CHARLES UNIVERSITY

Faculty of Science

Developmental and Cell Biology

Linn Amanda Syding

Mouse models for Angelman syndrome: generation and characterization

Doctoral thesis

Supervisor: Assoc. Prof. Radislav Sedlacek, Ph.D

Dept. of Transgenic Models of Diseases; Institute of Molecular Genetics AS CR, v.v.i

Prague, 2022

Declaration

I hereby declare that this thesis has been authored by me, Linn A. Syding, and all sources have been properly cited. I confirm that the content of this dissertation has not been used to obtain the same or a similar degree.

Tímto prohlašuji, že tuto práci jsem napsala já, Linn A. Syding, a všechny zdroje byly řádně citovány. Potvrzuji, že obsah této disertační práce nebyl využit k získání stejného nebo podobného titulu.

Prague, October 2022

Acknowledgements

I would like to thank my supervisor PD. Dr. rer. Nat. habil. Radislav Sedlacek, Ph.D. for his guidance, support, and advice during the doctoral study. I would also like to thank Dr. Agnieszka Kubik-Zahorodna, Ph.D., for her invaluable expertise, guidance and kindness during the PhD. Additionally, I would like to thank Dr. David Pajuelo-Reguera, Ph.D. and Dr. Jan Rozman, Ph.D. for their guidance and stimulating scientific discussions. I am also grateful for my colleagues in the Dept. of Transgenic Models of Diseases and the Czech Center for Phenogenomics for providing a vibrant, competent, and interdisciplinary workplace. Last, but not least, I thank my family and friends for their tremendous support, it could not have been done without you.

Abstract

Angelman syndrome (AS) is a neurodevelopmental disease found in 1 to 10,000 to 40,000 births, exhibiting an equal gender ratio. Key characteristics of the disease include an ataxic gait with tremor, severe mental retardation, profound speech impairment and seizures. Behavioral deficits such as increased anxiety and autism spectrum disorder features is found in affected individuals as well. The disease stems from the imprinted region 15q11.2-13q where genes are either maternally or paternally expressed as a result of parent-of-origin specific expression of the alleles. There are four main genetic etiologies causing AS namely, i) a large deletion ranging from 4-6 Mb on the maternally inherited allele including imprinted and bi-allelically expressed genes, ii) maternal deletion of the Ubitiquin ligase E3 (*UBE3A*) gene, iii) paternal uniparental disomy and iv) imprinting defect leading to inappropriate methylation of the locus. So far, there is no cure for AS rather the symptoms are ameliorated using a multidisciplinary approach. The goal of the doctoral study was to further decipher the role of *Ube3a* and *Gabra5* using two mouse models to gain more knowledge about the involvement of these two genes for future therapeutic interventions in for Angelman syndrome.

One model generated was a full gene deletion of *Ube3a* from 5'UTR to 3'UTR encompassing approximately 76 Kb with all coding and non-coding elements abolished. Although there are many mouse models available targeting the *Ube3a* gene in different manners there is no model with the entire gene missing, which offers a larger genetic similarity to the situation in patients as the majority harbor a large deletion. Also, a large variability of phenotypes in other AS models have been reported depending on experimenter, strain, and age of the animals, clearly presenting a barrier for development of therapeutics. To assess the suitability of the model in AS research we subjected it to a battery of tests particularly aimed towards the AS pathology, including motor skill evaluation and behavioral paradigms. We found that the novel AS model recapitulated motor skill deficits seen in DigiGait and rotarod tests. Furthermore, behavioral aberrancies were confirmed seen as underperformance in nest building and tail suspension test. The model did however not exhibit any underperformance in memory-dependent tests such as Barnes maze and novel object recognition. However, when subjected to the more difficult place reversal task in the IntelliCage setup, they did indeed underperform. We also observed differences in circadian rhythm activity and hypoactivity. The results obtained match well with phenotypes reported in other AS models

and has by the tests performed by us not provided any clear advantage in terms of studying AS. However, more tests addressing phenotypes such as autism spectrum disorder features, electrophysiology and EEG should be conducted and can lay basis for future publications.

Additionally, we targeted the Gamma-aminobutyric acid receptor alpha 5 (*Gabra5*) gene. This gene is frequently deleted on the maternal allele in patients with a large deletion. The cluster of Gamma-aminobutyric acid (GABA) subreceptor genes beta 3, gamma 3 and of course, alpha 5, is believed to be an important contributor to electrophysiological phenotypes but have also been linked to panic disorder and anxiety, phenotypes consistent in AS patients. We decided to study the anxiety-like behavior in *Gabra5* deficient mice by both behavioral tests but also assessing corticosterone levels, as dysregulation of the hypothalamic-pituary-adrenal- (HPA) axis has been linked to anxiety disorders. Furthermore, the HPA-axis is under GABAergic regulation however, the subreceptor expression and their contribution to the HPA-axis regulation, is still not clear, presenting a knowledge gap. We found that Gabra5$^{-/-}$ mice had lower corticosterone levels, which was rather surprising as disinhibition of GABAergic signaling has been reported to result in increased excitability. Additionally, the Gabra5$^{-/-}$ mice did not appear more anxious in open field and elevated plus maze tests. Furthermore, rearing behavior was decreased, suggesting a lower level of experienced anxiousness. Lastly, we did a functional analysis of hippocampal slices, a brain region known to contribute to anxiety regulation. The pact-clamp experiments revealed that Gabra5$^{-/-}$ derived neurons were hyperpolarized in several parameters tested. Based on this we believe that there must be a functional compensation of probably calcium or chloride channels to explain our observations. Although we were not able to attribute phentoypes to the alpha 5 channel we could clearly show the importance of examining functional compensation in constitutive models.

Finally, we conducted several gene expression analyses detecting expression of genes belonging to the AS locus using RT-qPCR. We generated two knock-out cell lines using CRISPR/Cas9 targeting resulting in a *Ube3a* deficient line and another line knocking out a putative enhancer residing within the intron 4-5 of said gene.

We evaluated expression of the genes in teratocarcinoma P19 cell line in both its pluripotent state and differentiated into neurons. We found a significant decrease in all paternally expressed genes. In rescue experiments with UBE3A overexpression, a restoration of gene expression was absent. We proceeded to do the same evaluation but with the putative enhancer knocked-out and found

that it recapitulated the observations made in *Ube3a* knock out cells. The results of the RT-qPCR generated experimental data pointing towards a possible function of the enhancer however additional tests are needed and eventually in the mouse organism.

Abstrakt

Angelmanův syndrom (AS) je neurovývojové onemocnění s celosvětovou incidencí 1:10 000, vyskytuje se tedy u 40 000 porodů ročně, poměr mezi pohlavími je stejný. Mezi klíčové charakteristiky onemocnění patří ataktická chůze s třesem, těžká mentální retardace, těžké poruchy řeči a záchvaty. U postižených jedinců se také vyskytují behaviorální deficity, jako je zvýšená úzkost a poruchy autistického spektra. Onemocnění pochází z imprintované oblasti 15q11.2-13q, kde jsou geny exprimovány buď maternálně, nebo paternálně jako výsledek exprese alel specifické pro rodiče. Existují čtyři hlavní genetické mutace způsobující AS, a to i) velká delece v rozsahu 4-6 Mb na alele zděděné maternálně včetně imprintovaných a bialelicky exprimovaných genů, ii) delece maternálního původu v genu Ubitiquin ligázy E3 (*UBE3A*), iii) paternální uniparentální disomie a iv) defekt imprintingu vedoucí k nevhodné metylaci lokusu. Dosud neexistuje žádný lék na AS, spíše se symptomy zmírňují pomocí multidisciplinárního přístupu. Cílem doktorského studia bylo dále dešifrovat roli UBE 3A a GABRA5 pomocí dvou myších modelů s cílem získat více znalostí o zapojení těchto dvou genů do generování modelů pro budoucí terapeutické intervence.

Jedním vytvořeným modelem byla úplná genová delece *Ube3a* z 5'UTR do 3'UTR zahrnující přibližně 76 Kb s vyloučením všech kódujících a nekódujících prvků. Ačkoli je k dispozici mnoho myších modelů zaměřujících se na gen *Ube3a* různými způsoby, neexistuje žádný model s chybějícím celým genem, který by nabízel větší genetickou podobnost se situací pacientů, protože většina z nich má velkou deleci. Také byla zjištěna velká variabilita fenotypů v jiných AS modelech v závislosti na experimentátorovi, kmeni a věku zvířat, což jasně představuje bariéru pro vývoj terapeutik. Abychom posoudili vhodnost modelu pro výzkum AS, podrobili jsme jej sérii testů zaměřených zejména na patologii AS, včetně hodnocení motorických dovedností a behaviorálních paradigmat. Zjistili jsme, že nový model AS opakoval deficity motorických dovedností pozorované v testech DigiGait a rotarod. Kromě toho byly potvrzeny odchylky chování při stavbě hnízda a testu zavěšení ocasu, na jejichž základě jsme výkonnost modelu vyhodnotili jako nedostatečnou.

Model však nevykazoval nedostatečnou výkonnost v testech závislých na paměti, jako je Barnesovo bludiště a nové rozpoznávání objektů. Když však byly podrobeny obtížnější úloze obrácení místa v nastavení IntelliCage, ukázalo se, že výkon skutečně nepodávaly. Pozorovali jsme také rozdíly v aktivitě cirkadiánního rytmu a hypoaktivitě. Získané výsledky se dobře shodují s fenotypy uváděnými v jiných AS modelech a námi provedené testy neposkytly žádnou jasnou výhodu z hlediska studia AS. Mělo by však být provedeno více testů zaměřených na fenotypy, jako jsou poruchy autistického spektra, elektrofyziologie a EEG, které mohou být základem pro budoucí publikace.

Dále jsme se zaměřili na gen receptoru alfa 5 kyseliny gama-aminomáselné (*Gabra5*). Tento gen je často deletován na mateřské alele u pacientů s velkou delecí. Shluk subreceptorových genů beta 3, gama 3 a samozřejmě alfa 5 kyseliny gama-aminomáselné (GABA) je považován za důležitého přispěvatele k elektrofyziologickým fenotypům, ale je také spojován s panickou poruchou a úzkostí, fenotypy konzistentními u pacientů s AS. Rozhodli jsme se studovat chování podobné úzkosti u myší s deficitem *Gabra5* pomocí behaviorálních testů, ale také hodnocením hladin kortikosteronu, protože dysregulace osy hypotalamus – hypofýza – nadledviny (HPA) byla spojena s úzkostnými poruchami. Kromě toho je osa HPA pod GABAergní regulací, exprese subreceptorů a jejich příspěvek k regulaci osy HPA však stále nejsou objasněny, což představuje mezeru ve znalostech. Zjistili jsme, že myši Gabra5 $^{-/-}$ měly nižší hladiny kortikosteronu, což bylo poměrně překvapivé, protože bylo popsáno, že dezinhibice GABAergické signalizace vede ke zvýšené excitabilitě. Navíc se myši Gabra5 $^{-/-}$ nezdály úzkostnější v testech v otevřeném poli a ve vyvýšeném křížovém bludišti. Současně „rearing behaviour“ byla snížena, což naznačuje nižší úroveň prožívané úzkosti. Nakonec jsme provedli funkční analýzu hipokampálních řezů, oblasti mozku, o které je známo, že přispívá k regulaci úzkosti. Experimenty pakt-clamp odhalily, že neurony odvozené z Gabra5 $^{-/-}$ byly hyperpolarizovány v několika testovaných parametrech. Na základě toho se domníváme, že k vysvětlení našich pozorování musí existovat funkční kompenzace pravděpodobně vápníkových nebo chloridových kanálů. Přestože jsme nebyli schopni přiřadit fentoypy alfa 5 kanálu, mohli jsme jasně ukázat důležitost zkoumání funkční kompenzace v konstitutivních modelech.

Nakonec jsme provedli několik analýz genové exprese detekující expresi genů patřících do lokusu AS pomocí RT-qPCR. Vytvořili jsme dvě knock-out buněčné linie pomocí CRISPR/Cas9 cílení,

což vedlo k *Ube3a* deficientní linii a další linii s vyřazeným domnělým enhancerem sídlícím v intronu 4-5 uvedeného genu.

Hodnotili jsme expresi genů v buněčné linii teratokarcinomu P19 jak v jejím pluripotentním stavu, tak diferencované na neurony. Zjistili jsme signifikantní pokles u všech paternálně exprimovaných genů. V záchranných experimentech s nadměrnou expresí UBE3A chyběla obnova genové exprese. Přistoupili jsme ke stejnému hodnocení, ale v linii s vyřazeným domnělým enhancerem, a zjistili jsme, že se pozorování provedená v knock-out buňkách *Ube3a* shodují. Výsledky RT-qPCR generovaly experimentální data ukazující na možnou funkci enhanceru, jsou však zapotřebí další testy a případně testy prováděné v myším organismu.

List of contents

1. Introduction

1.1.1 Angelman syndrome and its clinical manifestation

Angelman syndrome (AS) is a rare neurodevelopmental disease affecting approximately one in 10,000 to 40,000 births (1). The disease was first described by the pediatrician Dr. Harry Angelman in 1965 when he received several patients that were exhibiting severe developmental delay, complete or partial inability to use simple words or build sentences, ataxic gait, unprovoked laughter and seizures (2). At that time, it was assumed the disease was congenital but there were no findings yet to support it. It would take until the 1980s when the clinical observations were mapped to the chromosomal region 15q11.2-13q which is responsible for the disease (3). The clinical manifestation of AS patients can vary largely thus making it difficult at times to set a proper diagnosis. To facilitate this, there are several commonly occurring features the patient needs to exhibit such as sleep disturbances, unprovoked laughter, hyperactivity during childhood, inability to form coherent speech and a jerky ataxic gait with tremor (4). Young children with the disease often exhibit both hypo- and hypertonia with a stiff truncal part and loose flapping arms, especially at excitable states. The presence of seizures is not an official requisite for diagnosis but present in a vast majority of patients. The seizures includes all from tonic-clonic, myoclonic and atonic to full status epilepticus (5). The different phenotypes observed in patients have been divided into the following three categories; consistent, frequent and associated found in 100-, 80- and 20-80% of the patients (table 1.1) (6).

Table 1.1 The clinical features of Angelman syndrome. The associated, frequent, and consistent phenotypes summarized in the table. Table from Nickl et al. 2022 (unpublished).

Associated	Frequent	Consistent
• Flat occiput • Protruding tongue • Tongue thrusting; suck/swallowing disorders • Feeding problems during infancy • Prognathia • Wide mouth, widely spaced teeth • Frequent drooling • Excessive chewing/mouthing behaviours • Strabismus • Hypopigmented skin, light hair and eye colour (compared to family), seen only in deletion cases • Hyperactive lower limb deep tendon reflexes • Uplifted, flexed arm position especially during ambulation • Increased sensitivity to heat • Sleep disturbance • Attraction to/fascination with water	• Delayed, disproportionate growth in head circumference, usually resulting in microcephaly Seizures, onset usually • Characteristic EEG with large amplitude slow spike waves and triphasic waves	• Severe developmental delay • Speech impairment, no or minimal use of words • Movement or balance disorder, usually ataxia of gait and/or tremulous movement of limbs • Behavioral uniqueness: combination of frequent laughter/smiling; apparent happy demeanor; easily excitable personality, often with hand flapping movements; hypermotoric behaviour; short attention span

1.1.2 Angelman syndrome and imprinting diseases

Angelman syndrome is classified as an imprinting disease, which is a group of diseases stemming from imprinted regions with differentially expressed genes depending on their parental origin (7). Imprinted genes tend to exist in clusters and to date 13 different clusters on eight chromosomes have been identified but there are likely many more to be discovered (8). These clusters are largely conserved between mice and humans although they tend to be inversed on the mouse orthologue. Imprinted genes were first considered to only be involved in processes linked to the early development but it has since then become increasingly acknowledged that they are involved in a large number of different processes including metabolism and growth (9). So far, approximately 150 imprinted genes have been found in the murine genome and approximately half of those in humans (7). The expression of imprinted genes in the clusters are coordinated through a sophisticated interplay between DNA methylation, non-coding RNAs (ncRNAs), histone modification and chromatin structure (10). The clusters have in common that they tend to contain both maternally and paternally imprinted genes and both protein coding genes and ncRNA transcripts (9). The differentially expressed genes exhibit allele-specific methylation, histone

modification and with that, differential chromatin structure which in turn either allow for genes to be expressed or to silence them (11). The differential gene expression is under the control of an imprint control region (ICR), exerting an activating or repressing control on the genes in the imprinted region in *cis*. The ICR itself generally have a different methylation pattern depending on the parental origin, ICRs on maternally inherited chromosomes are in most cases hypermethylated and on paternally inherited chromosomes hypomethylated thus they are repressed and active, respectively (12). Additionally, the ICR usually contains the promoters of large ncRNAs that, when transcribed, silence the protein coding genes of which they overlap. The effect being subsequent silencing of large ncRNAs on the maternally inherited chromosome through a hypermethylated ICR but silencing of other genes due to methylation directly on the protein coding genes. The paternal mode of silencing thus entails the action of the large ncRNA to overlap protein coding genes as the genes themselves tend to be hypomethylated. In summary, the mode of imprinting varies depending on parental origin (13).

It is of utmost importance that the gene expression is kept at appropriate levels for normal development of the organism. When imprinted genes are expressed in a disturbed manner, either due to genetic mechanisms such as deletions or epigenetic mechanisms such as faulty methylation of ICRs, this leads to genetic diseases collectively called imprinting diseases (14). The four main etiologies for imprinting diseases are i) uniparental disomy (UPD) (15), ii) deletions, duplications or translocations of the chromosome in question (16), iii) DNA mutagenesis on protein coding genes (17), and iv) epigenetic mutations on ICRs or other differentially methylated regions (18).

There are eight known imprinting diseases with AS included (19). They are similar in their genetic etiologies but also in observed phenotypes, which generally include delayed development, growth aberrations, hormonal dysregulation, and cognitive impairment to varying degrees (table 1.2).

Table 1.2 **Imprinting diseases**. The diseases are summarized with phenotypes, epidemiological status, and chromosomal region. Table from Nickl et al. 2022 (Unpublished).

Imprinting disease	Occurrence	Chromosomal region	Clinical manifestation
Transient Neonatal Diabetes Mellitus (TNDM)	1:300.000	*6q24*	• Transient diabetes, hyperglycemia without ketoacidosis • Macroglossia • Omphalocele
Silver-Russell syndrome (SRS)	1:75 000-1:100 000	7 & *11p15*	• Small prematurely calcified placenta • Macrocephaly at birth • Hemihypotrophy • Prominent forehead • Triangular face • Feeding difficulties
Beckwith-Wiedemann syndrome (BWS	1:15 000	*11p15*	• Overgrowth (pre- & postnatal) • Organomegaly • Macroglossia • Omphalocele • Neonatal hypoglycemia • Hemihypertrophy
Kagami-Ogata syndrome (KOS14)	Unknown	*14q32*	• Polyhydramnion • Abdominal & thoracal wall defects • Bell-shaped thorax
Temple syndrome (TS14)	Unknown	*14q32*	• Neonatal hypotonia • Feeding difficulties in infancy • Truncal obesity • Scoliosis • Precocious puberty
Prader-Willi syndrome (PWS)	1: 10 000-1:25 000	*15q11-q13*	• Mental retardation • Neonatal hypotonia • Hypogenitalism • Hypopigmentation • Obesity/hyperphagia
Angelman syndrome (AS)	1:12 000-1/20 000	*15q11-q13*	• Mental retardation • No speech • Excessive & unmotivated laughter • Ataxia • Seizures susceptibility
Precocious puberty (central precocious puberty 2; cppb2)	Unknown	*15q11.2*	• Early activation of the hypothalamic-pituitary-gonadal axis results in gonadotropin-dependent precocious puberty
Pseudohypo-parathyroidism (PHP1B, PHP1C, PHP1A)	Unknown	*20q13*	• Resistance to PTH and other hormones • Albright hereditary osteodystrophy • Subcutaneous ossifications • Feeding behavior anomalies • Abnormal growth patterns

1.1.3 Angelman syndrome, locus arrangement and disease genetics

Angelman syndrome, classified as an imprinting disease, shares the genetic mechanisms with most of the other imprinting diseases. More specifically, the four main genetic etiologies causing AS are the following; i) a maternal *de novo* deletion of the 15q11.2-13q locus with an intact paternal copy (20); ii) DNA base mutations of the maternally inherited Ubiquitin-protein ligase E3A (*UBE3A*) gene, a gene where loss-of-function mutations alone are enough to cause AS thus it is labelled as the "AS gene" (21, 22); iii) paternal uniparental disomy of the 15q11.2-13q, leading to a paternal expression pattern (23); iv) and lastly, a failure to establish correct epigenetic modifications of the ICRs necessary for locus control (24).

Out of these four disease mechanisms, the by far most commonly occurring one is the maternal deletion of the locus, seen in approximately 70% of diagnosed patients. Patients harboring large deletions exhibit more severe symptoms than patients belonging to the other classes with albinism and physical growth retardation added to the list (25). This locus contains two proximal breakpoints and one distal, each consisting of low-copy repeats which facilitates for non-allelic homologous recombination between any of the proximal repeats with the distal repeat (26). This makes the region vulnerable for cytogenetic rearrangements such as deletions, inversions, and triplication with the first being the case in AS. The deletions between proximal breakpoint 1 and the distal breakpoint are labelled as a Class I deletion spanning ~6 Mb and the proximal breakpoint 2 with the distal as the Class II deletion involving 4-5 Mb (27). The Class I deletion presents with a more severe set of phenotypes as it includes more deleted genes than the Class II deletion (figure 1). In a study by Varela et al. (2004) (28) they found that Class I individuals acquired the skill to sit without support at 19 months whereas Class II were able to sit at 16 months of age (28). They also observed Class I patients being more affected regarding speech, as 38.1% of Class II subjects were able to utter syllabic sounds whereas the Class I patients could not.

Both deletions encompass all imprinted genes and several bi-allelically expressed genes. Both deletions have a cluster of Gamma-Aminobutyric Acid A ($GABA_A$) genes missing, which is likely the reason for more severe seizures and disturbed EEGs in deletion patients (27). The Class I deletion includes genes *NIPA1*, *NIPA2*, *CYF1P1* and *GCP5*, involved in magnesium transport, protein synthesis and microtubule association, respectively (figure 1.1) (29-31).

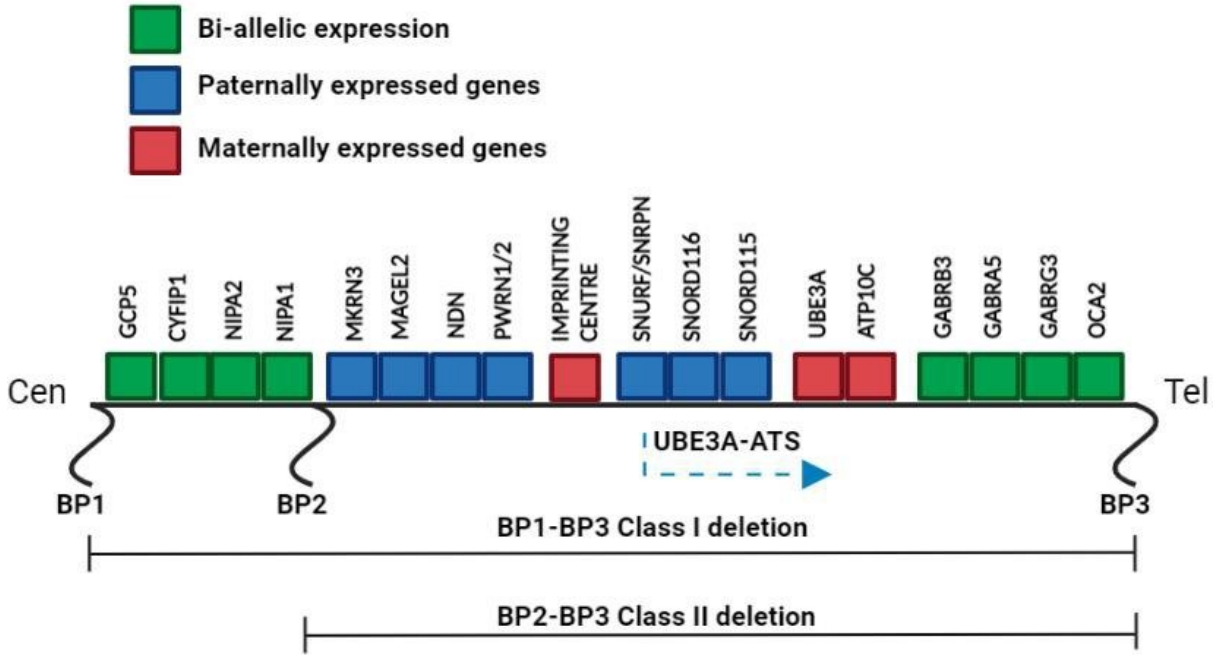

Figure 1.1 Simplified overview of the 15q11.3-15q chromosomal region. The figure presents the AS locus indicating the sets of genes deleted in the Class I and II deletion from break point 1 (BP1) and BP2, respectively until the distal breakpoint 3 (BP3). Genes marked in green are bi-allelically expressed, those in blue paternally expressed and genes in red maternally expressed. The figure also points out the ncRNA UBE3A-ATS which overlaps the *UBE3A* gene on the paternal chromosome, thus silencing it. Figure adapted from Nickl et al. 2022 (Unpublished).

This locus is also the root to a genetically mirrored disease named Prader-Willi syndrome (PWS). Prader-Willi syndrome shares its disease mechanisms with AS but is a result of paternal deletion or maternal UPD (32). In PWS, the deletion leads to loss of expression of the paternally expressed genes (PEGs) in the locus, a multi-gene disorder in contrast to the sole gene of *UBE3A* causing AS. The PEGs in the region include both protein coding genes and ncRNAs, with an involvement in a variety of cellular and physiological processes (table 1.3). Although PWS is genetically mirrored it presents with significantly different phenotypes such as hypogonadism, mild intellectual disability as opposed to the severe one seen in AS patients, hypotonia early in childhood with feeding difficulties but progressing to severe hyperphagia with age, physical growth retardation and craniofacial anomalies (33).

Table 1.3 Paternally expressed genes in the 15q11.2-13q locus. The function of PEGs in the AS/PWS locus. Table adapted from Nickl et al. 2022 (Unpublished).

Paternally expressed genes	Function
NDN	Likely plays a role in axonal outgrowth
MAGEL2	Expressed in the brain, lacking of the protein product is reported to be involved in autism spectrum disorders
MKRN3	Encodes for makorin proteins abundantly expressed in the brain and involved with hormone regulation and precocious puberty
SNURF-SNRPN	Bicitronic gene where exon 1-3 encodes protein involved in genomic imprinting and exon 4-10 involved in mRNA slicing
C/D box RNA (SNORDs)	SNORDs key in the development of PWS with involvement in RNA processing

In approximately 11% of AS patients the disease is caused by loss-of-function mutations in the maternally inherited *UBE3A* gene (22). The *UBE3A* gene is bi-allelically expressed ubiquitously in the organism except for in mature neuronal cells, where it exhibits a maternal only expression (figure 1.2) (34). The *UBE3A* gene is conserved in both invertebrate and vertebrate species, imprinting however, appears to have evolved after the divergence from the metatherian lineage (35). As the gene dosage of *UBE3A* is not decreased in neurons since the maternal copy compensates for the loss of the paternal one, there must be another advantage that imprinting of *UBE3A* has in eutherian species (35). A plausible reason is thought to be an advantage from expression of small nucleolar RNAs (snoRNAs) hosted by the UBE3A-ATS transcript, as they are present in eutherians but not in metatherians (36). This relationship has however not been proven yet. The *UBE3A* gene encodes the Homologous to E6AP Carboxy Terminus (HECT) ubitiquin ligase where it acts as an E3 enzyme, providing substrate specificity in the ubitiquin cascade (37). The HECT domain is crucial for the function of the protein and it is generally mutations in the gene region coding for the HECT domain that leads to AS (38). The *UBE3A* gene codes for three different isoforms, in humans the isoforms 2 and 3 has 23 and 20 extra amino acids in the N-termini in regards to isoform 1, respectively. Mutations in the N-termini leading to truncation of the protein

leads to AS phenotypes as the HECT is missing as does full length versions of the protein but with point mutations in the HECT domain, clearly showing that it is the crucial region of the gene (39).

As the UBE3A is an integral part of the ubitiquination cascade providing substrate specificity, ultimately resulting in proteosomal decay of proteins, it goes without saying that it has a multitude of potential substrates out of which only few have been identified (40). A list of downstream substrates should undoubtedly be developed but unfortunately, this would only be part of the story, as it is more complex. The UBE3A proteins subcellular location and the concentration of it differs over the development and by activity (41). The UBE3A protein is reduced in the mammalian brain in aged individuals however, they do not develop AS, clearly showing that it is a neurodevelopmental not neurodegenerative disease (42). It shows that UBE3A has a different role in the early developing versus aged CNS. As mentioned the UBE3A also changes its subcellular location with age, shifting from the cytoplasm to the nucleus as aging progresses (43). Additionally, activation of neurons leads to a nuclear localization of UBE3A, pointing to it being activity dependent (44). The timing and location thus seem to be crucial parameters to take in to account in its interaction with substrates, adding complexity to the matter.

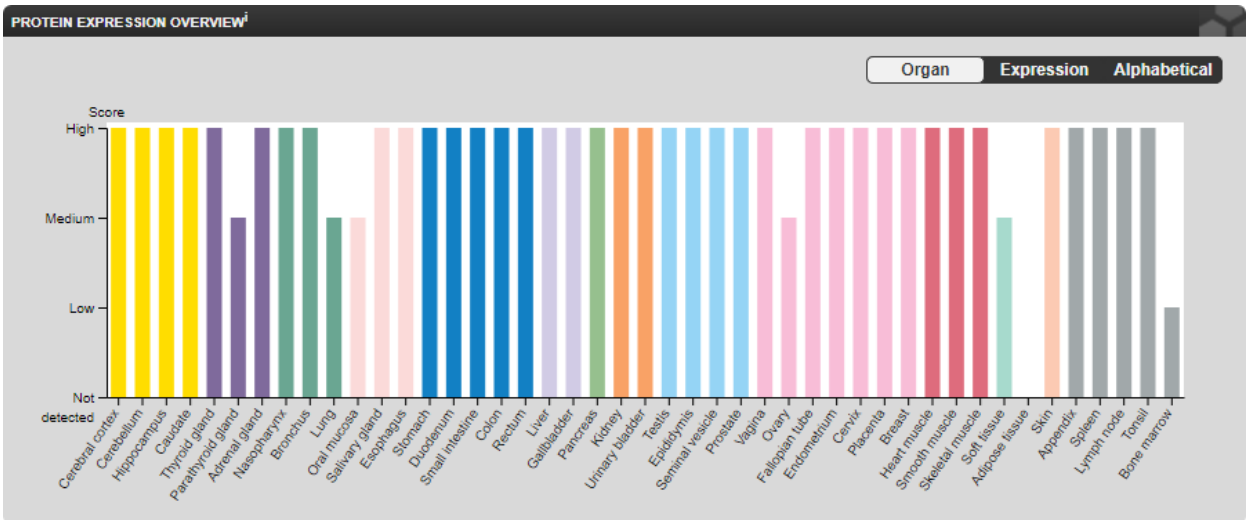

Figure 1.2. UBE3A tissue expression. The UBE3A expression estimated in human tissue. Source: The Human Protein Atlas.

The third category of AS patients are those with paternal UPD, found in 3-5% of cases. These patients usually presents with milder symptoms such as decreased seizure susceptibility, less ataxia and improved cognition (45). Uniparental disomy is caused by various mechanisms such as trisomy rescue, complementation of gametes, post-fertilization mitotic errors and monosomy rescue (46). These mechanisms are true for both maternal and paternal UPD. Patients with UPD should be given extra attention regarding the status of the duplicated genes, as recessive mutations may be expressed, causing additional harm.

Lastly, there are the patients affected by imprinting defects, accounting for ~3% of confirmed cases (47). These patients have the chromosomes from bi-parental origin but exhibit a paternal methylation pattern resulting in bi-allelic expression of PEGs and the subsequent silencing of UBE3A (48). In effect, subjects with imprinting aberrancies have similar expression profile of genes as the patient with paternal UPD. The imprinting defects can be a consequence of failure to replicate imprinting post-zygotically or a microdeletion in the AS imprinting center (IC) but can also possibly be a result of germline mosaicism in certain cases where the cause have not been found (49).

As mentioned, more generally for regulation of gene expression in imprinted gene clusters the paternal and maternal mode of imprinting tend to differ from one another. This is certainly the case in the AS locus regulation as well. On the maternally inherited chromosome, the AS-ICR is active throughout the embryonic development executing differential programs depending on parental allele (50). The AS-ICR on the maternally inherited 15q11.2-13q, methylates the distally located PWS-ICR, which in its turn acts as a bidirectional activator of PEGs. On the paternally inherited chromosome, the PWS-ICR remains hypomethylated and subsequently allows for PEGs to be expressed (51). Furthermore, the promoter/exon 1 of the bicistronic PEGs SNURF/SNRPN is the transcription start site (TSS) of the large antisense transcript SHNG14. The SHNG14 undergoes extensive alternative splicing and hosts the UBE3A-ATS transcript that overlaps the *UBE3A*, silencing it (52). The TSS of the SHNG14 is fully CpG methylated in maternally inherited chromosomes and fully unmethylated in the paternal ditto thus silencing the transcription or allowing for expression, respectively.

It has been proven beyond doubt that the UBE3A-ATS silences the paternal copy of *UBE3A* but the exact mechanism how is still debated (53). There are different models on how an antisense

transcript may silence the protein coding gene of which is overlaps. Two models worth mentioning are the collision model and the RNA-DNA interaction model (54). The collision model states that only one DNA strand can be transcribed at a time as the RNA polymerases would collide with one another if both strands were to be transcribed simultaneously, pushing one of them back (54). The other model put forth is the RNA-DNA interaction model hypothesizing that the transcription of the antisense transcript leads to modification of the chromatin structure. The change in chromatin structure would cause the transcription of the *UBE3A* transcript to be terminated, resulting in truncated, loss-of-function transcripts (52).

1.1.4 Angelman syndrome and experimental therapeutics

There is no cure for AS, rather the symptoms are managed by a multidisciplinary approach. It is common to address the lack of speech with teaching patients' non-verbal methods. The ability to communicate, if so only non-verbally, significantly reduces stress and anxiety tied to this (55). To help mitigate disturbances in the circadian rhythm melatonin may be provided and to prevent seizures it is recommended to administrate a combination of benzodiazepine and valproic acid (56, 57). This approach merely helps to reduce the severity of various symptoms, it does in no way cure the underlying cause, which is the lack of UBE3A. To combat this, experimental approaches reinstating the expression have been carried out in mouse models.

In a study by Daily et al. (2011) (58) they managed to significantly improve the AS mice performance in contextual fear conditioning, a hippocampus-dependent task, by delivering exogenous *Ube3a* in the form of plasmid DNA (58). The adeno-associated viruses (AAVs) utilized to deliver the plasmid had a differential distribution in the brain where the hippocampus of treated animals exhibited WT levels of UBE3A whereas there was no detection in the cerebellum. To little surprise, there was no rescue in motor skills impairments, such as latency to fall in the rotarod test (58). This approach faces one major drawback, which is the failure to precisely control the amount of UBE3A protein produced upon delivery of plasmid DNA. Increased amounts of UBE3A is reported in autism spectrum disorders (ASDs), clearly indicating the importance of the need of a tightly regulated amount of protein (59).

In another study, they were successful in activating the paternal copy of *Ube3a* by administrating AS mice with topetocan, a topoisomerase I inhibitor (60). Topetocan reinstated the *Ube3a* expression by reducing the Ube3a-ATS expression, which in its turn cannot silence the protein coding *Ube3a*. The expression was widespread in the CNS including the hippocampus, cortex, cerebellum, and spinal cord. Furthermore, it appears to have a long-term effect, as UBE3A was still detectable after 12 months post injection. The caveat to this method is the lack of specificity. The topoisomerase I inhibitor is not limited to Ube3a-ATS and could thus lead to adverse effects if patients were to be treated with topetocan.

Silencing of Ube3a-ATS was successfully performed in a more precise manner by delivering anti Ube3a-ATS oligonucleotides (ASOs) via intracerebroventricular injections in to adult AS mice (61). The ASOs degrade the Ube3a-ATS via hybridization of the two and subsequent cleavage by the endogenous RNase H endonuclease takes place. This approach resulted in partial restoration of UBE3A and amelioration of cognitive phenotypes (61). This approach offers the specificity lacking in the topetocan treatment but is short lasting as the UBE3A expression was lost within four months.

In 2016 Bailus and colleagues managed to restore *Ube3a* expression in the hippocampus and cerebellum by delivering an injectable engineered zinc-finger repressor via intraperitoneal or subcutaneous injections (62). It was able to cross the blood-brain barrier by linking it to the HIV TAT cell-penetrating peptide. The artificial transcription factor was engineered to bind to the *Snurf/Snrpn* promoter region which is also the TSS for the Ube3a-ATS (53). This clever approach shows promise as the zinc-finger used have already been successful in phase 2 clinical trials and could be safe for human use (63). However, artificial transcription factors are cleared out of the system rapidly and patients would need to get frequent injections for it to be an effective therapy.

The therapies show promise in their purpose to elevate UBE3A, but the timing of delivery is a crucial factor. As shown by Silva-Santos et al. (2015) there are several developmental windows for phenotype rescue (64). Using a temporally controlled Cre-dependent induction of *Ube3a*, they were able to reinstate *Ube3a* by delivering tamoxifen at various time points. The window to rescue behavioral phenotypes such as anxiety and repetitive behavior appear to close the earliest, where reinstatement needs to occur embryonically. Motor skill deficits were reversible in adolescent mice.

Hippocampal synaptic plasticity measured through evaluating the long-term potentiation (LTP) of neurons was reversible at any age (64).

Other approaches have included to reduce the levels of UBE3A substrate targets as the lack of UBE3A is postulated to result in an accumulation of its substrates. As there are mainly neurological phenotypes associated to AS it makes sense to investigate on brain-derived targets of UBE3A. GAT1, a GABA transporter has been identified as a target and has been found to be upregulated in the absence of UBE3A. This is believed to be an underlying cause of the loss of tonic inhibition as the GABA concentration is decreased in the extra synaptic space due to surplus of the transporter. By treating UBE3A deficient mice with THIP, a $GABA_A$ receptor agonist, electrophysiological and motor deficits were rescued (65). Arc, also a substrate of UBE3A is a regulator of trafficking AMPA receptor to the membrane (66). Investigators demonstrated that by reducing Arc and the recovery time after audiogenic seizures was decreased, it did however not ameliorate other impairments (67). Although modulating the UBE3A targets have shown to milden the severity of AS phenotypes it will not be plausible to use as a one-fits-all therapy. Furthermore, AS can develop from secondary and even tertiary changes downstream of UBE3A activity, making the pathways even more complex (40). Intriguingly, it appears there is significant overlap between dysregulated pathways between AS and other disorders such as ASD.

1.2.1 Mouse models of Angelman syndrome

Previous subchapter discussed AS disease manifestation, genetics and finally experimental therapeutics developed to cure or at least ameliorate disease symptoms. The latter being crucial for future pre-clinical and eventually clinical interventions. Experimental research would however not be possible without the employment of suitable animal models, AS research being no exception. The laboratory mouse poses as a good model organism for biomedical research as it is easy to handle, is genetically analogous to humans, inexpensive, breeds fast and can be genetically modified with ease (68). Furthermore, laboratory mice are often inbred thus representing a highly controlled system which, is suitable for medical research (69). To be suitable, the mouse model has to exhibit high construct validity, a genotypic similarity, and high face validity, similarity at a phenotypic level (70). Mice are highly appropriate for AS research as the AS locus 15q11.3-13q

has a syntenic region on chromosome 7 (71). However, the region between break point 2 and 3 is inversed in the mouse. The AS region in mice and humans contain the same genes and both are subjected to genomic imprinting and the mode of silencing *Ube3a* on the paternal chromosome is the same utilizing the Ube3a-ATS (72, 73).

There are multiple generated mouse models for AS research. These include different approaches such as *Ube3a* with conditional alleles, deletion models of *Ube3a*, inducible *Ube3a* isoforms, systems with reporters tagging *Ube3a* and larger deletion models including *Ube3a* and additional genes, more closely mimicking the genetics in patients (table 1.4). The different types of models are useful in different ways, for example, modifications within the gene can uncover details on specific gene domains and isoforms in particular (table 1.4) (74-77). *Ube3a* in conditioned models can be expressed in a cell-type, tissue, and even developmental stage specific manner, making it a highly dynamic system and showing much promise in deciphering spatio-temporal expression of Ube3a (64, 78, 79).

As mentioned in previous subchapter, there are three different isoforms of *Ube3a*, where isoform 2 and 3 have extra 23 and 20 amino acids in the N-terminus, respectively, in regards to isoform 1. The effect these additional amino acids have on the protein regulation could be deciphered using inducible models such as the Tg(tetO-Ube3a*2)^{884Svd} or Tg(tetO-Ube3a*1)^{1Svd} (Table 1.4). Models tagged with a reporter such as the YFP fused to the C-terminus of *Ube3a* namely the Ube3a^{tm2Alb} are invaluable for uncovering regulation, spatio-temporal distribution, and concentration of Ube3a expression (41, 80-82).

The by far most used model in regards to AS research is the Ube3a^{tm1Alb} model harboring a deletion of exon 5, referring to isoform 2, which leads to a truncated UBE3A without a HECT domain thus resulting protein deficiency (75). This mouse model has shown to recapitulate many of the AS features such as impaired motor skills, altered vocalization, increased seizure susceptibility and behavioral deficits such as repetitive behavior, however the cognitive abilities are usually not impaired or if so, only mildly (70).

Table 1.4. Table summarizing existing models for AS research. Previously generated models are summarized and grouped depending on type of mutation. Table adapted from Syding et al. (2022) (83).

Group	Strain	Genotype	Phenotype (AS heterozygote)	Ref.
Deletions and substitutions	Ube3a^{tm1Alb}	Deletion of 100 N-terminal amino acids in the encoded protein and a frameshift inactivating all putative protein isoforms	Neurobiological and behavioral, cellular, growth/size/body, homeostasis	(75)
	Ube3a^{tm2Yelg}	Nucleotide substitutions in exon 3 result in of a stop codon for glutamic acid at position 113 (E113X).	Neurophysiological	(76)
	Ube3a^{em2Yelg}	The ATG codon (exon 3) encoding the start-codon methionine of UBE3A isoform 2 was mutated into a TGA, resulting in expression of isoform 3 only.	Neurobiological, cellular	(74)
	Ube3a^{em1Yelg}	An ATG codon (Ube3a exon 4/5) encoding the initiating methionine of UBE3A isoform 3 was mutated into an alanine (GCG), therefore only isoform 2 is expressed in these mice.	Neurobiological, cellular	(74)
	Ube3a$^{em1(IMPC)Hmgu}$ (C57BL/6NCrl)	Intra-exon deletion (exon3)	Neurobiological and behavioral, hematopoietic, homeostasis,	(77)
Floxed alleles	Ube3a$^{tm1.1Bdph}$	A floxed allele, exon 5 flanked by loxP sites.	Neurobiological and behavioral	(78)
	Ube3a^{tm1Yelg}	A stop cassette with loxP sites is inserted in intron 3. Cre-mediated recombination reinstates gene expression.	Neurobiological and behavioral, cellular	(64)
	Ube3a$^{tm1a(KOMP)Wtsi}$	The critical exon(s) is/are flanked by loxP sites. FLP recombination generates conditional allele. Subsequent CRE expression results in a knockout mouse. If CRE expression occurs without FLP expression, a reporter knockout mouse is created.	N/A	(79)
Inducible isoforms	Tg(tetO-Ube3a*2)884Svd	The transgene under control of a modified Tet response element (TRE or tetO), transgene - mouse ubiquitin protein ligase E3A (Ube3a) cDNA sequence encoding transcript variant 2 (NM_011668.2) with FLAG tag, and an SV40 polyA signal.	NA	unpublished
	Tg(tetO-Ube3a*1)1Svd	The transgene under control of a modified Tet response element (TRE or tetO), transgene - mouse ubiquitin protein ligase E3A (Ube3a) cDNA sequence encoding transcript variant 1 (NM_173010.3) with FLAG tag, and an SV40 polyA signal.	N/A	unpublished
Modified Ube3a	Tg(Ube3a)1Mpan	Overexpression of Ube3a gene with three FLAG tags	Autism-like, neurophysiological	(80)
	Tg(Ube3a)5Mpan	Extra copy of Ube3a transgene in the genome	Seizures, social behavior	(81)
	Ube3a^{tm1Jwf}	A part of exon 15 and all of exon 16 fused to IRES-lacZ-neo cassette resulting in functional impairment of the C-terminal region responsible for ubiquitin protein ligase activity.	Neurobiology and behavior, nervous system	(82)

	Ube3a$^{tm2.1Alb}$/ Ube3a^{tm2Alb}	Fusion of Yellow fluorescent protein (YFP) to exon 10. Expression of YFP is through inheritance of the maternal allele and recapitulates endogenous expression.	Phenotype not analyzed, the strain is mainly used to track Ube3a expression	(41)
Large deletions	Del(7Gabra3-Ube3a)^{1Yhj}	The deletion extending from Gabra3 to Ube3a gene including Atp10a.	Neurobiology and behavior, cellular, craniofacial, digestive/alimentary, growth/size/body, mortality/aging, nervous system	(84)
	Dp(7Herc2-Mkrn3)1Taku	Insertion of selection cassettes and loxP sites proximal to Herc2 and distal to Mkrn3.CRE mediated recombination in ES cells led to balanced duplication and deletion of 6.3 Mb region between Herc2 and Mkrn3.	Neurobiological and behavioral, cellular, autistic	(85)
	Del(7Herc2-Mkrn3)13FRdni	5Mb deletion of entire AS/PWS locus spanning from Herc2 to Mkrn3 genes via Lmp2a transgene insertion	(Analyzed for PWS only) Neurobiology and behavior, cellular, homeostasis, metabolism, mortality, aging, respiratory	(86)
	Del(7Ube3a-Snrpn)1Alb	Deletion of genomic DNA from the loxP site within Snrpn to the loxP site within Ube3a.	(Analyzed for PWS only) Neurobiological and behavioral, growth, size, body, mortality, aging, muscle (hypotonia)	(87)
	Oca2$^{p-30PUb}$	This deletion expands distally from the p locus, Gabrb3, Ube3a, and Ipw. This deletion includes Atp10a.	Adipose (increased total fat), growth, size, body, hematopoietic, homeostasis, immune, liver and biliary, renal and urinary	(88)
	Ube3a^{genedel} (C57BL/6NCrl)	Gene deletion	Neurobiological and behavior, nervous system	(83)

1.2.2 Phenotyping of AS models

To evaluate the phenotypic similarity between AS mice and AS patients can be a difficult task as the two species differ significantly on the phenotypic level. However, there are plenty of tests developed for rodents where the results can be extrapolated for humans.

Cognition can be assessed in rodents with tests such as fear conditioning and water maze/Barnes maze (89, 90). Fear conditioning involves the association between a stimulus and an aversive penalty. The animal is conditioned to a stimulus such as light or sound paired with a mild foot shock. The innate fear response in rodents is freezing behavior. Freeze time is measured when eliciting the stimulus; this is cued-dependent fear. The context-dependent fear response is evaluated by placing the animal in the same apparatus without the stimulus (91). The context- versus cued-dependent freezing require different brain areas that can cleverly be assessed by one test with two modifications. Water maze and Barnes maze evaluate spatial memory, a hippocampal-dependent task (90). Water maze involves submerging the rodent in water which may cause the involvement

of confounding factors such as hypothermia and anxiety, while Barnes maze is on dry land thus offering an advantage to water maze testing (90).

Motor skill deficits are one of the hallmark features of AS (6). The rotarod test evaluates the animals motor coordination skills. The rotarod apparatus is comprised by a suspended rotating rod placed high up enough to elicit avoidance of fall but without harming the animal when they do fall. The latency to fall is often measured but the animals force and grip can be evaluated too (92). This test is sensitive to detect cerebellar dysfunction, which is affected in AS subjects (93, 94). Gait analysis such as the DigiGait system, is a useful tool to detect gait changes in rodent models, a relevant task to distinguish AS phenotypes in rodent models (95).

AS patients exhibit robust behavioral impairment with adaptive variability. A large population of AS children qualify for the autism diagnosis based on exhibited behavior, thus many of the behavioral paradigms used to test rodents are also suitable for detecting ASD (96). Anxiety in AS patients increases with age and manifests with tremors, tics and increased fits (97). The open field test evaluates animal anxiety-like behavior (98). The animal is placed in an arena with pre-defined zones such as periphery and center and has freedom to explore freely. The amount of time spent in the center versus periphery and distance moved are some for the parameters measured by an automatic tracking device (99, 100). Nest building test is a cheap and efficient way to assess neuro-developmental and degenerative disease and repetitive behavior. Small rodents have an innate urge to create a nest and normally do so with, for instance, paper provided. The amount that has not been used is weighed after one night (101). The exact translational value for nest building in AS animals is not fully elucidated, as it is dependent on several brain structures. However, due to its cheap and easy nature it is very often used in AS research and continues to be a recommended test (102). Marble burying is another inexpensive and simple test to use. It assesses repetitive behavior, a hallmark in ASDs (102). It also measures anxiety-like behavior, making it a recommended test in AS animals. The animals are given marbles in the cage and the number of marbles buried after a defined time is observed. When given anxiolytics the number of buried marbles generally increase, however in AS animals the number of marbles buried are decreased (101, 103).

Sleep disturbances are often present in AS patients manifested with changes in sleep/wake cycle and general hyperactivity (6). The IntelliCage setup can be used to observe both factors. The IntelliCage tracks animals with surgically placed transponders in their homecage environment

(104). The activity and the timing of individual animals are tracked automatically, giving a clear pattern of the circadian rhythmicity.

To assess AS phenotypes in mice, a combination of tests evaluating the model in regard to AS pathology should be employed. In a study by Sonozgni et al. (2018) they have put forth a behavioral battery of tests that can be used when characterizing a novel model or by evaluating the success of a therapy (103). Interestingly, they provided a statistical power study in addition, showing what kind of sample sizes are appropriate for certain tests. The highest number of animals needed to obtain statistical significance at $\alpha = 0.05$; $(1 - \beta) = 0.95$ was for the open field test where 21 animals were needed. In these test they used an F1 hybrid of C57BL/6 and 129sv mice, a frequently common strain in behavioral test in AS research (103). For rotarod and marble burying the sample number was 14 and 7, respectively.

The Ube3a^{tmAlb1} has undoubtedly been of great use in the AS field, recapitulating many of the hallmark features of AS but major inconsistencies in phenotypes between laboratories, strain and age of animals are however present, making standardized testing increasingly difficult (89). In a study by Born et al. (2017) the investigators subjected AS animals from the three different strains, C57BL/6J, 129, and the F1 hybrid of those, to tests evaluating the behavior, seizure susceptibility and EEG activity to determine how genetic background influence the phenotypes in AS animals (89). It was observed that AS animals on the C57BL/6J background exhibited robust behavioral impairments, displayed different cortical EEG power spectrum in both light and dark phases, hypoactvity and poor motor skills. The 129 strain exhibited decreased marble burying, impaired motor skills and lower seizure threshold. The F1 hybrid had the mildest phenotype, exhibiting impaired memory and hypoactivity. They all had significantly higher weight, a feature reported in some older AS individuals (105). Age is also a confounding factor in AS animals. It was observed that C57BL/6J animals had clear deficits in spatial learning acquisition at 16 weeks of age but not at 8 weeks, suggesting a progressive loss of cognition over time (106). On the contrary, sensorimotor gating and startle reactivity were affected in juvenile mice but not in adults, indicating a developmental window, further adding complexity to testing new drugs or evaluating other therapeutic interventions.

The reported phenotypic variations in AS animals depending on background strain and age have demanded an improved AS model of higher translational value. The majority of AS animals harbor

a large deletion in the AS locus while only a low percentage carry point mutations or small deletions in the *UBE3A* gene. The Ube3a^{tmAlb1} model and other smaller deletion models lack the genotypic similarity of the majority of patients (75). There has been increased demand for a model with a deletion spanning all coding and non-coding elements of the *Ube3a* gene. Such model could bring additional knowledge to the contribution of the gene. Furthermore, a putative enhancer is present in the *Ube3a* gene that may influence transcription of other genes, further worsening the phenotype. If such a model would confer less phenotypic variability and uncover additional information is yet to be elucidated.

1.3.1 Angelman syndrome and *Gabra5*

As mentioned in previous subchapters, the AS locus contains both imprinted and non-imprinted genes (1). The non-imprinted genes include a centromeric and a telomeric cluster (figure 1). The telomeric cluster contains three genes encoding $GABA_A$ subunits namely the Gamma-aminobutyric acid receptor subunit beta-3 (*GABRB3*), Gamma-aminobutyric acid receptor subunit alpha-5 (*GABRA5*) and Gamma-aminobutyric acid receptor subunit gamma-3 (*GABRG*3) genes. These encode for the β3-α5-γ3 $GABA_A$ receptor subunits, respectively. This GABAergic gene cluster is deleted on the maternal chromosome in most of the AS subjects, as they are included in both Class I and Class II deletions (27, 73). GABAergic dysfunction is known to add to the cognitive and behavioral impairments observed in AS subjects as well as contribute to impairments in electrophysiological phenotypes such as a disturbed EEG pattern and increased epileptic seizures (107). Based on the link of these genes to AS pathology there is enough motivation to investigate on the function that they have individually. As a lot of effort is required to evaluate gene function in mice, we chose to focus on only one of the genes in the GABAergic cluster, namely the *Gabra5* gene. The expression pattern of the protein product of the *Gabra5* gene, the α5 subunit, in the central nervous system (CNS) lead us to choose this gene as it exhibits remarkably high expression in the hippocampus attributing to 25% of GABAA receptors, in addition it is highly expressed in the hypothalamus, amygdala and cortex but at lower levels (108).

1.3.2 $GABA_A$ receptor function and *Gabra5* gene function

The GABAA receptor is a ligand-gated chloride ion channel that, when bound to GABA or an agonist such as benzodiazepines, lead to hyperpolarization of the cell, thus it is an inhibitory neurotransmitter receptor in the CNS (109). The functionality of the $GABA_A$ receptor ($GABA_AR$), such as pharmacological sensitivity, subcellular location, and channel properties, varies with the subunit assembly. The $GABA_AR$ is generally composed by two α (α1–6), two β (β1–3), and one γ (γ1–3) or δ subunit (108). The α5 subunit exhibit both synaptic and extra synaptic clustering via gephyrin and radixin, respectively thus the α5 subunit is involved in both in the slow tonic and fast phasic inhibition (110, 111).

1.3.3 *Gabra5* mouse models

As aforementioned, the generation of suitable animal models to study gene function is of utmost importance. The laboratory mouse is the most used one due to its genetic similarity to humans and its relatively easy manipulation (69). There are four mouse models for *Gabra5* gene evaluation produced and described, namely;

- A mouse model with loxP sites flanking exons 4-5, when bred to mice with tissue-specific Cre recombinase, the offspring will have tissue-specific deletion of the exons 4-5, resulting in a non-functional protein, named the α5fl model (112).
- A Gabra5 mouse model targeted at exon 3, a critical exon resulting in a non-functional protein, herein referred to as the $Gabra5^1$ model (113).
- A mouse with a point mutation of the H105 residue, a key residue for forming the benzodiazepine-binding site, resulting in a pharmacologically inactive subunit. The mouse model is referred to as the α5H105R in most literature. Furthermore, these mice exhibit a 25% decrease of the a5 subunit in the hippocampus, compared to WT mice (114).
- Additionally, our mouse model which harbors a 903 bp deletion including the whole exon 3 and parts of introns 2 and 3 with a predicted protein truncation from 463 amino acids to 47 amino acids. Syding et al. 2022 (submitted October 2022).

1.3.4 *Gabra5* and cognition

As the α5 subunit is expressed to such a high extent in the hippocampus, there is little surprise most researchers have focused on elucidating cognitive phenotypes (108). The two mouse models most extensively used to study the effect of *Gabra5* in learning and memory-dependent tasks are the α5H105R and the Gabra5^{1} models. Both models have normal lifespans, breed normally and do not exhibit any overt compensation in expression of other subunits (115). Both models have shown improved performance in hippocampal dependent trace fear conditioning paradigm but not in cued fear conditioning protocols (116, 117). The synaptic plasticity of brain slices from Gabra5^{1} mice and α5H105R mice was studied by applying high-frequency stimulation, however no changes in LTP was detected, despite the enhanced memory behaviors seen in the mice (113, 116). Pharmacological blocking of α5 subunits in WT mice, did however lead to increased LTP (118). The conflicting results may suggest that the a5 subunit can play a larger role in pharmacological enhancement of LTP but its role in the baseline plasticity may be smaller. Application of pharmacological α5 inverse agonist L-655,708 to WT mice also resulted in enhanced performance in hippocampal-dependent memory tasks (119).

While memory and learning has shown to improve with α5 pharmacological blockage and genetic ablation, the long-term effects of reduced α5 levels are connected to pathologies. Reduced α5 function has been linked to patients with neurodevelopmental disorders such as intellectual disabilities, epilepsy and ASDs (1, 120). Similar disorders have been seen in the Gabra5$^{-/-}$ mouse model too where they have shown that the Gabra5^{1} mice exhibit ASD, schizophrenia, anxiety, and distorted sleep/wake patterns (121, 122). Studies on the α5H105R mice identified behavioral changes such as hyperactivity (123). Furthermore, a mouse model mimicking Fragile X disorder (Fmr1$^{-/-}$) reported decreased α5 levels and impaired tonic inhibition (124).

1.3.5 *Gabra5* and stress response

Psychological and physical stress results from mental strain and from threatening conditions to the homeostasis, respectively (125, 126). The hypothalamic-pituitary-adrenal axis (HPA-axis) is the regulatory system that manages stress response. It starts with stimulation of hypophysiotropic neurons located in the paraventricular nucleus (PVN) receiving input from the limbic system and

culminating in the release of glucocorticoids through an oligocascade (127). Receptors binding to glucocorticoids are expressed ubiquitously throughout the organism and the physiological effect upon binding differs depending on the cell type and location (128). An increase of glucocorticoids in mammals, named cortisol in humans and corticosterone in rodents, have been linked to behavioral dysregulation such as increased anxiety and depression (129, 130). The regulation behind the HPA-axis function has been extensively studied but there are still knowledge gaps regarding the contribution of the GABAergic systems contribution to glucocorticoid secretion. The PVN is under substantial GABAergic control, mainly from hypothalamic GABAergic interneurons expressing, however the hippocampus, amygdala and prefrontal cortex which are limbic structures, also contribute (131, 132). The physiological role of GABA upon the HPA-axis was shown in one experiment where a GABA agonist was injected in to the hypothalamus and the following measurements shown a decrease of corticosterone secretion (133). As for the role of GABA regarding corticosterone response is known but there are significant gaps in knowledge in terms of the role of $GABA_AR$ subunits at play. Based on the behavioral phenotypes associated with *GABRA5* such as ASDs and anxiety, this subunit poses as an interesting subunit to conduct research on in terms of the stress response.

1.4 Aims of the project

Angelman syndrome is a rare neurodevelopmental disease characterized by severe mental retardation, gait ataxia, speech impairments and seizures. It stems from an imprinted locus consisting of paternal and imprinted genes as well as bi-allelically expressed ones. Several mouse models have been generated however, none spanning the entire gene including the non-protein coding elements within the gene. There is a demand for models closer mimicking the genetics of patients and further studies should be conducted regarding regulatory elements within the gene. Furthermore, studies on how the GABAergic cluster genes within the AS/PWS locus contribute to disease phenotype could shed additional light upon disease genetics.

The aims of the doctoral study were the following:

1. *Evaluation of the expression landscape of AS/PWS locus genes upon deletion of Ube3a*

2. *Expand the knowledge of 2 genes participating on the pathology of AS and prepare a model for development of therapeutic approaches*

   2i) Generate and characterize a model spanning the entire Ube3a gene from 5'UTR to 3'UTR

   2ii) Generate and characterize a model targeting the Gabra5 gene

2. Methods and materials

2.1 Animal husbandry and phenotyping by the Czech Center for Phenogenomics

To obtain set aims of the study involving animals we generated two mouse models deficient for *Ube3a* and *Gabra5*, detailed description of the generation can be found in supplementary manuscript 1 and 2, respectively. We had the advantage of working closely with the Czech Center for Phenogenomics (CCP) and could utilize their transgenic unit for model generation and highly optimized and precise phenotyping pipeline to catch phenotypes ranging from a wide range (figure 2.1). For the behavioral testing in supplementary manuscript 1 and 2, we had significant help from the neurobiology and behavior department head Dr. Agnieszka Kubik-Zahorodna, PhD and her team. The mice were bred and cared for by the technicians in the animal facility, part of the CCP services. All experiments utilized in this study were ethically reviewed and performed in accordance with European directive 2010/63/EU and were approved by the Czech Central Commission for Animal Welfare. All mouse models were kept on a C57Bl/6N background at 21 ± 2 C at 12 h light, 12 h dark Central European summer time. All experiments were performed during the light phase of the day.

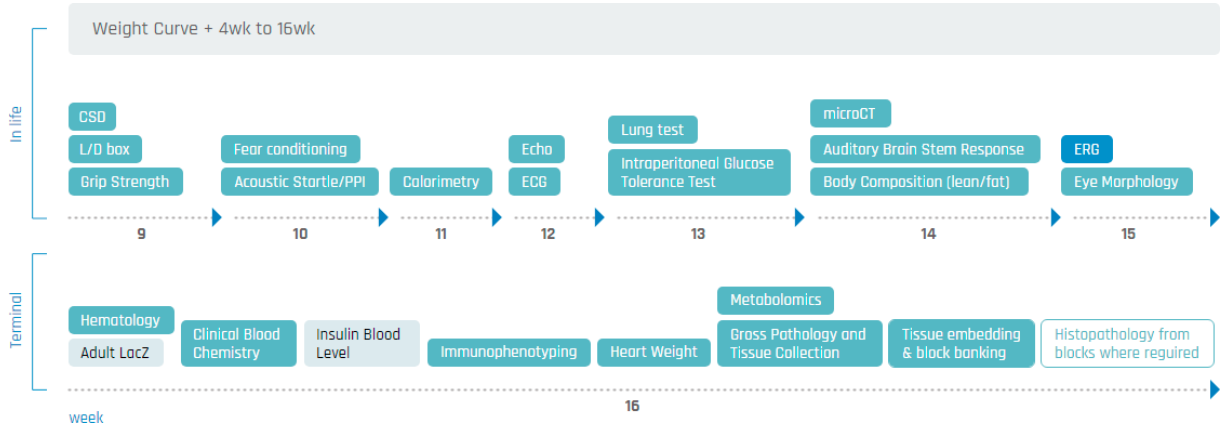

Figure 2.1. Phenotyping pipeline in the Czech Center for Phenogenomics. Tests starting from animal age of 9 weeks to 16 weeks. Source: Czech Center for Phenogenomics

2.2 Echocardiography

Echocardiography is used to assess cardiovascular structure and function. The mouse heart and heart rates are visualized by using the Vevo 2100 Imaging System (VisualSonics, Inc.) with a 30 MHz transducer (MS400) operating at a frequency that provides highly reliable and reproducible image quality. Echocardiography is performed on isoflourane-anaesthetized mice and the anesthesia is controlled to maintain a heart rate of 450-500 beats/min. The primary echocardiographic screen includes two-dimensional (2D) brightness mode imaging view of left

ventricle along the parasternal long axis and motion image of the heart in short-axis view for accurate linear measurements of left ventricular internal dimensions (134, 135).

2.3 Cell culture

The P19 teratocarcinoma cell line (CRL-1825, ATCC) was cultivated in MEM media (ThermoFisher, 22571038) constituted with 10% fetal bovine serum (A3840001, ThermoFisher), 2mM L-Glutamine (G5792, Sigma-Aldrich) and 1% standard cell culture antibiotics (15240096, Gibco). The cells were passaged every 2-3 days with 0.25% trypsin in PBS.

2.4 Neuronal differentiation of P19 cells

Differentiation of pluripotent P19 teratocarcinoma cells in to neuronal-like cells was done with a slightly adapted protocol from Nakayama et al. (2014) (136). Briefly, the dishes were coated with 2.5 ug laminin (L2020, Sigma-Aldrich) for 4 h and washed three times with PBS. P19 cells were seeded at a density of 3x10^4/cm^2 in medium 1 (table 2.1). The cells were cultivated for four days and had a media change once. After four days, the media was changed to media 2 and kept for two days for synapse maturation (table 2.1).

Table 2.1. Reagents for neuronal induction of P19 cells

	Reagent	Concentration	Source
1	HAM (DMEM:F12)	1x	Sigma (D8437)
	N2	1x	ThermoFisher (17502-048)
	Retinoic acid	1uM	Sigma (R2625)
	FGF8	10ng/mL	Sigma (SRP4053)
	DAPT	10uM	Sigma (D5942)
	Pen/strep	100X	
	FBS	100X	
2	Neurobasal	1X	ThermoFisher (21203049)
	B-27	50X	ThermoFisher (17504044)
	AraC	8uM	Sigma (C1768)

Details of reagents used for media 1 and 2.

2.5 Isolation and cultivation of primary neurons

Neurons were isolated from E17-19 mice and cultured for later purpose as control for evaluating differentiation success of P19 cells in to neuronal-like cells. Wells for culture were pre-coated with 50ug/ml poly-D-lysine (A-003-E, Sigma-Aldrich) and 2ug/ml laminin (L2020, Sigma-Aldrich) in sterile distilled H2O (dH2O) over night (O.N) at 37C. The next day, the coating solution was discarded, and the wells were washed thrice with sterile dH2O. Embryos were collected at E17-19 and the brains dissected in Hanks Balanced Salt solution (14185052, Life Technologies) with HEPES pH 7.3. Meninges were removed and the brain placed in dissecting media then further processed into cell suspension. The isolated brains were centrifuged at 900 rpm for 30 s and supernatant discarded. 500 ul of cultivation media consisting of neurobasal (21203049, ThermoFisher), B-27 (17504044, ThermoFisher) and 2uM L-Glutamine (G7513, Sigma Aldrich) was added to the brains and filtered through 40 uM cell strainer (734-2760, VWR international) and centrifuged at 1000 rpm for 2.5 min. The supernatant was discarded, and 1 ml of cultivation media added. The cells were counted and plated at 5x10^4 per cm^2 for 3-4 days before use.

2.6 Cloning of vectors

Assembly of the AAV-EF1a-Ube3a vector was performed using the backbone pAAV-CMV-GFP (AAV-400, CellBioLabs) plasmid further digested with EcoRI (ER0271, Life Technologies) and HindIII (ER0501, Life Technologies). *Ube3a* cDNA was amplified form cDNA obtained from P19 cells with forward primer 5'-TATCACCCTGATGTCACCGAATG-3' and reverse primer 5'-GCCCACAATGTCCCCAATGAA-3'. *Ube3a* cDNA was inserted into pAAV-CMV-GFP backbone using infusion recombinase (Takara) via EcoRI and HindIII restriction sites. The CMV promoter in pAAV-CMV-Ube3a vector was replaced by an EF1a promoter by double-digestion with MluI (ER0561, Life Technologies) and Bsu15I (ER0141, Life Technologies) and cloning done using infusion recombinase (639648, Takara). EF1a promoter sequence was amplified from the pXR001 plasmid (109049, Addgene) with forward primer 5'-CCTTCTAGGTCTTGAAAGGAGT-3' and reverse primer 5'-TACGTCACGACACCTGAAAT-3'.

Generation of plasmids for CRISPR/Cas9 targeted knock-out of *Ube3a* transcript ENSMUST00000200758.4 and the regulatory feature ENSMUSR00000716208, further called the Ube3a-enhancer, were assembled with the pX458 (48138, Addgene) and pX459 (62988, Addgene) digested with BbsI (ER1012, Life Technologies). *Ube3a* was knocked-out with oligos flanking the *Ube3a* gene 5'UTR 5'-CGCGGGTCCCGCATGAGACC-3' and 3'UTR 5'-CCTTGCGAGAATAGTTTCGT-3'. The Ube3a-enhancer was knocked out with flanking primers 5'- CCTCATGCTTCAGATCCACTACC-3' and 5'-ACTCTTCAAGGGTTTGGCTGTGG-3'. The plasmids were introduced to One Shot chemically competent bacteria (C404003, Carolina BioSystems), plasmid purification was done with the Miniprep kit (12125, Qiagen). Insert was

verified with sequencing using genotyping primers Ube3a-F 5'-CAGTCTCAAGATGGCGACGA-3' and Ube3a-R 5'- GCTACCATTATCCCCTGCCAA-3' and Ube3a-enhancer-F 5'- GCATGGGTTAATTGAGTCTTGGG-3' and Ube3a-enhancer-R 5'-TCAACCAATCATCTGGCCTCCT-3'.

2.7 Lipofectamine transfection and monoclonal expansion

P19 cells plates at 5x10^5 cells per well (9.6cm2) and at a density of 70% the day after were transfected with 4ug plasmid DNA using Lipofectamine 2000 (11668027, Life Technologies) for 48h. Media was changed and 2ug/ml puromycin was added and incubated for 48h. Surviving cells were sorted into single cell suspensions in 96 well plates using the BD FACS ARIA IIu cell sorter. Colonies were screened using junction PCR and western blot for the *Ube3a* KO line.

2.8 Western blotting

Cells were lysed in RIPA buffer (0.05 M Tris-HCl, pH 8, 0.15 M NaCl, 0.5% deoxycholic acid, 1% NP-40, and 0.1% sodium dodecyl sulfate (SDS)), cOmplete™, EDTA-free Protease Inhibitor Cocktail (5056489001, Roche), and PhosSTOP™, phosphatase inhibitor tablets (4906845001, Roche).

Lysates were sonicated and cleared by centrifugation. Protein concentration was determined using the Pierce™ BCA Protein Assay Kit (23225, ThermoScientific). Equal amounts of protein (20 µg) were denatured in reducing sample buffer, separated by SDS-PAGE (polyacrylamide gel electrophoresis) gels, and blotted to nitrocellulose membranes (Bio-Rad). Blots were blocked with 5% milk in PBS-T (0.2%) for 40 min at room temperature, and then incubated overnight at 4 °C with primary antibodies. The primary antibodies used were mouse anti-Ube3a (1:2000, 611416, BD Biosciences) and mouse anti-B-actin (1:5000, A2228, Sigma-Aldrich). After washing with PBS-T (0.2%) membranes were incubated with horse anti-mouse IgG HRP-conjugated (7076, Cell Signaling) diluted in blocking buffer for one hour at room temperature. Blots were washed with PBS-T and detection was performed with SuperSignal™ West Pico PLUS Chemiluminescent Substrate (34579, ThermoScientific).

2.9 RNA isolation, cDNA synthesis and RT-qPCR

RNA was isolated and used as a template for reverse transcription into cDNA with M-MLV Reverse Transcriptase (Promega, USA). RT-qPCR was performed using the TATAA SYBR ® GrandMaster ® Mix (TATAA Biocenter Sweden) in Cycler LightCycler® 480 Instrument II (Roche, Germany).

Primers were designed using the primer blast tool from NCBI. The primer combination with the least self-complementarity was chosen. Primers were optimized using serial dilution of template and efficiency was assessed. Primers used in the study are summarized in table 2.2).

Table 2.2. Primer list for RT-qPCR

Gene	Forward	Reverse	Exon	Transcript
Ube3a	TGGGAGACTCTCACCCAGTT	TCATCTTCCACACTCCCTTCA	8-9	ENSMUSG00000025326.12
Ube3a-ATS	GAAGAGTCTGGGAGAACAGTAAA	AACTGGGAGACATGAGGTTAGA	Ube3a intron 1	ENSMUSG00000025326.12
Snord115	GACAACCCACTGTCATGAAGAAA	CAGCGTAATCCTATTGAGCATGA	115-"1"	AF357427.1
Snord116	TCCTTGGAAAAGCTGAACAAAATGA	GACCTCAGTTCCGATGAGAG	116-"1"	XR_004934666.1
Snrpn	TGTGATTGTGATGAGTTCAGGAAGA	ACCAGACCCAAAACCCGTTT	5-6	NM_013670.4
Snurf	GGTCGAGGTCCAGGTCAAAC	CGTCGTGGGTACAAGTGACA	2-3	NM_013670.4
Ndn	CATCGGTCCTGCTCTGATCC	TTAGGGTCGCTCAGGTCCTT	5utr-1	NM_010882.3
Magel2	ATCCAGTCTCAAGTCATAAGGGC	CTGCCATGTCAAAGGCGTT	1	NM_013779.2
Mkrn3	ACAGGTGTGCATACCCCCA	GCAGGCCCTTCTATGAGCTTC	1	NM_011746.3
Map2	CCTCTAGCAGCCGAAGAAACA	GCCTGAGCCAAGTCACCACT	3-4	ENSMUST00000077355.12
Oct4	CAGCAGATCACTCACATCGC	GGGGCAGAGGAAAGGATACAG	4-5	ENSMUST00000025271.17

Primer sequences used in the study and exon location and transcript

2.10 Restraint stress test and corticosterone ELISA measurement

Fecal corticosterone metabolites (FCM) concentration was assessed by processing fecal samples as it offers a non-invasive method and is less stressful for the animal (137). Feces were collected on day 1 at 12 pm and day 2 at 16 pm to serve as samples for baseline measurements. On day 4 at 8 am mice were incapacitated in transparent tubes for 30 minutes, herein called the restraint stress. Feces were then collected after 4 and 8 h. The fecal samples were dried at 60C O.N. and weighed. For every 50 mg of feces, 1 ml of 80% methanol was added. It was further seal homogenized using beads in Tissue Lyzer II (Qiagen, Germany). The lysates were incubated at 20 C, at 1000 rpm O.N. The lysates were cleared by centrifugation for 10 min at 4 C at 2500 rpm. The supernatants were transferred to new tubes and stored at -20C until use. The FCM values were assessed using mouse/rat corticosterone ELISA kit (RTC002R, BioVendor) according to manufacturer's protocol

with use of Epoch™ Microplate Spectrophotometer (BioTek, USA). The values were computed with Ri386 version 4.1.2 using the drc package.

2.11 Statistical analyses

Statistical analyses were performed using GraphPad Prism software version 7.0 (GraphPad, USA). Statistics on data from RT-qPCR were computed with ordinary one-way ANOVA and data from echocardiography and FCM readings were processed with two-way ANOVAs. For post hoc analysis, Sidaks multiple comparisons test was used.

3. Results

3.1 Generation of Ube3a KO and Ube3a-enhancer KO cell lines

The *Ube3a* gene and the putative Ube3a-enhancer were separately knocked-out in the P19 cell line using the CRISPR/Cas9 system. Sequencing data revealed that the Ube3a KO cell line resulted in a deletion of 76 220 bp encompassing all coding exons of the gene and all introns. Western blot analysis of cell lysates confirmed that the protein is abolished in the Ube3a KO cell line (figure 2.2A).

The Ube3a-enhancer is an element annotated to 399 bp within intron 4-5 in the *Ube3a* gene, regarding isoform 2. Junction PCR (figure 2.2B) and sequencing confirmed a deletion of 450 bp spanning the entire Ube3a-enhancer, ranging from -10 to +445 in regard to the start of the Ube3a-enhancer.

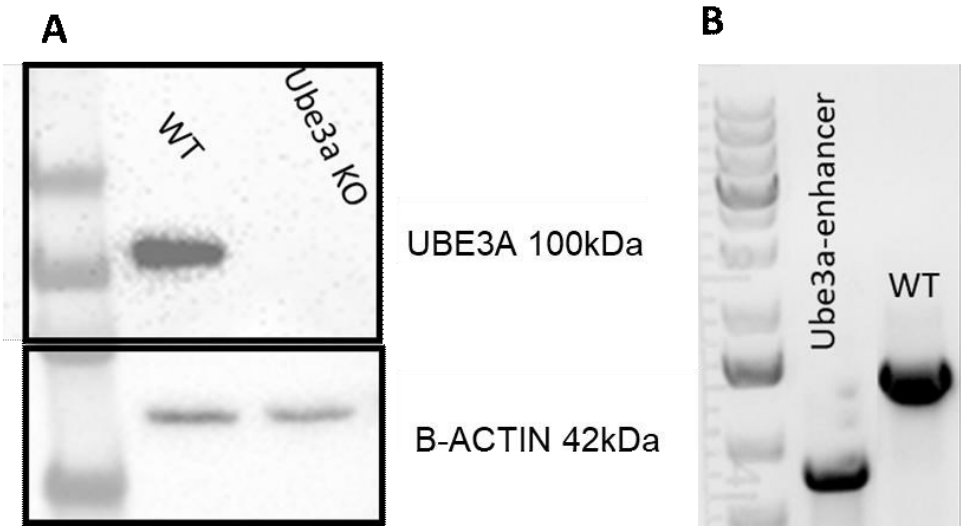

Figure 2.2. Knock-out cell line generation. **A** UBE3A was detected at 100kDa in the WT lysates but absent in the KO lysate, the loading control B-ACTIN is present in both samples. **B** Junction PCR of Ube3a-enhancer and WT DNA. The WT sample shows a band of 1397 bp and the Ube3a-enhancer KO exhibits a band of 947 bp.

3.2 UBE3A overexpression

A plasmid vector was produced to overexpress UBE3A for rescue experiments in the Ube3a KO cell line. Successful insertion of the *Ube3a* cDNA in to the AAV-EF1a backbone was verified by restriction digestion using the BglI enzyme resulting in fragments of 3569, 1625, 1053, 898, 176 and 117 bp (figure 2.3A). Subsequent western blot of transfected P19 cells showed an overexpression of UBE3A in all transfected lysates (figure 2.3B).

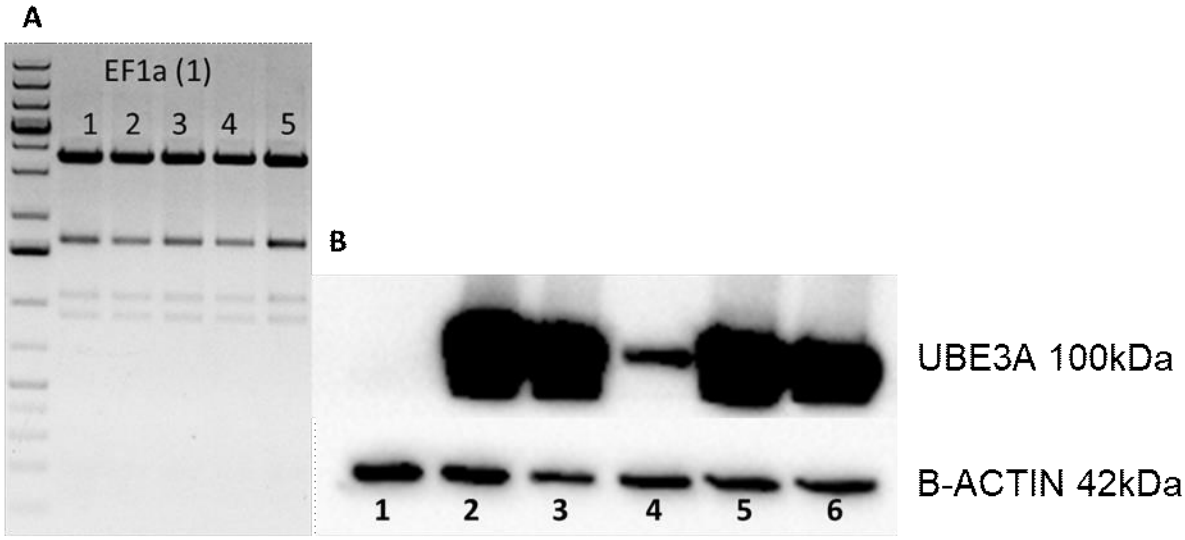

Figure 2.3. Overexpression of UBE3A. **A** Restriction analysis shows four corresponding bands, the two lower bands are not visible. **B** Western blot of UBE3A shows overexpression in transfected lysates, no expression in Ube3a KO

line and moderate expression in WT line. All lysates exhibit the B-ACTIN loading control. **1**: Ube3a KO, **2 & 3**: Ube3a KO + AAV-EF1a-Ube3a, **4**: WT, **5 & 6**: WT + AAV-EF1a-Ube3a

3.3 Paternally expressed genes belonging to the AS/PWS locus are downregulated in KO cell lines

The expression of genes within the AS/PWS locus was evaluated with RT-qPCR. Both P19 in its pluripotent state and P19 induced to neuronal-like cells exhibited a downregulation of PEGs, however more pronounced in pluripotent P19 cells (figure 2.4A-B). The successful differentiation of induced neuronal-like cells was confirmed by evaluating gained expression of the neuronal specific marker Microtubule Associated Protein 2 (Map2) and loss of pluripotent marker Oct-4 (figure 2.4B).

3.4 UBE3A overexpression does not rescue WT expression of PEGs

P19 WT and Ube3a KO cells in their pluripotent state were transfected with AAV-EF1a-Ube3a to rescue the decreased expression of PEGs. RT-qPCR of cell lysates from WT and Ube3a KO with mock and AAV-EF1a-Ube3a transfection revealed that the expression of *Ube3a* was approximately 20-fold upregulated in the Ube3a-KO transfected cells and about 50-fold upregulated in transfected WT cells, normalized to P19 WT cells with mock transfection (figure 2.5). The Ube3a-ATS and Snord116 transcripts were significantly upregulated in P19 WT AAV-EF1a-Ube3a cells ($p < 0.05$; figure 2.5). The UBE3A overexpression did not rescue the expression of any PEGs to WT levels which points toward the action of a regulatory element within the Ube3a causing the downregulation of PEGs.

3.5 Ube3a-Enhancer KO cells mostly recapitulate the reduced expression of PEGs

As the overexpression of UBE3A did not rescue the expression of PEGs we proceeded with analysis of Ube3a-enhancer KO cells to assess whether the reduced expression would be recapitulated. Interestingly, we found that all genes exhibited reduced expression of PEGs except for Snord115 where the expression was increased (figure 2.6). With these results, we conclude that the annotated enhancer within the Ube3a intron 4-5 is likely involved in regulating the expression of genes in the AS/PWS locus.

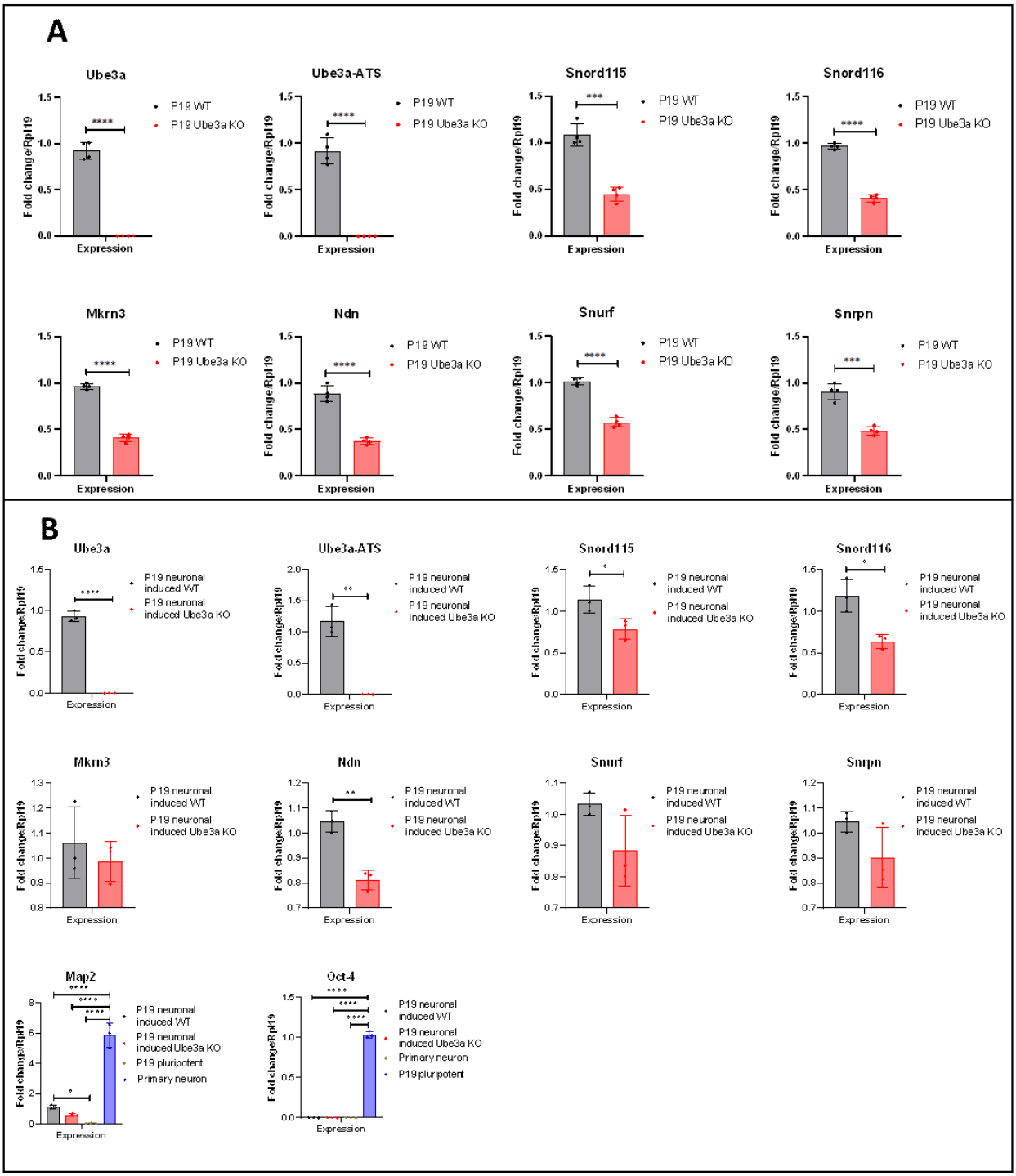

Figure 2.4. Expression of genes in the AS/PWS locus. A RT-qPCR of P19 WT and P19 Ube3a KO cells. **B** RT-qPCR of P19 WT neuronally induced cells and P19 Ube3a KO neuronally induced cells. Unpaired t-tests were used for comparisons of two parameters and Ordinary one-way ANOVA for comparisons of multiple parameters. All figures are depicted with mean ± SD. Significant differences are indicated as *p < 0.05, **p < 0.01, ***p <0.001 and ****p <0.0001

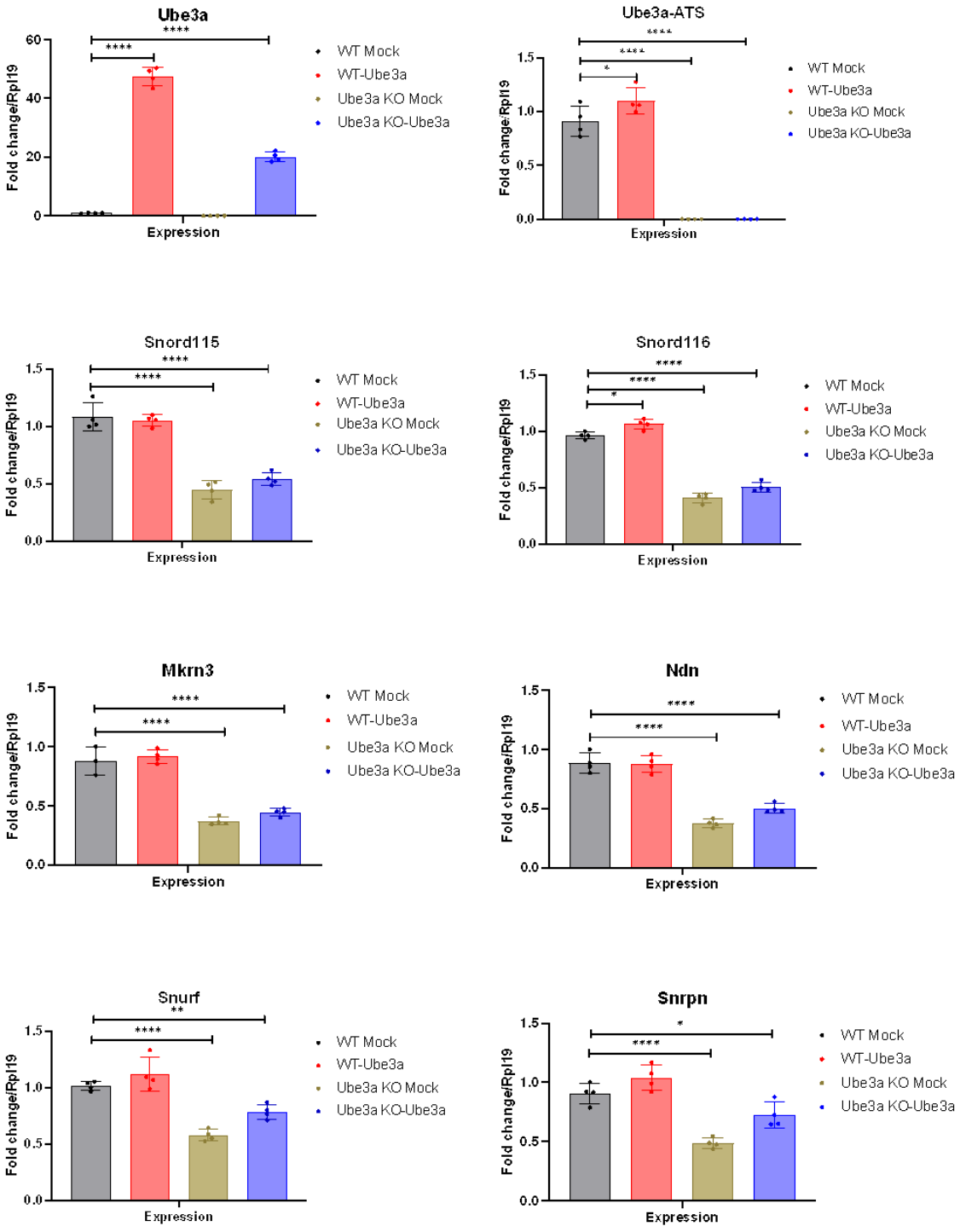

Figure 2.5. Expression of genes in the AS/PWS locus with UBE3A overexpression. RT-qPCR analysis of WT and Ube3a KO P19 cells with mock and AAV-EF1a-Ube3a transfection showed no rescue of downregulated PEGs. Ube3a-ATS and Snord116 transcripts were upregulated in P19 WT AAV-EF1a-Ube3a lysates. Ordinary one-way ANOVA was used for all analyses. All figures are depicted with mean ± SD. Significant differences are indicated as *p < 0.05, **p < 0.01, ***p <0.001 and ****p <0.0001as compared with the control column WT Mock.

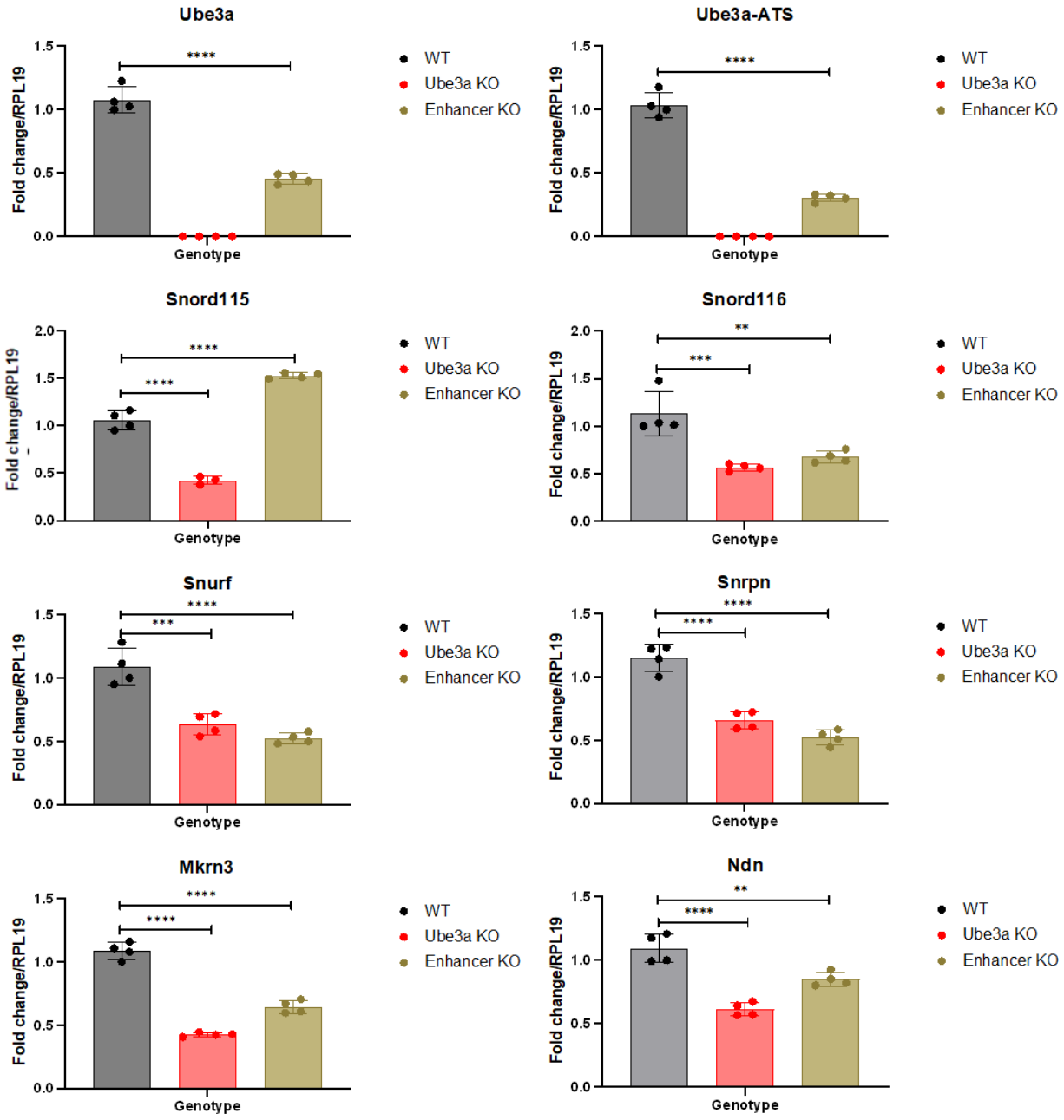

Figure 2.6. Expression of genes in the AS/PWS locus in Ube3a-enhancer KO cells. RT-qPCR analysis of the gene expression landscape P19 WT, Ube3a KO and Ube3a-enhancer KO cells. Ordinary one-way ANOVA was used for all analyses. All figures are depicted with mean ± SD. Significant differences are indicated as *p < 0.05, **p < 0.01, ***p <0.001 and ****p <0.0001 as compared with the control column WT.

3.6 Echocardiography reveals differences between WT and novel AS strain

We generated a novel mouse model for AS research where the entire *Ube3a* gene was deleted from 5'UTR to 3'UTR encompassing all coding and non-coding elements, detailed model production can be found in supplementary manuscript 1. The model went through the phenotyping pipeline to evaluate putative phenotypes ranging from a wide variety of parameters. We found behavioral changes and weight being increased (supplementary manuscript 1). We published a detailed description on the behavior, cognition, and circadian rhythmicity in the manuscript. From what we found but did not publish is the significant changes in echocardiography between the WT and AS mice. In AS animals the aortic diameter was found to be smaller (genotype effect $p<0.05$; genotype/sex interaction $p>0.05$; figure 2.7A), the cardiac output decreased (genotype effect $p<0.001$; genotype/sex interaction $p>0.05$; figure 2.7B), the heart rate also decreased (genotype effect $p<0.0001$; genotype/sex interaction $p>0.05$; figure 2.7C) and left ventricle anterior wall (LVAW) increased in thickness (genotype effect $p<0.05$; genotype/sex interaction $p>0.05$; figure 2.7D). The systolic LVAW and the right ventricle anterior wall (DVAW) were not significantly different between the genotypes (genotype effect $p>0.05$; data not shown). Stroke volume, an important parameter for calculating blood flow was not different from WT animals (genotype effect $p>0.05$; data not shown).

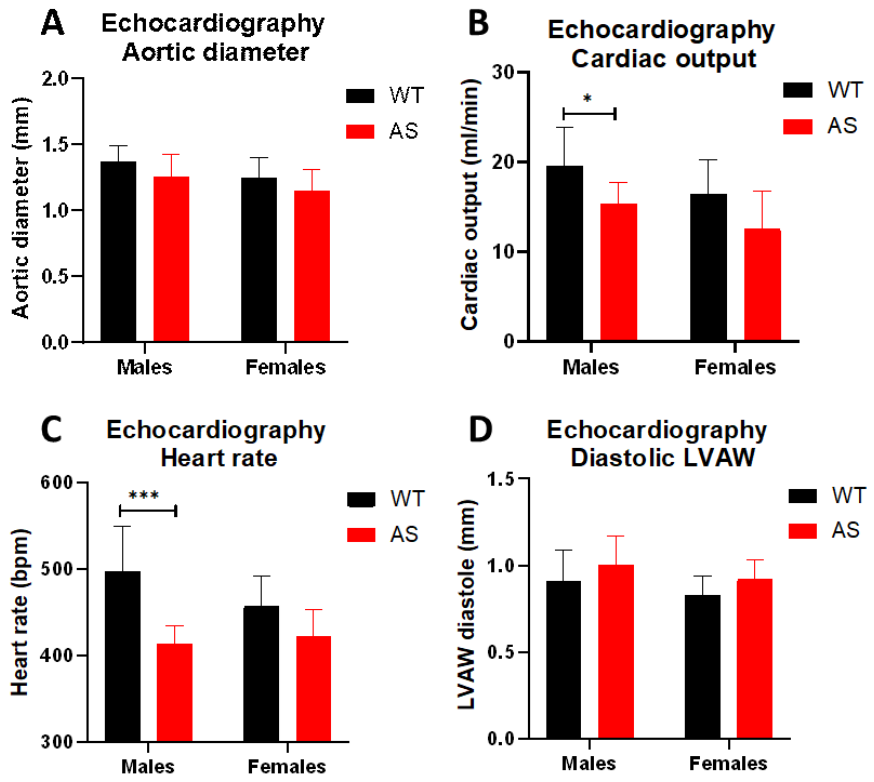

Figure 2.7. Echocardiography of WT and AS animals. **A** Aortic diameter is decreased in AS animals. **B** Cardiac output is lower in AS animals. **C** Heart rate is lower in AS animals. **D** The diastolic left ventricle anterior wall (LVAW) is thicker in AS animals. Two-way ANOVA with Sidak's multiple comparisons test Sidak's multiple comparisons test. All figures are depicted with mean ± SD. Significant differences are indicated as *p < 0.05, **p < 0.01 and ***p <0.001.

3.7 Fecal corticosterone metabolites are decreased in Gabra5$^{-/-}$ mice

We generated a mouse model deficient for *Gabra5* by deleting the crucial exon 3 leading to loss of function of the protein product; detailed description of model generation is supplied in manuscript 2). In the manuscript, we have evaluated corticosterone, anxiety-like behavior and electrophysiology. We did additional test evaluating how Gabra5$^{-/-}$ mice versus WT mice respond to stress, which we did not publish. Briefly, we subjected animals to restraint stress and collected feces after 4 and 8 h and measured the FCM levels with ELISA. We found that both treatment and genotype were significant factors after both 4 and 8 h ($p<0.05$; treatment/genotype interaction $p>0.05$; figure 2.8A-B). However, the stress treatment was more pronounced in WT females compared to Gabra5$^{-/-}$ females after 8 h (figure 2.8B). Gabra5$^{-/-}$ males exhibited significantly less FCM than WT males after 4 h (genotype effect $p<0.0001$; figure 2.8C) and after 8 h as well however the differences in FCM were less pronounced (genotype effect $p<0.05$; figure 2.8D). The

effect of stress treatment in FCM levels was significant at both times (treatment effect $p<0.001$; figure 2.8C-D) however, more pronounced after 8 h in the Gabra5$^{-/-}$ mice (figure 2.8D).

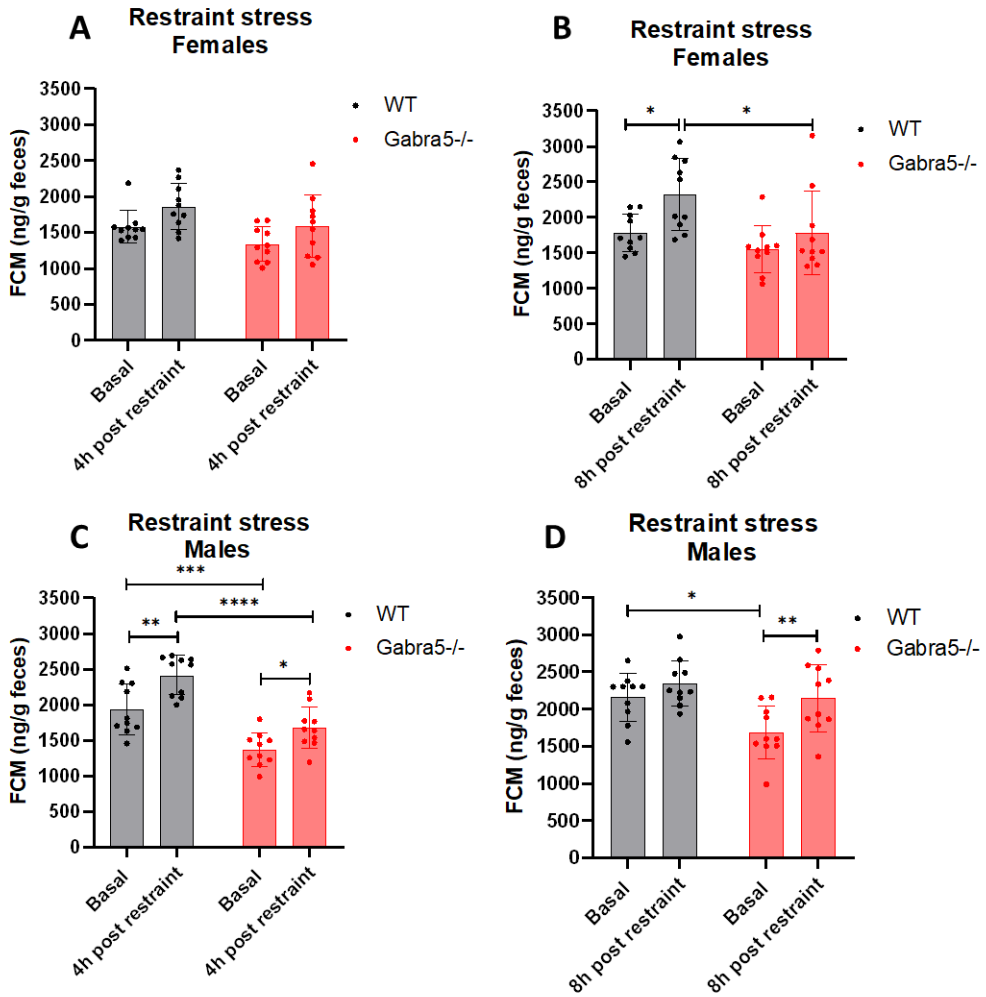

Figure 2.8. Fecal corticosterone metabolite assessment following restraint stress. AB measurements from females after 4 and 8 h following restraint. **CD** measurements from males after 4 and 8 h following restraint. Two-way ANOVA with Sidak's multiple comparisons test. All figures are depicted with mean ± SD. Significant differences are indicated as *p < 0.05, **p < 0.01, ***p <0.001 and ****p <0.0001.

3. Discussion

4.1 Recapitulation of project aims

The aim of the doctoral study was to generate and characterize two mouse models relevant for AS but also to study the expression profile of genes belonging to the AS/PWS locus. We generated a new *Ube3a* deficient line with the entire gene deleted, coding and non-coding elements included and a line with a loss of function of the protein product the *Gabra5* gene.

3.2 Aim 1) *Evaluation of the expression landscape of AS/PWS locus genes upon deletion of Ube3a*

We set out to evaluate the expression of genes belonging to the AS/PWS locus upon deletion of the *Ube3a* gene. The region is a highly regulated locus due to its parent-of-origin specific expression of a multitude of genes (24). As described, the mode of imprint in this region is either due to hypermethylation of promoters or due to the act of the Ube3a-ATS transcript, leading to gene suppression on the maternally and paternally inherited allele, respectively (8). As the *UBE3A* gene is completely absent, including non-coding regions, in most patients we were interested to find out whether the deletion of the gene from 5'UTR to 3'UTR could possibly have effect on the integrity of expression of other genes located in its vicinity. Furthermore, a putative enhancer within the intronic region of the *Ube3a* has been annotated, however, its existence has not been proven experimentally but frequent binding of histone acetyltransferases to the region has been reported (138). Acetylation of histones leads to a disperse configuration of the chromatin and thus allows for transcription factors to bind, leading to gene activation (139). Furthermore, deletion of a larger gene may lead to destabilization of the genetic landscape which, could affect the genes in the region.

We employed CRISPR/Cas9 targeting to delete the *Ube3a* gene from 5'UTR to the 3'UTR encompassing all coding and non-coding regions of the gene, including the annotated enhancer. Analysis of genes belonging to the region (Figure 1.1) using RT-qPCR showed a decrease of PEGs in both pluripotent P19 cells, where the *Ube3a* is not imprinted, and in neuronally induced P19 cells. We proceeded with overexpressing the UBE3A protein to see if the PEGs expression would be rescued. We found that the protein did not restore expression in PEGs, making it unlikely that it would be the HECT region of UBE3A responsible for the skewed expression either directly or

indirectly by other substrate. However, we did not perform an ubitiquination assay of the protein thus we cannot say with certainty that the HECT domain of the protein was functional although we had a 50-fold upregulation. However, many of the PEGs do not code for a protein product thus they are not targeted for proteosomal decay via this pathway. Finally, we knocked out the putative enhancer located in intron 4-5 regarding isoform 2. Again we found a decreased expression of PEGs except for the *Snord115* transcript, a C/D box small nucleolar RNA expressed from the Ube3a-ATS (53). Not only was the *Snord115* expression not decreased but it was significantly increased in the enhancer KO cell line. More studies are needed to further explain the results we obtained. However, as far as our knowledge goes, there has been no other studies focusing on the expression levels of PEGs upon *Ube3a* deletion, making these observations novel. Furthermore, these results were all seen in cell lines and with homozygous deletion. The CCP has generated a mouse model using the same gRNAs to further test if this is a phenomenon seen on organism level as well. Proving a dysregulation of PEGs due to an enhancer within *Ube3a* would have high novelty and could shed light on the behavioral deficits of AS. Many of the PEGs are genes associated with hormone regulation and behavior, two phenotypes cardinal of PWS where PEG expression is absent (140).

4.3 Aim 2i) *Generate and characterize a model deleting the entire Ube3a from 5'UTR to 3'UTR*

We generated a model using the CRISPR/Cas9 system to generate a mouse model harboring a deletion of the entire *Ube3a* gene ranging from 5'UTR to 3'UTR with all coding and non-coding elements. The *Ube3a* gene is paternally imprinted in neurons but bi-allelically expressed in other cell types (21). In our AS mice, heterozygotes with a maternal deletion, this was clearly seen in western blot lysates from CNS tissue and the non-imprinted liver tissue where we observed ~5-10% and ~50% of UBE3A, respectively. The small amount of UBE3A detected in the CNS tissue lysates is attributed from the paternal expression in glial and endothelial cells. As aforementioned, there are plentiful mouse models mimicking AS ranging from constitutive, conditional and tagged models (83). There are even models harboring larger deletions, encompassing genes *Ube3a-Gabrb3* but no model with solely *Ube3a* deleted in its entirety (84). Other models with loss-of-function mutations of UBE3A recapitulate many AS phenotypes but they would still contain putative regulatory elements within the non-coding parts (103). Thus, the model that we produced could bring additional knowledge.

To properly evaluate phenotypes most associated with AS we subjected the mice to a battery of tests particularly aimed to detect AS pathology, thus expanding the phenotypic evaluation from the standard CCP pipeline. We adopted the suggested behavioral and motor test battery put forth by the Elgersma lab, with some modification (103).

Ataxia and impaired motor skills are hallmark features of AS (137). We analyzed motor skills using the rotarod test where the AS mice significantly underperformed. AS mice exhibited significantly shorter latencies to fall, indicating impaired motor skills (100). We did a linear regression analysis to exclude possible weight/latency correlation as the increased weight of AS animals could be a confounding factor. We did however not find such correlation thus the underperformance should be due to affected motor skills and not weight.

To further evaluate any putative ataxic phenotype, we employed detailed gait analysis with the DigiGait system that records the placement and frequency of the movement of the four limbs. This defined the animals' posture and kinematics which is extrapolated to evaluate the animals coordination and balance but also its strength (141). We evaluated the duration of swing, stance, propel and stride parameters, which are commonly used gait characteristics for extrapolation of gait (141). We found an increase in these four parameters. The increase of the duration of propel indicates reduced strength in the movement and of control (142). In addition, we analyzed recorded data on the deceleration and the paw area at peak stance, both of which were increased. The increase in deceleration indicates a reduction in muscle strength (143). The increase in the area of paw stance can help to stabilize posture and balance of the animals (141). The results obtained from both rotarod and DigiGait tests indicates that the novel AS model do recapitulate ataxia and motor skills impairment.

Profound behavioral impairment is characterizing for AS patients, anxiety and ASD both commonplace (70). When evaluating anxiety-like behavior in open field tests we did not observe any indication of such. The time spent in the center and number of entries to the center remained comparable to WT animals. Neither did we observe any difference in anxiety in the elevated plus maze recordings, again indicating an absence of anxiety. It appears AS mice, our and other generated models generally do not recapitulate this feature, at least not with the sample size we used. In an interesting paper by Sonzogni et al. (2018) the authors performed a power study showing that a sample size of 17 is needed to detect anxiety in open field test, we had a sample size

of the recommended 12, making the phenotype and test relatively weak for AS animals (103). The open field test did however reveal hypoactivity in the AS animals, a commonly reported phenotype in other AS models generated (70). Hypoactivity is however not seen in AS individuals, rather children with the disease often display hyperactivity (144). The reason for the hypoactivity in AS animals could possibly be explained by the increased weight in AS animals, also something not frequently seen in patients. Nest building is another test often employed to assess behavioral impairments in AS mice (103). Our AS model exhibited significantly decreased nest building activity, especially female mice, extrapolated as an indicator of distress, decreased nest building is also often reported in mice with neurodegenerative diseases (145). Lastly, we subjected the animals to the tail suspension test, which can be interchanged with the forced swim test, both often used in assessing AS animals and to evaluate the success of antidepressants (103, 146). The AS mice from our study spent more time immobile than WT controls, which is in line with other generated AS models (89).

Severe cognitive malfunction is a cardinal feature in patients but not recapitulated in AS animals, cognitive deficits are either mild of absent (70). We utilized Barnes maze to test spatial learning, a hippocampal-dependent task, where we did not observe any cognitive malfunctions. We used the novel object recognition test to possibly reveal any differences in short term memory yet again, there were no significant differences between the genotypes. We used animals that were in the age between 9-13w for these tests, which according to a study by Huang et al. (2013) could be a reason for the lack of phenotype (106). They used the B6 strain in the study, similarly to us, and they showed that cognitive deficits in Barnes maze was apparent at age 16 weeks but not at 8 weeks. Another possibility might be that these tests are not complicated enough to reveal milder impairments. Hence, we utilized the sophisticated IntelliCage system with the place preference and reversal place preference learning paradigms. In these tests, the mice have to unlearn and relearn, which is a more complicated task (104). We did indeed find impairments in the AS animals in the reversal learning phase but not in the initial place preference test, suggesting that impairments do appear in more complicated tests. Furthermore, deficits in the reversal learning have been reported in rodent models of autism but in Morris water maze and T-maze (147-149).

We further utilized the IntelliCage system to measure the circadian activity and response to novelty. In the novelty response, we observed increased latency to corner visits, indicating a decreased

exploratory drive. This is however different from anxiety behavior as we further on observed the animal activity to be lower during the light phase of the day (150). Although we saw differences in circadian activity, we still need to take the general hypoactivity in to account when extrapolating behavior from the results. The total number of visits were not decreased when including visits with licks for water dispersal but when excluding visits with licks, meaning just the non-motivated visits, there was indeed a significant decrease. Furthermore, we observed increased frequency in water licks in the AS animals, measured by the number of licks per corner visits. This could be explained by the larger size of the animals or it could be possible that the mice harbor an increased affinity to water, as do AS patients, however, we cannot claim that with certainty (151).

Additionally, apart from the battery of behavioral and motor tests our AS mice were subjected to phenotyping in the CCP facility where the animals were evaluated for a large variety of phenotypes using their standardized pipeline. The CCP phenotyping pipeline caught heart defects in AS mice such as anatomical aberrations manifesting in smaller aortic diameter and thicker diastolic left ventricle anterior walls and physiological manifestation such as lower cardiac output and a slower heart rate. Lower cardiac output is the cause of the low cardiac output syndrome, which leads to fatigue due to less circulating oxygen and buildup of by products at the cellular level (152). The cardiac function is to distribute enough oxygenated blood to meet the organs demand, a failure to do so may lead to detrimental effects (153). The diastolic phase of the cardiac cycle is important for blood distribution, a too rapid heart rate may lead to insufficient relaxation of the left ventricle and thus it fills up with too little blood, anatomical aberrations such as a too thick wall, which we found in our AS mice, can also be a cause of insufficient filling of the ventricle resulting in less circulating blood (154). Physiologically, the cardiac output is depending on the heart rate and stroke volume and as we found the heart rate to be lower but no difference in stroke volume, it is only natural that the cardiac output is lower (152). This could quite possibly explain the hypoactivity seen in AS mice. However, there are no reports to our knowledge where the investigators have observed possible cardiac phenotypes.

We produced a new model mimicking AS that harbors a deletion of the entire gene from 5' UTR to 3'UTR regarding the isoform 2. This model mimics the disease genetics in AS patients more closely than the Ube3a^{tmAlb}1 model that is the by far most use one in AS research (75). To assess the presented phenotypes in our model we subjected it to a battery of tests particularly aimed

towards the AS pathology, as suggested by the Elgersma lab specifically but with modifications (103). We observed robust behavioral impairment, absent cognitive malfunctions in simpler tests such as Barnes maze and novel recognition but impairments in the more complicated reversal place preference learning. Furthermore, we revealed severe gait impairments and motor skills.

The differences in presented phenotypes depending on strain and age of the mice but also on the laboratory where the experiments were conducted presents a clear barrier for testing therapeutic interventions for the disease. Based on the results we obtained from our mouse model we can claim that this model is suitable as a mouse model for AS as it did recapitulate most of the main features of AS. However, at this point it is unclear whether it provides additional advantage to other models, as the phenotypes were very similar. The model would need additional testing on other strain backgrounds and ages to be able to state if this model is more robust in its presented phenotypes or not.

4.4 Aim 2ii) *Generate and characterize a mouse model targeting the Gabra5 gene*

One of the aims of the doctoral study was to generate and characterize a model deficient for *Gabra5*, a gene heterozygously deleted from the maternal chromosome in most AS patients (155). More specifically, we investigated the effect that *Gabra5* functional ablation may have on corticosterone levels and anxiety-like behavior in mice. We initially hypothesized that we would observe an increase in corticosterone as the inhibitory GABAergic neurons would be disinhibited, thus leading to increased excitation. We also hypothesized that anxiety-like behavior in mice would be increased as corticosterone has a documented relationship with increased anxiety (156). Surprisingly, we observed the contrary, decreased FCM and decreased anxiety suggested by decreased rearing behavior.

We generated the model by targeting the exon 3, a critical exon, using the CRISPR/Cas9 technique. Analysis of founders revealed one harboring a deletion of 903 bp encompassing the entire exon and parts of intron 2-3 and intron 3-4. For FCM evaluation, we analyzed feces of mice in both single- and group-housed conditions twice at 24 h apart. We chose to measure FCM from feces and not plasma corticosterone as it is a less invasive method which bypasses potential confounding factors on corticosterone secretion associated with blood sampling (157).

We found differences in males depended on housing. Gabra5$^{-/-}$ males exhibited significantly lower FCM levels in group-housed conditions but not in single-housed ones. The Gabra5 $^{-/-}$ females had significantly lower FCM in single-housed conditions but a trend was observed in group-housed conditions. We proceeded to analyze the effect that housing alone has on the same sex-genotype groups with the obtained data. There we found that housing was only a significant factor in WT males, where the FCM was clearly decreased in single-housed animals.

Group-housed male mice often exhibit aggression towards one another to establish hierarchal roles, which can be very stressful for the animals (158). We followed up on the observation made on FCM levels by analyzing the testosterone levels in the plasma of male mice. Testosterone is linked to aggressiveness and was used to extrapolate aggressiveness in the same type of setup as the FCM experiment (159). We hypothesized that the Gabra5$^{-/-}$ mice might have lower testosterone, hence less aggression rendering them more stable towards housing-conditions. We did not observe any significant differences in plasma testosterone between the genotypes, but we did find that males that were group-housed had an increase of testosterone at the second handling time. The handling likely triggers stress to the animals and a need to re-establish dominance leading to increased testosterone. This was phenomenon not observed in single-housed males, further strengthening the plausible explanation. We could also exclude testosterone levels and associated aggression as a reason for robustness towards housing as there were no differences between genotypes, only housing. Furthermore, we measured the FCM levels in mice that had been subjected to restraint stress. Again, we found lower FCM levels in Gabra5$^{-/-}$ mice but a similar response to stress, not indicative of increased anxiety-like behavior.

We followed up by performing anxiety assessing tests open field and elevated plus maze (160, 161). We initially expected to find increased anxiety-like behavior as mutations and/or deletions of the GABRA5 gene has been linked to increased anxiety in human subjects (120). Furthermore, distribution of allosteric modulators of the α5 subunit in mice have shown effect on exhibited anxiety (162). We did however not see any sign of increased anxiety as there were no significant differences in any parameter of the tests.

Next, we recorded rearing behavior, locomotion, energy expenditure and gas measurements utilizing an indirect calorimetry setup that automatically tracks given parameters. Rearing is the occurrence when quadrupedal animals stands only on its two hind-legs when placed in a new

environment to gather information (163). Rearing is dependent on several brain structures, the hippocampus being one of the more important ones, also where the α5 subunit is highly expressed (163). Anxiety level can thus affect rearing behavior, with more anxiety comes increased rearing behavior (164, 165). Furthermore, it was proven that anxiolytics decreased rearing in subjects placed in stressful situations, clearly indicating that decreased anxiety is linked to decreased rearing(166). We found decreased rearing in our Gabra5$^{-/-}$ animals during the active phases for a duration of three consecutive days in a new environment. Putative confounding factors such as energy expenditure, food and drink intake and general locomotion were not significantly different except for general locomotion in Gabra5$^{-/-}$ females, which was decreased.

We evaluated the functional properties specifically on CA1 pyramidal neurons upon *Gabra5* deletion. We recorded the responses of neurons under control and during condition with the α5 $GABA_AR$ selective inverse agonist L655, 708 (167). We found that the minimal current to elicit an action potential, also referred to as the rheobase, was actually increased in Gabra5$^{-/-}$ mice, which would suggest a decrease in excitability (168). Furthermore, the resting membrane in cells derived from the Gabra5$^{-/-}$ mice was hyperpolarized, consistent with the rheobase measurement. The resting membrane recordings were also not affected by the inverse agonist suggesting these differences between genotypes are not attributed to the α5 subunit specifically. This implies activity by another channel, likely chloride, or potassium. Our findings contradict findings from another very similar model where they observed increased excitability with reduced tonic inhibition. However, the neurons were derived from mice on a mixed C57/BL6 and half 129SvEv background whereas ours were on a C57/BL6N background (169).

The reduced excitability in our recordings is likely a consequence of developmental adaptation (functional compensation), which is often found in constitutive KO mice (170). For instance, in a constitutive mouse model lacking the *Pkm2* gene, the mice are viable and fertile but in cells with a conditional knock-out of the very same gene in embryonic fibroblasts results in a limitation of nucleotide synthesis and following cell cycle arrest (171). Genetic robustness, the ability to maintain fitness despite genetic perturbations are important in evolution. Genetic compensation in KOs is a common occurrence where other associated genes are upregulated or expression is modified in the instance of a deleted gene (170). For example, in a constitutive mouse model lacking the ribosomal *Rpl22* gene, the translation is not hampered as its paralogue *Rpl22l1* is

upregulated in the absence of the *Rpl22* gene that normally inhibits its expression (172). When mutants do not exhibit a phenotype, it may be a result of a loss of a negative feedback loop, allowing for paralogs to rescue, here a knockdown approach might be useful to test it. This means that when deleting a gene of interest and examining the phenotype upon deletion, the phenotype seen may not solely reflect the role of the gene itself but the effect it has on the interaction of remaining genes, which have not been manipulated.

We aimed to evaluate the effect deletion of a critical exon in the Gabra5$^{-/-}$ gene could have on stress regulation measured through corticosterone response and anxiety-like behavior. The functional evaluation of CA1 pyramidal neurons suggest a functional compensation because of a constitutive deletion of the gene. It becomes apparent just how important it is to take compensations or masking by pleiotropy into account when interpreting phenotypes in constitutive models.

4. Summary

Angelman syndrome is a rare neurodevelopmental disease characterized by ataxia, severe mental retardation, inability to communicate verbally and by epileptic seizures. The disease stems from an imprinted region on chromosome 15 where most patients harbor a large deletion of 4-6 Mb other contain mutations on the *UBE3A* gene, imprinting disturbances or paternal disomy. There is currently no cure for the condition rather, symptoms are treated in a multidisciplinary approach. This project aimed to generate and characterize two mouse models connected to Angelman syndrome and additionally to understand the genetic landscape of the AS locus better by performing gene expression analyses. We successfully generated a large deletion model deleting the entire *Ube3a* gene from 5'UTR to 3'UTR and to study the phenotypic presentation. The model recapitulated several cardinal features of AS such as motor skill dysfunction, behavioral deficits and skewed circadian rhythm activity. However, based on tests done so far, the model does not offer any clear advantage to other already studied models harboring smaller deletions. This model is however suitable to study gene expression as it encompasses a deletion of coding and non-coding elements, including a putative promoter within intron 4-5. We showed that the genes within the AS locus were indeed downregulated upon deletion of *Ube3a* and of the putative enhancer. Additional studies *in vivo* are needed to confirm its activity. We also characterized an additional model targeting the *Gabra5* gene and more specifically studied the stress response and anxiety-like behavior. We found a decrease in fecal corticosterone metabolites in the deletion model and decreased anxiety-like behavior. However, functional studies by electrophysiology revealed that is very likely we have a functional compensation by other channel or subunit and the results can thus not be appointed due to *Gabra5* itself, however it does show how important it is to take possible functional compensation to mind in constitutive models. We conclude that the *Ube3a* deletion model is suitable for future development of AS therapeutics the *Gabra5* model needs to be further studied in case functional compensation is present or not.

Publications and contributions

The doctoral dissertation contains the following publications

Publication 1:

Syding, L.A.; Kubik-Zahorodna, A.; Nickl, P.; Novosadova, V.; Kopkanova, J.; Kasparek, P.; Prochazka, J.; Sedlacek, R. **Generation and Characterization of a Novel Angelman Syndrome Mouse Model with a Full Deletion of the Ube3a Gene**. Cells 2022, 11, 2815. https://doi.org/10.3390/cells11182815

Author Contributions: R.S. and A.K.-Z. contributed to methodology of the behavioral experiments. **L.A.S**., A.K.-Z. and V.N. analyzed and interpreted the data. **L.A.S.** and P.K. designed the Ube3a deletion model. P.N. and J.K. generated the mouse models. **L.A.S**. and P.N. made the figures and table. **L.A.S**. and J.K. performed genotyping and breeding. **L.A.S**. and A.K.-Z. designed the study. **L.A.S**., A.K.-Z., P.N. and R.S. prepared the manuscript. J.P. directed the phenotyping of the model. R.S. acquired the funding.

This model describes the generation and characterization of the *Ube3a* KO model.

Publication 2: (submitted October 2022)

Linn Amanda Syding, Agnieszka Kubik-Zahorodna, David Pajuelo-Reguera, Bohdana Hruskova, Michaela Kralikova, Jana Kopkanova, Vendula Novosadova, Petr Kasparek, Jan Prochazka, Jan Rozman, Rostislav Turecek, Radislav Sedlacek. **The effect of *Gabra5* functional ablation on corticosterone levels and anxiety-like behavior in mice.**

Author contributions: **L.A.S**, A.K-Z, D.P-R, J.R, R.S designed the experiments. **L.A.S**, A.K-Z, D.P-R, B.H, M.K performed experiments. **L.A.S** and J.K genotyped and prepared animal cohorts. **L.A.S** and P.K designed the mouse model. P.K and J.K generated the animals. **L.A.S**, A.K-Z and V.N performed data analysis. **L.A.S** generated the figures and tables. J.P performed experimental phenotyping. **L.A.S**, A.K-Z, D.P-R, B.H, J.R, R.T and R.S prepared the manuscript. R.T and R.S acquired funding.

This model describes the generation and characterization of the *Gabra5* model

Publication 3:

Syding LA, Nickl P, Kasparek P, Sedlacek R. **CRISPR/Cas9 Epigenome Editing Potential for Rare Imprinting Diseases: A Review.** Cells. 2020 Apr 16;9(4):993. doi: 10.3390/cells9040993. PMID: 32316223; PMCID: PMC7226972.

Author contributions:

Conceptualization: P.N. and **L.A.S**.; writing—original draft preparation: P.N. and **L.A.S**.; writing—review and editing: P.N., **L.A.S**.; visualization: P.N. and **L.A.S**.; writing and manuscript preparation: **L.A.S,** P.N, P.K. and R.S.; funding: R.S.

This review goes through imprinting diseases including Angelman syndrome and what benefit they might have of new CRISPR/Cas9 advancements.

Publication 4:

Nickl P, Raishbrook MJ, **Syding LA** and Sedlacek R (2022). **Advances in Modelling COVID-19 in Animals.** Front. Drug. Discov. 2:899587. doi: 10.3389/fddsv.2022.899587

Author contributions:

PN, MJR, and LAS wrote the article with equal contributions. RS supervised.

This review paper summarizes mouse models utility in COVID research. The paper is not directly linked to the goals of the doctoral study but as the project include mouse models mainly I decided to include this one in the dissertation.

7. References

1. Bird LM. Angelman syndrome: review of clinical and molecular aspects. The application of clinical genetics. 2014;7:93-104.
2. Angelman H. 'Puppet' Children A Report on Three Cases. Developmental Medicine & Child Neurology. 1965;7(6):681-8.
3. Magenis RE, Brown MG, Lacy DA, Budden S, LaFranchi S, Opitz JM, et al. Is angelman syndrome an alternate result of del(15)(qllql3)? American Journal of Medical Genetics. 1987;28(4):829-38.
4. Jolleff N, Ryan MM. Communication development in Angelman's syndrome. Archives of disease in childhood. 1993;69(1):148-50.
5. Viani F, Romeo A, Viri M, Mastrangelo M, Lalatta F, Selicorni A, et al. Seizure and EEG patterns in Angelman's syndrome. Journal of child neurology. 1995;10(6):467-71.
6. Clayton-Smith J, Laan L. Angelman syndrome: a review of the clinical and genetic aspects. Journal of medical genetics. 2003;40(2):87-95.
7. Eggermann T, Netchine I, Temple IK, Tümer Z, Monk D, Mackay D, et al. Congenital imprinting disorders: EUCID.net - a network to decipher their aetiology and to improve the diagnostic and clinical care. Clinical Epigenetics. 2015;7(1):23-.
8. Syding LA, Nickl P, Kasparek P, Sedlacek R. CRISPR/Cas9 Epigenome Editing Potential for Rare Imprinting Diseases: A Review. Cells. 2020;9(4):993-.
9. Peters J. The role of genomic imprinting in biology and disease: an expanding view. Nature Reviews Genetics. 2014;15(8):517-30.
10. Edwards CA, Ferguson-Smith AC. Mechanisms regulating imprinted genes in clusters. Current opinion in cell biology. 2007;19(3):281-9.
11. Barlow DP. Genomic imprinting: A mammalian epigenetic discovery model. Annual Review of Genetics. 2011;45:379-403.
12. Chotalia M, Smallwood SA, Ruf N, Dawson C, Lucifero D, Frontera M, et al. Transcription is required for establishment of germline methylation marks at imprinted genes. Genes & development. 2009;23(1):105-17.
13. Monk D, Mackay DJG, Eggermann T, Maher ER, Riccio A. Genomic imprinting disorders: lessons on how genome, epigenome and environment interact. Nature Reviews Genetics. 2019;20(4):235-48.
14. Wilkins JF, Úbeda F. Diseases associated with genomic imprinting. Progress in molecular biology and translational science. 2011;101:401-45.
15. Shaffer LG, Agan N, Goldberg JD, Ledbetter DH, Longshore JW, Cassidy SB. American College of Medical Genetics statement of diagnostic testing for uniparental disomy. Genetics in medicine : official journal of the American College of Medical Genetics. 2001;3(3):206-11.
16. Abi Habib W, Azzi S, Brioude F, Steunou V, Thibaud N, Das Neves C, et al. Extensive investigation of the IGF2/H19 imprinting control region reveals novel OCT4/SOX2 binding site defects associated with specific methylation patterns in Beckwith-Wiedemann syndrome. Human molecular genetics. 2014;23(21):5763-73.
17. Brioude F, Oliver-Petit I, Blaise A, Praz F, Rossignol S, Le Jule M, et al. CDKN1C mutation affecting the PCNA-binding domain as a cause of familial Russell Silver syndrome. Journal of medical genetics. 2013;50(12):823-30.
18. Uyar A, Seli E. The impact of assisted reproductive technologies on genomic imprinting and imprinting disorders. Current opinion in obstetrics & gynecology. 2014;26(3):210-21.
19. Eggermann T, Perez de Nanclares G, Maher ER, Temple IK, Tümer Z, Monk D, et al. Imprinting disorders: a group of congenital disorders with overlapping patterns of molecular changes affecting imprinted loci. Clinical Epigenetics. 2015;7(1):123-.

20. Sandanam T, Beange H, Robson L, Woolnough H, Buchholz T, Smith A. Manifestations in institutionalised adults with Angelman syndrome due to deletion. American journal of medical genetics. 1997;70(4):415-20.
21. Matsuura T, Sutcliffe JS, Fang P, Galjaard RJ, Jiang YH, Benton CS, et al. De novo truncating mutations in E6-AP ubiquitin-protein ligase gene (UBE3A) in Angelman syndrome. Nature genetics. 1997;15(1):74-7.
22. Kishino T, Lalande M, Wagstaff J. UBE3A/E6-AP mutations cause Angelman syndrome. Nature genetics. 1997;15(1):70-3.
23. Malcolm S, Clayton-Smith J, Nichols M, Robb S, Webb T, Armour JA, et al. Uniparental paternal disomy in Angelman's syndrome. Lancet (London, England). 1991;337(8743):694-7.
24. Buiting K, Gross S, Lich C, Gillessen-Kaesbach G, el-Maarri O, Horsthemke B. Epimutations in Prader-Willi and Angelman syndromes: a molecular study of 136 patients with an imprinting defect. American journal of human genetics. 2003;72(3):571-7.
25. Lossie AC, Whitney MM, Amidon D, Dong HJ, Chen P, Theriaque D, et al. Distinct phenotypes distinguish the molecular classes of Angelman syndrome. Journal of medical genetics. 2001;38(12):834-45.
26. Amos-Landgraf JM, Ji Y, Gottlieb W, Depinet T, Wandstrat AE, Cassidy SB, et al. Chromosome Breakage in the Prader-Willi and Angelman Syndromes Involves Recombination between Large, Transcribed Repeats at Proximal and Distal Breakpoints. The American Journal of Human Genetics. 1999;65(2):370-86.
27. Valente KD, Varela MC, Koiffmann CP, Andrade JQ, Grossmann R, Kok F, et al. Angelman syndrome caused by deletion: a genotype-phenotype correlation determined by breakpoint. Epilepsy research. 2013;105(1-2):234-9.
28. Varela MC, Kok F, Otto PA, Koiffmann CP. Phenotypic variability in Angelman syndrome: comparison among different deletion classes and between deletion and UPD subjects. European Journal of Human Genetics. 2004;12(12):987-92.
29. Goytain A, Hines RM, El-Husseini A, Quamme GA. NIPA1(SPG6), the basis for autosomal dominant form of hereditary spastic paraplegia, encodes a functional Mg2+ transporter. The Journal of biological chemistry. 2007;282(11):8060-8.
30. Fricano-Kugler C, Gordon A, Shin G, Gao K, Nguyen J, Berg J, et al. CYFIP1 overexpression increases fear response in mice but does not affect social or repetitive behavioral phenotypes. Molecular Autism. 2019;10(1):25-.
31. Murphy SM, Preble AM, Patel UK, O'Connell KL, Dias DP, Moritz M, et al. GCP5 and GCP6: two new members of the human gamma-tubulin complex. Molecular biology of the cell. 2001;12(11):3340-52.
32. Butler MG, Miller JL, Forster JL. Prader-Willi Syndrome - Clinical Genetics, Diagnosis and Treatment Approaches: An Update. Current pediatric reviews. 2019;15(4):207-44.
33. Angulo MA, Butler MG, Cataletto ME. Prader-Willi syndrome: a review of clinical, genetic, and endocrine findings. Journal of endocrinological investigation. 2015;38(12):1249-63.
34. Yamasaki K, Joh K, Ohta T, Masuzaki H, Ishimaru T, Mukai T, et al. Neurons but not glial cells show reciprocal imprinting of sense and antisense transcripts of Ube3a. Human molecular genetics. 2003;12(8):837-47.
35. Hillman PR, Christian SGB, Doan R, Cohen ND, Konganti K, Douglas K, et al. Genomic imprinting does not reduce the dosage of UBE3A in neurons. Epigenetics & Chromatin. 2017;10(1):27-.
36. Zhang Y-J, Yang J-H, Shi Q-S, Zheng L-L, Liu J, Zhou H, et al. Rapid birth-and-death evolution of imprinted snoRNAs in the Prader-Willi syndrome locus: implications for neural development in Euarchontoglires. PloS one. 2014;9(6):e100329-e.

37. Edelmann MJ, Nicholson B, Kessler BM. Pharmacological targets in the ubiquitin system offer new ways of treating cancer, neurodegenerative disorders and infectious diseases. Expert Reviews in Molecular Medicine. 2011;13:e35-e.
38. Khatri N, Man H-Y. The Autism and Angelman Syndrome Protein Ube3A/E6AP: The Gene, E3 Ligase Ubiquitination Targets and Neurobiological Functions. Frontiers in Molecular Neuroscience. 2019;12.
39. Tomaić V, Banks L. Angelman syndrome-associated ubiquitin ligase UBE3A/E6AP mutants interfere with the proteolytic activity of the proteasome. Cell Death & Disease. 2015;6(1):e1625-e.
40. Sell G, Margolis S. From UBE3A to Angelman syndrome: a substrate perspective. Frontiers in Neuroscience. 2015;9.
41. Dindot SV, Antalffy BA, Bhattacharjee MB, Beaudet AL. The Angelman syndrome ubiquitin ligase localizes to the synapse and nucleus, and maternal deficiency results in abnormal dendritic spine morphology. Human molecular genetics. 2008;17(1):111-8.
42. Williams CA, Driscoll DJ, Dagli AI. Clinical and genetic aspects of Angelman syndrome. Genetics in medicine : official journal of the American College of Medical Genetics. 2010;12(7):385-95.
43. Judson MC, Sosa-Pagan JO, Del Cid WA, Han JE, Philpot BD. Allelic specificity of Ube3a expression in the mouse brain during postnatal development. The Journal of comparative neurology. 2014;522(8):1874-96.
44. Filonova I, Trotter Jh Fau - Banko JL, Banko Jl Fau - Weeber EJ, Weeber EJ. Activity-dependent changes in MAPK activation in the Angelman Syndrome mouse model. (1549-5485 (Electronic)).
45. Bottani A, Robinson WP, DeLozier-Blanchet CD, Engel E, Morris MA, Schmitt B, et al. Angelman syndrome due to paternal uniparental disomy of chromosome 15: a milder phenotype? American journal of medical genetics. 1994;51(1):35-40.
46. Robinson WP. Mechanisms leading to uniparental disomy and their clinical consequences. BioEssays : news and reviews in molecular, cellular and developmental biology. 2000;22(5):452-9.
47. Beygo J, Grosser C, Kaya S, Mertel C, Buiting K, Horsthemke B. Common genetic variation in the Angelman syndrome imprinting centre affects the imprinting of chromosome 15. European Journal of Human Genetics. 2020;28(6):835-9.
48. Saitoh S, Buiting K, Rogan PK, Buxton JL, Driscoll DJ, Arnemann J, et al. Minimal definition of the imprinting center and fixation of chromosome 15q11-q13 epigenotype by imprinting mutations. Proceedings of the National Academy of Sciences of the United States of America. 1996;93(15):7811-5.
49. Bürger J, Buiting K, Dittrich B, Gross S, Lich C, Sperling K, et al. Different mechanisms and recurrence risks of imprinting defects in Angelman syndrome. American journal of human genetics. 1997;61(1):88-93.
50. Horsthemke B, Wagstaff J. Mechanisms of imprinting of the Prader-Willi/Angelman region. American journal of medical genetics Part A. 2008;146A(16):2041-52.
51. Rabinovitz S, Kaufman Y, Ludwig G, Razin A, Shemer R. Mechanisms of activation of the paternally expressed genes by the Prader-Willi imprinting center in the Prader-Willi/Angelman syndromes domains. Proceedings of the National Academy of Sciences of the United States of America. 2012;109(19):7403-8.
52. Mabb AM, Judson MC, Zylka MJ, Philpot BD. Angelman syndrome: insights into genomic imprinting and neurodevelopmental phenotypes. Trends in neurosciences. 2011;34(6):293-303.
53. Meng L, Person RE, Beaudet AL. Ube3a-ATS is an atypical RNA polymerase II transcript that represses the paternal expression of Ube3a. Human molecular genetics. 2012;21(13):3001-12.
54. Faghihi MA, Wahlestedt C. Regulatory roles of natural antisense transcripts. Nature reviews Molecular cell biology. 2009;10(9):637-43.
55. Laan LA, v Haeringen A, Brouwer OF. Angelman syndrome: a review of clinical and genetic aspects. Clinical neurology and neurosurgery. 1999;101(3):161-70.
56. Saitoh S, Harada N, Jinno Y, Hashimoto K, Imaizumi K, Kuroki Y, et al. Molecular and clinical study of 61 Angelman syndrome patients. American journal of medical genetics. 1994;52(2):158-63.

57. Ostergaard JR, Balslev T. Efficacy of different antiepileptic drugs in children with Angelman syndrome associated with 15q11-13 deletion: the Danish experience. 2001. p. 718-9.
58. Daily JL, Nash K, Jinwal U, Golde T, Rogers J, Peters MM, et al. Adeno-Associated Virus-Mediated Rescue of the Cognitive Defects in a Mouse Model for Angelman Syndrome. PLoS ONE. 2011;6(12):e27221-e.
59. Vatsa N, Jana NR. UBE3A and Its Link With Autism. Frontiers in molecular neuroscience. 2018;11:448-.
60. Huang H-S, Allen JA, Mabb AM, King IF, Miriyala J, Taylor-Blake B, et al. Topoisomerase inhibitors unsilence the dormant allele of Ube3a in neurons. Nature. 2011;481(7380):185-9.
61. Meng L, Ward AJ, Chun S, Bennett CF, Beaudet AL, Rigo F. Towards a therapy for Angelman syndrome by targeting a long non-coding RNA. Nature. 2015;518(7539):409-12.
62. Bailus BJ, Pyles B, McAlister MM, O'Geen H, Lockwood SH, Adams AN, et al. Protein delivery of an artificial transcription factor restores widespread Ube3a expression in an angelman syndrome mouse brain. Molecular Therapy. 2016;24(3):548-55.
63. Sangamo Therapeutics NCT. A Phase 2 Repeat Dosing Clinical Trial of SB-509 in Subjects With Moderate to Severe Diabetic Neuropathy and Unmeasurable Nerve Conduction Velocity. 2010.
64. Silva-Santos S, van Woerden GM, Bruinsma CF, Mientjes E, Jolfaei MA, Distel B, et al. Ube3a reinstatement identifies distinct developmental windows in a murine Angelman syndrome model. The Journal of clinical investigation. 2015;125(5):2069-76.
65. Egawa K, Kitagawa K, Inoue K, Takayama M, Takayama C, Saitoh S, et al. Decreased tonic inhibition in cerebellar granule cells causes motor dysfunction in a mouse model of Angelman syndrome. Science translational medicine. 2012;4(163):163ra57-ra57.
66. Greer PL, Hanayama R, Bloodgood BL, Mardinly AR, Lipton DM, Flavell SW, et al. The Angelman Syndrome protein Ube3A regulates synapse development by ubiquitinating arc. Cell. 2010;140(5):704-16.
67. Mandel-Brehm C, Salogiannis J, Dhamne SC, Rotenberg A, Greenberg ME. Seizure-like activity in a juvenile Angelman syndrome mouse model is attenuated by reducing Arc expression. Proceedings of the National Academy of Sciences of the United States of America. 2015;112(16):5129-34.
68. Sellers RS. Translating Mouse Models. Toxicologic pathology. 2017;45(1):134-45.
69. Nickl P, Raishbrook MJ, Syding LA, Sedlacek R. Advances in Modelling COVID-19 in Animals. Frontiers in Drug Discovery. 2022;2.
70. Rotaru DC, Mientjes EJ, Elgersma Y. Angelman Syndrome: From Mouse Models to Therapy. Neuroscience. 2020;445:172-89.
71. Albrecht U, Sutcliffe JS, Cattanach BM, Beechey CV, Armstrong D, Eichele G, et al. Imprinted expression of the murine Angelman syndrome gene, Ube3a, in hippocampal and Purkinje neurons. Nature genetics. 1997;17(1):75-8.
72. Nicholls RD, Knepper JL. Genome Organization, Function, and Imprinting in Prader-Willi and Angelman Syndromes. Annual Review of Genomics and Human Genetics. 2001;2(1):153-75.
73. Lalande M, Calciano MA. Molecular epigenetics of Angelman syndrome. Cellular and Molecular Life Sciences. 2007;64(7):947-.
74. Avagliano Trezza R, Sonzogni M, Bossuyt SNV, Zampeta FI, Punt AM, van den Berg M, et al. Loss of nuclear UBE3A causes electrophysiological and behavioral deficits in mice and is associated with Angelman syndrome. Nature Neuroscience. 2019;22(8):1235-47.
75. Jiang YH, Armstrong D, Albrecht U, Atkins CM, Noebels JL, Eichele G, et al. Mutation of the Angelman ubiquitin ligase in mice causes increased cytoplasmic p53 and deficits of contextual learning and long-term potentiation. Neuron. 1998;21(4):799-811.
76. Wang T, van Woerden GM, Elgersma Y, Borst JGG. Enhanced Transmission at the Calyx of Held Synapse in a Mouse Model for Angelman Syndrome. Frontiers in cellular neuroscience. 2018;11.

77. Ube3a Mouse Gene Details | ubiquitin protein ligase E3A | International Mouse Phenotyping Consortium. 2022 [updated 2022. Available from: https://www.mousephenotype.org/.
78. Berrios J, Stamatakis AM, Kantak PA, McElligott ZA, Judson MC, Aita M, et al. Loss of UBE3A from TH-expressing neurons suppresses GABA co-release and enhances VTA-NAc optical self-stimulation. Nature Communications. 2016;7.
79. Skarnes WC, Rosen B, West AP, Koutsourakis M, Bushell W, Iyer V, et al. A conditional knockout resource for the genome-wide study of mouse gene function. Nature. 2011;474(7351):337-44.
80. Smith SEP, Zhou Y-D, Zhang G, Jin Z, Stoppel DC, Anderson MP. Increased gene dosage of Ube3a results in autism traits and decreased glutamate synaptic transmission in mice. Science translational medicine. 2011;3(103):103ra97-ra97.
81. Krishnan V, Stoppel DC, Nong Y, Johnson MA, Nadler MJS, Ozkaynak E, et al. Autism gene Ube3a and seizures impair sociability by repressing VTA Cbln1. Nature. 2017;543(7646):507-.
82. Matsumoto A, Kumagai T, Miura K, Miyazaki S, Hayakawa C, Yamanaka T. Epilepsy in Angelman syndrome associated with chromosome 15q deletion. Epilepsia. 1992;33(6):1083-90.
83. Syding LA, Kubik-Zahorodna A, Nickl P, Novosadova V, Kopkanova J, Kasparek P, et al. Generation and Characterization of a Novel Angelman Syndrome Mouse Model with a Full Deletion of the Ube3a Gene. 2022;11(18):2815.
84. Jiang Y-h, Pan Y, Zhu L, Landa L, Yoo J, Spencer C, et al. Altered Ultrasonic Vocalization and Impaired Learning and Memory in Angelman Syndrome Mouse Model with a Large Maternal Deletion from Ube3a to Gabrb3. PLOS ONE. 2010;5(8):e12278-e.
85. Nakatani J, Tamada K, Hatanaka F, Ise S, Ohta H, Inoue K, et al. Abnormal behavior in a chromosome-engineered mouse model for human 15q11-13 duplication seen in autism. Cell. 2009;137(7):1235-46.
86. Gabriel JM, Merchant M, Ohta T, Ji Y, Caldwelli RG, Ramsey MJ, et al. A transgene insertion creating a heritable chromosome deletion mouse model of Prader-Willi and angelman syndromes. Proceedings of the National Academy of Sciences of the United States of America. 1999;96(16):9258-63.
87. Tsai TF, Jiang YH, Bressler J, Armstrong D, Beaudet AL. Paternal deletion from Snrpn to Ube3a in the mouse causes hypotonia, growth retardation and partial lethality and provides evidence for a gene contributing to Prader-Willi syndrome. Human molecular genetics. 1999;8(8):1357-64.
88. Russell LB, Montgomery CS, Cacheiro NLA, Johnson DK. Complementation analyses for 45 mutations encompassing the pink-eyed dilution (p) locus of the mouse. Genetics. 1995;141(4):1547-62.
89. Born HA, Dao AT, Levine AT, Lee WL, Mehta NM, Mehra S, et al. Strain-dependence of the Angelman Syndrome phenotypes in Ube3a maternal deficiency mice. Scientific Reports. 2017;7(1):8451-.
90. Pitts MW. Barnes Maze Procedure for Spatial Learning and Memory in Mice. Bio-protocol. 2018;8(5):e2744-e.
91. Panlab. No Title.
92. Jones BJ, Roberts DJ. The quantitative measurement of motor inco-ordination in naive mice using an accelerating rotarod. Journal of Pharmacy and Pharmacology. 1968;20(4):302-4.
93. Shiotsuki H, Yoshimi K, Shimo Y, Funayama M, Takamatsu Y, Ikeda K, et al. A rotarod test for evaluation of motor skill learning. Journal of neuroscience methods. 2010;189(2):180-5.
94. Maranga C, Fernandes TG, Bekman E, da Rocha ST. Angelman syndrome: a journey through the brain. The FEBS Journal. 2020;287(11):2154-75.
95. Dorman CW, Krug HE, Frizelle SP, Funkenbusch S, Mahowald ML. A comparison of DigiGait™ and TreadScan™ imaging systems: assessment of pain using gait analysis in murine monoarthritis. Journal of pain research. 2013;7:25-35.
96. Steffenburg S, Gillberg CL, Steffenburg U, Kyllerman M. Autism in Angelman syndrome: a population-based study. Pediatric neurology. 1996;14(2):131-6.

97. Prasad A, Grocott O, Parkin K, Larson A, Thibert RL. Angelman syndrome in adolescence and adulthood: A retrospective chart review of 53 cases. American Journal of Medical Genetics Part A. 2018;176(6):1327-34.
98. Demuyser T, Deneyer L, Bentea E, Albertini G, Van Liefferinge J, Merckx E, et al. In-depth behavioral characterization of the corticosterone mouse model and the critical involvement of housing conditions. Physiology & behavior. 2016;156:199-207.
99. Stanford. Open field.
100. Deacon RMJ. Measuring motor coordination in mice. Journal of visualized experiments : JoVE. 2013(75):e2609-e.
101. Deacon RMJ. Digging and marble burying in mice: simple methods for in vivo identification of biological impacts. Nature protocols. 2006;1(1):122-4.
102. Au - Angoa-Pérez M, Au - Kane MJ, Au - Briggs DI, Au - Francescutti DM, Au - Kuhn DM. Marble Burying and Nestlet Shredding as Tests of Repetitive, Compulsive-like Behaviors in Mice. JoVE. 2013(82):e50978-e.
103. Sonzogni M, Wallaard I, Santos SS, Kingma J, Du Mee D, Van Woerden GM, et al. A behavioral test battery for mouse models of Angelman syndrome: A powerful tool for testing drugs and novel Ube3a mutants. Molecular Autism. 2018;9(1):1-19.
104. Winslow W, McDonough I, Tallino S, Decker A, Vural AS, Velazquez R. IntelliCage Automated Behavioral Phenotyping Reveals Behavior Deficits in the 3xTg-AD Mouse Model of Alzheimer's Disease Associated With Brain Weight. Frontiers in aging neuroscience. 2021;13:720214-.
105. Smith JC. Angelman syndrome: evolution of the phenotype in adolescents and adults. Developmental medicine and child neurology. 2001;43(7):476-80.
106. Huang H-S, Burns AJ, Nonneman RJ, Baker LK, Riddick NV, Nikolova VD, et al. Behavioral deficits in an Angelman syndrome model: effects of genetic background and age. Behavioural brain research. 2013;243:79-90.
107. Roden WH, Peugh LD, Jansen LA. Altered GABA(A) receptor subunit expression and pharmacology in human Angelman syndrome cortex. Neuroscience letters. 2010;483(3):167-72.
108. Jacob TC. Neurobiology and Therapeutic Potential of α5-GABA Type A Receptors. Frontiers in Molecular Neuroscience. 2019;12(July):1-10.
109. Förstera B, Castro PA, Moraga-Cid G, Aguayo LG. Potentiation of Gamma Aminobutyric Acid Receptors (GABAAR) by Ethanol: How Are Inhibitory Receptors Affected? Frontiers in Cellular Neuroscience. 2016;10.
110. Herd MB, Haythornthwaite AR, Rosahl TW, Wafford KA, Homanics GE, Lambert JJ, et al. The expression of GABAA beta subunit isoforms in synaptic and extrasynaptic receptor populations of mouse dentate gyrus granule cells. The Journal of physiology. 2008;586(4):989-1004.
111. Loebrich S, Bähring R, Katsuno T, Tsukita S, Kneussel M. Activated radixin is essential for GABAA receptor alpha5 subunit anchoring at the actin cytoskeleton. The EMBO journal. 2006;25(5):987-99.
112. Engin E, Zarnowska ED, Benke D, Tsvetkov E, Sigal M, Keist R, et al. Tonic Inhibitory Control of Dentate Gyrus Granule Cells by α5-Containing GABAA Receptors Reduces Memory Interference. (1529-2401 (Electronic)).
113. Collinson N, Kuenzi FM, Jarolimek W, Maubach KA, Cothliff R, Sur C, et al. Enhanced learning and memory and altered GABAergic synaptic transmission in mice lacking the alpha 5 subunit of the GABAA receptor. The Journal of neuroscience : the official journal of the Society for Neuroscience. 2002;22(13):5572-80.
114. Balic E, Rudolph U Fau - Fritschy J-M, Fritschy Jm Fau - Mohler H, Mohler H Fau - Benke D, Benke D. The alpha5(H105R) mutation impairs alpha5 selective binding properties by altered positioning of the alpha5 subunit in GABAA receptors containing two distinct types of alpha subunits. (1471-4159 (Electronic)).

115. Martin LJ, Bonin RP, Orser BA. The physiological properties and therapeutic potential of alpha5-GABAA receptors. Biochemical Society transactions. 2009;37(Pt 6):1334-7.
116. Crestani F, Keist R, Fritschy JM, Benke D, Vogt K, Prut L, et al. Trace fear conditioning involves hippocampal alpha5 GABA(A) receptors. Proceedings of the National Academy of Sciences of the United States of America. 2002;99(13):8980-5.
117. Martin LJ, Oh GHT, Orser BA. Etomidate targets alpha5 gamma-aminobutyric acid subtype A receptors to regulate synaptic plasticity and memory blockade. Anesthesiology. 2009;111(5):1025-35.
118. Dawson GR, Maubach KA, Collinson N, Cobain M, Everitt BJ, MacLeod AM, et al. An inverse agonist selective for alpha5 subunit-containing GABAA receptors enhances cognition. The Journal of pharmacology and experimental therapeutics. 2006;316(3):1335-45.
119. Atack JR, Bayley PJ, Seabrook GR, Wafford KA, McKernan RM, Dawson GR. L-655,708 enhances cognition in rats but is not proconvulsant at a dose selective for alpha5-containing GABAA receptors. Neuropharmacology. 2006;51(6):1023-9.
120. Hodges LM, Fyer AJ, Weissman MM, Logue MW, Haghighi F, Evgrafov O, et al. Evidence for linkage and association of GABRB3 and GABRA5 to panic disorder. Neuropsychopharmacology : official publication of the American College of Neuropsychopharmacology. 2014;39(10):2423-31.
121. Zurek AA, Kemp SWP, Aga Z, Walker S, Milenkovic M, Ramsey AJ, et al. α5GABAA receptor deficiency causes autism-like behaviors. Annals of clinical and translational neurology. 2016;3(5):392-8.
122. Mesbah-Oskui L, Penna A, Orser BA, Horner RL. Reduced expression of α5GABA(A) receptors elicits autism-like alterations in EEG patterns and sleep-wake behavior. Neurotoxicology and teratology. 2017;61:115-22.
123. Hauser J, Rudolph U, Keist R, Möhler H, Feldon J, Yee BK. Hippocampal α5 subunit-containing GABAA receptors modulate the expression of prepulse inhibition. Molecular Psychiatry. 2005;10(2):201-7.
124. Curia G, Papouin T, Séguéla P, Avoli M. Downregulation of tonic GABAergic inhibition in a mouse model of fragile X syndrome. Cerebral cortex (New York, NY : 1991). 2009;19(7):1515-20.
125. Goodnite PM. Stress: a concept analysis. Nursing forum. 2014;49(1):71-4.
126. Kagias K, Nehammer C, Pocock R. Neuronal Responses to Physiological Stress. Frontiers in Genetics. 2012;3.
127. Smith SM, Vale WW. The role of the hypothalamic-pituitary-adrenal axis in neuroendocrine responses to stress. Dialogues in clinical neuroscience. 2006;8(4):383-95.
128. Goncharova N, Chigarova O, Rudenko N, Oganyan T. Glucocorticoid Negative Feedback in Regulation of the Hypothalamic-Pituitary-Adrenal Axis in Rhesus Monkeys With Various Types of Adaptive Behavior: Individual and Age-Related Differences. Frontiers in Endocrinology. 2019;10.
129. Raglan GB, Schmidt LA, Schulkin J. The role of glucocorticoids and corticotropin-releasing hormone regulation on anxiety symptoms and response to treatment. Endocrine connections. 2017;6(2):R1-R7.
130. Sapolsky RM. Why zebras don't get ulcers: The acclaimed guide to stress, stress-related diseases, and coping: Holt paperbacks; 2004.
131. Cullinan WE, Ziegler DR, Herman JP. Functional role of local GABAergic influences on the HPA axis. Brain structure & function. 2008;213(1-2):63-72.
132. Gunn B, Brown A, Lambert J, Belelli D. Neurosteroids and GABAA Receptor Interactions: A Focus on Stress. Frontiers in Neuroscience. 2011;5.
133. Cullinan WE, Helmreich DL, Watson SJ. Fos expression in forebrain afferents to the hypothalamic paraventricular nucleus following swim stress. The Journal of comparative neurology. 1996;368(1):88-99.
134. Moreth K, Fischer R, Fuchs H, Gailus-Durner V, Wurst W, Katus HA, et al. High-throughput phenotypic assessment of cardiac physiology in four commonly used inbred mouse strains. Journal of comparative physiology B, Biochemical, systemic, and environmental physiology. 2014;184(6):763-75.

135. Stypmann J, Engelen MA, Troatz C, Rothenburger M, Eckardt L, Tiemann K. Echocardiographic assessment of global left ventricular function in mice. Laboratory animals. 2009;43(2):127-37.
136. Nakayama Y, Wada A, Inoue R, Terasawa K, Kimura I, Nakamura N, et al. A rapid and efficient method for neuronal induction of the P19 embryonic carcinoma cell line. Journal of Neuroscience Methods. 2014;227:100-6.
137. Margolis SS, Sell GL, Zbinden MA, Bird LM. Angelman Syndrome. Neurotherapeutics : the journal of the American Society for Experimental NeuroTherapeutics. 2015;12(3):641-50.
138. Ensembl. Ube3a gene mouse organism.
139. Sun XJ, Man N, Tan Y, Nimer SD, Wang L. The Role of Histone Acetyltransferases in Normal and Malignant Hematopoiesis. (2234-943X (Print)).
140. Bittel DC, Butler MG. Prader-Willi syndrome: clinical genetics, cytogenetics and molecular biology. Expert reviews in molecular medicine. 2005;7(14):1-20.
141. Rinalduzzi S, Trompetto C, Marinelli L, Alibardi A, Missori P, Fattapposta F, et al. Balance dysfunction in Parkinson's disease. BioMed research international. 2015;2015:434683-.
142. Dodge A, Peters MM, Greene HE, Dietrick C, Botelho R, Chung D, et al. Generation of a Novel Rat Model of Angelman Syndrome with a Complete Ube3a Gene Deletion. Autism research : official journal of the International Society for Autism Research. 2020;13(3):397-409.
143. Rostosky CM, Milosevic I. Gait Analysis of Age-dependent Motor Impairments in Mice with Neurodegeneration. Journal of visualized experiments : JoVE. 2018(136):57752-.
144. Pelc K, Cheron G, Dan B. Behavior and neuropsychiatric manifestations in Angelman syndrome. Neuropsychiatric disease and treatment. 2008;4(3):577-84.
145. Jirkof P. Burrowing and nest building behavior as indicators of well-being in mice. Journal of neuroscience methods. 2014;234:139-46.
146. Porsolt RD, Bertin A, Jalfre M. Behavioral despair in mice: a primary screening test for antidepressants. Archives internationales de pharmacodynamie et de therapie. 1977;229(2):327-36.
147. Moy SS, Nadler JJ, Young NB, Nonneman RJ, Segall SK, Andrade GM, et al. Social approach and repetitive behavior in eleven inbred mouse strains. Behavioural Brain Research. 2008;191(1):118-29.
148. Silverman JL, Yang M, Lord C, Crawley JN. Behavioural phenotyping assays for mouse models of autism. Nature reviews Neuroscience. 2010;11(7):490-502.
149. Guariglia SR, Chadman KK. Water T-maze: a useful assay for determination of repetitive behaviors in mice. Journal of neuroscience methods. 2013;220(1):24-9.
150. Heinz DE, Schöttle VA, Nemcova P, Binder FP, Ebert T, Domschke K, et al. Exploratory drive, fear, and anxiety are dissociable and independent components in foraging mice. Translational Psychiatry. 2021;11(1):318-.
151. Sarkar PA, Shigli A, Patidar C. Happy Puppet syndrome. BMJ case reports. 2011;2011:bcr0920114747-bcr.
152. Massé L, Antonacci M. Low cardiac output syndrome: identification and management. Critical care nursing clinics of North America. 2005;17(4):375-83, x.
153. Hauser M, Bengel FM, Hager A, Kuehn A, Nekolla SG, Kaemmerer H, et al. Impaired myocardial blood flow and coronary flow reserve of the anatomical right systemic ventricle in patients with congenitally corrected transposition of the great arteries. Heart (British Cardiac Society). 2003;89(10):1231-5.
154. Carcillo JA, Fields AI. Clinical practice parameters for hemodynamic support of pediatric and neonatal patients in septic shock. Critical care medicine. 2002;30(6):1365-78.
155. Frohlich J, Miller MT, Bird LM, Garces P, Purtell H, Hoener MC, et al. Electrophysiological Phenotype in Angelman Syndrome Differs Between Genotypes. Biological psychiatry. 2019;85(9):752-9.

156. Mitra R, Sapolsky RM. Acute corticosterone treatment is sufficient to induce anxiety and amygdaloid dendritic hypertrophy. Proceedings of the National Academy of Sciences of the United States of America. 2008;105(14):5573-8.
157. Jacobsen KR, JØRgensen P, Pipper CB, Steffensen AM, Hau J, Abelson KSP. The Utility of Fecal Corticosterone Metabolites and Animal Welfare Assessment Protocols as Predictive Parameters of Tumor Development and Animal Welfare in a Murine Xenograft Model. In Vivo. 2013;27(2):189 LP-96.
158. Lidster K, Owen K, Browne WJ, Prescott MJ. Cage aggression in group-housed laboratory male mice: an international data crowdsourcing project. Scientific Reports. 2019;9(1):15211-.
159. Giammanco M, Tabacchi G, Giammanco S, Di Majo D, La Guardia M. Testosterone and aggressiveness. Medical science monitor : international medical journal of experimental and clinical research. 2005;11(4):RA136-45.
160. Kulesskaya N, Voikar V. Assessment of mouse anxiety-like behavior in the light-dark box and open-field arena: role of equipment and procedure. Physiology & behavior. 2014;133:30-8.
161. Lister RG. The use of a plus-maze to measure anxiety in the mouse. Psychopharmacology. 1987;92(2):180-5.
162. Piantadosi SC, French BJ, Poe MM, Timić T, Marković BD, Pabba M, et al. Sex-Dependent Anti-Stress Effect of an α5 Subunit Containing GABAA Receptor Positive Allosteric Modulator. Frontiers in Pharmacology. 2016;7.
163. Lever C, Burton S, O'Keefe J. Rearing on hind legs, environmental novelty, and the hippocampal formation. Reviews in the neurosciences. 2006;17(1-2):111-33.
164. Kaesermann HP. Stretched attend posture, a non-social form of ambivalence, is sensitive to a conflict-reducing drug action. Psychopharmacology. 1986;89(1):31-7.
165. Molewijk HE, van der Poel AM, Olivier B. The ambivalent behaviour "stretched approach posture" in the rat as a paradigm to characterize anxiolytic drugs. Psychopharmacology. 1995;121(1):81-90.
166. Blanchard DC, Blanchard RJ, Rodgers RJ. Risk Assessment and Animal Models of Anxiety BT - Animal Models in Psychopharmacology. In: Olivier B, Mos J, Slangen JL, editors. Basel: Birkhäuser Basel; 1991. p. 117-34.
167. Quirk K, Blurton P, Fletcher S, Leeson P, Tang F, Mellilo D, et al. [3H]L-655,708, a novel ligand selective for the benzodiazepine site of GABAA receptors which contain the alpha 5 subunit. Neuropharmacology. 1996;35(9-10):1331-5.
168. Chase MH, Morales FR. Chapter 12 - Control of Motoneurons during Sleep. In: Kryger MH, Roth T, Dement WCBTP, Practice of Sleep M, editors. Philadelphia: W.B. Saunders; 2005. p. 154-68.
169. Bonin RP, Martin LJ, MacDonald JF, Orser BA. Alpha5GABAA receptors regulate the intrinsic excitability of mouse hippocampal pyramidal neurons. Journal of neurophysiology. 2007;98(4):2244-54.
170. El-Brolosy MA, Stainier DYR. Genetic compensation: A phenomenon in search of mechanisms. PLoS genetics. 2017;13(7):e1006780-e.
171. Lunt Sophia Y, Muralidhar V, Hosios Aaron M, Israelsen William J, Gui Dan Y, Newhouse L, et al. Pyruvate Kinase Isoform Expression Alters Nucleotide Synthesis to Impact Cell Proliferation. Molecular Cell. 2015;57(1):95-107.
172. O'Leary MN, Schreiber KH, Zhang Y, Duc A-CE, Rao S, Hale JS, et al. The Ribosomal Protein Rpl22 Controls Ribosome Composition by Directly Repressing Expression of Its Own Paralog, Rpl22l1. PLOS Genetics. 2013;9(8):e1003708-e.

8. List of abbreviations

AS- Angelman syndrome

WT- Wild type

ICR- Imprint control region

ID- Imprinting disorder

UBE3A- Ubiquitin-protein ligase E3A

PEG- Paternally expressed gene

UPD- Uniparental disomy

ncRNA- Non-coding RNA

PWS- Prader-Willi syndrome

snoRNA- Small nucleolar RNA

IC- Imprinting center

TSS- Transcription start site

AAV- Adeno-associated virus

LTP- Long-term potentiation

YFP- Yellow fluorescent protein

GABA- Gamma-Aminobutyric Acid

GABRB3- Gamma-aminobutyric acid receptor beta 3

GABRA5- Gamma-aminobutyric acid receptor alpha 5

GABRG3- Gamma-aminobutyric acid receptor gamma 3

CNS- Central nervous system

HPA- Hypothalamic-pituary-adrenal

PVN- Paraventricular nucelus

MAP2- Microtubule-associated protein 2

OCT-4- Octamer-binding transcription factor 4

MKRN3- Makorin ring finger protein 3

NDN- Necdin

SNRPN- Small nuclear ribonucleoprotein polypeptide N

SNURF- SNRPN upstream open reading frame

FCM: Fecal corticosterone metabolite

List of figures

List of tables

cells

MDPI

Article

Generation and Characterization of a Novel Angelman Syndrome Mouse Model with a Full Deletion of the *Ube3a* Gene

Linn Amanda Syding [1], Agnieszka Kubik-Zahorodna [2], Petr Nickl [1,2], Vendula Novosadova [2], Jana Kopkanova [2], Petr Kasparek [2], Jan Prochazka [1,2] and Radislav Sedlacek [1,2,*]

[1] Laboratory of Transgenic Models of Diseases, Institute of Molecular Genetics of the Czech Academy of Sciences, 252 50 Vestec, Czech Republic
[2] Czech Centre for Phenogenomics, Institute of Molecular Genetics of the Czech Academy of Sciences, 252 50 Vestec, Czech Republic
* Correspondence: radislav.sedlacek@img.cas.cz

Abstract: Angelman syndrome (AS) is a neurodevelopmental disorder caused by deficits in maternally inherited *UBE3A*. The disease is characterized by intellectual disability, impaired motor skills, and behavioral deficits, including increased anxiety and autism spectrum disorder features. The mouse models used so far in AS research recapitulate most of the cardinal AS characteristics. However, they do not mimic the situation found in the majority of AS patients who have a large deletion spanning 4–6 Mb. There is also a large variability in phenotypes reported in the available models, which altogether limits development of therapeutics. Therefore, we have generated a mouse model in which the *Ube3a* gene is deleted entirely from the 5^1 UTR to the 3^1 UTR of mouse *Ube3a* isoform 2, resulting in a deletion of 76 kb. To investigate its phenotypic suitability as a model for AS, we employed a battery of behavioral tests directed to reveal AS pathology and to find out whether this model better mirrors AS development compared to other available models. We found that the maternally inherited Ube3a-deficient line exhibits robust motor dysfunction, as seen in the rotarod and DigiGait tests, and displays abnormalities in additional behavioral paradigms, including reduced nest building and hypoactivity, although no apparent cognitive phenotype was observed in the Barnes maze and novel object recognition tests. The AS mice did, however, underperform in more complex cognition tasks, such as place reversal in the IntelliCage system, and exhibited a different circadian rhythm activity pattern. We show that the novel UBE3A-deficient model, based on a whole-gene deletion, is suitable for AS research, as it recapitulates important phenotypes characteristic of AS. This new mouse model provides complementary possibilities to study the *Ube3a* gene and its function in health and disease as well as possible therapeutic interventions to restore function.

Keywords: Angelman syndrome; UBE3A; mouse model; neurodevelopmental disease; autism spectrum disorder

Citation: Syding, L.A.; Kubik-Zahorodna, A.; Nickl, P.; Novosadova, V.; Kopkanova, J.; Kasparek, P.; Prochazka, J.; Sedlacek, R. Generation and Characterization of a Novel Angelman Syndrome Mouse Model with a Full Deletion of the *Ube3a* Gene. *Cells* **2022**, *11*, 2815. https://doi.org/10.3390/cells11182815

Academic Editor: Edor Kabashi

Received: 1 August 2022
Accepted: 31 August 2022
Published: 9 September 2022

1. Introduction

Angelman syndrome (AS) is a rare congenital neurodevelopmental disease affecting one in 10,000 to 40,000 births. The clinical manifestations in individual patients differ considerably. However, frequent phenotypes include a jerky ataxic gait, little to non-existent speech, profound mental retardation, sleep disturbances, and hyperactivity early in childhood [1,2]. Seizures occur in approximately 80% of patients and are often considered a characteristic of AS [3]. The disease stems from the imprinted 15q11.2–13q locus, meaning that it exhibits parent of origin specific expression of certain genes, hence defying classic Mendelian genetics. The main causative gene of AS is *UBE3A,* which encodes a ubiquitin E3 ligase. The gene is paternally imprinted in neurons, only allowing for maternal expression. However, it exhibits bi-allelic expression in non-CNS tissue. The paternal allele is silenced by a large antisense transcript, commonly referred to as UBE3A-ATS, by a mechanism still

being discussed [4]. The differential expression of genes in the locus are under the overall control of an imprint control region (ICR) acting in cis [4].

There are four main genetic etiologies causing AS, namely, (i) the de novo interstitial deletion of 15q11.2–13q on the maternally inherited chromosome [5]; (ii) paternal uniparental disomy [6]; (iii) imprinting defects due to aberrant epigenetic modification of the AS imprinting control region necessary for correct regulation [7]; and (iv) point mutations on the maternally inherited *UBE3A* gene. As mutations of this gene alone can cause AS, albeit with a milder phenotype, it is thus labeled as the AS gene [8,9]. The most common genetic cause for AS is the large deletion of the maternal 15q11.2–13q, which is found in approximately 70% of patients [10].

Although the occurrence of AS is equally distributed in both sexes, there is very little reported on the sex-dependent differences in humans [11,12]. However, few studies have reported sex-dependent differences in weight, anxiety, and cognitive and sensory phenotypes in AS mice [12–15]. In a study published by Koyavski et al. (2019) [12], they reported multiple genes exhibiting opposite sex-dependent transcriptional profiles between wild-type and AS mice. Many of them were linked to sensory phenotypes and several were estrogen-dependent, clearly showing the importance of sex on behavioral assessment [12].

For AS research, in terms of construct validity, the mouse organism serves as a useful and relevant model, as it has a syntenic region to the 15q11.2–13q locus on its chromosome 7, although with inverted orientation [16]. As for phenotypic similarity, the model needs to recapitulate robust phenotypes representative of AS to be useful for translational research.

Various mouse models mimicking AS have been generated and characterized, including deletions and substitutions of *Ube3a*, conditional *Ube3a* alleles, inducible *Ube3a* isoforms, *Ube3a* fusion to reporters, and large deletions encompassing multiple genes including *Ube3a* (Table 1) [17–19]. Models with intragenic modifications have been used to uncover the functions of the gene and its specific domains or isoforms (Table 1) [18,20–22]. Conditioned models allow for the cell-type-, tissue-, or developmental-stage-specific knockout of *Ube3a* and show the importance of spatiotemporal *Ube3a* expression [23–25]. Moreover, the role of individual *Ube3a* isoforms can be studied with inducible models such as Tg(tetO-Ube3a*2)^{884Svd} or Tg(tetO-Ube3a*1)^{1Svd} (Table 1). The models with tagged *Ube3a* were shown to be invaluable for the research, especially in deciphering the regulation, dynamics, and distribution of *Ube3a* expression in the studied models [26–29].

Table 1. Summary of Angelman mouse models (previously generated models are summarized and grouped depending on type of mutation).

Group	Strain	Genotype	Phenotype (Ube3a −/+)	Ref.
Deletions and substitutions	Ube3a^{tm1Alb}	Deletion of 100 N-terminal amino acids in the encoded protein and a frameshift inactivating all putative protein isoforms	Deficits in context-dependent learning (FC), impaired LTP (EP), increased abundance of p53 in PC (IHC), seizures, and motor disfunction (RRT, RCT)	[20]
	Ube3a^{tm2Yelg}	Nucleotide substitutions in exon 3 result in a stop codon for glutamic acid at position 113 (E113X).	MNTB neurons decreased failure rate (IJWR), faster recovery after AP in neurons, elevated AP amplitude (IJWR), AIS length increased (IHC), reduced STD and fast recovery from STD (IJWR)	[21]
	Ube3a^{em2Yelg}	The ATG codon (exon 3) encoding the start codon methionine of UBE3A isoform 2 was mutated into a TGA, resulting in expression of isoform 3 only.	Cytosolic Ube3a isoform, not critical for development of severe AS symptoms	[18]
	Ube3a^{em1Yelg}	An ATG codon (Ube3a exon 4/5) encoding the initiating methionine of UBE3A isoform 3 was mutated into an alanine (GCG). Therefore, only isoform 2 is expressed in these mice.	Nuclear Ube3a isoform, crucial for development. Deficiency leads to synaptic changes and impacts excitation and inhibition balance (VCR). Neurobehavioral phenotype confirmed by RRT NB, MB, FST, OF.	[18]
	Ube3a$^{em1(IMPC)Hmgu}$ (C57BL/6NCrl)	Intra-exon deletion (exon 3)	Assessed by IMPC pipeline, decreased locomotor activity (OF), decreased food intake (IC), decreased respiratory quotient (IC), increased hematocrit (HEM)	[22]
Floxed alleles	Ube3a$^{tm1.1Bdph}$	A floxed allele, exon 5 flanked by loxP sites.	Enhanced reward-seeking behavior (OS) due to lack of Ube3a in TH neurons (EP, VCR, IHC)	[23]
	Ube3a^{tm1Yelg}	A stop cassette with loxP sites inserted in intron CRE-mediated recombination reinstates gene expression.	Non-CRE recombined mouse recapitulates murine AS phenotype. Recombination leads to partial rescue of the phenotype on the protein (WB), neuronal (EP), and motor behavior levels (OF, MB, RRT, NB, FST)	[24]
	Ube3a$^{tm1a(KOMP)Wtsi}$	The critical exon(s) is/are flanked by loxP sites. FLP recombination generates a conditional allele. Subsequent CRE expression results in a knockout mouse. If CRE expression occurs without FLP expression, a reporter knockout mouse is created.	N/A	[25]

Table 1. *Cont.*

Group	Strain	Genotype	Phenotype (Ube3a −/+)	Ref.
Inducible isoforms	Tg(tetO-Ube3a*2)884Svd	The transgene under control of a modified Tet response element (TRE or tetO), transgene of mouse ubiquitin protein ligase E3A (Ube3a) cDNA sequence encoding transcript variant 2 (NM_011668.2) with FLAG tag, and an SV40 polyA signal	Anxiety-like behavior (EPMT, LD) autism (TCSIT), contextual learning deficit (FC), lower seizure threshold (EEG), reduced brain volume (MRI)	[30] unpublisde
	Tg(tetO-Ube3a*1)1Svd	The transgene under control of a modified Tet response element (TRE or tetO), transgene of mouse ubiquitin protein ligase E3A (Ube3a) cDNA sequence encoding transcript variant 1 (NM_173010.3) with FLAG tag, and an SV40 polyA signal	N/A	[31] unpublished
Modified Ube3a	Tg(Ube3a)1Mpan	Overexpression of Ube3a gene with three FLAG tags	Overexpression leads to development of autistic symptoms, impaired social behavior (TCSIT, RRT, OF, EMPT), decreased communication and repetitive behavior, impaired glutamatergic synaptic transmission, and glutamate release (EP).	[26]
	Tg(Ube3a)5Mpan	Extra copy of Ube3a transgene in the genome	Increased seizures, impaired social behavior (TCSIT, VT)	[27]
	$Ube3a^{tm1Jwf}$	A part of exon 15 and all of exon 16 are fused to IRES-lacZ-neo cassette, resulting in functional impairment of the C-terminal region responsible for ubiquitin protein ligase activity.	Allows Ube3a expression tracing based on LacZ staining, motor disfunction (RRT, BCT, FST), abnormal EEG), increased abundance of p53 in PC (IHC).	[28,32]
	$Ube3a^{tm2.1Alb}$ /$Ube3a^{tm2Alb}$	Fusion of yellow fluorescent protein (YFP) to exon expression of YFP is through inheritance of the maternal allele and recapitulates endogenous expression.	Phenotype not analyzed; the strain is mainly used to track Ube3a expression.	[29]
Large deletions	$Del(7Gabra3\text{-}Ube3a)^{1Yhj}$	The deletion extending from Gabra3 to Ube3a gene including Atp10a.	Homozygotes exhibit cleft palate and perinatal lethality. In AS mice, impaired behavior (LD, HP, USV, MWM, PPI), motor function (RRT, OF), and seizures	[17]
	Dp(7Herc2-Mkrn3)1Taku	Insertion of selection cassettes and loxP sites proximal to Herc2 and distal to Mkrn3. CRE-mediated recombination in ES cells led to balanced duplication and deletion of 6.3 Mb region between Herc2 and Mkrn3.	Duplication of the paternal allele results in poor social interaction, behavioral inflexibility, and abnormal ultrasonic vocalizations and correlates with anxiety (TCSIT, MWM, BMT, USV, FC) and altered 5-HT2c receptor signaling (EP).	[15]
	Del(7Herc2-Mkrn3)13FRdni	5Mb deletion of entire AS/PWS locus spanning from Herc2 to Mkrn3 genes via Lmp2a transgene insertion	Neurophysiological and behavioral phenotype, cellular morphology, impaired homeostasis and metabolism, increased mortality, aging, and respiratory problems. Analyzed for PWS only.	[19]
	Del(7Ube3a-Snrpn)1Alb	Deletion of genomic DNA from the loxP site within Snrpn to the loxP site within Ube3a	Neurophysiological and behavioral phenotype, impaired growth, increased mortality, aging, and muscle hypotonia. Analyzed for PWS only.	[33]
	$Oca2^{p-30PUb}$	This deletion expands distally from the p locus to Gabrb3, Ube3a, and Ipw. This deletion includes Atp10a.	Used for PWS and Atp10c research, homozygosity lethal, impaired modulation of body fat and/or affecting lipid metabolism (increased total fat)	[34]
	C57BL/6NCrl-Ube3a<em1(IMPC)Ccpcz>/Ph	Gene deletion	Impaired motor functions (RRT, GB, TST) and altered behavior (OF, EPMT, NB, BMT InteliCage)	This article

LTP: long-term potentiation, PC: Purkinje cells, FC: fear conditioning, EP: electrophysiology, TMF: testing motor function, RRT: rotating rod test, BCT: bar-crossing test, IHC: immunohistochemistry, WB: Western blot MNTB: medial nucleus of the trapezoid body, AP: action potential, AIS: axon initial segment, STD: short- term synaptic depression, IJWR: In vivo juxtacellular and whole-cell recordings, VCR: voltage-clamp recording, NB: Nest building, MB: Marble burying, FST: Forced-swim test, OF: Open field test, IC: indirect calorimetry, HEM: hematology, TH: tyrosine-hydroxylase-expressing neurons, OS: Optogenic stimulation, TCSIT: three-chamber social interaction test, EPMT: elevated plus maze tests, VT: video tracking, MWM: Morris water maze, PPI: prepulse inhibition, HP: hot plate, USV: ultrasonic vocalization, LD: light–dark exploration, BMT: Barnes maze test, GB: gait bait, TST: tail suspension test, NOR: novel object recognition, MRI: magnetic resonance imaging.

The most used mouse model in Angelman research is the $Ube3a^{tm1Alb1}$ generated by Beaudet and colleagues [20]. This model, based on a deletion of exon 5, referring to isoform 2, with a truncated and non-functional UBE3A, has proven to have a high face validity in phenotypes linked to motor skills, vocalization, seizure susceptibility, and behavioral patterns such as repetitive behavior but does not recapitulate severe cognitive deficits normally assessed by fear conditioning and water maze or similar test. Instead, the cognitive malfunction presents as mild or absent, depending on the strain and experimenter [35]. In a recent study, it was demonstrated that AS mice on the C57BL/6J background displayed behavioral impairments and the B6 AS mice differed in the cortical EEG power spectrum compared to WT mice during the light cycle, with significant increases in delta and theta power. The AS mice on the 129 background exhibited poor performance on the wire hang and contextual fear conditioning. The $Ube3a^{tmAlb1}$ animals also had a lower seizure threshold, both chemically and audiogenically induced, in comparison to wild-type animals [36]. The $Ube3a^{tmAlb1}$ F1 hybrid mice on the 129 and C57BL/6 backgrounds appeared to have milder phenotypes altogether [36]. The reported variations have demanded a further improved AS model with higher translational value.

The majority of AS patients harbor a large deletion including the entire *UBE3A* gene. However, the mouse model used in AS research is limited to a 3kb deletion [8]. We are describing a new mouse model in which the entire *Ube3a* gene is deleted, encompassing both the coding and non-coding elements of the gene, to obtain a higher similarity to the patients' situation. Furthermore, this new model was generated as part of the International Mouse

Phenotyping Consortium (IMPC, www.mousephenotype.org accessed: 25 March 2022), which is aiming to produce and phenotype a knockout mouse model for every protein-coding gene on a similar genetic background and utilizing shared standard operating procedures for phenotyping. The model was assigned the strain name C57BL/6NCrl-Ube3a<em1(IMPC)Ccpcz>/Ph, further referred to as Ube3a^{Genedel}. We characterized the Ube3a^{Genedel} model using a battery of phenotyping tests, adapted from the Sonzogni et al. (2018) [15], describing the AS pathology. These include tests connected to motor performance, stereotypic behavior, anxiety, and seizure susceptibility [15]. We adopted this test battery to either prove or disprove its utility in AS research. We found impaired motor skills, robust behavioral differences, changed circadian activity, and underperformance in memory flexibility.

2. Materials and Methods

2.1. Generation of the Ube3a^{genedel} Model

The Ube3a^{Genedel} mouse (C57BL/6NCrl-Ube3a<em1(IMPC)Ccpcz>/Ph) was generated on a C57BL/6N background (Charles River Laboratories) by targeting the 5^{1}UTR and the 3^{1}UTR of isoform 2 flanking the *Ube3a* gene (transcript Ube3a-203 ENSMUST00000200758.4) for a gene deletion by using the CRISPR/Cas9 technique. The guide RNAs (gRNAs) of highest score and specificity were designed using http://crispor.tefor.net/, accessed on 31 July 2022. The following guides were selected: Ube3a 5^{1}UTR gRNAs, U5-1: 5^{1}-CGCGGGTCCCGCATGA GACC-3^{1} and U5-2: 5^{1}-GCGCTTCAGCGCCGACTTCA-3^{1} and Ube3a 3^{1}UTR gRNAs, U3-1: 5^{1}-CCTTGCGAGAATAGTTTCGT-3^{1} and U3-2: 5^{1}-CTGTCCTTTCATATACTAAG-3^{1}. The gRNAs were assembled into a ribonucleoprotein (RNP) complex with Cas9 protein (1081058, 1072532, Integrated DNA technologies), electroporated into 1-cell zygotes, and transferred into pseudopregnant foster mice. Putative founders were analyzed by PCR and sequencing. A founder harboring a 76,225 bp deletion spanning the entire *Ube3a* gene was chosen for subsequent breeding. Genotyping was performed by junction PCR with 5^{1}UTR forward (5F) 5^{1}-CAGTCTCAAGATGGCGACGA-3^{1}, 5^{1}UTR reverse (5R) 5^{1}-CAATCCACCCCCAATACCCC-3^{1}, and 3^{1}UTR reverse (3R) 5^{1}-GCTACCATTATCCCCTGCCAA-3^{1}. The 5F and 5R products are 1183 bp, seen in all wild-types and AS mice. The 5F and 3R, only present in AS animals, have a size of 1602 bp, otherwise located ~77 kb apart in wild-type animals.

2.2. Mouse Husbandry, Breeding, and Experimental Cohorts

All animals and experiments used in this study were ethically reviewed and performed in accordance with European directive 2010/63/EU and were approved by the Czech Central Commission for Animal Welfare. Mice were housed in individually ventilated cages (Techniplast), genotyped at 14–21 days of age, and regenotyped after a battery of tests. All animals were kept at 22 ± 2 °C with a 12 h dark and light cycle and were tested during the light period and provided with mouse chow (Altramion) and water ad libitum. The transgenic mice were maintained on a *Ube3a*$^{+/-}$ zygosity, and animals for experiments were generated by crossing female *Ube3a*$^{+/-}$ animals with wild-type males to attain *Ube3a*$^{-/+}$ progeny and control littermates. Weight measurements started at four weeks and were repeated once per week until 15 weeks (WT n = 50; AS n = 26). All testing was performed during the light phase of the day on 9–18-week-old male and female mice. The testing was conducted on three animal cohorts consisting of an approximate 1:1 ratio between female and male mice for both genotypes (Table 2). Male and female mice were tested separately on different days. The tests in each cohort were conducted as follows: cohort 1 was tested with the rotarod, DigiGait, and tail suspension tests and nest building, cohort 2 was tested with the elevated plus maze, open field, novel object recognition test, and Barnes maze; and cohort 3 was tested with IntelliCage. Testing arenas, mazes, objects, and animal enclosures were thoroughly cleaned with 75% ethanol and then dried to remove olfactory traces before the first tested animal and between the tested animals.

Table 2. Sample sizes of animals used for cohorts (number of animals used in groups of every cohort).

Cohort	WT Males	Ube3a^{Genedel} Males	WT Females	Ube3a^{Genedel} Females
1	14	11	10	10
2	10	11	9	10
3	12	12	12	12

2.3. Western Blotting

Tissues were dissected, snap-frozen in liquid nitrogen, and lysed in RIPA buffer (0.05 M Tris-HCl, pH 8, 0.15 M NaCl, 0.5% deoxycholic acid, 1% NP-40, and 0.1% sodium dodecyl sulfate (SDS)), cOmplete™, EDTA-free Protease Inhibitor Cocktail (Roche, 5056489001), and PhosSTOP™ phosphatase inhibitor tablets (Roche, 4906845001, Darmstadt, Germany). Lysates were sonicated and cleared by centrifugation; the protein concentration was determined using the Pierce™ BCA Protein Assay Kit (Thermo Scientific, 23225, Rockford, IL, USA). Equal amounts of protein (20 µg) were analyzed by Western blotting, where anti-Ube3a (1:2000, BD Biosciences, 611416, Brno, Czech Republic) and anti-B-actin (1:5000, Sigma-Aldrich, A2228, Darmstadt, Germany) were used as primary antibodies. Blots were washed with PBS-T, and detection was performed with SuperSignal™ West Pico PLUS Chemiluminescent Substrate (ThermoScientific, 34579, Rockford, IL, USA). The Western blots were quantified using ImageJ analysis, and the sample size was $n = 8$ with a 1:1 ratio for the sexes.

2.4. Rotarod

The rotarod system was used to assess the sense of balance, motor learning, and motor coordination in the animals [37]. Three trials per day for each mouse were recorded on a rod with an accelerating speed of rotation (4–40 rpm/5 min, RotaRod, TSE Systems GmhB, Berlin, Germany) during five consecutive days. The average latency to fall was determined from the three trials with 15 min intratrial intervals (ITI).

2.5. Gait Analysis

Each animal was placed on a motorized treadmill with a belt speed of 20 cm/s (DigiGait, Mouse Specifics, Ins., Framingham, MA, USA). A minimum of five fluent strides were recorded by a camera positioned below the belt to focus on the ventral view of the animal. The DigiGait software (Mouse Specifics, Ins., Framingham, MA, USA), which recognizes and evaluates over 50 gait indices describing walk quantitative metrics, kinematics, and animal posture, automatically analyzed the recordings [38].

2.6. Tail Suspension Test

The tail suspension test (TST) was used to assess tendencies for depressive-like behavior [39]. The tested animal was attached to an apparatus hook and left suspended for six minutes. The immobility time, energy, and power in motion were analyzed using BIO-TST 4.0.2.1 (Bioseb, Vitrolles, France) software.

2.7. Open Field

The activity of the animals in a novel environment and the displayed level of anxiety were evaluated in open field (OF) tests as previously described [40]. The area of the open field was a square of 42 × 42 cm that was uniformly illuminated with a light intensity of 200 lux at the center of the field. The testing arena was virtually divided into periphery and center zones, where the center zone constituted 38% of the whole arena. Each mouse was placed in the corner of the arena for a 10 min period of free maze exploration. The time spent in each zone, the distance travelled, and other indices were automatically computed based on video recordings (Viewer, Biobserve GmbH, Bonn, Germany).

2.8. Elevated plus Maze

The elevated plus maze (EPM) apparatus consisted of two closed and two open elevated arms, with a light intensity of 60 lux at the center of the maze [41]. The subject animal was placed at the center and was left to explore the EPM for five minutes. The total time spent in the open and closed arms and the center of the EPM were tracked and evaluated automatically (Viewer software, Biobserve GmbH, Bonn, Germany).

2.9. Novel Object Recognition

The novel object recognition test (NOR) was used to evaluate animal exploration of a novel object as a measure of working memory and attention [42]. The test, fully automated and based on a video tracking system (Viewer, Biobserve GmbH, Bonn, Germany), was preceded by two days of 10 min-long habituation to the testing maze. Familiarization with two identical objects was performed on the following day. The probe trial with one familiar and one new object took place after a three-hour-long retention time. All trials were undertaken with 70 lux illumination at the center of the maze. The objects were placed 7.5 cm from the walls, alternating to different sides of the quadrant, and the subject was always placed on the opposite wall from the objects to counterbalance the relative position. Object visits, object exploration time, and the percentages of listed parameters were automatically computed for each object.

2.10. Nest Building

An evaluation of material usage for nest building was performed as previously described by Sonzogni et al. [15]. Mice were first separated to single cages for a week. Following accommodation to single housing, 12 g of FDA Nestlets (Datesand Ltd., Manchester, UK) were introduced to each cage for five consecutive days. The unused material in the nest was weighed at the same time each day.

2.11. Barnes Maze

Spatial learning and memory were analyzed according to a previously published protocol [43]. We used a random pattern of holes to prevent mice from using a serial strategy to find the escape box [44]. Except for the first habituation day, where a low-light condition (70 lux) and no noise were used, the entire procedure was performed in high-aversive conditions, with an illumination of 200 lux and moderate background noise, to motivate the animals to search for the escape target box. During the two-day habituation phase, the mice were allowed to explore the maze for 7 min to find an escape box positioned in a different place each day. If the subject animal failed to find the escape box, it was gently guided in a glass container to the target and left there for 30 s. The next stage was a 5-day training session, during which four different escape box positions in the maze were used alternately as follows: The specific escape box position for each individual animal varied, but each individual animal was trained for the same escape box position during all 5 days of the training session. The mice were allowed to find the target hole during two 3 min-long trials with an approximately 2 h ITI on each day of the acquisition stage. The animals were tested in a probe trial 24 h after the last day of the acquisition. During the 1 min of the probe trial, no escape box was present in the maze. Video recordings were automatically analyzed by the Viewer software (Biobserve GmbH, Germany). Primary distance, latency, and errors to reach the target hole were used for further analysis. Additionally, the time and distance in the target quadrant were evaluated during the probe trial.

2.12. Testing in Home-Cage Environment IntelliCage

For the evaluation of circadian activity, we used the free adaptation protocol in the IntelliCage system (TSE Systems GmbH), which enables the testing of grouped animals in a home-cage environment [45], eliminating stressful conditions originating from animal handling during experimentation. Each IntelliCage is equipped with four operant corners with access to water. Each corner detects animal presence and identifies every individual

with a radio-frequency identification (RFID) antenna that detects subcutaneously implanted transponder signals. The IntelliCage system collects information on entries and exits from the corner during a real time scale and records information on the frequency and duration of licks during each visit in every corner. The number of corner visits without licks was calculated to remove the effect of drinking motivation on general activity. Males and females were tested in separate cages. The mice were introduced to the IntelliCage for a free-adaptation regime for a week, and the animals had free access to water. The latencies to the first visit and lick were recorded to evaluate the animal novelty response. The temporal distribution of visits and their frequency were recorded to compare experimental group circadian activity. To assess spatial learning in place preference, each mouse was assigned to one rewarding (correct) corner to drink for five consecutive days. Upon visiting the correct corner, the mice were rewarded with 7 s of access to water. After the behavioral acquisition of the task, the learning flexibility was evaluated with a reversal place preference phase, where the correct corner was changed to the diagonally opposite one for each animal for five consecutive days.

2.13. Statistical Analyses

For the main genotype, sex, and interaction effects, a two-way ANOVA, with dependent measurements where needed, was used if the data distribution met the normality assumption. A robust ANOVA of aligned rank transformed data, with dependent measurement where needed, was used if the data distribution did not meet the normality assumption. Tukey's post hoc test for normally distributed data or the Wilcoxon post hoc test for non-normal data distributions were used to assess differences within sex and genotype. Statistical analysis was performed in R version 4.1.2 (2021-11-01) with the stats version 4.1.2, ARTool version 0.11.1, and rstatix version 0.7.0 packages. All data are presented as means ± SD or medians with interquartile ranges.

3. Results

3.1. The New Ube3a^{genedel} Model Harbors a Large Deletion Spanning the Entire Ube3a Gene

The Ube3a^{genedel} model was generated using CRISPR/Cas9, resulting in a founder harboring a deletion of the gene from the 5′UTR to the 3′UTR (Figure 1A). Subsequent sequencing confirmed a deletion of 76,225 bp, mediated by corresponding gRNAs (Figure 1A); this founder was further selected for by the breeding of the F1 progeny.

Screening the putative founders with junction PCR revealed one founder with an appropriate amplification using the 5F, 5R, and 3R primer triplet (Figure 1B). Western blotting confirmed a near complete abolishment of protein expression in CNS tissue, with the limited detectable expression coming from non-neuronal cells. In the non-imprinted liver tissue, there was a decrease in UBE3A to half of that seen in WT animals (main genotype effect; $p < 0.001$; Figure 1C,D). The Ube3a^{genedel} mice and controls were weighed once per week from four weeks to 15 weeks of age, and both female and male Ube3a^{genedel} mice were significantly heavier than their litter mate controls (main genotype effect; $p < 0.001$; Figure 1E,F).

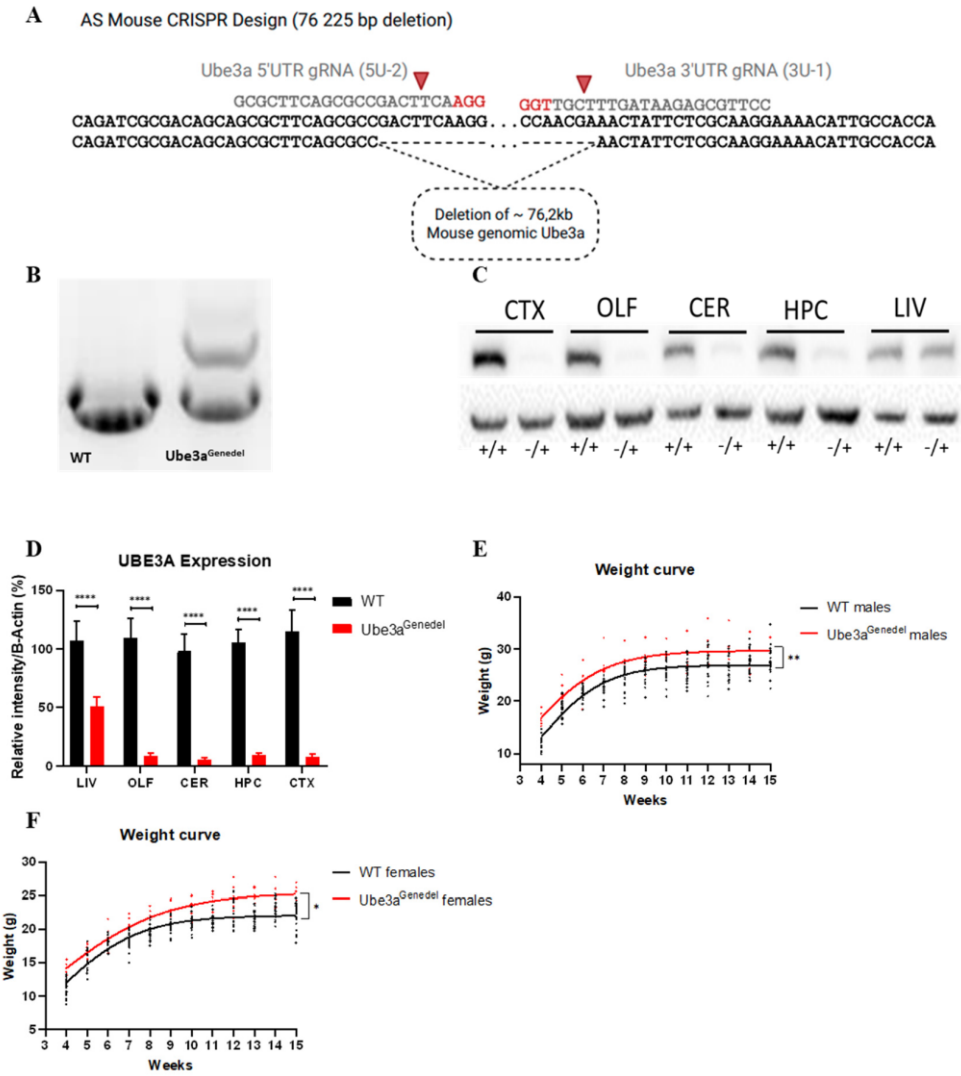

Figure 1. The Ube3a^{Genedel} mouse model. (**A**) Schematic of the Ube3a^{Genedel} deletion, a 76,225 bp deletion range from 58,878,821 to 58,955,045, *Mus musculus* strain C57BL/6J chromosome 7, GRCm39 (NC_000073.7). The gRNA generating the cut are indicated. (**B**) Representative amplification of WT control and Ube3a^{Genedel} DNA, with the WT showing one band of 1183 bp and the Ube3a^{genedel} showing an additional at 1602 bp. (**C**) A representative Western blot showing a near complete reduction in UBE3A in several brain regions and a decrease to half in liver tissue. (**D**) A quantification of the UBE3A expression from Western blot; two-way ANOVA main genotype effect $p < 0$. CTX: cortex, OLF: olfactory bulb, CER: cerebellum, HPC: hippocampus, LIV: liver. (**E**,**F**) Graph of weight recordings from 4 weeks to 15 weeks. All data represent means ± SD. Significant effects of genotype are indicated as * $p < 0.05$, ** $p < 0.01$ and **** $p < 0.0001$ for genotype significance.

3.2. Gait Impairment and Impaired Motor Skills Are Recapitulated in The Novel Ube3a^{genedel} Mouse

Ataxia and severely impaired motor skills are consistently present in individuals with AS, manifesting with an ataxic gait with tremor. Furthermore, this phenotype is one of the key clinical features for diagnosis [46]. We performed a detailed gait analysis using the DigiGait platform to assess the gait in the animals. This system allows for both spatial and temporal analyses of gait parameters. We found that the Ube3a^{genedel} mice exhibited prolonged durations in parameters such as swing, stance, stride, and propel (main genotype effect; F = 48.131; F = 54.346; F = 94.802; F = 20.098; $p < 0.001$ for all parameters; Figure 2A–E). Other characteristics, such as MAX dA/dt (maximal rate of change of paw area in contact with the treadmill belt during the braking phase), paw area at peak stance, and stride length,

were increased (main genotype effect; F = 26.929; F = 33.725; $p < 0.001$ for all parameters; Figure 2F,G).

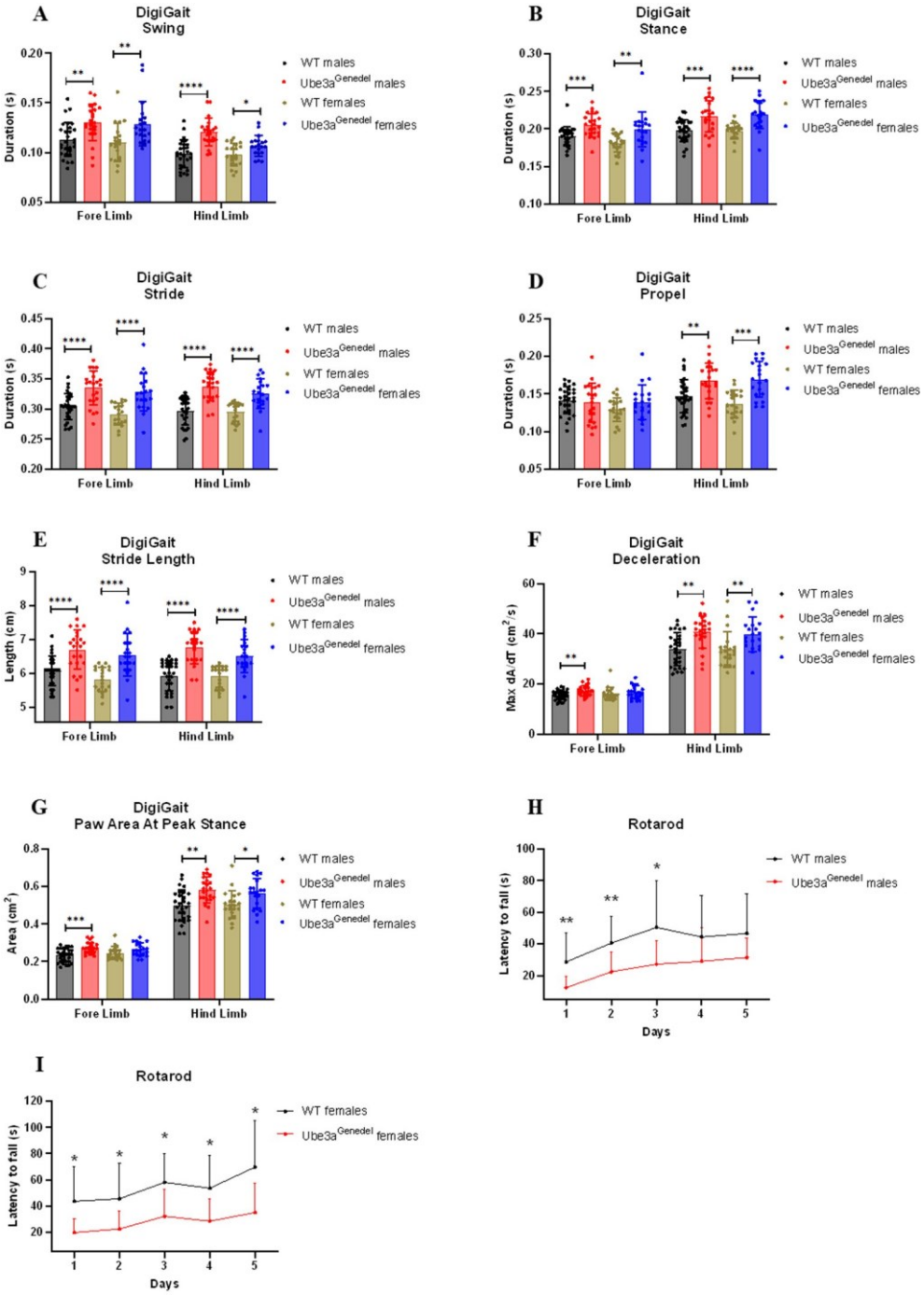

Figure 2. Results of gait analysis and rotarod. (**A**–**G**) Gait parameters were measured with the DigiGait platform. The data show an increase in the duration of swing, stance, stride, and propel in Ube3a^{genedel} animals. Stride length, MAX dA/dt, and the paw area at peak stance were also increased in Ube3a^{genedel} animals in both sexes; two-way ANOVA: genotype main effect, $p < 0$. (**H**,**I**) Ube3a^{genedel} mice had significantly shorter latency to fall; two-way ANOVA with dependent measurements genotype main effect: $p < 0$. All data represent means ± SD. Significant effects of genotype are indicated as * $p < 0.05$, ** $p < 0.01$, *** $p < 0.001$, and **** $p < 0.0001$ for genotype significance.

The motor coordination and balance of the mice were evaluated on the rotarod apparatus. We found that the Ube3a^{genedel} mice had a significantly shorter latency to fall, which further confirmed the observation that the mice have motor skill dysfunction (main genotype effect; F = 54.111; $p < 0.001$; Figure 2H,I). The weights of the mice were plotted against the latency to fall to investigate any putative weight bias. However, weight was not a significant factor (factor of weight; $p > 0.05$; Supplementary Figure S1).

3.3. The Ube3a^{genedel} Model Exhibits Robust Behavioral Impairment

To assess general activity and anxiety, we used open field and elevated plus maze tests. In the open field test, male Ube3a^{genedel} mice appeared to be hypoactive, as the distance walked and average speed were decreased, whereas the resting time was increased (main genotype effect; F = 9.233; F = 9.268; F = 10.033; $p < 0.01$ for each parameter; sex/genotype interaction $p > 0.05$; Figure 3A–C); females exhibited similar tendencies, but the results were not significant. However, no significant differences in the number of entries into the anxiogenic center nor the time spent there were observed, which indicates that there is no general anxiety-like phenotype in Ube3a^{genedel} mice (main genotype effect $p > 0.05$; F = 3.34; F = 0.00; Figure 3D,E). The observation was confirmed by the results from the elevated plus maze, where mice of both genotypes spent comparable time in the anxiogenic open arms (main genotype effect; F = 2.88759; $p > 0.05$; sex/genotype interaction $p > 0.05$; Figure 3F–H).

The mice were further tested for other behavioral phenotypes, such as their innate instinct to create a nest via the nest building test [47]. Here, we found that Ube3a^{genedel} mice underperformed in the task, as commonly occurs in mice with neurodegenerative disease [47] (main genotype effect; F = 4.86599; $p < 0.05$; sex/genotype interaction $p > 0.05$; Figure 4A,B). The results from TST showed that Ube3a^{genedel} mice spent a significantly longer time immobile compared to the WT controls (main genotype effect; F = 20.326; $p < 0.001$ sex/genotype interaction $p > 0.05$; Figure 4C) which is a characteristic of depressive-like behavior.

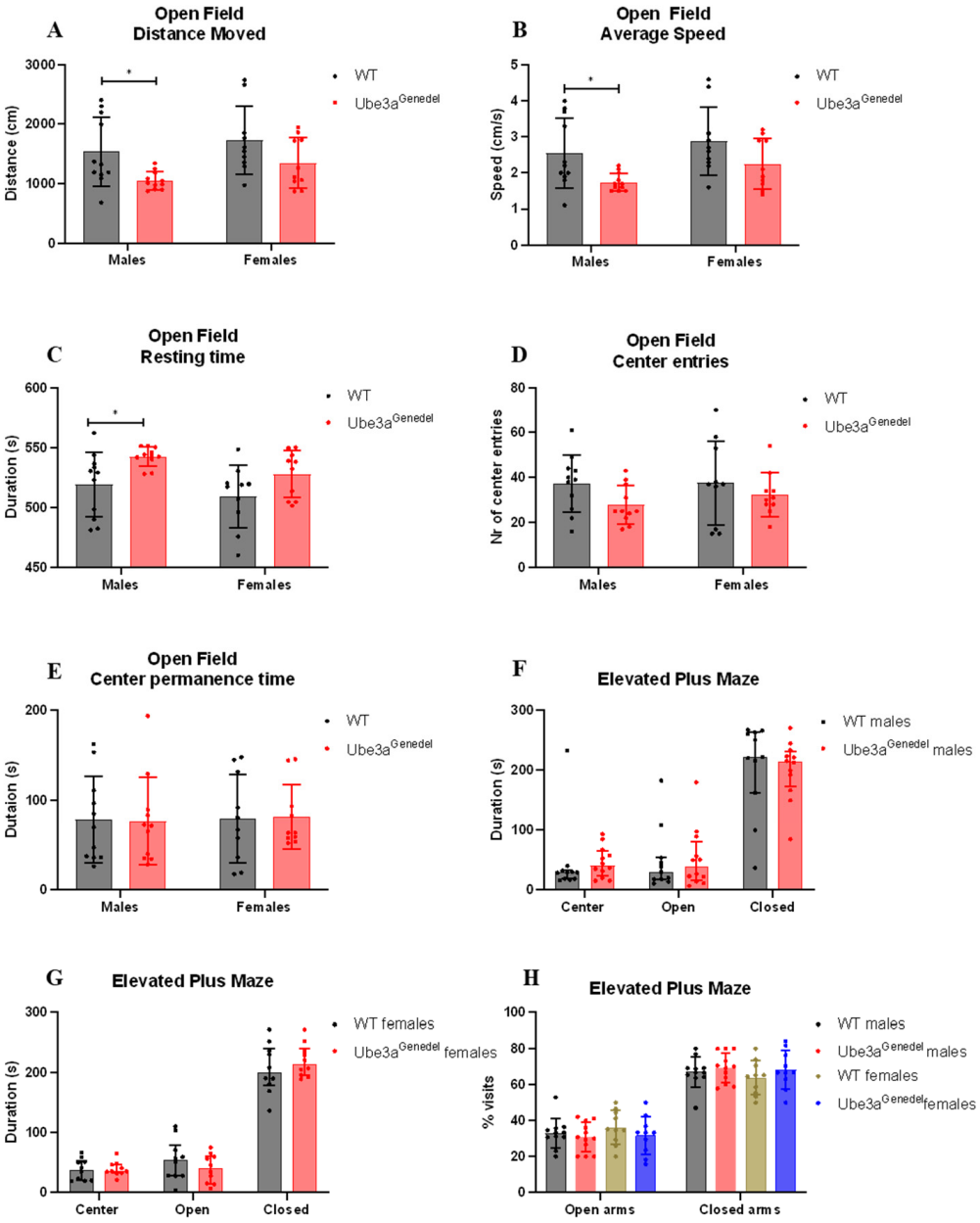

Figure 3. Activity and assessment of general anxiety with open field and elevated plus maze. (**A**–**E**) The performance in the open field for the parameters total distance moved, average speed, resting time, center entries, and center permanence time. The Ube3a^{genedel} mice exhibited increased resting time, while the total distance moved and average speed were decreased; two-way ANOVA with dependent measurements genotype main effect, $p < 0.01$, depicted with means ± SD. (**F**–**H**) Time spent in the center, open, and closed configuration of the EPM, showing no significant alteration in duration or percentage between the genotypes; robust ANOVA of aligned rank transformed data with dependent measurements genotype main effect, $p > 0.05$, depicted with medians and interquartile ranges. Significant effects of genotype are indicated as * $p < 0.05$ for genotype significance.

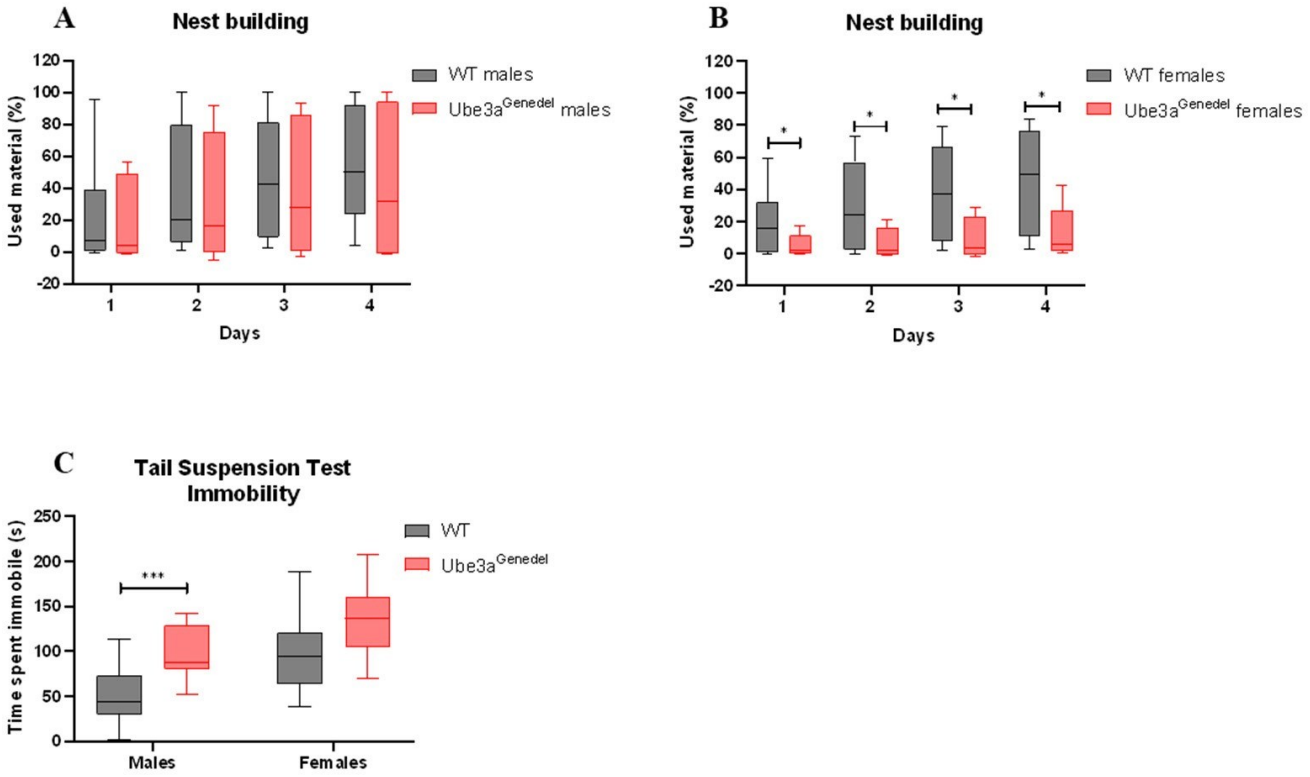

Figure 4. Results from nest building and tail suspension tests. (**A**,**B**) The Ube3a^{genedel} mice used significantly less material for nesting; robust ANOVA of aligned rank transformed data with dependent measurements, genotype main effect, $p < 0.05$, depicted with medians and interquartile ranges. (**C**) Ube3a^{genedel} mice spent significantly more time immobile during the last four minutes of the test; two-way ANOVA with dependent measurements, genotype main effect, $p < 0.001$, depicted with means ± SD. Significant effects of genotype are indicated as * $p < 0.05$ and *** $p < 0.001$ for genotype significance.

3.4. Memory and Learning Were Not Impaired in Ube3a^{genedel} Mice in Barnes Maze and Novel Object Recognition Tests

Severe cognitive disabilities are a key characteristic of AS, and we aimed to assess the cognitive phenotype in the Ube3a^{genedel} model using the Barnes maze and NOR tests. The learning curve, measured by the latency and primary distance needed to find an escape box during the Barnes maze learning phase, did not differ between genotypes (main genotype effect $p > 0.05$; F = 0.478; sex/genotype interaction $p > 0.05$; Figure 5A,B). The memory of the animals also did not differ in the probe trial, where the time spent and distance walked in the target quadrant were estimated (main genotype effect $p > 0.05$; F = 2.566; sex/genotype interaction $p > 0.05$; Figure 5C).

When subjecting the mice to the NOR test, we found no significant difference in the percentage of the duration spent with the new object between the genotypes or sexes (main genotype effect; F = 0.088525; $p > 0.05$; sex/genotype interaction $p > 0.05$; Figure 5D). We conclude, based on these experiments, that the animals do not exhibit cognitive impairments in easier tasks.

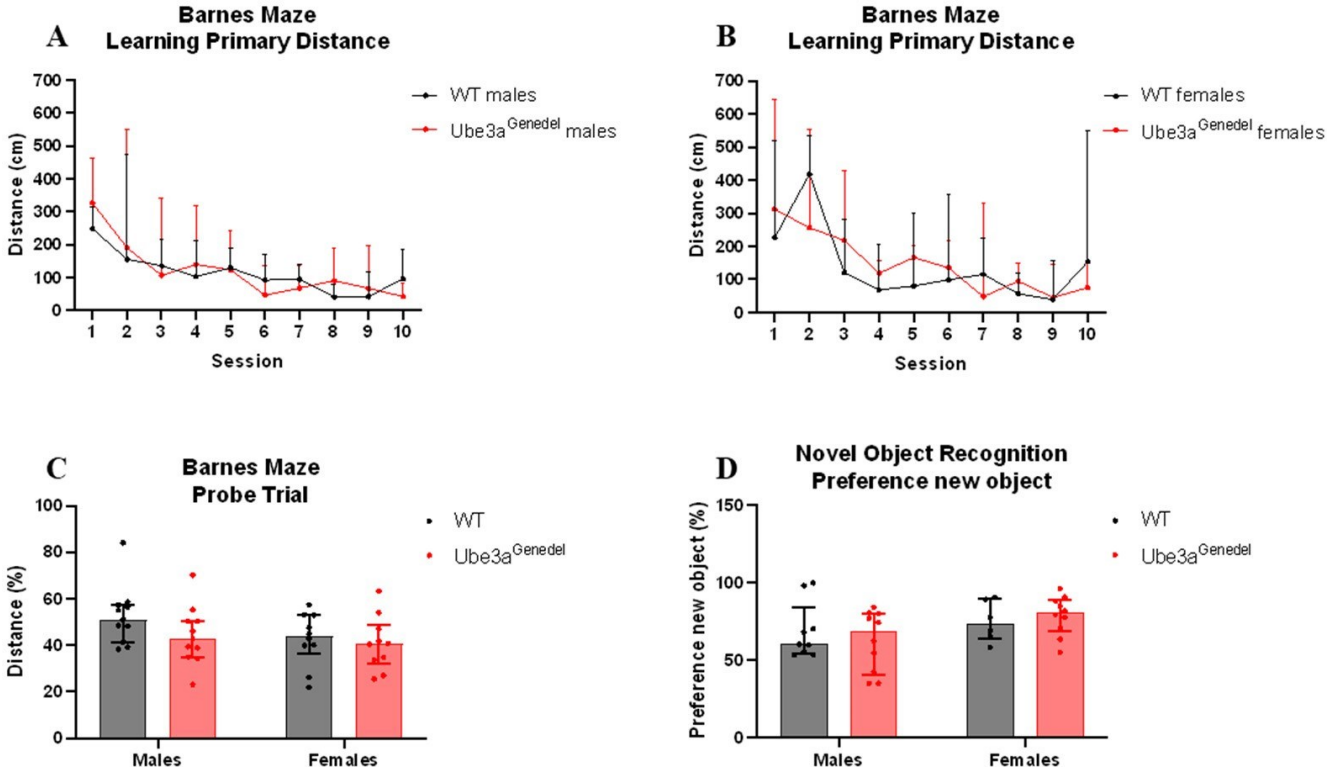

Figure 5. Learning and memory assessment. (**A**–**C**) The durations of the learning phase and probe trial were not significantly altered between genotypes; robust ANOVA of aligned rank transformed data with dependent measurement, $p > 0$. (**D**) No significant differences in the percentage of time spent with a new object between the genotypes, robust ANOVA of aligned rank transformed data with dependent measurement main effect, $p > 0$. All data represent medians with interquartile ranges.

3.5. Home-Cage Circadian Activity, Response to Novelty, and Performance in Place Reversal Tasks Differ in Ube3a^{genedel} Animals

The circadian activity, drinking behavior, and memory of the mice were evaluated using the IntelliCage paradigm. Male Ube3a^{genedel} mice exhibited significant increases in latency to the first corner visit and the first lick after introducing animals into the IntelliCage (main genotype $p < 0.001$; F = 20.139, F = 4.561; genotype/sex interaction $p < 0.05$; Figure 6A,B). A post hoc analysis showed that only the Ube3a^{genedel} males exhibited increased latency in the tested parameters (Figure 6A,B).

The number of corner visits was recorded and displayed over the course of the day (Figure 6C,D). There were no significant differences in total visits (main genotype effect $p > 0.05$; Supplementary Figure S2C). However, there were differences in activity depending on the phase of the day (main genotype effect; $p < 0.001$; F = 1.35; genotype/time interaction $p < 0.05$; Figure 6C,D). A subsequent post hoc analysis revealed that the Ube3a^{genedel} mice's decrease in corner visits was pronounced during the light phase of the day (Figure 6C,D). When visits with licks were included, the significant difference disappeared (main genotype effect $p > 0.05$; Supplementary Figure S2A–C).

The number of licks was increased in the Ube3a^{genedel} mice during a 24 h period (main genotype effect; F = 10.52; $p < 0.01$; sex/genotype interaction $p > 0.05$; Figure 6E,F). A subsequent post hoc analysis showed that this was pronounced during the dark phase, but the opposite tendency was seen during the light phase. However, the overall number of licks during a 7-day period showed a clear increase in licks in Ube3a^{genedel} animals (main genotype effect $p < 0.001$; Supplementary Figure S2D). An additional analysis showed that AS animals made more licks per visit (main genotype effect $p < 0.001$; sex; genotype interaction $p > 0.05$; Supplementary Figure S2E).

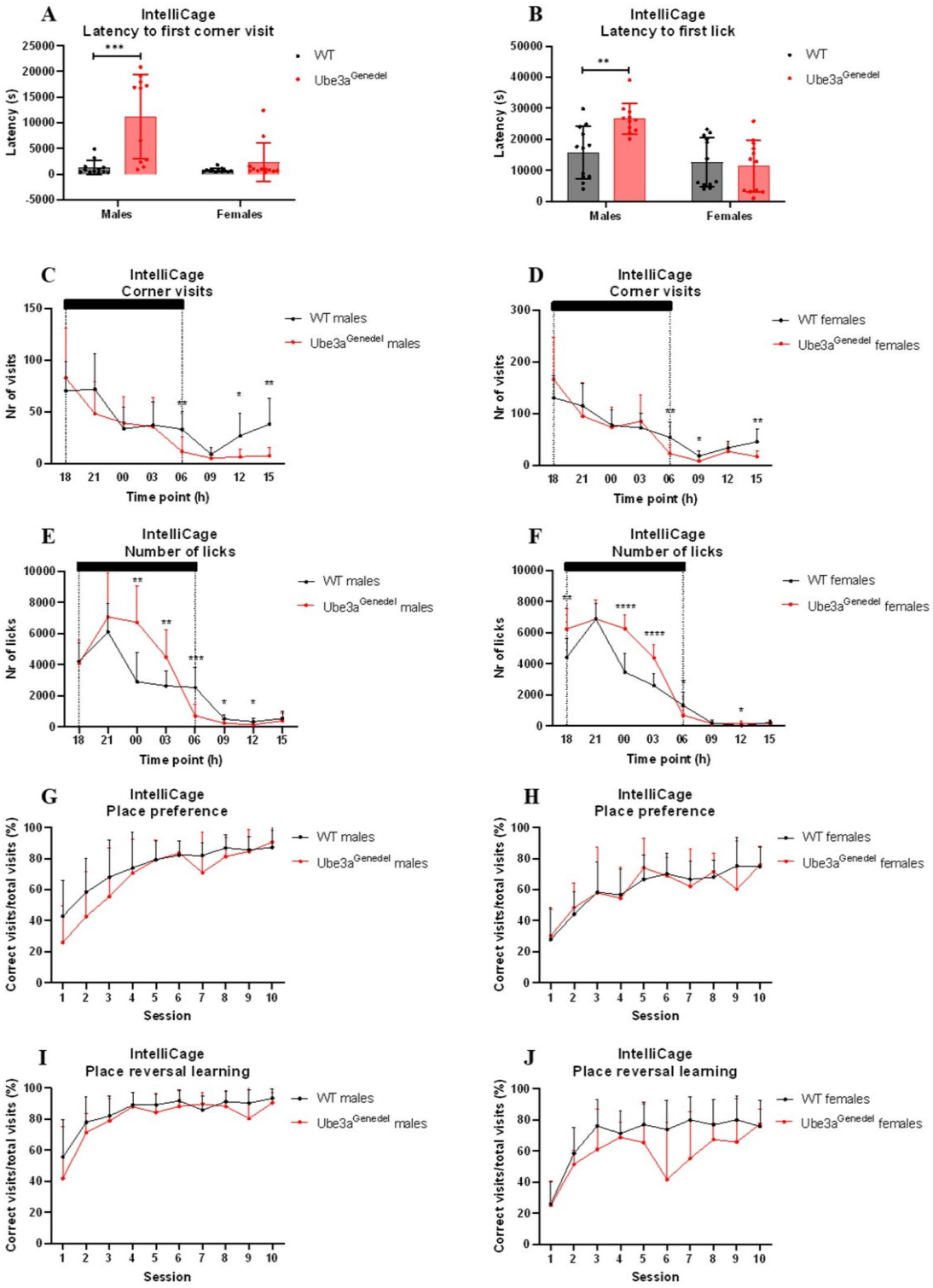

Figure 6. Results from IntelliCage measurements. (**A**,**B**) Ube3a^{genedel} male mice exhibited increased latency to first corner visit and first lick over 7 days. (**C**,**D**) Ube3a^{genedel} mice visited the corners less than WT littermates, which was pronounced during dark phases (shadowed). (**E**,**F**) Ube3a^{genedel} mice exhibited an increase in lick number over the entire period. (**G**,**H**) Control and Ube3a^{genedel} mice exhibited similar learning memory in place preference test. (**I**,**J**) Ube3a^{genedel} mice exhibited less correct visits to rewarding corners than control animals during 10 sessions of reversal learning. Two-way ANOVA with dependent measurements, genotype main effect, $p < 0.001$, depicted with means ± SD. Significant effects of genotype are indicated as * $p < 0.05$, ** $p < 0.01$, *** $p < 0.001$, and **** $p < 0.0001$ for genotype significance.

We found no significant difference between Ube3a^{genedel} and WT mice in place preference phase (main genotype effect $p > 0.05$; F = 0.01; Figure 6G,H).

Place preference reversal learning showed that Ube3a^{genedel} animals significantly underperformed, exhibiting a lower percentage of correct visits to the rewarding corner (main genotype effect $p < 0.05$; F = 5.04; sex/genotype interaction $p > 0.05$; F = 0.10; Figure 6I,J).

4. Discussion

We employed the CRISPR/Cas9 technology to produce a new AS model, deleting *Ube3a* from the 5^{I}UTR to the 3^{I}UTR. In regard to the isoform in lysates from the Ube3a^{genedel} mice, a Western blot analysis of several regions in the CNS showed a near complete reduction in the UBE3A protein, with parts of it remaining due to the paternal contribution from non-neuronal cells [48]. The liver, a tissue exhibiting bi-allelic expression of UBE3A, was also analyzed, showing a near 50% reduction in the protein.

The rationale to produce a mouse model mimicking AS, in addition to the already existing and well-characterized models, was to generate a model harboring a deletion encompassing the entire *UBE3A* gene, as ~70% of AS patients have a large deletion of the locus [20]. This could complement other AS models and reveal additional information about gene importance in addition to the most studied model generated by the Beaudet lab [20].

To evaluate our new model in terms of its phenotypic suitability for AS research, we subjected it to a battery of tests aimed at the characterization of AS phenotypes. We used the behavioral test battery put forth by the Elgersma lab, with some adaptation [15]. Ataxia and severely impaired motor skills are consistently present in AS patients, manifesting in an ataxic gait with tremor. This phenotype, one of the key clinical features for diagnosis [49], was demonstrated in the Ube3a^{tmAlb1} model [50]. For instance, the mice performed poorly on the accelerating rotarod and exhibited a distorted gait with wider, longer, and fewer steps compared to wild-type littermates [36,51].

We evaluated motor skills with the rotarod test and with the detailed gait analysis in DigiGait. It was revealed that the Ube3a^{genedel} mice significantly underperformed in the rotarod task, with a shorter latency to fall. This was true for both female and male Ube3a^{genedel} mice, although the increased weight in Ube3a^{genedel} mice could be a confounding factor. However, a linear regression analysis revealed no significant weight/latency correlation, thereby excluding the influence of animal weight on rotarod performance (Supplementary Figure S1A,B). Our data also corresponded to observations made in another study, clearly indicating that the increased weight in AS animals is not a reason for underperformance [15]. In addition, we performed a detailed gait analysis using the DigiGait system to evaluate each of the four limbs, ultimately defining the posture and kinematics and allowing for the extrapolation of strength, coordination, and balance in the animals. We assessed the duration of common gait characteristics such as swing, stance, propel, and stride. We found an increase in the duration of all four parameters and longer strides. An increase in the propel duration, defined as the time spent in the air between steps, indicates reduced strength and control of movement [52]. Additionally, we collected data on the deceleration and the paw area at peak stance. We found that the Ube3a^{genedel} mice exhibited increased deceleration, which has been reported to be an indicator of reduced muscle strength [53]. A larger contact area of the paws at peak stance may act to stabilize the posture and balance [54].

Based on our data collected from the rotarod and DigiGait, we conclude that the novel Ube3a^{genedel} mice recapitulate the motor deficits seen in AS patients and could be of translational value for therapeutics aimed towards improving the motor phenotype.

We set out to evaluate whether our new Ube3a^{genedel} model exhibits any behavioral impairments, which are a hallmark phenotype in AS patients [1], and found that both sexes of Ube3a^{genedel} mice were hypoactive in the open field test. This has been reported in multiple studies using other AS mouse models [15,35]. The Ube3a^{genedel} mice showed

significantly increased resting time and decreased average speed and total distance walked. The detected hypoactive phenotype in our Ube3a^{genedel} model opposes what is found in AS patients. AS patients are frequently reported to exhibit hyperactivity during childhood. However, this was shown to decrease with age [55]. Regarding the evaluation of anxiety, there were no differences in time spent in the center or the number of entries into the center, suggesting that the mice are not more anxious than their WT littermates. We also subjected mice to the elevated plus maze test, where we did not observe any significant differences between the genotypes, again suggesting an absence of an anxiety-like phenotype. This is opposed to the findings in other studies, where the investigators have observed increased anxiety-like behavior when using the open field and elevated plus maze tests [15,24,36,56]. Our results are, however, in line with previously conducted studies on the Ube3a^{tmAlb1} model, where the mice clearly exhibit hypoactivity in open field tests. The reason for the observed hypoactivity could be the increased weight of the animals [15].

Another relevant neurobehavioral parameter is nest building, and the Ube3a^{genedel} mice exhibited a reduction in nest building activity, thus showing a sign of distress, a hallmark of neurodegenerative diseases [48]. Although we observed a main genotype effect, a subsequent post hoc analysis revealed that females were more affected, aligning with the fact that females are more likely to nest. Lastly, we evaluated the animals' behavior in the tail suspension test, a commonly used tool to assess depressive-like behavior. Our Ube3a^{genedel} mice were significantly more immobile in this test, corresponding well with similar tests performed on the Ube3a^{tmAlb1} model [36], exhibiting no sex-dependent differences.

Regarding the cognitive functions, the Barnes maze test was used to assess any impairments in hippocampal-dependent learning, a phenotype presented in AS patients [44,57]. The results did not reveal any hippocampal-dependent cognitive malfunctions. Additionally, there were no significant differences in the NOR test assessing the short-term memory of animals. A possible reason for the lack of a cognitive phenotype is likely the age of the mice. In a study by Huang et al. (2013) [56], the authors showed that the AS mice from the B6 strain had deficits in spatial learning acquisition after 16 weeks but not at 8 weeks of age, showing that cognitive function becomes impaired with time [56]. As our cohort of mice were younger than 16 weeks at the time of testing in the Barnes maze and NOR test, this could potentially be the reason as to why we did not observe any cognitive dysfunction. We did, however, test the animals in place preference and reversal place preference learning paradigms, where mice needed to modify already learned behavior, observed using the IntelliCage setup at the age of 18 weeks. We observed a specific cognitive impairment of reversal learning in the Ube3a^{genedel} animals, but no impairment was seen in the initial place preference acquisition. A deficit in reversal learning has also been described in animal models of autism, where the Morris water maze or T-maze task were used [58–60]. Ube3a^{genedel} animals performed equally in reward-motivated place preference learning but showed deficiency in behavioral flexibility measured by reversal learning.

Lastly, we evaluated our Ube3a^{genedel} model for circadian activity and novelty response using the IntelliCage paradigm. The latency to the first visit of the corners and the latency to the first lick were increased in Ube3a^{genedel} males but not in females. The increased latency could be interpreted as a decreased exploratory drive and not necessarily due to increased anxiety-like behavior, which was strengthened by a detailed analysis of animal activity that revealed a marked attenuation of corner exploration during the light phase of the day [61]. Nonetheless, an important factor to take into account is the hypoactivity seen in our Ube3a^{genedel} mice in both sexes. However latency was only affected in males. The total number of corner visits over 24 h did not differ, whereas visits not motivated by drinking, visits without licks, were decreased during the light phase of the day. Ube3a^{genedel} animals drank more during the dark phase due to higher number of licks per visit. This could be due to the overall larger size of the Ube3a^{genedel} mice, but it could also be possible that the Ube3a^{genedel} mice are drawn to the water per se, as AS patients are characterized by a fascination with water [62]. However, we do not have the data to make such a statement.

The variation in animal ages needed for the different behavioral and cognitive paradigms is a clear barrier for testing new drugs or evaluating other therapeutic interventions in the Ube3a^{tmAlb1} mouse model, as cognitive deficits appear later on, while the reflex phenotype is seen only in juvenile mice [56].

As briefly mentioned in the introduction, it is important to take sex-dependent differences into account when evaluating behavioral and cognitive phenotypes in mice. Indeed, we did observe differences in nest building, where AS females used significantly less material for nest building than WT littermates, a difference that was not seen between WT and AS males. We also detected a more pronounced impairment in place reversal in AS females compared to WT than in males. The sex-dependent differences in the cognitive and behavioral aspects correspond well to findings reported by Koyavski and colleagues. They observed differences in neurobehavioral aspects where the AS mice either lacked differences between the sexes or showed opposed differences from WTs [12]. They did not observe any sex-dependent differences in motor phenotypes, again corresponding well with our results, as the AS mice of both sexes underperformed in the rotarod test and displayed distorted gait. Interestingly, they found sex-dependent differences in the transcriptome of AS mice as well, with several genes being estrogen-dependent [12]. Indeed, where the mice are in the estrous cycle plays a role in behavior and cognition, as the estrous-related hormones estrogen, progesterone, and their metabolites bind to steroid receptors in the brain, exerting influence on the mentioned parameters [63,64]. Unfortunately, we did not assess the estrous cycle in our females, which can be considered a limitation of the study method. There is limited information on sex-dependent differences in AS individuals, but the cycle in AS female subjects could possibly impact the assessment of the efficacy of therapeutic interventions and likely should be addressed.

In conclusion, we generated a new model in which the whole *Ube3a* gene was deleted. This target design differs from other existing models where smaller deletions are present, such as in the Ube3a^{tmAlb1} model harboring a 3kb deletion of exon 5 [20]. Genetic elements in the non-coding parts of the gene could possibly be present, thus potentially worsening the phenotype. We observed similar phenotypes in behavioral, motor, and cognitive tasks as in the Ube3a^{tmAlb1} model [36], although further studies, for instance with aged animals, are needed to confirm its usefulness. The motor impairment was particularly robust in our model and, based on previous work by Silva-Santos et al. (2015) [24], we now know that the developmental window for rescuing motor skills closes in adolescence, significantly later than the behavioral deficits that need *Ube3a* reinstatement during early development [24], which makes tests relying on the motor skills of the animal a good indicator of the success of therapeutics. This model provides several similarities to AS patients as well as several dissimilarities. We did not observe any cognitive deficits in simpler tasks, such as the Barnes maze and NOR tests, but that could be due to the age of the animals [56]. The memory flexibility was, however, affected in the Ube3a^{genedel} animals. There are other phenotypes associated with AS that were not evaluated in this study, such as electrophysiological phenotypes, abnormal EEG, and autistic behavior. The investigation of these phenotypes could lay a foundation for future publications. Nevertheless, this model can be rendered suitable for AS research and the potential testing of therapeutic interventions.

Supplementary Materials: The following supporting information can be downloaded at: https://www.mdpi.com/article/10.3390/cells11182815/s1, Figure S1: Weight and latency to fall in rotarod; Figure S2: IntelliCage results: licks and corner visits.

Author Contributions: R.S. and A.K.-Z. contributed to methodology of the behavioral experiments. L.A.S., A.K.-Z. and V.N. analyzed and interpreted the data. L.A.S. and P.K. designed the Ube3a deletion model. P.N. and J.K. generated the mouse models. L.A.S. and P.N. made the figures and table. L.A.S. and J.K. performed genotyping and breeding. L.A.S. and A.K.-Z. designed the study. L.A.S., A.K.-Z., P.N. and R.S. prepared the manuscript. J.P. directed the phenotyping of the model. R.S. acquired the funding. All authors contributed intellectually to this study. All authors have read and agreed to the published version of the manuscript.

Funding: This research was supported by the Czech Academy of Sciences RVO 68378050, LM2018126 Czech Centre for Phenogenomics provided by MEYS CR, OP RDE CZ.02.1.01/0.0/0.0/16_013/0001789 (Upgrade of the Czech Centre for Phenogenomics: developing towards translation research by MEYS and ESIF), OP RDE CZ.02.1.01/0.0/0.0/18_046/0015861 (CCP Infrastructure Upgrade II by MEYS and ESIF), and OP RDI CZ.1.05/2.1.00/19.0395 (Higher quality and capacity for transgenic models by MEYS and ERDF), and funding was received from the European Union's Horizon 2020 research and innovation program under the Marie Skłodowska–Curie grant agreement "Improving Genome Editing Efficiency (IMGENE)", grant agreement no 765269. In addition, this study received funding from the NGO "Association of Gene Therapy (ASGENT)", Czechia (https://asgent.org/).

Institutional Review Board Statement: All animals and experiments used in this study were ethically reviewed and performed in accordance with European directive 2010/63/EU and were approved by the Czech Central Commission for Animal Welfare.

Informed Consent Statement: Not applicable.

Data Availability Statement: The datasets used and/or analyzed during the current study are available from the corresponding author on reasonable request.

Acknowledgments: We thank our technicians Katarina Kanasova, Pavlina Kucerova, and Pavel Jina who helped perform the behavioral testing.

Conflicts of Interest: The authors declare no conflict of interest.

References

1. layton-Smith, J.; Laan, L. Angelman syndrome: A review of the clinical and genetic aspects. *J. Med. Genet.* **2003**, *40*, 87–95. [CrossRef] [PubMed]
2. Jolleff, N.; Ryan, M.M. Communication development in Angelman's syndrome. *Arch. Dis. Child.* **1993**, *69*, 148–150. [CrossRef]
3. Viani, F.; Romeo, A.; Viri, M.; Mastrangelo, M.; Lalatta, F.; Selicorni, A.; Gobbi, G.; Lanzi, G.; Bettio, D.; Briscioli, V.; et al. Seizure and EEG Patterns in Angelman's Syndrome. *J. Child. Neurol.* **1995**, *10*, 467–471. [CrossRef] [PubMed]
4. Meng, L.; Person, R.E.; Beaudet, A.L. Ube3a-ATS is an atypical RNA polymerase II transcript that represses the paternal expression of Ube3a. *Hum. Mol. Genet.* **2012**, *21*, 3001–3012. [CrossRef] [PubMed]
5. Sandanam, T.; Beange, H.; Robson, L.; Woolnough, H.; Buchholz, T.; Smith, A. Manifestations in institutionalised adults with Angelman syndrome due to deletion. *Am. J. Med. Genet.* **1997**, *70*, 415–420. [CrossRef]
6. Malcolm, S.; Clayton-Smith, J.; Nichols, M.; Pembrey, M.; Armour, J.; Jeffreys, A.; Robb, S.; Webb, T. Uniparental paternal disomy in Angelman's syndrome. *Lancet* **1991**, *337*, 694–697. [CrossRef]
7. Buiting, K.; Gross, S.; Lich, C.; Gillessen-Kaesbach, G.; el-Maarri, O.; Horsthemke, B. Epimutations in Prader-Willi and Angelman syndromes: A molecular study of 136 patients with an im-printing defect. *Am. J. Hum. Genet.* **2003**, *72*, 571–577. [CrossRef]
8. Matsuura, T.; Sutcliffe, J.S.; Fang, P.; Galjaard, R.-J.; Jiang, Y.-H.; Benton, C.S.; Rommens, J.M.; Beaudet, A.L. De novo truncating mutations in E6-AP ubiquitin-protein ligase gene (UBE3A) in Angelman syndrome. *Nat. Genet.* **1997**, *15*, 74–77. [CrossRef]
9. Kishino, T.; Lalande, M.; Wagstaff, J. UBE3A/E6-AP mutations cause Angelman syndrome. *Nat. Genet.* **1997**, *15*, 70–73. [CrossRef]
10. Syding, L.A.; Nickl, P.; Kasparek, P.; Sedlacek, R. CRISPR/Cas9 Epigenome Editing Potential for Rare Imprinting Diseases: A Review. *Cells* **2020**, *9*, 993. [CrossRef]
11. Williams, C.A.; Beaudet, A.L.; Clayton-Smith, J.; Knoll, J.H.; Kyllerman, M.; Laan, L.A.; Magenis, R.E.; Moncla, A.; Schinzel, A.A.; Summers, J.A.; et al. Angelman syndrome 2005: Updated consensus for diagnostic criteria. *Am. J. Med. Genet. Part A* **2006**, *140A*, 413–418. [CrossRef] [PubMed]
12. Koyavski, L.; Panov, J.; Simchi, L.; Rayi, P.R.; Sharvit, L.; Feuermann, Y.; Kaphzan, H. Sex-Dependent Sensory Phenotypes and Related Transcriptomic Expression Profiles Are Differentially Affected by Angelman Syndrome. *Mol. Neurobiol.* **2019**, *56*, 5998–6016. [CrossRef] [PubMed]
13. van Woerden, G.M.; Harris, K.D.; Hojjati, M.R.; Gustin, R.M.; Qiu, S.; de Avila Freire, R.; Jiang, Y.H.; Elgersma, Y.; Weeber, E.J. Rescue of neurological deficits in a mouse model for Angelman syndrome by reduction of alphaCaMKII inhibitory phosphorylation. *Nat. Neurosci.* **2007**, *10*, 280–282. [CrossRef]
14. Sidorov, M.S.; Judson, M.C.; Kim, H.; Rougie, M.; Ferrer, A.I.; Nikolova, V.D.; Riddick, N.V.; Moy, S.S.; Philpot, B.D. Enhanced Operant Extinction and Prefrontal Excitability in a Mouse Model of Angelman Syndrome. *J. Neurosci.* **2018**, *38*, 2671–2682. [CrossRef] [PubMed]
15. Sonzogni, M.; Wallaard, I.; Santos, S.S.; Kingma, J.; Du Mee, D.; Van Woerden, G.M.; Elgersma, Y. A behavioral test battery for mouse models of Angelman syndrome: A powerful tool for testing drugs and novel Ube3a mutants. *Mol. Autism* **2018**, *9*, 1–19. [CrossRef]
16. Albrecht, U.; Sutcliffe, J.S.; Cattanach, B.M.; Beechey, C.V.; Armstrong, D.; Eichele, G.; Beaudet, A.L. Imprinted expression of the murine Angelman syndrome gene, Ube3a, in hippocampal and Purkinje neurons. *Nat. Genet.* **1997**, *17*, 75–78. [CrossRef]

17. Jiang, Y.-H.; Pan, Y.; Zhu, L.; Landa, L.; Yoo, J.; Spencer, C.; Lorenzo, I.; Brilliant, M.; Noebels, J.; Beaudet, A.L. Altered Ultrasonic Vocalization and Impaired Learning and Memory in Angelman Syndrome Mouse Model with a Large Maternal Deletion from Ube3a to Gabrb3. *PLoS ONE* **2010**, *5*, e12278. [CrossRef]
18. Avagliano Trezza, R.; Sonzogni, M.; Bossuyt, S.N.V.; Zampeta, F.I.; Punt, A.M.; van den Berg, M.; Rotaru, D.C.; Koene, L.M.C.; Munshi, S.T.; Stedehouder, J. Loss of nuclear UBE3A causes electrophysiological and behavioral deficits in mice and is asso-ciated with Angelman syndrome. *Nat. Neurosci.* **2019**, *22*, 1235–1247. [CrossRef]
19. Gabriel, J.M.; Gabriel, J.M.; Merchant, M.; Ohta, T.; Ji, Y.; Caldwell, R.G.; Ramsey, M.J.; Tucker, J.D.; Longnecker, R.; Nicholls, R.D. A transgene insertion creating a heritable chromosome deletion mouse model of Prader-Willi and angelman syn-dromes. *Proc. Natl. Acad. Sci. USA* **1999**, *96*, 9258–9263. [CrossRef]
20. Jiang, Y.H.; Armstrong, D.; Albrecht, U.; Atkins, C.M.; Noebels, J.L.; Eichele, G.; Sweatt, J.D.; Beaudet, A.L. Mutation of the Angelman ubiquitin ligase in mice causes increased cytoplasmic p53 and deficits of con-textual learning and long-term potentiation. *Neuron* **1998**, *21*, 799–811. [CrossRef]
21. Wang, T.; Van Woerden, G.M.; Elgersma, Y.; Borst, J.G.G. Enhanced Transmission at the Calyx of Held Synapse in a Mouse Model for Angelman Syndrome. *Front. Cell. Neurosci.* **2018**, *11*, 418. [CrossRef]
22. Ube3a Mouse Gene Details | Ubiquitin Protein Ligase E3A | International Mouse Phenotyping Consortium. Available online: https://www.mousephenotype.org/ (accessed on 25 March 2022).
23. Berrios, J.; Stamatakis, A.M.; Kantak, P.A.; McElligott, Z.A.; Judson, M.C.; Aita, M.; Rougie, M.; Stuber, G.D.; Philpot, B.D. Loss of UBE3A from TH-expressing neurons suppresses GABA co-release and enhances VTA-NAc optical self-stimulation. *Nat. Commun.* **2016**, *7*, 10702. [CrossRef] [PubMed]
24. Silva-Santos, S.; Van Woerden, G.M.; Bruinsma, C.F.; Mientjes, E.; Jolfaei, M.A.; Distel, B.; Kushner, S.; Elgersma, Y. Ube3a reinstatement identifies distinct developmental windows in a murine Angelman syndrome model. *J. Clin. Investig.* **2015**, *125*, 2069–2076. [CrossRef] [PubMed]
25. Skarnes, W.C.; Rosen, B.; West, A.P.; Koutsourakis, M.; Bushell, W.; Iyer, V.; Mujica, A.O.; Thomas, M.; Harrow, J.; Cox, T.; et al. A conditional knockout resource for the genome-wide study of mouse gene function. *Nature* **2011**, *474*, 337–342. [CrossRef] [PubMed]
26. Smith, S.E.P.; Zhou, Y.-D.; Zhang, G.; Jin, Z.; Stoppel, D.C.; Anderson, M.P. Increased Gene Dosage of *Ube3a* Results in Autism Traits and Decreased Glutamate Synaptic Transmission in Mice. *Sci. Transl. Med.* **2011**, *3*, 103ra97. [CrossRef]
27. Krishnan, V.; Stoppel, D.C.; Nong, Y.; Johnson, M.A.; Nadler, M.J.S.; Ozkaynak, E.; Teng, B.L.; Nagakura, I.; Mohammad, F.; Silva, M.A.; et al. Autism gene Ube3a and seizures impair sociability by repressing VTA Cbln1. *Nature* **2017**, *543*, 507–512. [CrossRef]
28. Matsumoto, A.; Kumagai, T.; Miura, K.; Miyazaki, S.; Hayakawa, C.; Yamanaka, T. Epilepsy in Angelman Syndrome Associated with Chromosome 15q Deletion. *Epilepsia* **1992**, *33*, 1083–1090. [CrossRef]
29. Dindot, S.V.; Antalffy, B.A.; Bhattacharjee, M.B.; Beaudet, A.L. The Angelman syndrome ubiquitin ligase localizes to the synapse and nucleus, and maternal deficiency results in abnormal dendritic spine morphology. *Hum. Mol. Genet.* **2007**, *17*, 111–118. [CrossRef]
30. Copping, N.A.; Christian, S.G.B.; Ritter, D.G.; Islam, M.S.; Buscher, N.; Zolkowska, D.; Pride, M.C.; Berg, E.L.; LaSalle, J.M.; Ellegood, J.; et al. Neuronal overexpression of Ube3a isoform 2 causes behavioral impairments and neuroanatomical pathology relevant to 15q11.2-q13.3 duplication syndrome. *Hum. Mol. Genet.* **2017**, *26*, 3995–4010. [CrossRef]
31. The Jackson Laboratory, I.o.f.T.J.L., Bar Harbor, ME. Unpublished. 2005–2017. Available online: https://www.jax.org/ (accessed on 25 March 2022).
32. Miura, K.; Kishino, T.; Li, E.; Webber, H.; Dikkes, P.; Holmes, G.L.; Wagstaff, J. Neurobehavioral and Electroencephalographic Abnormalities in Ube3aMaternal-Deficient Mice. *Neurobiol. Dis.* **2002**, *9*, 149–159. [CrossRef]
33. Tsai, T.F.; Jiang, Y.H.; Bressler, J.; Armstrong, D.; Beaudet, A.L. Paternal deletion from Snrpn to Ube3a in the mouse causes hypotonia, growth retardation and partial le-thality and provides evidence for a gene contributing to Prader-Willi syndrome. *Hum. Mol. Genet.* **1999**, *8*, 1357–1364. [CrossRef]
34. Russell, L.B.; Montgomery, C.S.; Cacheiro, N.L.; Johnson, D.K. Complementation analyses for 45 mutations encompassing the pink-eyed dilution (p) locus of the mouse. *Genetics* **1995**, *141*, 1547–1562. [CrossRef] [PubMed]
35. Rotaru, D.C.; Mientjes, E.J.; Elgersma, Y. Angelman Syndrome: From Mouse Models to Therapy. *Neuroscience* **2020**, *445*, 172–189. [CrossRef] [PubMed]
36. Born, H.A.; Dao, A.T.; Levine, A.T.; Lee, W.L.; Mehta, N.M.; Mehra, S.; Weeber, E.J.; Anderson, A.E. Strain-dependence of the Angelman Syndrome phenotypes in Ube3a maternal deficiency mice. *Sci. Rep.* **2017**, *7*, 1–15. [CrossRef]
37. Shiotsuki, H.; Yoshimi, K.; Shimo, Y.; Funayama, M.; Takamatsu, Y.; Ikeda, K.; Takahashi, R.; Kitazawa, S.; Hattori, N. A rotarod test for evaluation of motor skill learning. *J. Neurosci. Methods* **2010**, *189*, 180–185. [CrossRef]
38. Hampton, T.G.; Kale, A.; Amende, I.; Tang, W.; McCue, S.; Bhagavan, H.N.; VanDongen, C.G. Gait Disturbances in Dystrophic Hamsters. *J. Biomed. Biotechnol.* **2011**, *2011*, 1–8. [CrossRef] [PubMed]
39. Porsolt, R.D.; Bertin, A.; Jalfre, M. Behavioral despair in mice: A primary screening test for antidepressants. *Arch. Int. Pharmacodyn. Ther.* **1977**, *229*, 327–336. [PubMed]
40. Kulesskaya, N.; Voikar, V. Assessment of mouse anxiety-like behavior in the light–dark box and open-field arena: Role of equipment and procedure. *Physiol. Behav.* **2014**, *133*, 30–38. [CrossRef] [PubMed]
41. Lister, R.G. The use of a plus-maze to measure anxiety in the mouse. *Psychopharmacology* **1987**, *92*, 180–185. [CrossRef]

42. Chiba, A.A.; Kesner, R.P.; Reynolds, A.M. Memory for spatial location as a function of temporal lag in rats: Role of hip-pocampus and medial prefrontal cortex. *Behav. Neural Biol.* **1994**, *61*, 123–131. [CrossRef]
43. Youn, J.; Ellenbroek, B.A.; van Eck, I.; Roubos, S.; Verhage, M.; Stiedl, O. Finding the right motivation: Genotype-dependent differences in effective reinforcements for spatial learning. *Behav. Brain Res.* **2012**, *226*, 397–403. [CrossRef]
44. O'Leary, T.P.; Brown, R.E. The effects of apparatus design and test procedure on learning and memory performance of C57BL/6J mice on the Barnes maze. *J. Neurosci. Methods* **2012**, *203*, 315–324. [CrossRef] [PubMed]
45. Benner, S.; Endo, T.; Endo, N.; Kakeyama, M.; Tohyama, C. Early deprivation induces competitive subordinance in C57BL/6 male mice. *Physiol. Behav.* **2014**, *137*, 42–52. [CrossRef] [PubMed]
46. Margolis, S.S.; Sell, G.L.; Zbinden, M.A.; Bird, L.M. Angelman Syndrome. *Neurotherapeutics* **2015**, *12*, 641–650. [CrossRef] [PubMed]
47. Jirkof, P. Burrowing and nest building behavior as indicators of well-being in mice. *J. Neurosci. Methods* **2014**, *234*, 139–146. [CrossRef]
48. Yamasaki, K.; Joh, K.; Ohta, T.; Masuzaki, H.; Ishimaru, T.; Mukai, T.; Niikawa, N.; Ogawa, M.; Wagstaff, J.; Kishino, T. Neurons but not glial cells show reciprocal imprinting of sense and antisense transcripts of Ube3a. *Hum. Mol. Genet.* **2003**, *12*, 837–847. [CrossRef]
49. Duca, D.G.; Craiu, D.; Boer, M.; Chirieac, S.M.; Arghir, A.; Tutulan-Cunita, A.; Barca, D.; Iliescu, C.; Lungeanu, A.; Magureanu, S.; et al. Diagnostic approach of angelman syndrome. *Maedica (Bucur)* **2013**, *8*, 321–327.
50. Heck, D.; Zhao, Y.; Roy, S.; LeDoux, M.S.; Reiter, L.T. Analysis of cerebellar function in Ube3a-deficient mice reveals novel genotype-specific behaviors. *Hum. Mol. Genet.* **2008**, *17*, 2181–2189. [CrossRef]
51. Berg, E.L.; Petkova, S.P.; Born, H.A.; Adhikari, A.; Anderson, A.E.; Silverman, J.L. Insulin-like growth factor-2 does not improve behavioral deficits in mouse and rat models of Angelman Syndrome. *Mol. Autism* **2021**, *12*, 1–16. [CrossRef]
52. Dodge, A.; Peters, M.M.; Greene, H.E.; Dietrick, C.; Botelho, R.; Chung, D.; Willman, J.; Nenninger, A.W.; Ciarlone, S.; Kamath, S.G.; et al. Generation of a Novel Rat Model of Angelman Syndrome with a Complete *Ube3a* Gene Deletion. *Autism Res.* **2020**, *13*, 397–409. [CrossRef]
53. Rostosky, C.M.; Miloševic´, I. Gait Analysis of Age-dependent Motor Impairments in Mice with Neurodegeneration. *J. Vis. Exp.* **2018**, *136*, e57752. [CrossRef]
54. Rinalduzzi, S.; Trompetto, C.; Marinelli, L.; Alibardi, A.; Missori, P.; Fattapposta, F.; Pierelli, F.; Currà, A. Balance dysfunction in Parkinson's disease. *Biomed. Res. Int.* **2015**, *2015*, 434683. [CrossRef] [PubMed]
55. Dan, B.; Pelc, K.; Cheron, G. Behavior and neuropsychiatric manifestations in Angelman syndrome. *Neuropsychiatr. Dis. Treat.* **2008**, *4*, 577–584. [CrossRef] [PubMed]
56. Huang, H.-S.; Burns, A.J.; Nonneman, R.J.; Baker, L.K.; Riddick, N.V.; Nikolova, V.D.; Riday, T.T.; Yashiro, K.; Philpot, B.D.; Moy, S.S. Behavioral deficits in an Angelman syndrome model: Effects of genetic background and age. *Behav. Brain Res.* **2013**, *243*, 79–90. [CrossRef]
57. Maranga, C.; Fernandes, T.G.; Bekman, E.; Da Rocha, S.T. Angelman syndrome: A journey through the brain. *FEBS J.* **2020**, *287*, 2154–2175. [CrossRef] [PubMed]
58. Moy, S.S.; Nadler, J.J.; Young, N.B.; Nonneman, R.J.; Segall, S.K.; Andrade, G.M.; Crawley, J.N.; Magnuson, T.R. Social approach and repetitive behavior in eleven inbred mouse strains. *Behav. Brain Res.* **2008**, *191*, 118–129. [CrossRef] [PubMed]
59. Silverman, J.L.; Yang, M.; Lord, C.; Crawley, J.N. Behavioural phenotyping assays for mouse models of autism. *Nat. Rev. Neurosci.* **2010**, *11*, 490–502. [CrossRef]
60. Guariglia, S.R.; Chadman, K.K. Water T-maze: A useful assay for determination of repetitive behaviors in mice. *J. Neurosci. Methods* **2013**, *220*, 24–29. [CrossRef]
61. Heinz, D.E.; Schöttle, V.A.; Nemcova, P.; Binder, F.P.; Ebert, T.; Domschke, K.; Wotjak, C.T. Exploratory drive, fear, and anxiety are dissociable and independent components in foraging mice. *Transl. Psychiatry* **2021**, *11*, 1–12. [CrossRef]
62. Sarkar, P.A.; Shigli, A.; Patidar, C. Happy Puppet syndrome. *BMJ Case Rep.* **2011**, *2011*, bcr0920114747. [CrossRef]
63. Ter Horst, J.P.; De Kloet, E.R.; Schächinger, H.; Oitzl, M.S. Relevance of Stress and Female Sex Hormones for Emotion and Cognition. *Cell. Mol. Neurobiol.* **2011**, *32*, 725–735. [CrossRef] [PubMed]
64. Marques, A.A.; Bevilaqua, M.C.D.N.; da Fonseca, A.M.P.; Nardi, A.E.; Thuret, S.; Dias, G.P. Gender Differences in the Neurobiology of Anxiety: Focus on Adult Hippocampal Neurogenesis. *Neural Plast.* **2016**, *2016*, 1–14. [CrossRef] [PubMed]

The effect of *Gabra5* functional ablation on corticosterone levels and anxiety-like behavior in mice

Linn Amanda Syding[1], Agnieszka Kubik-Zahorodna[2], David Pajuelo Reguera[2], Bohdana Hrušková[3], Michaela Králíková[3], Jana Kopkanova[2], Vendula Novosadová[2], Petr Kasparek[2] Jan Procházka[1, 2], Jan Rozman[2], Rostislav Tureček[3], Radislav Sedláček[1, 2*]

Author affiliations and email addresses

[1] Laboratory of Transgenic Models of Diseases, Institute of Molecular Genetics of the CAS, v.v.i, 252 50 Vestec, Czech Republic
[2] Czech Centre for Phenogenomics, Institute of Molecular Genetics of the CAS, v.v.i, 252 50 Vestec, Czech Republic
[3] Department of Auditory Neuroscience, Institute of Experimental Medicine of the Czech Academy of Sciences, v. v. i., 14220 Prague, Czech Republic
* Author to whom correspondence should be addressed

linn.syding@img.cas.cz
agnieszka.kubik-zahorodna@img.cas.cz
david.pajuelo-reguera@img.cas.cz
bohdana.hruskova@iem.cas.cz
michaela.kralikova@iem.cas.cz
jana.kopkanova@img.cas.cz
Vendula.novosadova@img.cas.cz
Petr.Kasparek@img.cas.cz
Jan.Prochazka@img.cas.cz
jan.rozman@img.cas.cz
rostislav.turecek@iem.cas.cz
radislav.Sedlacek@img.cas.cz

Key words: corticosterone; GABA receptor, anxiety, behavior

Summary statement

Functional ablation of the α5 subunit of the GABA receptor leads to lowering of fecal corticosterone levels and decreased rearing behavior suggesting decreased anxiety-like behavior.

Abstract

Stress responses are activated by the hypothalamic-pituitary-adrenal-axis (HPA-axis), culminating in the release of glucocorticoids. During prolonged periods of secretion of glucocorticoids or inappropriate behavioral responses to a stressor, pathologic conditions may occur. Increased glucocorticoid concentration is linked to generalized anxiety, a widespread condition in society. Although the stress response has been well studied, there are knowledge gaps regarding its regulation. It is known that the HPA-axis is under GABAergic control but the contribution of the individual subunits of the GABA receptor is unknown. Here, we investigated the relationship between the α5 subunit and corticosterone levels in a new mouse model deficient for *Gabra5*, which is known to be linked to anxiety-disorders in humans and phenologs observed in mice. Although anxiety-like behavior using open field and elevated plus maze tests could not be detected, decreased rearing behavior was observed during indirect calorimetry. We also found decreased levels of fecal corticosterone metabolites in Gabra5$^{-/-}$ mice. Moreover, based on the electrophysiological recordings, we hypothesize that the constitutive ablation of the *Gabra5* gene leads to functional compensation with other channels or GABA receptor subunits.

Introduction

Stress is defined as a state of mental or physical strain resulting from demanding circumstances mirroring internal or external conditions threatening the homeostasis of the organism (Kagias, Nehammer and Pocock, 2012; Goodnite, 2014). The hypothalamic-pituitary-adrenal-axis (HPA-axis) is the main system mediating stress responses through physiological and/or behavioral adaptations. The response to stress starts with the stimulation of hypophysiotropic neurons, innervated by afferents from limbic brain regions in the paraventricular nucleus (PVN) of the hypothalamus (Hill, 2012). The HPA-mediated response culminates in the release of glucocorticoids through several intermediate steps (Smith and Vale, 2006) that bind to their ubiquitously expressed receptors, activating the transcription of target genes (Jubb *et al.*, 2017).

The relationship between glucocorticoids commonly referred to as cortisol in humans and corticosterone in rodents, and increased anxiety and behavioral impairments has been established (Raglan, Schmidt and Schulkin, 2017). Increased secretion of glucocorticoids is tied to increased general anxiety, depressive disorders and social anxiety (Sapolsky, 2004). Although the physiology behind the stress response and its role in psychological disorders has been extensively studied, there are still gaps in the knowledge of the contribution of the GABA(A) subunit contribution in terms of its regulation.

The PVN receives considerable GABAergic innervation from local hypothalamic regions and areas of the amygdala that exert a substantial inhibitory tone upon the HPA axis (Cullinan, Ziegler and Herman, 2008). Limbic regions such as the hippocampus and prefrontal cortex do not directly innervate the PVN, but control HPA action via projections to GABAergic nuclei surrounding the

PVN (Gunn *et al.*, 2011). The functional role of GABA in regards to corticosterone secretion was shown when microinjection of the GABA agonist muscimol into the hypothalamus resulted in inhibited secretion of glucocorticoids (Cullinan, Helmreich and Watson, 1996). The GABA(A) receptor is a ligand-gated chloride ion channel that, when activated by GABA or a positive allosteric modulator leads to hyperpolarization of the cell, thus being an inhibitory neurotransmitter receptor in the CNS (Everington *et al.*, 2018). The functionality of the heteropentameric GABA(A) receptor including the pharmacological sensitivity, subcellular location and channel properties varies according to subunit assembly (Jacob, 2019). The GABA(A)R subunit composition in terms of regulating the stress response still has left to be elucidated as the contribution of single subunits is still being discovered. Interestingly, it was shown that in stressed mice GABA has an excitatory effect on the HPA axis potentiated via the GABA(A) delta subunit-containing receptors (Sarkar *et al.*, 2011). The individual contribution of other subunits in regards to the stress response is still unclear.

Perturbations in the *GABRA5* gene, encoding the α5 subunit, were found in patients with panic disorder and heterozygous expression of the gene is commonly present in patients with Angelman syndrome, where anxiety and autism are commonly reported conditions (Bird, 2014; Hodges *et al.*, 2014). Assumptions about the function of the gene were corroborated by corresponding phenotypes in Gabra5$^{-/-}$ mutant mice (Zurek *et al.*, 2016; Mesbah-Oskui *et al.*, 2017). In addition, high α5 subunit expression is described in the hippocampus, part of the limbic system, which is rich in glucocorticoid receptors (Olsen and Sieghart, 2009; Myers, McKlveen and Herman, 2014).

Besides hippocampus the receptors are found in the cortex, hypothalamus, and amygdala (Martin, Bonin and Orser, 2009), although at lower levels. The brain regions with substantial α5 expression are all involved in the fear circuitry, which is a central component of anxiety (Shin and Liberzon, 2010). As outlined above, the hypothalamus is the master regulator of the HPA-axis, where the cascade starts (Herman *et al.*, 2016). However, structures such as the hippocampus play an important role when anxiety-like behavior is exhibited (Cominski *et al.*, 2014). It has been shown that α5 GABA(A) receptors generate tonic inhibitory conductance in CA1 hippocampal pyramidal neurons (Caraiscos *et al.*, 2004). Taken together these findings make the *Gabra5* gene an interesting candidate for studies on glucocorticoids and anxiety-like behavior.

Based on reported anxiety-like phenotype in Gabra5$^{-/-}$ mice and the link between glucocorticoids and anxiety, we aimed to elucidate the putative relationship between the α5 subunit and corticosterone in mice. In this new experimental model based on the targeting critical exon 3 to functionally ablate the gene we evaluated if the corticosterone levels are affected. In particular, we investigated whether housing conditions based on single- and group-housed individuals affects the corticosterone levels. We also assessed general anxiety using open field and elevated plus maze tests, locomotor activity and rearing behavior under home cage conditions and energy expenditure was evaluated by indirect calorimetric devices. Finally, we employed electrophysiological recordings for functional evaluation of the mouse model.

To summarize, we hypothesize that an ablation of the α5 subunit results in increased corticosterone secretion and increased anxiety-like behavior due to disinhibition of the GABAergic neurons. Altogether, we observed decreased corticosterone levels in Gabra5$^{-/-}$ mice

and decreased rearing, suggesting lower anxiety levels as well as hyperpolarization of pyramidal hippocampal neurons in α5 deletion neurons, as the recordings were not sensitive to the α5 inverse agonist L655,708, suggesting a functional compensation.

Materials and methods

Mouse husbandry

All animal models and experiments used in this study were ethically reviewed and performed following European directive 2010/63/EU and were approved by the Czech Central Commission for Animal Welfare. Mice were housed in individually ventilated cages (Techniplast) in a barrier facility. Mice were genotyped when they were 14-21 days old. All animals were kept at 22 ± 2 °C with a 12-h dark and light cycle and were tested during the light period, provided with mouse chow (Altromin 1314, Altromin, Lage, Germany) and water ad libitum. Mice were group-housed with two to six animals of the same sex and genotype per cage.

Model generation

The Gabra5 knockout mouse on C57BL/6N background (Charles River Laboratories) used for this study was generated by targeting exon 3 of the Gabra5 gene (transcript Gabra5-201 ENSMUST00000068456.8) for an exon deletion by using the CRISPR/Cas9 technique at Institute of Molecular Genetics, Prague. The gRNAs were generated using (http://crispor.tefor.net/) where the gRNAs with the highest score were selected. The gRNAs for electroporation were the following: Gabra5 forward 5'- GGCCGCAGTCTGTTGTCATA-3' and Gabra5 reverse 5'-

ACTAGTTCTGTACAAGACGA-3'. The gRNAs were introduced to the fertilized oocytes of C57BL/6N strain and transferred into pseudo-pregnant foster mice. Putative founders were analyzed by PCR, gel electrophoresis, and sequencing. One animal harboring a 903 nucleotide deletion spanning exon 3 and parts of intron 2 and 3 was chosen for subsequent breeding to F1 progeny. Genotyping was performed using following primers: forward: 5'- TACAGAAGCAAGGGGTTCAGG - 3', reverse: 5'- GCCTCCCTGTTCTTATTGTCG-3' with Ta 65°C.

Western blotting

Hippocampi were dissected and snap frozen in liquid nitrogen. The tissue was lysed in RIPA buffer (0.05 M Tris-HCl, pH 8, 0.15 M NaCl, 0.5% deoxycholic acid, 1% NP-40, and 0.1% sodium dodecyl sulfate (SDS)), cOmplete™, EDTA-free Protease Inhibitor Cocktail (Roche, 5056489001), and PhosSTOP™, phosphatase inhibitor tablets (Roche, 4906845001). Lysates were sonicated and cleared by centrifugation. Protein concentration was determined using the Pierce™ BCA Protein Assay Kit (ThermoScientific, 23225). 8µg of protein from hippocampus was denatured in reducing sample buffer, separated by SDS-PAGE (polyacrylamide gel electrophoresis) gels, and blotted to nitrocellulose membranes (Bio-Rad). The primary antibodies used were rabbit anti-Gabra5 (1:4000, Synaptic Systems, 224 503) and mouse anti-B-actin (1:5000, Sigma-Aldrich, A2228). Blots were washed with PBS-T and detection was performed with SuperSignal™ West Pico PLUS Chemiluminescent Substrate (ThermoScientific, 34579).

Fecal corticosterone assessment and housing

For the detection of fecal corticosterone metabolites and the effect of housing we used a total of 6 animals per sex, genotype and housing-condition. All animals were group-housed at the

initiation of the experiment. On the first day, the animals were placed individually on a mesh inside compartments and egested feces was collected. The animals were subsequently placed in single-housing for those selected, group-animals were kept in their home-cage. Feces were collected at 8 am at 24h and 48h post the initial collection. The fecal samples were dried overnight at 60C and weighed; 1ml of 80% methanol was added per 50 mg of feces. The samples were seal homogenized and then left shaking at 1000 rpm at room temperature overnight. The fecal samples were spun down at 4C at 2500 rpm for 10 min and the supernatant moved to a new tube. The fecal corticosterone metabolites were assessed using corticosterone ELISA (Biovendor, RTC002R) according to manufacturer's protocol.

Testosterone sampling and ELISA

Males at 11w of age were used for testosterone analysis. The animals were either group-housed at six animals per cage or single-housed in six different cages. After 24h and 48h of separation at 10 am we collected 25ul blood from the tail in lithium/heparin microvettes (Sarstedt, 16.443) and spun down at 2500 g for 10 minutes at 4C to obtain plasma. We analyzed the testosterone levels using testosterone ELISA measurements according to the manufacturer's protocol (Biovendor, RTC001R).

Open field

The activity of the animals in a novel environment and the level of anxiety displayed were evaluated in open field tests as previously described (Kulesskaya and Voikar, 2014). The area of the open field was a square of 42 × 42 cm uniformly illuminated with a light intensity of 200 lux in the center of the field. The testing arena was virtually divided into periphery and center zones,

where the center zone constituted 38% of the whole arena. Each mouse was placed in the corner of the arena for a 10 min period of free maze exploration. The time spent in each zone, the distance travelled and other indices were automatically computed based on a video recordings (Viewer, Biobserve GmbH, Germany). In total 23 WT mice and 21 Gabra5$^{-/-}$ were tested with an approximate 1:1 gender ratio.

Elevated plus maze

The elevated plus maze (EPM) apparatus consisted of two closed and two open elevated arms, with a light intensity of 60 lux in the center of the maze (35). The animals were placed in the center and were left to explore the EPM for five minutes. The total time spent in the open and closed arms and the center of EPM were tracked and evaluated automatically (Viewer software, Biobserve GmbH).

Slice preparation

For electrophysiology experiments, transversal hippocampal slices were prepared from P36–P44 WT and Gabra5$^{-/-}$ mice. Animals were decapitated in accordance with Animal Protection Law of the Czech Republic (compatible with European Community Council directives 86/609/EEC). The brains were excised in ice-cold low Ca2+ artificial CSF (aCSF) containing the following (in mM): 130 NaCl, 3.5 KCl, 3 MgCl2, 0.5 CaCl2, 10 glucose, 1.25 NaH2PO4, 24 NaHCO2, 0.5 ascorbic acid, 3 myo-inositol, and 2 sodium pyruvate; bubbled with 5% CO2/95% O2 to pH 7.3. Slices (300 µm thick) were cut in the low Ca2+ aCSF using a VT1200S vibratome (Leica) after slicing the connection between CA1 and CA3 region was cut and slices were incubated at 34°C for 60 min and then stored at room temperature (21–23°C) in low Ca2+ aCSF.

Electrophysiology

During recording slices were perfused with a standard aCSF containing (in mM): 125 NaCl, 2.5 KCl, 1 MgCl2, 2 CaCl2, 25 glucose, 1.25 NaH2PO4, 25 NaHCO2; gassed with 5% CO2/95% O2 to pH 7.3. The recordings were performed at physiological temperature (35°C). Whole cell patch-clamp recordings of membrane potentials were performed from CA1 stratum pyramidale; neurons were viewed using infrared and differential interference contrast optics.

Borosilicate glass electrodes (~2-3 MΩ) were filled with a solution containing the following: 107 mM K-gluconate, 32.5 KCl, 5 mM EGTA, 10 mM HEPES, 4 mM MgATP, 10 mM Tris-phosphocreatine, 0.6 mM NaGTP, at pH 7.25 with KOH and 295 mOsm).

Drugs, applied by perfusion into the recording chamber, were kept as aliquots, and solutions were freshly prepared on the day of the experiment. Recordings were performed in (±)-CPP (5µM), DNQX (10µM), CGP 54626 (1µM), SR-95531 (5µM) to block Glutamate, GABAB and synaptic GABAA receptors and with or without L655,708 (10nM) a selective inverse agonist of extrasynaptic α5GABAA receptors. GABA (5µM) was added to substitute background GABA in the hippocampus. Current clamp recordings were performed to discover whether α5GABAA activity influences neuronal excitability. Current steps with increasing amplitude were delivered through the patch electrode (to monitor membrane input resistance and time constant (150 µs, -10 pA), and to determine rheobase (1000 µs, 0.05-0,215 nA). Voltage responses were recorded with an Axopatch 200B amplifier (Molecular Devices); signals were filtered at 10 kHz, digitized at 50 kHz, and acquired using pCLAMP software (Molecular Devices).

Indirect calorimetry

Indirect calorimetry was performed using an 8 cage multiplex setup including monitoring of food and water uptake, and physical activity (distance travelled and rearing, PhenoMaster, TSE Systems, Bad Homburg, Germany, software version v.7.1.2). Before starting the indirect calorimetry measurements, we performed a complete calibration protocol for the gas analysers according to the manufacturer's recommendations using compressed air, CO_2 1% and N_2 100%. We weighed the mice before introducing them into the calorimetric cages. Mice were measured individually. Mice had *ad libitum* access to water and food, (Altromin 1314, Lage, Germany). The volume of bedding material was limited to approximately 150 ml per cage during indirect calorimetry measurements to properly detect locomotor activity of the mice by infrared beam breaks frame surrounding the cage in the horizontal plane (ActiMot2).

The mice were individually housed in a multiplex system with 8 cages plus reference cage. In total, 8 animals per sex and genotype were used for testing. Sampling frequency to measure the CO_2 and O_2 gas measurements was every 15 min. The environmental conditions inside the climatic chamber were 23 degrees centigrade, 55% relative humidity and a light cycle of 12 hours of light and 12 hours of darkness synchronized with the animal facility where the mice were housed. The following 72 h period was used for measurements of the CO_2 production and O_2 consumption, where the energy expenditure (EE), locomotor activity including rearing behavior, and food and water intake were monitored. When the experiment was stopped, the mice were weighed and placed to their original cages.

In vivo body composition analysis

Time domain – Nuclear Magnetic resonance (TD-NMR) is a method based on the acquisition of radiofrequency signals generated by hydrogen spins from fluid and soft tissues, such as muscle and adipose tissue. The Minispec LF90 II was calibrated for mice body composition measurements following (Morla *et al.*, 2020). The measurement is non-invasive and does not require anesthesia or other preparation.

Statistical analyses

Recorded voltage responses were analyzed using pClamp v.11 and GraphPad Prism v.8 software. Time constant was determined based on exponential fit of the course of voltage change evoked by a small hyperpolarizing current injection (-10nA). The input resistance was determined from amplitude of the steady state membrane potential was divided by the amount of injected current (10pA). For statistical comparison of the experimental data, a two-way ANOVA was used with Bonferroni's *Post hoc* test. A probability level of $p<0.05$ was chosen as a threshold for statistical significance (*). A linear mixed model was applied sex and genotype as main factors and body weight as covariate.

Results

Generation of Gabra5$^{-/-}$ mouse model

The mouse line was generated by CRISPR-based on targeting of exon 3 deleting 903 nucleotides encompassing the crucial exon 3 of Gabra5$^{-/-}$ (Fig. 1A). The elimination of the protein product was confirmed using western blot on hippocampal lysates. The α5 protein was detected at its predicted size of 55kDa in WT controls whereas no detection was visible in the Gabra5$^{-/-}$ sample and reduced expression in heterozygotes (Fig. 1B).

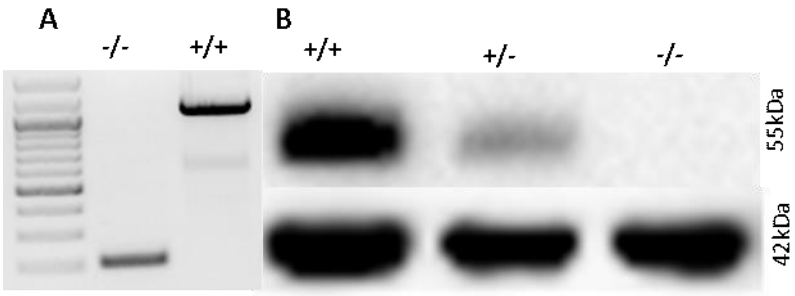

Figure 1. Model validation. A representative genotyping gel where the KO has a band of 197 bp and the WT 1100 bp**. B** western blot of WT and Gabra5 $^{-/-}$ hippocampi. The α5 subunit protein was detected at 55kDa in WTs, non-detectable in Gabra5$^{-/-}$ and reduced in the heterozygote. Loading control B-Actin (42kDa) was detected in both samples.

Gabra5$^{-/-}$ mice exhibit decreased levels of fecal corticosterone metabolite

We were first interested in stress levels of Gabra5$^{-/-}$ control and mutant mice under regular home cage conditions reflected by concentrations of fecal corticosterone metabolites (FCM). As extension of this we also compared FCM of mice that were either group- or single-housed over

24 and 48 h. Originally kept in groups of up to six individuals, the test animals were separated and kept single-housed. The group-housed mice remained under these conditions as controls. We found that male Gabra5$^{-/-}$ mice had significantly lower FCM levels when group-housed both times collectively (main genotype effect $p<0.01$; $F=14.28$; genotype/time interaction $p>0.05$; Fig. 2A; Table S1). However, when single-housed Gabra5$^{-/-}$ males did not differ significantly from WT males (main genotype effect $p>0.05$: $F=0.51$; genotype/time interaction $p>0.05$; Fig. 2B; Table S1). In group-housed females we could not detect significant differences in FCM between genotypes but there was a trend towards lower FCM (main genotype effect $p=0.07$; $F=4.23$; genotype/time interaction $p>0.05$; Fig. 2C; Table S1). However, when the Gabra5$^{-/-}$ females were single-housed FCM were significantly lower (main genotype effect $p<0.01$; $F=19.2$; genotype/time interaction $p>0.05$; Fig. 2D; Table S1).

Using the same data from the previous paragraph but looking at the effects of housing conditions on FCM levels within the same sex-genotype groups revealed that single-housing significantly decreased FCM concentrations in WT males, decreasing from a mean of 2715 to a mean of 1858 ng FCM per g feces (main housing effect $p<0.05$; $F=7.235$; housing/time interaction $p>0.05$: Fig. 2E; Table S1). In Gabra5$^{-/-}$ males and both WT and Gabra5$^{-/-}$ females there were no statistically significant effects of housing on FCM concentrations (main genotype effects $p>0.05$; $F=2.04$; 0.7; 0.05; Fig. 2F-H; Table S1). Time was not a significant factor for any of the sex-genotype combinations (main time effect $p>0.05$; figure 2).

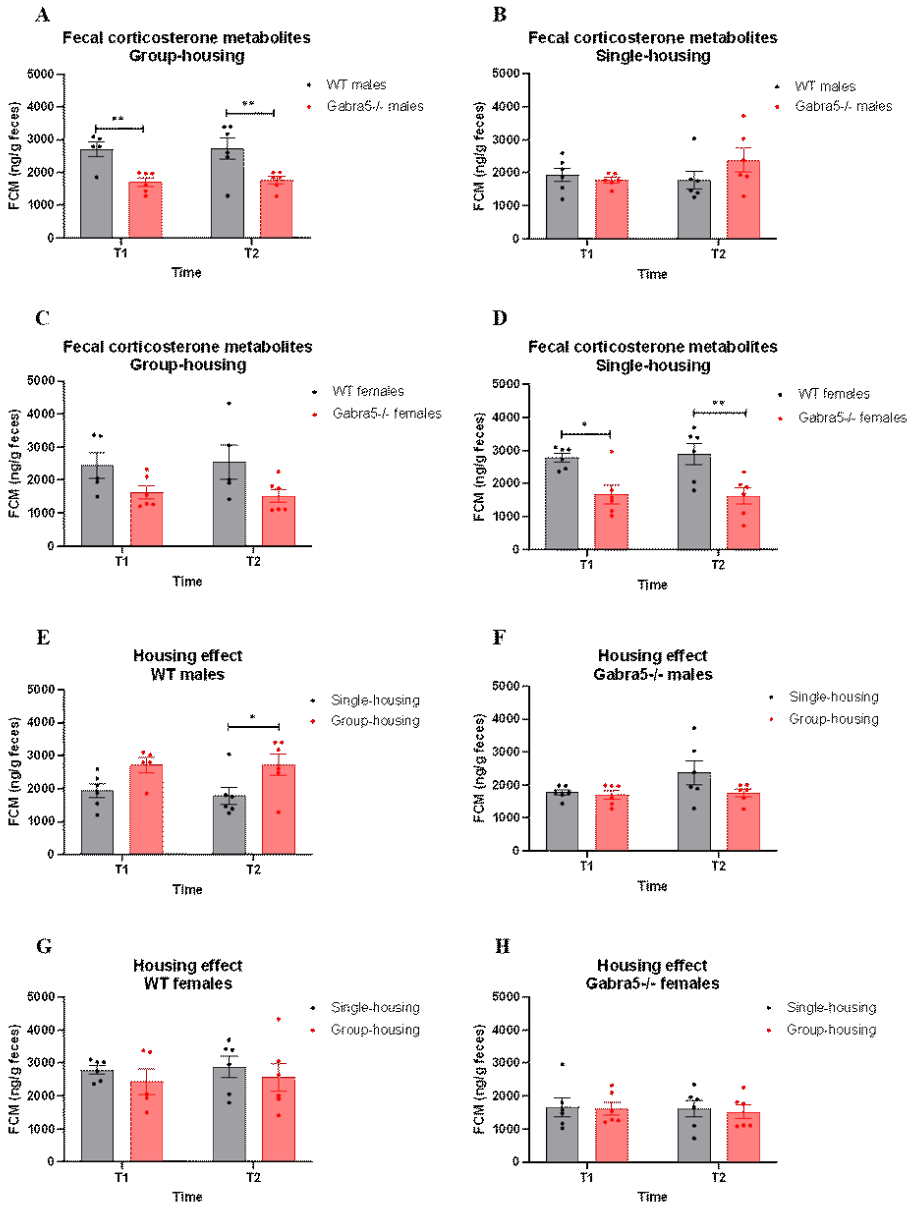

297

298 **Figure 2.** Fecal corticosterone metabolites concentration and effects of housing. **A-D** FCM concentrations depending
299 on genotype within same housing-conditions. **E-H** Same FCM concentrations but depending on housing within sex
300 and genotype. Two-way ANOVA with dependent measurements with Bonferroni's post-hoc test, *n*=6. All graphs
301 were depicted with mean ± SEM. Significant effects of genotype or housing are indicated as *p < 0.05 and **p < 0.01.

302

The significant effect of housing detected in WT males corticosterone levels urged us to investigate whether the stress caused by group-housing could be linked to aggression. Group housing could lead to more pronounced dominance behavior within groups of males, which could also affect testosterone levels in the blood. Therefore, we measured testosterone levels in single- and group-housed males 24 h and 48 h after separation representing the state at once (T1) and twice (T2) handled and blood sampled. There was a significant increase in testosterone when handled twice for both genotypes in group-housed conditions (main time effect $p<0.01$; $F=10.3$; time/genotype interaction $p>0.05$; Fig. S1A; Table S2). Time and handling did not affect the levels of testosterone in single-housed animals regardless of genotype (main time effect $p>0.05$; $F=0.317$; Fig. S1B; Table S2). Comparing the effect of housing within each genotype did not reveal significant changes with time however trends were observed for both WT and Gabra5$^{-/-}$ at T2 (main housing effect $p>0.05$; $F=3.48$; $F=4.27$; Fig. S1C-D; Table S2).

Open field and elevated plus maze tests do not suggest general anxiety in Gabra5$^{-/-}$ mice

We then performed more specialized behavioral testing like open field and elevated plus maze tests to investigate whether Gabra5$^{-/-}$ mice and WTs differ in general anxiety-like behavior. Based on the time spent in the aversive center, the latency to enter the center and the number of center entries we observed that Gabra5$^{-/-}$ mice do not exhibit anxiety-like tendencies (main genotype effect $p>0.05$; $F=1.49$; 0.82; 0.21; genotype/sex interaction $p>0.05$; Fig. 3A-C) nor the average speed, total resting time and total distance travelled differed ($p>0.05$; $F=2.03$; 2.24; 2.05; genotype/sex interaction $p>0.05$; Fig. 3D-F). Time spent in the open and closed arms in the

elevated plus maze test did not significantly differ between the genotypes ($p>0.05$; $F=0.006$; $F=0.19$; sex/genotype interaction $p>0.05$; genotype/zone interaction $p>0.05$; Fig. 3G-H).

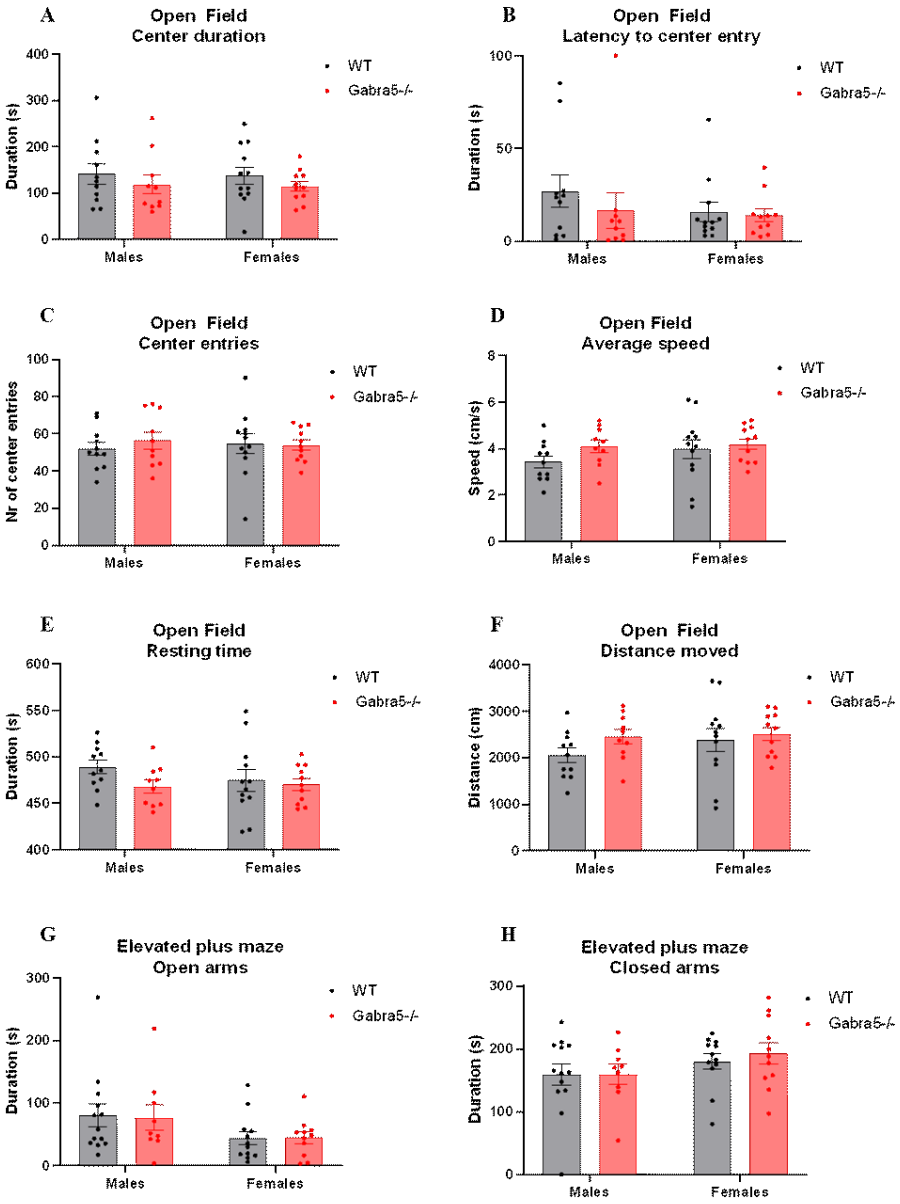

Figure 3. Open field and elevated plus maze tests. **A-C** OF anxiety-like test parameters; center duration, latency to enter center and number of center entries. **D-F** OF activity parameters; average speed, resting time and distance moved. **G-H** Elevated plus maze open arms and closed arms duration. Two-way ANOVA main genotype effects all above $p>0.05$. All figures are depicted with mean ± SEM, *n*=12.

Gabra5$^{-/-}$ KO animals exhibit different rearing behavior

As an approach to monitor specific behavioral domains like drinking and feeding behavior, locomotor activity and metabolic rate, animals were then placed into calorimetric cages. These parameters cover behavioral and metabolic functions in rodents that are affected by corticosterone (Mitra and Sapolsky, 2008; Sturman, Germain and Bohacek, 2018; Izzi-Engbeaya *et al.*, 2020). Gabra5$^{-/-}$ mice exhibited significantly less rearings per time interval during the three combined dark phases (main genotype effect $p<0.05$; Fig. 4A-B). Total locomotion for both sexes was not significantly altered but trended to be decreased over the cumulative period (main genotype effect $p=0.07$; Fig. 4C-D). Additional analysis showed that Gabra5$^{-/-}$ females moved significantly less than control animals (female genotype effect $p<0.05$; Fig. 4C-D) which was not detected in males. Energy expenditure was not significantly different for neither sex (main genotype effect $p>0.05$; Fig 4E-F). Food and water intake were also monitored. The animals did not differ in food intake ($p>0.05$; Fig. S2A-B), but Gabra5$^{-/-}$ males drank significantly less than controls ($p<0.001$; Fig. S2C-D).

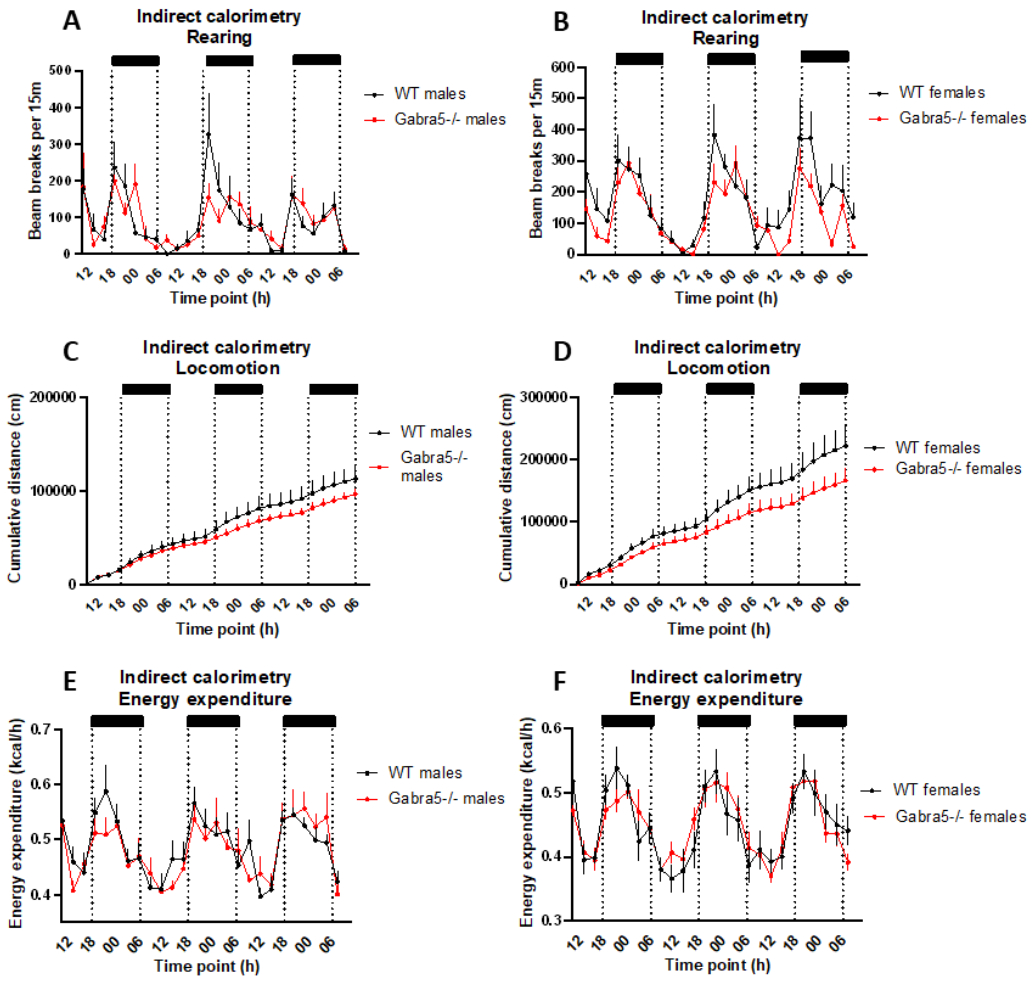

346

347 **Figure 4.** Indirect calorimetry- Rearing, locomotion and energy expenditure. **A-B** rearing was decreased during the
348 dark phases (shaded) in KO animals. **C-D** a tendency of decreased locomotion was observed in Gabra5$^{-/-}$ animals of
349 both sexes however significant for females. **E-F** Energy expenditure was not significantly altered for either sex.
350 Regression analysis, *n*=8. All figures depict mean ± SEM.

351

352

353 Body composition was measured to investigate if small differences in energy fluxes affect
354 endogenously stored energy in white adipose tissue or result in a lean phenotype. However,

there were no significant differences in the relationship between fat and lean mass when regressed versus bodyweight (genotype effect on slope and intercept $p>0.05$; Fig. S3A-D).

Hippocampal CA1 pyramidal neurons exhibit reduced excitability in Gabra5$^{-/-}$ mice

To test whether deletion of Gabra5 leads to functional changes in central neurons, we examined the electrical properties of pyramidal cells in acutely isolated live CA1 hippocampal slices using the patch-clamp technique. These cells typically express α5 receptors at both synaptic and extrasynaptic sites where they mediate phasic and tonic GABAergic inhibition (Serwanski et al., 2006, Glykys et al., 2008) Compared with those found in WT neurons, the resting membrane potential and membrane time constant in Gabra5$^{-/-}$ neurons showed a shift to more negative and lower values, respectively (main genotype effect $p<0.001$; $F=14.26$; $F=12.67$; Fig. 5A-B). This rather unexpected observation indicated reduced excitability of hippocampal neurons with deleted α5 receptors and suggested the presence of tonic hyperpolarizing conductance. The conductance did not appear to be affected by the α5-specific inverse agonist L655,708 and its properties were not investigated further (Fig. 5A-D) (Jacob, 2019). Consistent with the presence of increased hyperpolarizing and shunting inhibition in Gabra5$^{-/-}$ neurons, we observed a significant increase in their rheobase values for action potentials evoked by long depolarizing stimuli ($p<0.0001$; $F=24.02$; Fig. 5C-D). These results thus show that deletion of α5-containing GABA(A)R on CA1 pyramidal neurons leads to changes in their functional properties. The findings also suggest the activity of a different type of channel affecting the responses of Gabra5$^{-/-}$ hippocampal pyramidal neurons.

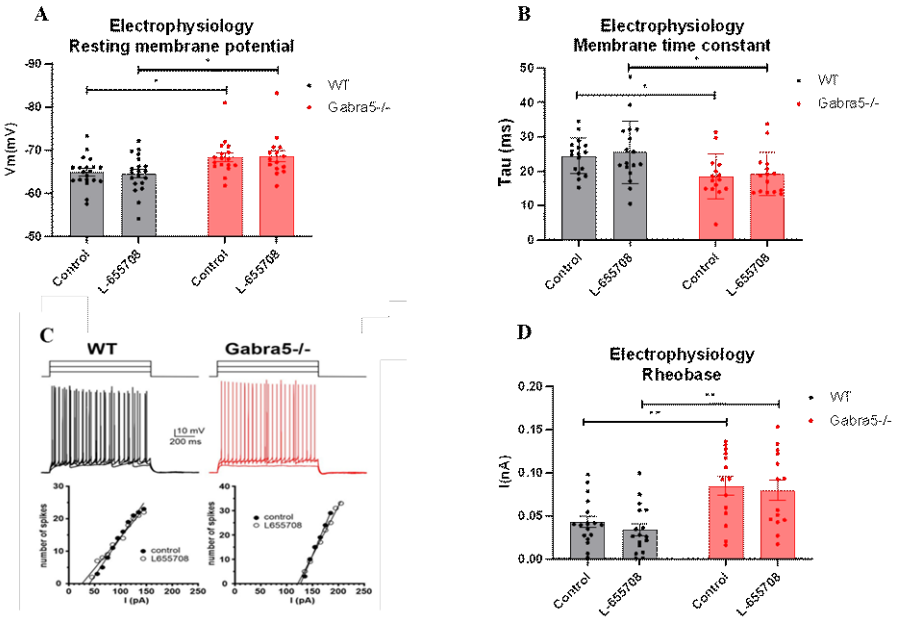

Figure 5. Deletion of Gabra5 reduces neuronal excitability in CA1 hippocampal slices. AB Comparison of resting membrane potential (V_m) and the membrane time constant (τ_m) of CA1 pyramidal neurons from WT and Gabra5$^{-/-}$ mice in the absence or presence of L655,708. Values are mean ± SEM of 20 (WT) and 17 (Gabra5$^{-/-}$) *p < 0.05; Two-way ANOVA followed by Sidak's multiple comparisons test. **C** Example traces showing voltage responses of pyramidal neurons evoked by current step stimulations of amplitude 55, 95 and 135 pA (WT) or 95, 135 and 175 pA (Gabra5$^{-/-}$). The plots below show spike frequency as a function of injected current for the same neurons as above recorded in the absence or presence of L655,708. The minimum current required to elicit an action potential (rheobase) was determined by fitting the dependence to a linear function (solid line; see Methods). **D** Comparison of mean rheobase in WT and Gabra5$^{-/-}$ neurons in the presence or absence of L655,708. Gabra5$^{-/-}$ show significantly increased rheobase independent of the presence of L655,708. Values are mean ± SEM of 17 (WT) and 14 (Gabra5$^{-/-}$) experiments. **p < 0.01; Two-way ANOVA followed by Sidak's multiple comparisons test.

Discussion

Gabra5$^{-/-}$ is a gene frequently missing from the maternal chromosome in Angelman syndrome patients that may harbor a large deletion ranging from 4-6Mb (Syding *et al.*, 2020). We generated a new mouse model deficient for Gabra5 by targeting the critical exon 3 of the *Gabra5* gene with the CRISPR/Cas9 technique. The model was used to evaluate how GABA(A)R influences behavioral anxiety-like behavior in correlation to corticosterone levels. Our study revealed significantly lower fecal corticosterone metabolites in the Gabra5$^{-/-}$ mice and decreased anxiety-like behavior exhibited by decreased rearing behavior.

Regarding the effect of functional *Gabra5* ablation and its neurobehavioral effects, we assayed corticosterone in feces (in single- and group-housed conditions twice during a period of 24 h). Measuring FCM and not plasma corticosterone offers an advantage as it is less invasive to the animal and the confounding effect that blood sampling may have on corticosterone is eliminated using this methodology. Furthermore, it is an integrated value to evaluate general levels and not spot values affected by peakwise secretion underlying circadian rhythms (JACOBSEN *et al.*, 2013). The Gabra5$^{-/-}$ males exhibited lower FCM levels in group-housed conditions but when single-housed, the significant difference disappeared. Gabra5$^{-/-}$ females had significantly less secreted FCM when single-housed but no significance appeared in FCM levels in group-housed conditions although a tendency could be observed, suggesting less anxiety-like behavior. Interestingly, we found that the housing-conditions only had a significant effect on FCM levels in WT males but not in any of the other sex-genotype groups.

Male mice can exhibit aggression towards one another when group-housed which would lead to higher FCM levels under such group-housed conditions (Lidster *et al.*, 2019). As testosterone is

linked to aggressive behavior (Giammanco *et al.*, 2005), we found that testosterone concentration in males in the same setup as the FCM test is increased at the second time of handling in group-housed males irrespective of the genotype. As there were no significant differences between Gabra5$^{-/-}$ and WT males, differences in aggression or stress are likely not the cause of lower FCM levels in Gabra5$^{-/-}$ males.

Based on reports from patients with impairments in the *GABRA5* gene and animal studies with allosteric modulators to the α5 subunit, we were expecting to see an increase in anxiety-like behavior in our Gabra5$^{-/-}$ model (Hodges *et al.*, 2014; Piantadosi *et al.*, 2016). However, the open field and elevated plus maze tests could not detect an anxiety phenotype in the Gabra5$^{-/-}$ animals.

Another aspect we followed is rearing behavior that is largely hippocampal-dependent as its formation is a pivotal component of the neural structure responsible for anxiety (Lever, Burton and O'Keefe, 2006). Rearing can be strengthened by anxiety (Kaesermann, 1986; Molewijk, van der Poel and Olivier, 1995). Rearing is a phenomenon when four-legged animals stand on their hind-legs and explore their environment which is a common response to novelty in rodents (Lever, Burton and O'Keefe, 2006). It has been suggested that the benefits of rearing in terms of information gathering are traded off by the risks of exploration. In a study by Blanchard and Blanchard (1991) it was found that anxiolytics decreased rearing in situations interpretable as eliciting anxiety in the subjects (Blanchard, Blanchard and Rodgers, 1991). Based on this, one would argue that rearing occurs the least during low levels of anxiety. We identified decreased rearing in our Gabra5$^{-/-}$ animals during the dark phase of the day, the period when the animals are active, suggesting lower levels of anxiety in a new environment. General locomotion was only

reduced in Gabra5$^{-/-}$ females however not in males and energy expenditure and feeding did not differ in any sex, thus the reduced rearing is not a result of other possible confounding factors.

Lastly, we evaluated the impact of *Gabra5* deletion on the functional properties of CA1 pyramidal neurons. We recorded their voltage responses under control conditions and during the application of the α5 GABA(A)R selective inverse agonist L655, 708 (Quirk *et al.*, 1996). Rheobase, the minimal current needed to elicit an action potential, was increased in Gabra5$^{-/-}$ mice suggesting decreased excitability of CA1 neurons (Chase and Morales, 2005). Consistent with this, Gabra5$^{-/-}$ cells showed slightly hyperpolarized resting membrane potential and a shorter membrane time constant compared to cells isolated from WT mice. Both parameters were insensitive of the L655,708 in both WT and Gabra5$^{-/-}$ derived neurons, indicating that the observed differences are not attributed to the α5 subunit. The lack of effect of the inverse agonist L655,708 but recorded differences in excitability suggests the activity of another type of channel influencing the responses of CA1 neurons in Gabra5$^{-/-}$ mice. Our findings differ from previous experiments done on a very similar model harboring a deletion of crucial exon 3 where the authors reported a reduced tonic inhibitory conductance and increased excitability of principal neurons in the hippocampus. However, these neurons were derived from mice on a mixed C57/BL6-129SvEv background whereas our model was on a C57/BL6N background (Bonin *et al.*, 2007). The reduced excitability in our recordings might be a consequence of developmental adaptation (functional compensation), found occasionally in constitutive KO mice (El-Brolosy and Stainier, 2017). Genetic robustness, the ability to maintain fitness despite genetic perturbations is important in evolution. Genetic compensation in KOs is a common occurrence where other associated genes are upregulated or expression is modified in the instance of a deleted gene (El-

Brolosy and Stainier, 2017). Therefor one needs to be careful when interpreting results based on KO models as phenotypes may be a result of remaining genes interacting and not the absence of the gene of interest.

In this work we studied effects of the α5 subunit ablation on behavior connected to anxiety and stress, linked to corticosterone concentration. Based on the electrophysiological recordings, we assume that the functional ablation of the *Gabra5* gene leads to functional compensation with other channels or GABA receptor subunits.

Acknowledgments

We thank the technicians at the Czech Centre for Phenogenomics for contributing with phenotyping data generation.

Competing interests

The authors declare no competing interests.

Funding

This research was supported by Czech Academy of Sciences RVO 68378050, LM2018126 Czech Centre for Phenogenomics provided by MEYS CR, OP RDE CZ.02.1.01/0.0/0.0/16_013/0001789 (Upgrade of the Czech Centre for Phenogenomics: developing towards translation research by MEYS and ESIF), OP RDE CZ.02.1.01/0.0/0.0/18_046/0015861 (CCP Infrastructure Upgrade II by MEYS and ESIF), OP RDI CZ.1.05/2.1.00/19.0395 (Higher quality and capacity for transgenic

models by MEYS and ERDF), and funding was received from the European Union's Horizon 2020 research and innovation program under the Marie Skłodowska–Curie grant agreement no. 765269.

Rostislav Turecek was supported by GACR 19-09283S

Data availability

Data is available from the authors upon reasonable request.

Author contributions statement

Author contributions: L.A.S, A.K-Z, D.P-R, J.R, R.S designed the experiments. L.A.S, A.K-Z, D.P-R, B.H, M.K performed experiments. L.A.S and J.K genotyped and prepared animal cohorts. L.A.S and P.K designed the mouse model. P.K and J.K generated the animals. L.A.S, A.K-Z and V.N performed data analysis. L.A.S generated the figures and tables. J.P performed experimental phenotyping. L.A.S, A.K-Z, D.P-R, B.H, J.R, R.T and R.S prepared the manuscript. R.T and R.S acquired funding.

References

Bird, L. M. (2014) 'Angelman syndrome: review of clinical and molecular aspects.', *The application of clinical genetics*, 7, pp. 93–104. doi: 10.2147/TACG.S57386.

Blanchard, D. C., Blanchard, R. J. and Rodgers, R. J. (1991) 'Risk Assessment and Animal Models of Anxiety BT - Animal Models in Psychopharmacology', in Olivier, B., Mos, J., and Slangen, J. L. (eds). Basel: Birkhäuser Basel, pp. 117–134. doi: 10.1007/978-3-0348-6419-0_13.

494 Bonin, R. P. *et al.* (2007) 'Alpha5GABAA receptors regulate the intrinsic excitability of mouse
495 hippocampal pyramidal neurons.', *Journal of neurophysiology*. United States, 98(4), pp. 2244–
496 2254. doi: 10.1152/jn.00482.2007.

497 Caraiscos, V. B. *et al.* (2004) 'Tonic inhibition in mouse hippocampal CA1 pyramidal neurons is
498 mediated by alpha5 subunit-containing gamma-aminobutyric acid type A receptors.',
499 *Proceedings of the National Academy of Sciences of the United States of America*, 101(10), pp.
500 3662–3667. doi: 10.1073/pnas.0307231101.

501 Chase, M. H. and Morales, F. R. (2005) 'Chapter 12 - Control of Motoneurons during Sleep', in
502 Kryger, M. H., Roth, T., and Dement, W. C. B. T.-P. and P. of S. M. (Fourth E. (eds). Philadelphia:
503 W.B. Saunders, pp. 154–168. doi: https://doi.org/10.1016/B0-72-160797-7/50019-7.

504 Cominski, T. P. *et al.* (2014) 'The role of the hippocampus in avoidance learning and anxiety
505 vulnerability', *Frontiers in behavioral neuroscience*. Frontiers Media S.A., 8, p. 273. doi:
506 10.3389/fnbeh.2014.00273.

507 Cullinan, W. E., Helmreich, D. L. and Watson, S. J. (1996) 'Fos expression in forebrain afferents
508 to the hypothalamic paraventricular nucleus following swim stress.', *The Journal of*
509 *comparative neurology*. United States, 368(1), pp. 88–99. doi: 10.1002/(SICI)1096-
510 9861(19960422)368:1<88::AID-CNE6>3.0.CO;2-G.

511 Cullinan, W. E., Ziegler, D. R. and Herman, J. P. (2008) 'Functional role of local GABAergic
512 influences on the HPA axis.', *Brain structure & function*. Germany, 213(1–2), pp. 63–72. doi:
513 10.1007/s00429-008-0192-2.

514 Demuyser, T. *et al.* (2016) 'In-depth behavioral characterization of the corticosterone mouse
515 model and the critical involvement of housing conditions.', *Physiology & behavior*. United
516 States, 156, pp. 199–207. doi: 10.1016/j.physbeh.2015.12.018.

517 El-Brolosy, M. A. and Stainier, D. Y. R. (2017) 'Genetic compensation: A phenomenon in search
518 of mechanisms', *PLoS genetics*. Public Library of Science, 13(7), pp. e1006780–e1006780. doi:
519 10.1371/journal.pgen.1006780.

520 Everington, E. A. *et al.* (2018) 'Molecular Characterization of GABA-A Receptor Subunit Diversity
521 within Major Peripheral Organs and Their Plasticity in Response to Early Life Psychosocial
522 Stress', *Frontiers in Molecular Neuroscience*, 11. doi: 10.3389/fnmol.2018.00018.

523 Giammanco, M. *et al.* (2005) 'Testosterone and aggressiveness.', *Medical science monitor :
524 international medical journal of experimental and clinical research*. United States, 11(4), pp.
525 RA136-45.

526 GLYKYS, J., MANN EO FAU - MODY, I. & MODY, I. 2008. Which GABA(A) receptor subunits are necessary
527 for tonic inhibition in the hippocampus?

528 Goodnite, P. M. (2014) 'Stress: a concept analysis.', *Nursing forum*. United States, 49(1), pp. 71–
529 74. doi: 10.1111/nuf.12044.

530 Gunn, B. *et al.* (2011) 'Neurosteroids and GABAA Receptor Interactions: A Focus on Stress',
531 *Frontiers in Neuroscience*, 5. doi: 10.3389/fnins.2011.00131.

532 Herman, J. P. *et al.* (2016) 'Regulation of the Hypothalamic-Pituitary-Adrenocortical Stress
533 Response', *Comprehensive Physiology*, 6(2), pp. 603–621. doi: 10.1002/cphy.c150015.

534 Hill, J. W. (2012) 'PVN pathways controlling energy homeostasis', *Indian journal of*
535 *endocrinology and metabolism*. Medknow Publications & Media Pvt Ltd, 16(Suppl 3), pp. S627–
536 S636. doi: 10.4103/2230-8210.105581.

537 Hodges, L. M. *et al.* (2014) 'Evidence for linkage and association of GABRB3 and GABRA5 to
538 panic disorder', *Neuropsychopharmacology : official publication of the American College of*
539 *Neuropsychopharmacology*. 2014/05/23. Nature Publishing Group, 39(10), pp. 2423–2431. doi:
540 10.1038/npp.2014.92.

541 Izzi-Engbeaya, C. *et al.* (2020) 'Effects of corticosterone within the hypothalamic arcuate
542 nucleus on food intake and body weight in male rats', *Molecular Metabolism*, 36, p. 100972.
543 doi: https://doi.org/10.1016/j.molmet.2020.02.015.

544 Jacob, T. C. (2019) 'Neurobiology and Therapeutic Potential of α5-GABA Type A Receptors',
545 *Frontiers in molecular neuroscience*. Frontiers Media S.A., 12, p. 179. doi:
546 10.3389/fnmol.2019.00179.

547 JACOBSEN, K. R. *et al.* (2013) 'The Utility of Fecal Corticosterone Metabolites and Animal
548 Welfare Assessment Protocols as Predictive Parameters of Tumor Development and Animal
549 Welfare in a Murine Xenograft Model', *In Vivo*, 27(2), pp. 189 LP – 196. Available at:
550 http://iv.iiarjournals.org/content/27/2/189.abstract.

551 Jubb, A. W. *et al.* (2017) 'Glucocorticoid Receptor Binding Induces Rapid and Prolonged Large-
552 Scale Chromatin Decompaction at Multiple Target Loci.', *Cell reports*, 21(11), pp. 3022–3031.
553 doi: 10.1016/j.celrep.2017.11.053.

554 Kaesermann, H. P. (1986) ‘Stretched attend posture, a non-social form of ambivalence, is
555 sensitive to a conflict-reducing drug action.’, *Psychopharmacology*. Germany, 89(1), pp. 31–37.
556 doi: 10.1007/BF00175185.

557 Kagias, K., Nehammer, C. and Pocock, R. (2012) ‘Neuronal Responses to Physiological Stress ’,
558 *Frontiers in Genetics* . Available at:
559 https://www.frontiersin.org/article/10.3389/fgene.2012.00222.

560 Kulesskaya, N. and Voikar, V. (2014) ‘Assessment of mouse anxiety-like behavior in the light-
561 dark box and open-field arena: role of equipment and procedure.’, *Physiology & behavior*.
562 United States, 133, pp. 30–38. doi: 10.1016/j.physbeh.2014.05.006.

563 Lever, C., Burton, S. and O’Keefe, J. (2006) ‘Rearing on hind legs, environmental novelty, and
564 the hippocampal formation.’, *Reviews in the neurosciences*. Germany, 17(1–2), pp. 111–133.
565 doi: 10.1515/revneuro.2006.17.1-2.111.

566 Lidster, K. *et al.* (2019) ‘Cage aggression in group-housed laboratory male mice: an international
567 data crowdsourcing project’, *Scientific Reports*, 9(1), p. 15211. doi: 10.1038/s41598-019-51674-
568 z.

569 Martin, L. J., Bonin, R. P. and Orser, B. A. (2009) ‘The physiological properties and therapeutic
570 potential of alpha5-GABAA receptors.’, *Biochemical Society transactions*. England, 37(Pt 6), pp.
571 1334–1337. doi: 10.1042/BST0371334.

572 Mesbah-Oskui, L. *et al.* (2017) ‘Reduced expression of α5GABA(A) receptors elicits autism-like
573 alterations in EEG patterns and sleep-wake behavior.’, *Neurotoxicology and teratology*. United

States, 61, pp. 115–122. doi: 10.1016/j.ntt.2016.10.009.

Mitra, R. and Sapolsky, R. M. (2008) 'Acute corticosterone treatment is sufficient to induce anxiety and amygdaloid dendritic hypertrophy', *Proceedings of the National Academy of Sciences of the United States of America*. 2008/04/07. National Academy of Sciences, 105(14), pp. 5573–5578. doi: 10.1073/pnas.0705615105.

Molewijk, H. E., van der Poel, A. M. and Olivier, B. (1995) 'The ambivalent behaviour "stretched approach posture" in the rat as a paradigm to characterize anxiolytic drugs.', *Psychopharmacology*. Germany, 121(1), pp. 81–90. doi: 10.1007/BF02245594.

Morla, L. *et al.* (2020) 'A noninvasive method to study the evolution of extracellular fluid volume in mice using time-domain nuclear magnetic resonance', *American Journal of Physiology-Renal Physiology*. American Physiological Society, 319(1), pp. F115–F124. doi: 10.1152/ajprenal.00377.2019.

Myers, B., McKlveen, J. M. and Herman, J. P. (2014) 'Glucocorticoid actions on synapses, circuits, and behavior: implications for the energetics of stress', *Frontiers in neuroendocrinology*. 2013/12/18, 35(2), pp. 180–196. doi: 10.1016/j.yfrne.2013.12.003.

Olsen, R. W. and Sieghart, W. (2009) 'GABA A receptors: subtypes provide diversity of function and pharmacology.', *Neuropharmacology*, 56(1), pp. 141–148. doi: 10.1016/j.neuropharm.2008.07.045.

Piantadosi, S. C. *et al.* (2016) 'Sex-Dependent Anti-Stress Effect of an α5 Subunit Containing GABAA Receptor Positive Allosteric Modulator ', *Frontiers in Pharmacology* . Available at:

https://www.frontiersin.org/article/10.3389/fphar.2016.00446.

Quirk, K. *et al.* (1996) '[3H]L-655,708, a novel ligand selective for the benzodiazepine site of GABAA receptors which contain the alpha 5 subunit.', *Neuropharmacology*. England, 35(9–10), pp. 1331–1335. doi: 10.1016/s0028-3908(96)00061-5.

Raglan, G. B., Schmidt, L. A. and Schulkin, J. (2017) 'The role of glucocorticoids and corticotropin-releasing hormone regulation on anxiety symptoms and response to treatment', *Endocrine connections*. 2017/01/24. Bioscientifica Ltd, 6(2), pp. R1–R7. doi: 10.1530/EC-16-0100.

Sapolsky, R. M. (2004) *Why zebras don't get ulcers: The acclaimed guide to stress, stress-related diseases, and coping*. Holt paperbacks.

Sarkar, J. *et al.* (2011) 'Neurosteroidogenesis is required for the physiological response to stress: role of neurosteroid-sensitive GABAA receptors.', *The Journal of neuroscience : the official journal of the Society for Neuroscience*, 31(50), pp. 18198–18210. doi: 10.1523/JNEUROSCI.2560-11.2011.

SERWANSKI, D. R., MIRALLES CP FAU - CHRISTIE, S. B., CHRISTIE SB FAU - MEHTA, A. K., MEHTA AK FAU - LI, X., LI X FAU - DE BLAS, A. L. & DE BLAS, A. L. 2006. Synaptic and nonsynaptic localization of GABAA receptors containing the alpha5 subunit in the rat brain.

Shin, L. M. and Liberzon, I. (2010) 'The neurocircuitry of fear, stress, and anxiety disorders', *Neuropsychopharmacology : official publication of the American College of Neuropsychopharmacology*. Nature Publishing Group, 35(1), pp. 169–191. doi:

614 10.1038/npp.2009.83.

615 Smith, S. M. and Vale, W. W. (2006) 'The role of the hypothalamic-pituitary-adrenal axis in
616 neuroendocrine responses to stress.', *Dialogues in clinical neuroscience*, 8(4), pp. 383–395. doi:
617 10.31887/DCNS.2006.8.4/ssmith.

618 Sturman, O., Germain, P.-L. and Bohacek, J. (2018) 'Exploratory rearing: a context- and stress-
619 sensitive behavior recorded in the open-field test', *Stress*. Taylor & Francis, 21(5), pp. 443–452.
620 doi: 10.1080/10253890.2018.1438405.

621 Zurek, A. A. *et al.* (2016) 'α5GABAA receptor deficiency causes autism-like behaviors', *Annals of*
622 *Clinical and Translational Neurology*, 3(5), pp. 392–398. doi: 10.1002/acn3.303.

623

624

625

626

627

628

629

630

631

Supplementary material

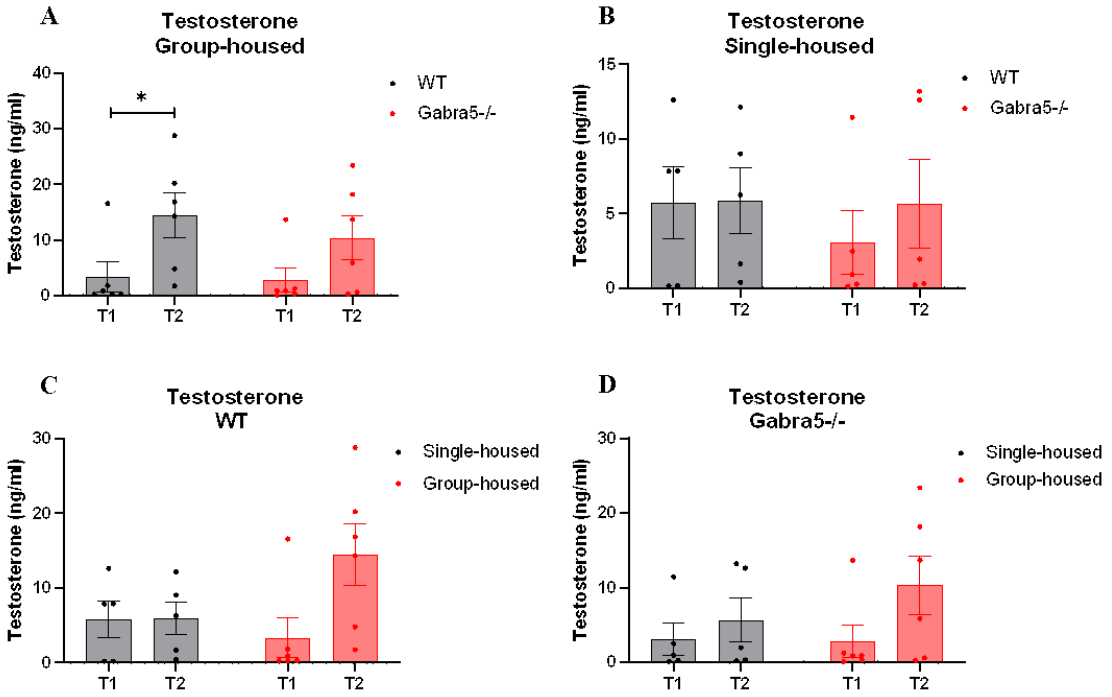

Figure S1. Testosterone levels in single- and group-housed males. AB testosterone levels comparison between genotypes in group- and single-housing. **CD** Same testosterone values but depending on housing within genotype. Two-way ANOVA with dependent measurements with Bonferroni's post-hoc test, *n*=6. Graphs show mean ± SEM. Significant effects of genotype or housing are indicated as *p < 0.05.

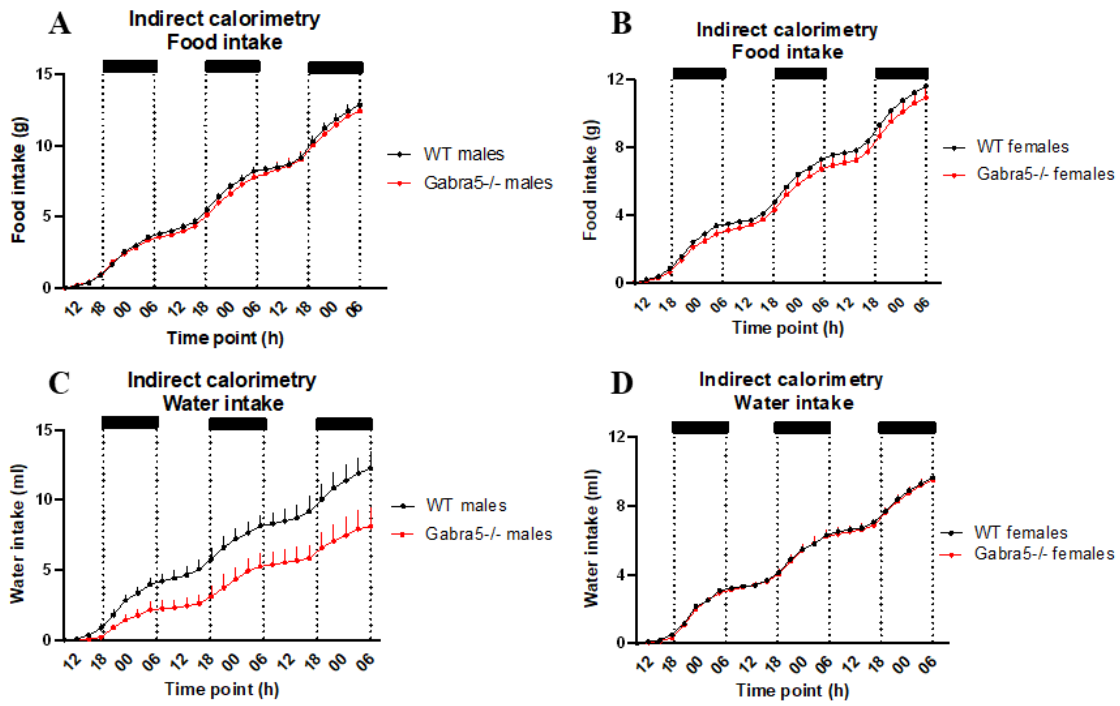

639

640 **Figure S2. Indirect calorimetry food and water intake**. **AB** Food intake monitored over three consecutive days where

641 shaded areas represent dark periods. **CD** Water intake monitored over three consecutive days where shaded areas

642 represent dark periods

643

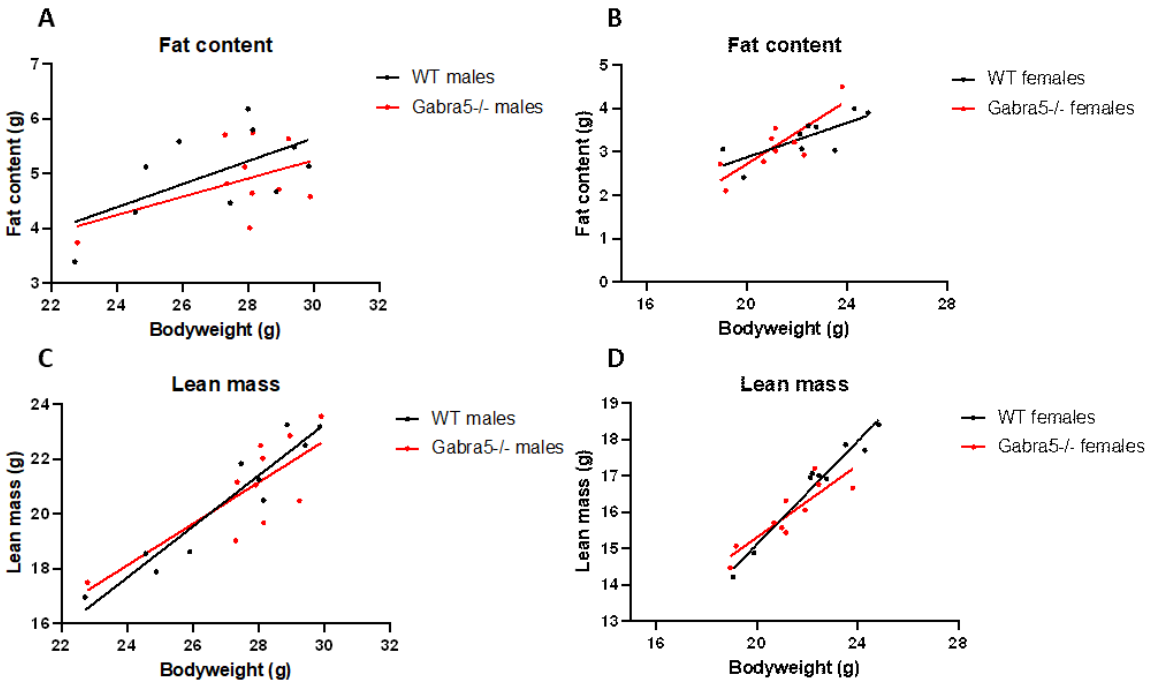

644

645 **Figure S3. Body composition analyses. AD** Fat and lean body mass plotted over bodyweight in WT and Gabra5$^{-/-}$

646 animals.

cells

MDPI

Review

CRISPR/Cas9 Epigenome Editing Potential for Rare Imprinting Diseases: A Review

Linn Amanda Syding [1,†], Petr Nickl [1,†], Petr Kasparek [1,2] and Radislav Sedlacek [1,2,*]

[1] Laboratory of Transgenic Models of Diseases, Institute of Molecular Genetics of the CAS, v.v.i, 252 50 Vestec, Czech Republic

[2] Czech Centre for Phenogenomics, Institute of Molecular Genetics of the CAS, v.v.i, 252 50 Vestec, Czech Republic

* Correspondence: Radislav.Sedlacek@img.cas.cz; Tel.: +420-325-873-243

† These authors contributed equally to this work.

Received: 21 March 2020; Accepted: 15 April 2020; Published: 16 April 2020

Abstract: Imprinting diseases (IDs) are rare congenital disorders caused by aberrant dosages of imprinted genes. Rare IDs are comprised by a group of several distinct disorders that share a great deal of homology in terms of genetic etiologies and symptoms. Disruption of genetic or epigenetic mechanisms can cause issues with regulating the expression of imprinted genes, thus leading to disease. Genetic mutations affect the imprinted genes, duplications, deletions, and uniparental disomy (UPD) are reoccurring phenomena causing imprinting diseases. Epigenetic alterations on methylation marks in imprinting control centers (ICRs) also alters the expression patterns and the majority of patients with rare IDs carries intact but either silenced or overexpressed imprinted genes. Canonical CRISPR/Cas9 editing relying on double-stranded DNA break repair has little to offer in terms of therapeutics for rare IDs. Instead CRISPR/Cas9 can be used in a more sophisticated way by targeting the epigenome. Catalytically dead Cas9 (dCas9) tethered with effector enzymes such as DNA de- and methyltransferases and histone code editors in addition to systems such as CRISPRa and CRISPRi have been shown to have high epigenome editing efficiency in eukaryotic cells. This new era of CRISPR epigenome editors could arguably be a game-changer for curing and treating rare IDs by refined activation and silencing of disturbed imprinted gene expression. This review describes major CRISPR-based epigenome editors and points out their potential use in research and therapy of rare imprinting diseases.

Keywords: rare disease; CRISPR/Cas9; epigenome editing; transcriptome editing; genomic imprinting; Angelman syndrome; Prader-Willi syndrome; transient neonatal diabetes mellitus; Silver-Russell syndrome

1. Introduction

1.1. CRISPR Epigenome Editors

The current course of genome engineering is set by tools derived from the bacterial immune system referred to as CRISPR/Cas9 (Clustered Regularly Interspaced Short Palindromic Repeats/CRISPR-associated protein 9). The system uses a ribonucleoprotein complex consisting of a short RNA molecule, a guide RNA (gRNA) and protein with nuclease activity Cas9 protein. The canonical CRISPR/Cas9 system acts as a site-specific nuclease, targeting a substrate DNA sequence, dictated by gRNA. Nuclease activity is executed by two Cas9 cleavage domains, RuvC (endonuclease domain termed after E.coli protein associated with DNA repair) and HNH (endonuclease domain termed after characteristic histidine and asparagine residues), which together mediate a double-strand

break (DSB) [1,2]. This mechanism has been broadly used for generating disease or transgenic models [3–5]. However, further improvement of the canonical CRISPR/Cas9 system led to more accurate genetic manipulations, exceeding the 'double-cut-based' editing.

An example of a more specific editor is the Cas9 nickase, a modified Cas9 protein with an inactivation mutation in one of the DNA cleavage domains, which results in single-strand breaks (SSB). The use of two adjacent nickases instead of the canonical Cas9 protein has proven to be more precise, with lower off-target effects and increased probability of the cell shifting towards homology-directed repair [6,7]. Further mutations of RuvC and HNH domains gave rise to a catalytically inactive "dead" Cas9 (dCas9). Establishment of dCas9 has further extended the application of CRISPR technology to gene regulation editing and opened a new venue to the understanding of diseases etiologies linked to epigenetic dysregulations [8–10].

Epigenetics, literal translation "on top of the genetics", involves mechanisms of gene regulation without changing the DNA sequence. The most critical processes participating in gene regulation are DNA methylation, histone modification, and chromatin remodeling [11]. Epigenetic machinery is controlled by groups of enzymes which are divided into three groups: writers, erasers, and readers.

DNA methylation is an epigenetic modification playing a crucial role in many regulatory processes. It is involved in regulation of transcriptional gene expression, genomic imprinting, X inactivation, silencing of mobile elements, and maintenance of genome integrity [12]. In the mammalian genome, DNA methylation or demethylation occurs at CpG sites, which are distributed throughout the genome, mainly in CpG-rich regions such as CpG islands. CpG islands can be part of promoters and distal regulatory elements where their methylation status contributes to gene transcriptional regulation. DNA methylation serves as a signal for the recruitment of epigenetic modifiers affecting the histone code or chromatin remodeling factors and often has a repressive effect [13,14].

The biochemistry of DNA methylation is based on the enzymatic addition of a methyl group to cytosine. This process is catalyzed by the "writer"—DNA methyltransferases (DNMTs). DNMTs are divided according to their function. Maintaining DNMT1 is responsible for methylation of hemimethylated DNA after replication. Methyltransferases DNMT3A, DNMT3B, and DNMT3L (co-factor DNA methyltransferase without enzymatic activity) are crucial for de novo DNA methylation, including the establishment of imprinting or gene silencing during embryonic development [15,16].

Removal of the methyl group from methylated cytosine (5mC) is either passive or active. The passive process of demethylation is replication-dependent and occurs throughout replication when a new DNA strand is not re-methylated yet. The active demethylation is a replication-independent process coupled with the conversion of methyl-cytosine to cytosine through oxidation or deamination [17]. Major 'erasers' or enzymes involved in the active demethylation are dioxygenases from the ten-eleven translocation family (TET1, TET2, and TET3) [18]. TET enzymes oxidize 5mC and produce 5-hydroxymethylcytosine (5hmC) intermediate, which is then oxidized to 5-formylcytosine (5fC) and 5-carbocylcytosine (5caC). These two intermediates are recognized and excised by thymine DNA glycosylase (TDG) [19]. The deamination pathway converts 5mC or 5hmC into 5-hydroxymethyluracil (5hmU) by the activation-induced deaminase (AID) and apolipoprotein B mRNA-editing enzyme complex (APOBEC), and 5hmU is then removed by uracil DNA glycosylase (UNG) [20,21].

Another regulatory process is histone modification, which involves chemical alternations on unstructured ends of histone proteins. Histone modification, essential for gene regulation, is conferred by methylation and acetylation on histones located in the vicinity of promoters or enhancers. The most studied histone modifications associated with gene activation are methylation of lysine 4 on histone 3 (H3K4) and lysine 36 (H3K36), or acetylation of lysine 9 (H3K9) and lysine 27 (H3K27) [22–24]. In contrast, modification, such as methylation of lysine 9 on histone 3 (H3K9), lysine 27 (H3K27) or lysine 20 (H3K20), are often linked to transcriptionally-repressed genes [22,25,26]. Enzymes responsible for histone modifications are designated as "writers" (adding methyl and acetyl residues), histone acetyltransferase (HAT) and histone methyltransferase (HMT), and "erasers" (removing the residues) histone demethylase (HDM) and histone deacetylase (HDAC) [27,28].

The epigenetic code is read by "readers", molecules perceiving the information encoded in the epigenetic code and recruiting other factors influencing the epigenetic landscape. Readers dispose of specialized domains through which they recognize changes in chromatin marks and attract a particular group of proteins, activators or repressors, depending on the epigenetic context [28]. Examples of DNA methylation readers are proteins MeCP2, MBD1–6 or SETDB1/2. In the case of the histone code, for instance, methylation is read by HP1 or Polycomb proteins, and acetylation by CREBBP or EP300 proteins and many others. The readers potentiate gene activation or repression and are a crucial part of epigenetic machinery utilized by epi-editor systems [28,29].

The field of genome engineering has adopted writers, erasers and, indirectly, readers, and developed new epigenome editing tools, enabling modulation of gene expression without altering genetic information.

1.2. Genomic Imprinting, Rare Imprinting Diseases, and Epigenome Engineering

Genomic imprinting, a term describing the parent-of-origin expression of specific genes was first described in 1984 when it was shown that both the maternal and paternal genome were crucial for normal development of mouse embryos [30,31]. Since then, over 150 imprinted genes have been verified in the murine genome, and approximately half of them have been found in humans [32]. Most imprinted genes have important placental and developmental functions. Increasing evidence has shown that they also regulate metabolism, stem cell function, sleep patterns, and feeding. The imprinted genes tend to be organized in clusters and 13 clusters have been identified so far. The clusters vary significantly in size from only a few genes to several megabases containing both maternally- and paternally-expressed genes [33]. These gene clusters are modulated by imprinting control regions (ICRs) that regulate the expression of the imprinted genes in cis [32]. The ICRs are methylated either maternally or paternally in the gametes by a robust mechanism involving transcription [34]. A methylated ICR is inactive, whereas an unmethylated ICR is active and alterations of the methylation on the ICRs lead to disrupted expression levels of the genes under its control. ICRs on the maternally inherited chromosomes are mostly hypermethylated as a mode of imprinting, the methylation is conferred by DNMT3A and its co-factor DNMT3L during oogenesis. The ICRs from the maternally inherited copies generally encompasses the promoters of large untranslated antisense transcript, overlapping protein-coding genes, when transcribed [35]. In male germ cells, these ICRs are fully unmethylated, allowing for the long non-coding antisense transcripts to be expressed, thus silencing the protein-coding genes, of which they overlap. The exact mode of action by which it silences the gene is still under debate [36]. Although the majority of the DNA methylated ICRs are acquired in the female germline, there are paternally-methylated imprinted loci described. The ICRs regulate the H19/IGF2, Rasgrf1 and Dlk1/Gtl2 loci [37].

The IGF2/H19 ICR is present on chromosome 11 and regulates fetal growth. Aberrations on this loci such as paternal hypomethylation of the ICR is present in the majority of patients with the imprinting disease Silver–Russell syndrome [38].

Disturbed expression of imprinted genes can occur either through genetic or epigenetic mechanisms. Genetic perturbation of imprinted genes can occur through mutations in the gene, duplications and deletions of larger segments. Uniparental disomy, a phenomenon where the chromosome is inherited from one parent-of-origin is also commonly occurring in diseases caused by imprinting defects. Epigenetic mutations cause aberrant expression via alteration in DNA methylation marks of ICRs in the imprinting clusters [39].

Imprinting diseases (IDs) are a group of rare congenital diseases that are caused by the aforementioned perturbations in imprinted genes. There are eight separate diseases known to us, but there are most likely more to be discovered and described [40]. Patients with rare IDs commonly carry intact genes but that are silenced through epigenetic mechanisms or by overexpression of imprinted genes. This taken together makes it evident that rare IDs have little benefit of first-generation CRISPR genome editing, relying on dsDNA breaks subsequently repaired through the error-prone

pathway NHEJ or the low-frequency HDR pathway. Rather, they are in dire need of sophisticated editing of the epigenome to activate existing but silenced genes. In the following sections, we will describe the molecular genetics of four known rare IDs and the possible applications new generation CRISPR epigenome editors could offer.

2. CRISPR-Based Epigenome Editors (CRISPR Epi-Editors)

The epigenetic landscape can be manipulated by small molecules referred to as epigenetic drugs. These drugs target writers and erasers and alter or inhibit their function, causing changes in the epigenetic state [41]. Although epigenetic drugs represent promising treatment for cancer, cardiovascular, neurological diseases, and metabolic disorders, their effect is broad, and they lack locus specificity [42,43].

A more specific alternative to epigenetic drugs might be epigenome editing by CRISPR/dCas9, which enables locus-specific epigenome alternations [44]. CRISPR-based epigenome editors (CRISPR epi-editors) consist of dCas9 and epigenetic effector, fused or non-covalently bound to dCas9 [3,44–47]. This complex is navigated by gRNA to a target sequence in which vicinity the epigenetic landscape is edited by the effector. The effector is either activator or repressor of gene transcription depending on the origin of the effector. The effectors are derived from epigenetic writers and erasers, such as DNMTs, HATs, HMTs and TETs, HDM, and HDAC, respectively [10,48,49]. Therefore, compared to the small molecules, that can relatively easy penetrate tissues of interest, CRISPR epi-editors might have a problem to be efficiently delivered in vivo. The most promising delivery system for CRISPR epi-editors with prolonged expression is AAV (adeno-associated virus) vectors with a packaging capacity of ~5 kb [50]. In spite the size of the SpCas9-gRNA-effector (*Streptococcus pyogenes* Cas9) complex exceeds an average packaging limit, the effective in vivo delivery is achievable with smaller dCas9 variants, or a different, less immunogenic delivery systems, such as EVs (extracellular vesicles), carrying CRISPR epi-editor plasmids or viral vectors [50–54]. Achieving the efficient delivery, high specificity, and non-immunogenicity represent the most crucial challenges standing before epigenome editing [55].

CRISPR epi-editors may be divided into four groups by their mode of action: chromatin reorganization, expression regulation, covalent histone and DNA modification [3,10,49,56]. Current research employs mainly the last three groups. Expression regulators, referred to as CRISPR activation (CRISPRa) and CRISPR interference (CRISPRi), use domains of transcriptional activators or repressors which mediate recruitment or blockage of transcription factors affecting transcriptional machinery [10,45,46,57]. In contrast, epi-editors with catalytic domains responsible for covalent histone modifications or DNA methylation are actors with own enzymatic activity [58–61].

The following sections provide an overview of the most relevant CRISPR epi-editors and their prospects in research or treatment of mentioned IDs.

2.1. DNA De/Methylation Mediated by CRISPR Epigenome Editors

Knowledge of the molecular mechanisms linked to methylation and demethylation contributed to the development of epigenome editors. Catalytic domains of enzymes responsible for DNA methylation have been adopted by CRISPR technology and given rise to programmable epi-editors capable of editing DNA methylation.

The first programmable DNA methylation editors were based on a fusion of the catalytic residues of programmable DNA binding molecules, such as ZFN or TALEN [62–65]. CRISPR epi-editors are designed by similar principles, through fusion or non-covalent attachment of active domains to DNA binding molecules; in this case, dCas9 [60,66–68]. However, CRISPR epi-editors, in contrast to ZFN and TALEN based epi-editors allow inexpensive and easily programmable epigenome engineering with a possibility of large-scale throughput analysis [69].

The current research focused on epigenome editing through DNA methylation mainly takes advantage of DNMTs or TETs. As mentioned above, DNMTs enzymes add the methyl group to cytosine, which has a silencing effect [15,16]. Therefore, the DNMTs catalytic domains have been

attached to dCas9 protein and produced a programmable silencing complex. In contrast, TETs, in combination with dCas9, have been used for demethylation leading to decondensation of chromatin and subsequent binding of transcription factors [16,60,67,70].

DNA methylation status can be edited by gRNA/dCas9-effector complex where the effectors are often DNA methyltransferases, mostly DNMT3A and DNMT3L (Figure 1B). DNMT3L lacks a catalytic domain mediating DNA methylation but enhances methylation by DNMT3A [16,60]. The effector can be either fused to the dCas9 protein through a linker or attached to RNA aptamers (e.g., MS2, com, PP7) or repetitive peptide epitopes via binding proteins (RNA aptamer binding proteins, e.g., MCP, COM, PCP; repetitive peptide epitopes binding proteins, e.g., single-chain variable fragment (ScFv) antibody). The advantage of the attached effector system is the potential recruitment of multiple copies of the effector, leading to a more robust change in methylation status (Figure 1F,G) [60,66–68]. Epi-editors with DNMT catalytic domains modify CpG-rich loci in the manner described above, leading to silencing of gene expression and chromatin rearrangements [15,16]. Locus-specific DNA methylation is enhanced while combinations of epi-editors are used, for instance, triple recruitment of DNMT3A, DNMT3L, and KRAB domains [66,71].

It has been reported that site-specific DNA methylation is achievable with the dCas9-DNMT complex. However, multiple studies have pointed out a higher efficiency of site-specific DNA methylation when DNMTs are multimerized. For example, Huang et al. (2017) showed that tethering of DNMT3A domains via SunTag system can lead to more robust and precise locus-specific DNA methylation due to a multimerization of DNMTs [66]. A similar synergistic effect has been shown by Amabile et al. (2016) after combinatorial use of DNMT3A, DNMT3L, and KRAB, fused to ZFP, followed by Stepper at al. (2016) with DNMT3A and DNMT3L fused to dCas9 [60,71].

In the past, DNA demethylation epi-editors were TALEN- or ZFP-based and fused with TET1 catalytic domain. Afterwards, CRISPR technology came and took over the locus-specific DNA demethylation [47,64,65,67,70]. CRISPR demethylation editors are structured in a similar way as DNA methylation systems but employ catalytic domains (CD) of functionally antagonistic enzymes, such as TET1 or TET3 (Figure 1B) [67,71]. Catalytic residues can be fused to dCas9 or attached to the gRNA/dCas9 complex via RNA aptamers or peptide repeats as described above [47,67,71].

TET catalytic domains have been proven effective in regards of site-specific DNA demethylation. Xu et al. (2016) have demonstrated demethylation of genes with CpG-rich promoters mediated by TET1-CD tethered via gRNA scaffold to dCas9 in vitro [67]. Furthermore, the potential of dCas-TET constructs was also proven in vivo by Xu et al. (2018). The Xu group targeted dCas9-TET3CD complex to genes essential for suppression of renal fibrosis. After treatment of affected mice, researchers observed elevated expression of targeted genes, together with decreased promoter methylation and reduced fibrogenesis in kidneys [70]. These studies imply that CRISPR epi-editor systems with TET catalytic domains are capable of effective demethylation in a locus-specific manner.

2.2. Histone Modifications by CRISPR Epi-Editors

Targeting the histone code represents another approach of intentional manipulation of the epigenetic landscape. Thus, catalytic domains of histone code maintaining enzymes have been adopted for epigenome editing. For instance, catalytic domains of PRDM9 (HMT), LSD1 (HDM), p300 (HAT), or HDAC3 (HDAC) have been fused to ZF, TALE, or dCas9 proteins.

Each of the listed domains is involved in the modification of lysine residues on histone 3 as a group of the crucial marks affecting gene regulation. Dead Cas9 fused to the SET domain of human PRDM9 mediates the addition of methyl groups to H3K4 and attaches the gene expression inducing mark, H3K4me3 (Figure 1B) [61]. The dCas9-LSD1 complex has an antagonistic effect and catalyzes the removal of the methyl group from H3K4me1/2 and H3K9me2, which has a repressive effect (Figure 1B). dCas9-LSD1 generally downregulates expression of the target gene through histone modification in a site of the cis-regulatory element or promoter [72,73]. Gene regulation can also be regulated through histone acetylation. The fusion of dCas9 and p300 catalytic domain enables the locus-specific addition

of acetyl groups on H3K27, resulting in transcriptional activation (Figure 1B) [58]. Partially in contrast to the dCas9-p300 complex, dCas9 fused to HDAC3 can either repress or promote transcription by removing the acetyl group on H327ac depending on the chromatin context (Figure 1B) [74]. The precise application of histone code targeting epi-editors has the potential to be used for deciphering the basis of rare diseases caused by dysregulation of histone modifications.

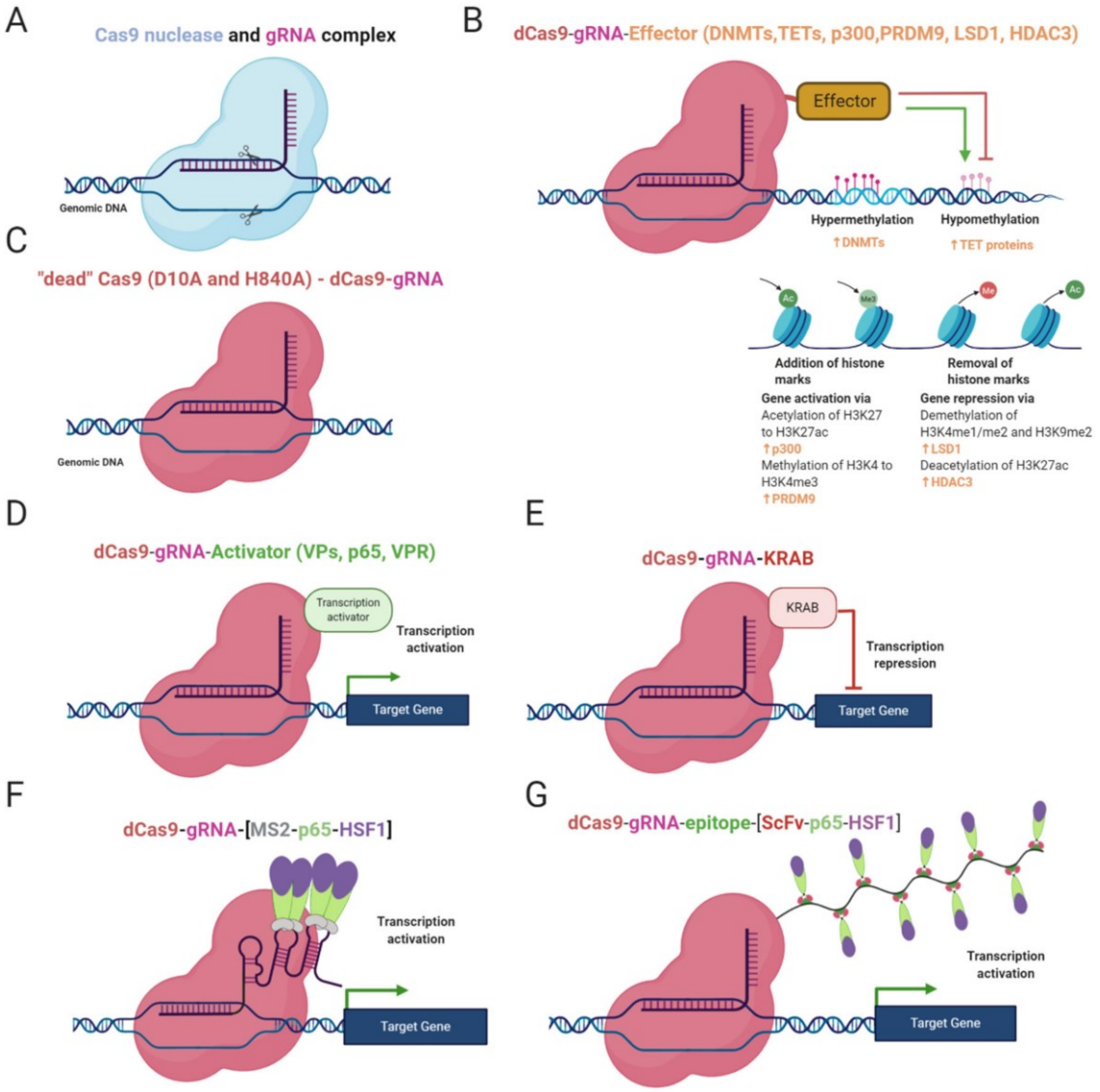

Figure 1. Epi-editor systems and their constitution. (**A**) Cas9 nuclease executing site-specific DSB; (**B**) dCas9 protein with effector domain of DNMTs or TETs or p300 or PRDM9 or LSD1 or HDAC3. DNMTs repress gene regulation through DNA methylation, TETs mediate demethylation of DNA and activate gene expression. p300 acetylates H3K27 and PRDM9 adds a third methyl residue on H3K4, with both effectors promoting gene expression. LSD1 removes methyl groups from H3K4me1/2 and H3K9me2, and HDAC3 deacetylates H3K27ac, with both modifications leading to repression of gene expression; (**C**) dCas9 protein with inactivation mutations, D10A and H84A in domain RvuC and HNH, respectively (**D**); CRISPR activator, dCas9 fused to distinct trans-activation proteins, such as VP64, p65, Rta; (**E**) CRISPR interference complex, dCas9 with KRAB repressing gene expression (**F**) CRISPRa, synergistic activation modulator (SAM) tethering trans-activating molecules (p65 and HSF1) on RNA scaffold through MS2 proteins. (**G**) CRISPRa, gene activating SunTaq system, consisting of dCas9 with repetitive peptide epitopes bound by single-chain variable fragment antibodies (ScFv) fused to trans-activation proteins (p65 and HSF1).

2.3. Gene Regulation by CRISPRa and CRISPRi Systems

CRISPR activation and CRISPR interference systems are CRISPR-based epi-editors consisting of dCas9 and an effector domain. Unlike the previous epi-editors, the effector domains of CRISPRa and CRISPRi are not catalytically active [9,48]. The mode of action is the recruitment of transcription promoting or repressing molecules, depending on features of the effector. CRISPRa system employs several activation factors, for instance, the transactivation domain of NF-κB p65 subunit (p65AD), herpes simplex viral protein 16 (VP16), four tandem copies of VP16 (VP64), or ten tandem copies of VP16 (VP160), (Figure 1D,F,G) [29,48,75,76].

The pursuit for more significant activation led to the development of tripartite target gene activator dCas9-VPR, consisting of dCas9 and tethered V64, p65AD, and Rta (Epstein–Barr virus trans-activator) proteins (Figure 1D). The system was proven to be a potent transcriptional activator, especially when multiplexing gRNAs along the promoter of interest [46].

Another approach for increasing the efficiency of activation is the use of synergistic activation mediator (SAM), using modified gRNA as a scaffold. As noted earlier, the scaffold is a tandem of aptamers (MS2, com, PP7) which are bound by RNA-binding proteins fused to a functional protein. In this case, functional proteins are p65AD, heat shock factor 1 (HSF1) with MCP proteins (Figure 1F). This scaffold can associate with dCas-V64 fusion protein and give rise to more efficient transcription activator [68,77].

An alternative to SAM is the SunTag system, tethering multiple V64 molecules through ScFv antibodies (Figure 1G) [78]. Although VPR, SAM, and SunTag systems are considered the most potent, they still cannot achieve maximal activation. Their high rate of performance is dependent on multiplexing gRNAs along the promoter, and their efficiency differs depending on the cell line, selected gRNAs, locus and chromatin environment [3,78]. An elegant solution for multiple gene regulation has been shown by Campa et al. [79]. The approach stands on expression of a relatively compact cassette consisting of ddCas12a (DNase dead Cas12a from *Acidaminococcus* sp.) fused to an effector and array of gRNAs, where each gRNA can affect different gene. Although the size of the cassette is reduced compared to other broadly used epigenome editing systems, it exceeds packaging capacity of AAV vectors. Therefore, use of more than one vector is still necessary, but this system represents a first step towards a robust, large-scale epigenome editing in vivo [79].

In the case of target gene repression, it can be achieved by using CRISPR interference tools which are based on dCas9 protein fused to a repressor domain, silencing the target gene. The first generation CRISPRi consisted of a gRNA/dCas9 complex (Figure 1C). The complex was targeted to the promoter sequence and sterically blocked gene expression. Even though this simple system could decrease the expression of target genes by 99% in prokaryotes, its performance in eukaryotic cells has not been so robust, 60–80% [80]. To produce more efficient programmable gene repressor, domains of mammalian transcriptional repressor were adopted and fused to dCas9 protein. CRISPRi system-mediated gene repression has been attempted with various dCas9 fusion proteins. For instance, Gilbert et al. have tested three different repressive domains: KRAB (Krüppel associated box) derived from transcription repressor Kox1 protein (ZNF10) (Figure 1E), CS domain (Chromo Shadow) of heterochromatin protein 1 (HP1), and the WRPW motif of transcription factor Hairy and enhancer of split-1 (HES1). The results showed that KRAB fusion is the most effective in target gene repression [48]. Therefore, the combination of KRAB repressor and dCas9 has been extensively used in other studies until the present day [57,81].

Activator and repressor systems can be combined with histone code epi-editors resulting in an extension of their ability to activate or repress target genes not only through recruitment of transcription machinery on the promoter but also affecting cis-regulatory elements [82].

2.4. Delivery

Therapeutic applications of epigenome editing require safe, efficient, tissue-specific delivery and sustained inducible expression, all of which can be partially achieved with viral vectors. Although lentiviral or retroviral delivery systems are capable of carrying large transgenic cassettes, their

immunogenicity, the potential to competent other viruses, and tendency to randomly integrate into the host genome make these systems less convenient for these types of therapeutic applications, even though attempts to reduce their integrative potential have been made [83,84]. In contrast, adenoviral vectors are non-integrative with transient expression and excellent transduction efficiency but with a risk of severe antigenicity [85]. According to many studies, potentially the least harmful vectors are derived from adeno-associated virus (AAV). Despite their low packaging capacity and transduction efficiency, these vectors are capable of delivering transgenes in a tissue-specific manner, with relatively long-term transient expression without significant pathogenicity effects [45,86,87].

Nonetheless, recombinant AAV serotypes with increased packaging capacity and the ability to cross the blood-brain barrier have been developed. These improvements make AAVs a serious candidate for the primary delivery system of epi-editors [88,89]. However, the capacity expansion is not sufficient enough for AAV particle to carry a whole epi-editor system. Therefore, multi-component, trans-splicing systems, or more compact orthologues of SpCas9 (1 366 aa) has been employed, e.g., dCas9 from *Neisseria meningitides* (NmCas9,1 082 aa) or *Staphylococcus aureus* (SaCas9,1 053 aa) [90,91].

The multi-component system has been used by Liao et al. where dCas9 and gRNA with the SAM complex were expressed separately from two and/or more vectors [45]. Furthermore, trans-splicing allowed delivery of sizable Cas9 protein which is divided into two vectors, and the RNA is put together and forms one functional Cas9 coding mRNA via RNA trans-splicing machinery [92]. Cas9 orthologues represent smaller versions of SpCas9 derived from different bacteria species. They are capable of reducing the size of the carried gene and open a possibility to be efficiently packaged into AAV particles [90,91].

An alternative to viral vectors are extracellular vesicles (EVs) which are lipid-bilayer particles naturally released from cells. EVs can be derived from autologous cells. Therefore, they have low immunogenicity and also the ability to target tissue or cell population of interest. Their affinity to specific tissues may be controlled through modification or removal of surface receptors [93]. A possible disadvantage of EVs is a short lifetime in vivo (up to 6 h) compared to AAV-mediated delivery (up to 2 days) [94,95]. It has been shown that cell-derived EVs enable efficient drug or gene delivery with minimal immune response. In addition, it has been successfully achieved to supply the tissue of interest with an AAV transgene cassette without an antigenic effect with so-called vexosomes, a combination of EVs and viral particles [54,96].

2.5. Inducible Systems

Furthermore, safer applications of the epi-editors have been examined by the utilization of inducible systems preventing the uncontrolled activity of the epi-editor cassette. Such an example is the optogenetic system, using two photoactivated binding proteins, cytochrome 2 (CRY2) and its interacting partner CIB1, to turn on epi-editor activity. In this case, the CRY2 domain is fused to the effector and CIB1 to dCas9 protein. The light-sensitive proteins, CRY2 and CIB1, interact when exposed to blue light. They activate the epi-editor by bringing together the effector and dCas9. The system is reversible, and after the removal of the blue light, the complex is destabilized and inactivated (Figure 2A) [97,98]. Another optogenetic system is CASANOVA (CRISPR–Cas9 activity switching via a novel optogenetic variant of AcrIIA4). Even though, this system has been used for gene editing it offers a new approach which can be adopted by epigenome editing system in the future. The CASANOVA system activates Cas9/gRNA complex upon blue light exposure. In the inactive state, the Cas9 complex is inhibited by a composite inhibitor AcrIIA4-LOV2, in which AcrIIA4 is an actuator derived from *Listeria monocytogenes* prophage fused to photosensor-LOV2 domain from A. sativa phototropin-1. When the inhibitor is exposed to blue light, it changes its conformation and allows the Cas9/gRNA complex to function. Upon removal of blue light, the inhibitor acquires its repressive conformation and binds back the Cas9/gRNA complex (Figure 2B) [99].

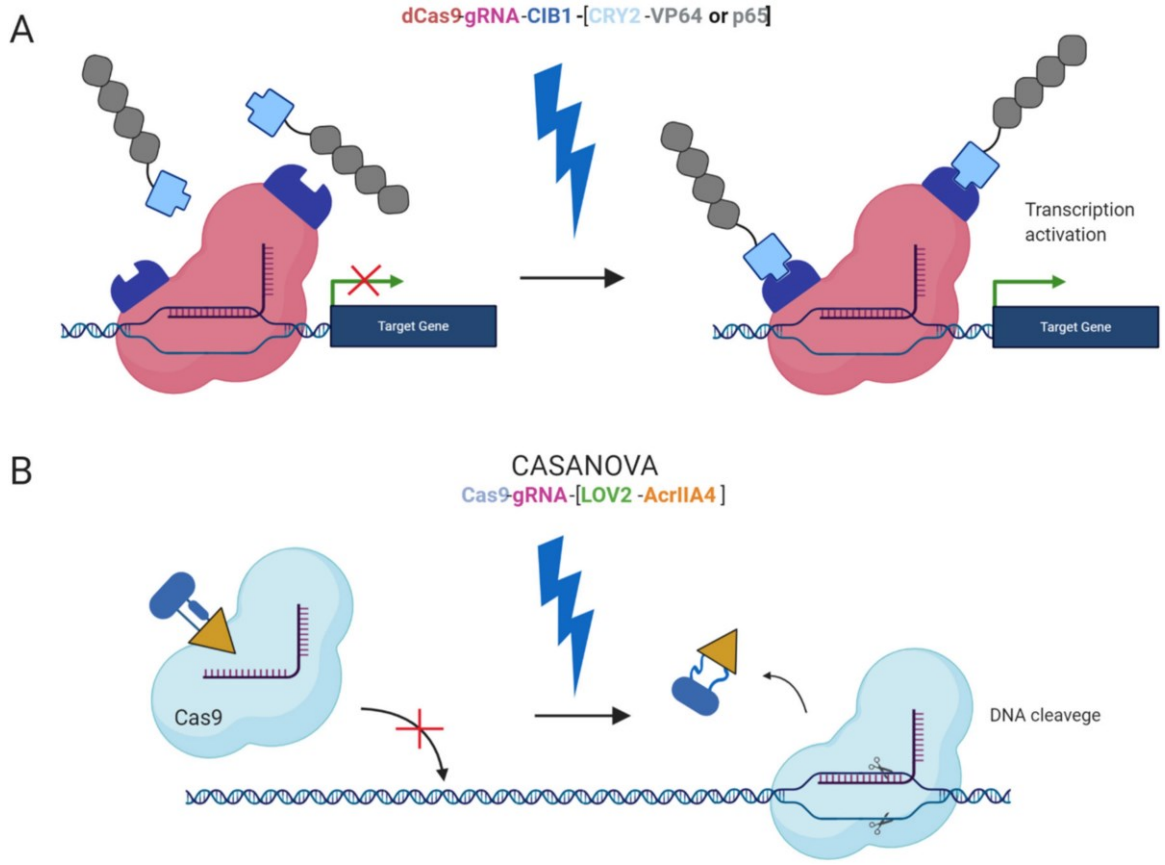

Figure 2. Light inducible CRISPR/Cas9 systems. (**A**) An inducible system based on blue light-dependent interaction between cytochrome 2 and CIB1 protein fused to CRISPRa components dCas9 and the effector (VP64 or p65). During exposure to the blue light two components are bound together and fully functional, upon removal of the blue light the complex is decomposed; (**B**) CASANOVA system, the blue light-inducible system controlling Cas9 nuclease activity via inhibitor LOV2-AcrIIA4. In the absence of the blue light, the inhibitor blocks Cas9 and prevents it from the binding the target sequence. In the presence of the blue light, the inhibitor is destabilized and released from Cas9 protein. Subsequently, Cas9 is active and executes DSB in the target locus when the blue light is removed the inhibitor binds back to Cas9.The chemically inducible systems are ligand-dependent. The interaction between the effector domain and dCas9 is conditioned by the presence of a ligand and two ligand-binding domains, linking two epi-editor components. Again, one of the binding domains fuses with the effector and the other with dCas9. In the presence of a ligand, both binding domains interact with the ligand and form a stable heterodimer resulting in the formation of an active epi-editor complex. Examples of ligand-binding domains are FK506 binding protein 12 (FKBP), and FKBP rapamycin binding protein (FRB) interacting together via rapamycin molecule (Figure 3A) [100], abscisic acid-induced dimerization of ABI and PYL1 domains (Figure 3B) [101], or gibberellin-induced dimerization of GID1 and GAI (Figure 3B) [101].

Moreover, other systems use ligands as inhibitors of proteolytic cleavage of a linker between dCas9 and the effector domain. The induction stands on the protease domain derived from the hepatitis C virus, ligand-inhibited NS3 protease. The protease domain connects dCas9 and the effector, the linker is cleaved unless the NS3 inhibitor is present. The inhibitor binds the NS3 domain and prevents separation of dCas9 from the effector (Figure 3D) [102]. A similar system takes advantage of proteasomal degradation, ligand-(Z)-4-hydroxytamoxifen (4OHT) binds a destabilized domain of the estrogen receptor fused to the effector domain and stabilizes it. In the absence of 4OHT, the whole effector complex is degraded in the proteasome. Thus, stabilization prevents degradation and the dCas9-effector complex is assembled and activated (Figure 3C) [103].

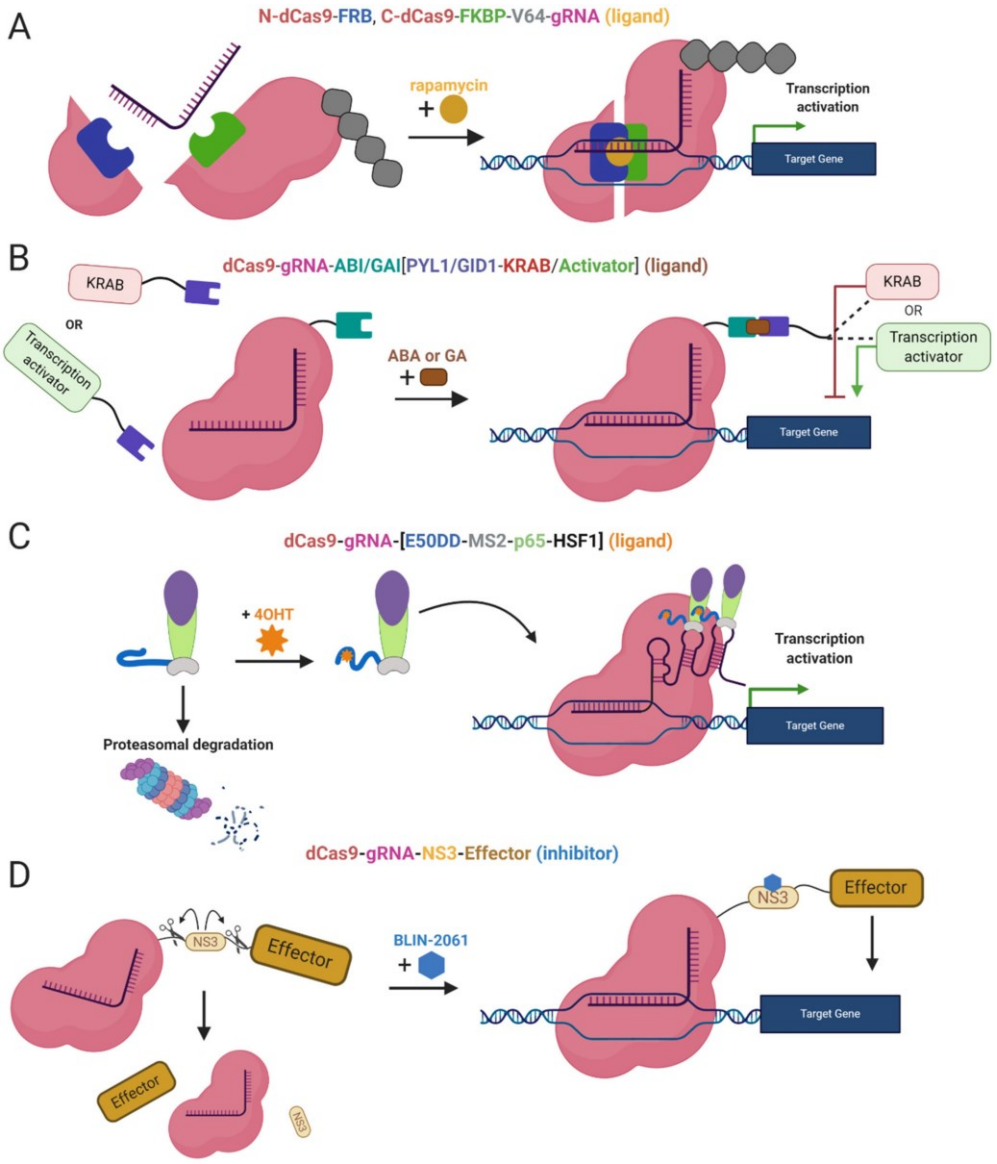

Figure 3. Chemically Inducible Epi-editors Systems. (**A**) Split dCas9-VP64 complex with one ligand-binding domain (LBD) at N-terminus of dCas9 and second LBD at C-terminus. Both LBDs bind a ligand (rapamycin, yellow) and bring together both halves of dCas9, resulting in the formation of functional gene activation complex; (**B**) Inducible system using phytohormones and phytohormone binding domains ABI or GAI fused to dCas9, and PYL1/GID1 fused to the effector-activator (VPR) or KRAB. The interaction via a ligand (abscisic acid or gibberellin) activates the epi-editor complex; (**C**) Inducible SAM system with a destabilized domain of estrogen receptor 50 (ER50DD). In the absence of a ligand-4OHT (4-hydroxytamoxifen), ER50DD protein is destabilized and leads the whole ER50DD-MS2-p65-HSF1 to proteasomal degradation, once the ligand is present it binds ER50DD and stabilizes it. Then complex is not degraded and therefore capable of interacting with RNA aptamers a form functional activation complex. (**D**) Inducible system with proteolytic cleavage. A part of the linker, between dCas9 and effector domain, is NS3 protein, protease from hepatitis C virus that cleaves peptide bonds in its vicinity. When NS3 is active, it cleaves the linked and abrogates the function of the epi-editor complex. The protease can be blocked by inhibitorBLIN-2061, leading to restoration of the epi-editor and its activity. The effect of ligands or inhibitors in the system mentioned above is reversible. After the inhibitor/ligand is diluted or metabolized, the chemical epi-editor systems are inactivated.

In conclusion, epi-editors represent a potent tool for gene regulation. Their combinatorial use provides a possibility of activation and repression of target genes at the same time without altering DNA or RNA sequence. They can compete with commonly used approaches such as RNAi or cDNA rescue with an advantage of higher, specificity, repression of all transcription variants or elevating the level of protein in isoform independent manner [104,105]. However, to make epi-editor systems safe for therapeutic purposes, many challenges must still be overcome—for instance, effective and non-immunogenic delivery with subsequent sustainable and tunable activity. Although off-target acting of epi-editor might seem less harmful compared to Cas9 gene editing, it is essential to make the epigenome editing as precise as possible due to the lack of complete knowledge of epigenome regulation. Therefore, the current research of epigenome editors aims for overcoming these challenges and possibly opens new avenues for treatment of diseases caused by epigenetic dysregulation.

3. Rare Imprinting Diseases and Therapy

Rare ID are in dire need of sophisticated editing of the epigenome to activate silenced genes. In the following sections, we review the molecular genetics of four rare IDs and how new-generation CRISPR epigenome editors could offer in terms of editing (Table 1).

Table 1. An overview of the chromosomal regions and frequency of mutations/epimutations for four selected rare ID.

Imprinting Disorder	Chromosome/Gene	Mutation/Epimutation	Frequency
Angelman Syndrome	15q11.2-13q	Maternal deletion UPD(15)Pat	1:12,000/1:20,000
	Ube3a	Methylation defects Point mutations	
Prader-Willi Syndrome	15q11.2-13q	Paternal deletion UPD(15)Mat Methylation defects	1:10,000/1:25,000
Transient Neonatal Diabetes Mellitus	6q24, PLAGL1/HYMA1	UPD(6)Pat Paternal duplication Methylation defects	1:400,000
Silver-Russell Syndrome	7	UPD(7)Mat	1:75,000/1:100,000
	11p15	UPD(11p15)Mat	
	IGF2/H19	Maternal duplication Paternal hypomethylation	

3.1. Angelman Syndrome

Angelman Syndrome (AS) is a rare neurodegenerative disease linked to the imprinted chromosomal region 15q11.2–13q [106]. Main features of AS include severe mental retardation, epileptic seizures, gait ataxia, sleep disturbances, and a fascination for water [107]. The disease genetics are comprised by mainly four genetic etiologies (i) de novo interstitial deletion of 15q11.2–13q on the maternal chromosome, spanning approximately 4 Mb in total [108]; (ii) paternal uniparental disomy, both regions are paternally inherited thus exhibiting paternal expression only [109]; (iii) imprinting defects due to incomplete or faulty epigenetic modification of the ICRs necessary for correct regulation [110]; and (iv) point mutations on the brain-specific paternally imprinted *Ube3a* gene, encoding a ubitiquin E3 ligase targeting substrate proteins for proteasomal decay. This gene has been proven to be solely capable of causing AS, labelling it as the AS gene [111,112].

The mode of imprinting differs maternally and paternally in the locus. The maternally-inherited locus is associated with hypermethylation, with the imprint established in the gametes [113,114]. The paternal mode of imprinting is associated with hypomethylation of the region where silencing of the *Ube3a* gene is mediated by an antisense transcript (further referred to as Ube3a-ATS) that blocks the expression of the paternal copy in cis [115]. The transcription start site (TSS) of Ube3a-ATS initiates at

the promoter/exon 1 region of the maternally imprinted gene *SNRPN* which is fully CpG methylated in the maternal copy and completely lacks methylation on the paternal one, rendering it transcriptionally active (Figure 4) [36].

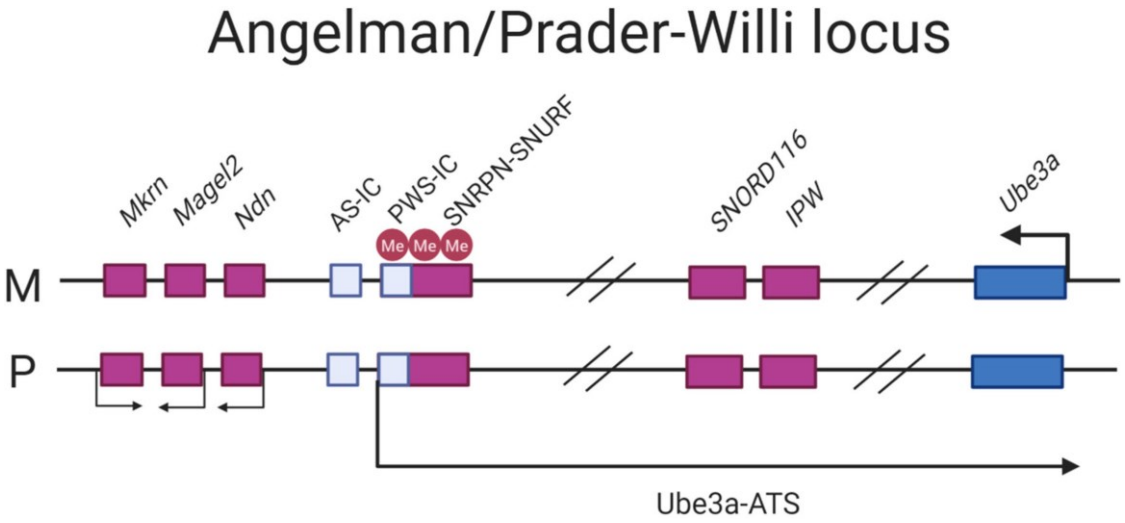

Figure 4. Schematic of the AS/PWS locus. The pink filled boxes: paternally expressed genes, blue filled boxes: maternally-expressed genes. The PWS/IC located in the promoter/exon 1 region of *SNRPN/SNURF* is hypermethylated on the maternally inherited chromosome thus silencing transcription of the Ube3a-ATS, allowing Ube3a to be expressed. The paternally-inherited PWS-IC is hypomethylated thus expressing the transcript, silencing *Ube3a*.

Ameliorating phenotypes associated with AS can be achieved by solely reinstating the expression of *Ube3a*. As recently demonstrated, pharmacological reinstatement of the paternal copy of *Ube3a* rescued cognitive defects in a murine mouse models and has proven to fully restore hippocampal synaptic plasticity [116–118]. The topoisomerase I inhibitor topotecan have significantly increased the paternal *Ube3a* expression, but its lack of specificity together with its toxicity are limitations that do not allow its efficient use in the disease treatment [117]. Anti-Ube3a-ATS oligonucleotides, administered via intracerebroventricular injections were tolerated as well as it provided the specificity that topotecan lacks but is limited by its transient nature, only allowing for Ube3a-ATS silencing up to four months [118]. Viral vectors carrying mouse *Ube3a* has been attempted to rescue AS by delivery into the hippocampus of an AS mouse. This study demonstrated rescue in hippocampus-dependent learning and memory but no alteration in the phenotypes, including movement deficits [119]. Further attempts to activate the silenced copy were conducted by providing AS patients with pro-methylation dietary supplements during one year, with the rationale that an increase of global DNA methylation should allow for Ube3a-ATS silencing; however, this study was not successful [120]. As discussed by Bi et al. (2016), for un-silencing of the paternal *Ube3a* to be rendered as a successful therapeutic option the effect should be long-lasting, non-toxic and specific, which has not yet been achieved by the efforts mentioned above [121].

The novel CRISPR epigenome editors could putatively provide a solution to previous limitations in regards to specificity, longevity and toxicity. For instance, programming gRNA to guide the catalytically inactive dCas9 tethered with DNMT3A for the CpG islands at the TSS for Ube3a-ATS should mimic the maternal inactive methylation pattern, associated with increased *Ube3a* expression. As discussed in by Silva-Santos et al. (2015) there is a window for improving motor-function deficits that does not extend beyond the postnatal stage in development [116]. For ameliorating cognitive deficits, it seems to be a window closing much earlier. However, at a cellular level the plasticity of the hippocampal neurons can be rescued later on as no critical window seems to exist [116]. How to overcome the limitations caused by critical time-windows and which the best mode of delivery of

treatments to patients would be, are two open questions for CRISPR based AS therapy. However, the CRISPR technology is continuously surmounting pitfalls such as off-target effects and delivery methods are being refined, preventing thus unspecific methylation and toxic reactions in the host. Furthermore, DNA methylation by dCas9-DNMT3A in cell lines has been proven to be stable and persisted through mitotic divisions [122]. Altogether, this points towards that CRISPR epigenome editing should be considered in the treatment of AS.

3.2. Prader–Willi Syndrome

Prader–Willi Syndrome (PWS) is linked to the locus 15q11–13q (Figure 4), as described for AS, distinguishing itself from AS by its clinical manifestation and parent-of-origin aberrancy. The majority of PWS patients harbor a 6 Mb or 5.4 Mb deletion, referred to as a type I and type II deletion on the paternal chromosome, respectively. Approximately 20–30% have maternal UPD; additional 1–3% have imprinting disorders leading to silencing of paternally expressed genes [123]. In contrast to AS where one main disease-causing gene has been confirmed, there are 15 genes in the PWS critical region [111,124]. However, evidence from collective efforts in deciphering the molecular genetics of PWS is suggesting that the C/D box snoRNA cluster SNORD116, expressed from its host transcript 116 HG, might be the key player in PWS [125]. C/D box snoRNAs are small nuclear RNAs that methylates ribosomal RNAs. Nevertheless, the SNORD116 cluster is considered non-canonical as it has no ribosomal RNA target and the function is largely unknown [126].

Additionally, sequencing of five patients with microdeletions has further narrowed the PWS critical region to 91 kb encompassing three non-coding genes; SNORD115, SNORD116, and IPW [127–131]. Where the loss of paternal inheritance leads to severe neuroendocrine and physical dysfunctions [132]. The full PWS phenotype is characterized by severe hypotonia with feeding difficulties in the first years of life that later progresses to hyperphagia, often leading to morbid obesity [133]. Moreover, PWS patients also exhibit hypogonadism, short stature, mild mental retardation, and psychotic behavior in adult life [134]. As the endocrine system is arguably the most affected system in PWS patients, growth hormone therapy ameliorates the aberrant growth, body composition, and behavioral phenotypes [135]. Prevention therapies, including ghrelin analogues, have been clinically tested and proven to significantly decrease the appetite in PWS patients [122]. Thus far, no treatment can rescue the full phenotype seen in patients.

As an increasing amount of studies are pointing towards SNORD116 to be the main causative player in PWS, reactivating it would be of interest as a possible therapeutic strategy [136]. Demonstrated by Cruvinal et al. (2014) the histone H3 lysine 9 (H3K9) methyltransferase SETDB1 together with the zinc finger protein ZN274 form a complex that silences the maternal SNORD116 cluster. Upon knockdown of SETDB1 in PWS induced pluripotent stem cells (iPSCs), these cells not only decreased the repressive H3K9me3 mark at the site but also partially restored the maternal 116HG RNA levels in the cells. In addition, knockdown of SETDB1 also disrupted the DNA methylation present on the PWS-IC, shifting it towards a paternal expression pattern [136]. Although a promising approach, the knockdown of SETDB1 lacks specificity as the SNORD116 cluster is not its only histone methylation target [137]. To consider the SETDB1 knockdown/out, it needs to acquire specificity. In another study, Kim et al. (2017) produced a knockout of the ZNF274 gene in neurons derived from PWS iPSCs and rescued SNORD116 expression without it affecting the methylation status in the PWS-IC [138].

Screenings of small molecule compounds possibly able to activate PWS candidate genes have been carried out in mouse fibroblasts derived from the transgenic SNRPN-EGFP mouse. Two inhibitors, UNC0642 and UNC0638, were able to inhibit the histone H3K9 methyltransferase G9a/EHMT2 and activate SNORD116 amongst other genes and subsequently rescued the perinatal lethality seen in this mouse model [139].

This taken together, activation of maternal SNORD116 would pose as a suitable candidate for PWS treatment strategy. To further narrow down the off-target effects, the modified CRISPR-Cas systems employ specificity and are considered to be largely tolerated. As discussed by Wang (2019),

the dCas9 tethered with LSD1—a H3K9 demethylase, would specifically reduce the repressive histone marks and allow for SNORD116 reactivation. As an option, manipulation of SETDB1 and ZNF274 could be considered although they could arguably lead to a more global effect [124]. However, in the experiments with ZNF274 and SETDB1 knockdown, the increase of maternally reactivated genes were far from being as expressed as on the paternal allele. The open question is whether a partial restoration is enough to rescue the phenotype. In addition, the experiments were conducted on iPSCs which reflects the conditions during early development, but it does not address the critical windows for restorations later on [136]

3.3. Transient Neonatal Diabetes Mellitus Type 1

Transient neonatal diabetes mellitus type 1 (TNDM) is a rare ID affecting 1:400,000 births. TNDM is characterized by intrauterine growth retardation, failure to thrive in the neonatal stage, dehydration, macroglossia, umbilical hernia, and hyperglycemia requiring exogenous insulin for approximately three months after birth [140]. Endogenous levels of insulin are extremely sparse; however, by 18 months of age, the affected individuals have recovered [141]. Given appropriate treatment and recovery, this rare imprinting disease gives transient phenotypes, but there is a relapse rate of 40% later in life with type 2 diabetes, typically during adolescence. The affected, although diagnosed with type 1 diabetes in infancy, exhibits a type 2 diabetes profile if relapse occurs, as the affected does not have islet cell antibodies characteristic of the immunogenic type I diabetes, nor do they have HLA haplotypes which are diabetes susceptible. A region of 5.4 Mb on 6q24 that is subjected to differential methylation has been linked to TNDM [142]. Genetic and epigenetic etiologies causing TNDM can be grouped as follows: (i) paternal UPD; (ii) interstitial duplications of the paternal locus; and (iii) hypomethylation of the maternal allele allowing for transcription from a normally silenced allele (Figure 5) [143,144]. Analysis of the TNDM region identified two genes which, when overexpressed, cause TNDM, namely; PLAGL1 (pleomorphic adenoma gene-like 1), a zinc finger protein coding gene and HYMAI, an untranslated mRNA [145–147]. The maternal imprinting of the genes is modulated by methylation of the promoter/exon 1 of HYMAI, previously shown to be crucial for controlling gene expression in the TNDM mouse model [147].

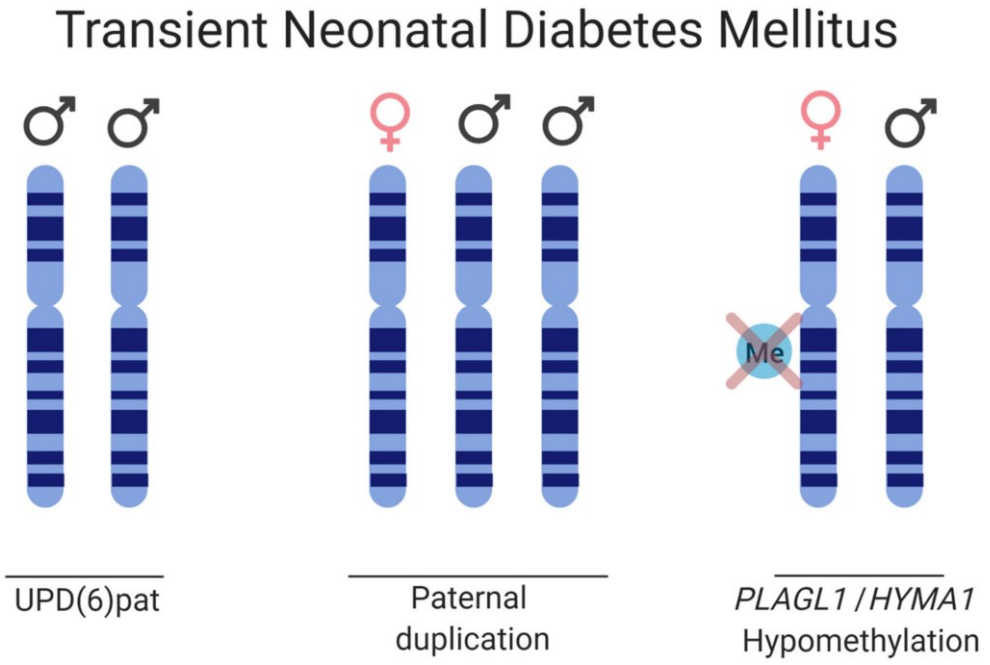

Figure 5. Schematic of the disease causes for TNDM. Three etiologies are depicted, paternal UPD of chromosome 6, paternal duplication of chromosome 6, and hypomethylation on the maternal HYMA1/PLAGL1 promoter, thus allowing for biallelic expression.

The PLAGL1 is a zinc finger transcription factor shown to control cell cycle regulation and apoptosis [148]. Furthermore, in mice, the PLAGL1 was shown to positively and negatively regulate beta-cell proliferation and glucose-stimulated insulin release through binding the promoter of the pituitary adenylate cyclase-activating polypeptide type 1 receptor (PACAP) [149]. The role of imprinted transcript HYMA1 is yet to be elucidated [150].

The first-line treatment for TNDM caused by chromosome 6 aberrations is exogenous insulin administered to the patient during the neonatal stage to manage the glucose levels [151]. Upon relapse, however, the consensus on treatment is lacking. In one patient case described by Zhang (2015), a Chinese teenager with a clinical history of maternal hypomethylation at 6q24 associated-TNDM was successfully treated with sulfonylurea, a class of organic compounds used as antidiabetic drugs for type 2 diabetes. The patient reached the glycemic goal of 7–10 mmol/L after sulfonylurea therapy with no subsequent organ damage or apparent side effects [152]. The drug acts by stimulating the release of insulin from the beta cells in the pancreas and can be administered given that the patient has functional receptors for sulfonylurea in the pancreatic beta cells. The rationale behind sulfonylurea treatment is that the patient would have a reduced sensitivity to glucose and its cellular uptake would be aided by sulfonylurea induced insulin secretion [153]. Treatment with insulin, however, is merely a treatment of existing symptoms, not a cure per se and is of little benefit to address other complications connected to the disease. Ideally, a genetic therapy that decreases the PLAGL1 and HYMA1 expression would be early onset treatment. As aforementioned, dCas9/gRNA complexes can be targeted to the promoter sequence and sterically block gene expression, with an efficiency of 60–80% in eukaryotes [69]. For higher silencing efficiencies, the dCas9 and KRAB domains would be employed. As for patients with paternal UPD or interstitial duplications a full silencing would not be beneficial, rather a decrease to mimic the wild-type situation should be considered. For patients harboring hypomethylation on the maternal allele, the dCas9-DNMT3A poses as a convenient candidate for methylating the promoter/exon 1 of HYMA1 and so decreasing the expression to the ordinary levels. The question when and how to therapeutically intervene remains as the TNDM is normally diagnosed after the first symptoms appears. Furthermore, silencing sterically or silencing through the KRAB effector domain is merely transient and more information must be obtained regarding the mode and frequency of administration.

3.4. Silver–Russell Syndrome

Silver–Russell Syndrome (SRS) is a rare ID caused by either (i) maternal UPD of chromosome 7, (ii) maternal UPD of the 11p15 locus, or (iii) paternal hypomethylation of the paternal H19/IGF2 DMR [154]. The disease manifestation varies greatly from very mild to severe phenotypes [155]. The primary locus of interest in SRS is the imprinted region at 11p15, a region with two imprinting domains consisting of the H19/IGF2 IG-DMR (ICR1) and KCNQ1OT1 TSS-DMR (ICR2) regulating the genes H19/IGF2 and the KCNQ1/CDKN1C, respectively [155–157]. The H19/IGF2 IG-DMR is paternally methylated, which in turns hinders the CTCF from binding it; this allows the shared enhancers to activate the transcription of IGF2 that is essential for fetal growth (Figure 6) [158]. KCNQ1OT1 TSS-DMR is maternally methylated, and loss of imprinted mutation is the most prevalent cause of Beckwith–Wiedemann syndrome (BWS), a syndrome considered as a distinct but mirrored syndrome of SRS, as they are both caused by aberrations on the 11p15 locus but from different parent-of-origin and have opposite phenotype in disturbed growth [159]. The most frequent cause of SRS is hypomethylation of the H19/IGF2 IG-DMR, displayed by 40% of the affected, in turn leading to a decreased expression of IGF2 and a biallelic expression of H19 [38]. Ten percent has maternal UPD of the chromosome 7 and additional 1–3% have a duplication of the maternally inherited 11p15; for an overview of the locus arrangement see Figure 6. The phenotypes vary drastically in severity, from nearly undetectable symptoms to severe clinical manifestations [160]. The predominant symptoms characterizing SRS is reduced intrauterine and postnatal growth but can also often include macrocephaly and a prominent forehead. In addition,

speech delays, organ asymmetry, hypoglycemia, and feeding difficulties are amongst symptoms that are part of the disease picture [161].

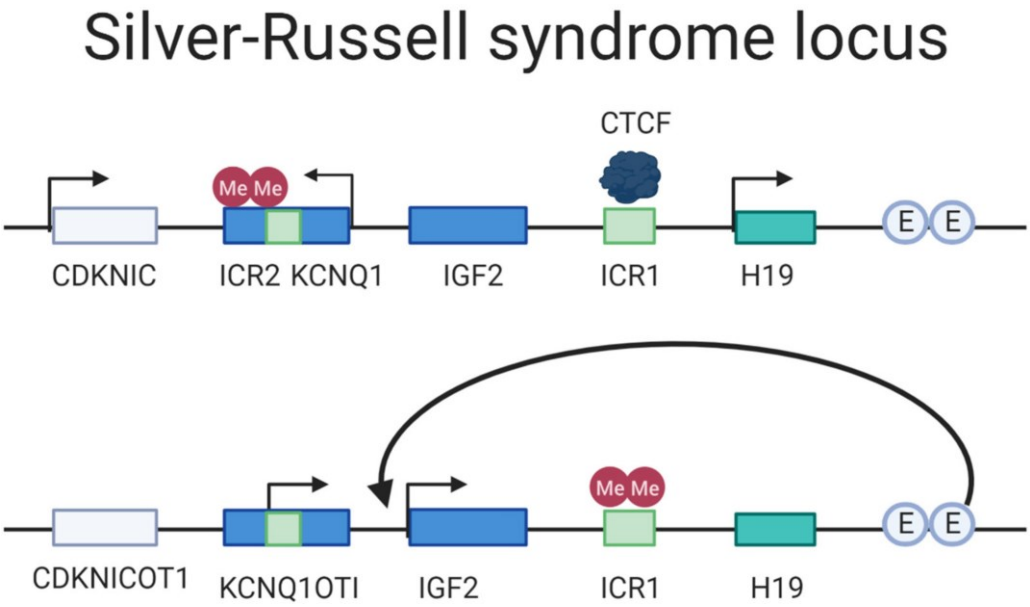

Figure 6. Locus overview of the SRS region. The upper drawing depicts the maternal regulation of the locus. The ICR2 is hypermethylated where the maternally expressed genes KCNQ1 and CDKNIC are expressed. The ICR1 is not methylated, allowing the CTCF motif to bind it and hindering the enhancers (E) to activate IGF2 expression. The lower drawing paternally inherited ICR1 is methylated, thus inhibiting CTCF binding and allowing the enhancers to regulate IGF2 transcription. The ICR2 is not methylated paternally and the non-coding transcript KCNQ1OTI is expressed. Adapted from: Azzi et al. (2009) [158].

Currently, the treatment of SRS aims to manage the symptoms for the patients that vary depending on how the disease manifests itself. Growth hormone therapy, nutritional and caloric supplements and therapy for oral-motor problems may be included as treatments. Moreover, in cases of cleft palate or micrognathia should be addressed by craniofacial surgery [162]. Aforementioned treatments do not provide an entirely satisfactory rescue of all symptoms. An introduction of a mutant ICR in maternal duplication distal chromosome 7 mouse fetuses resulted in activated IGF2 and H19 correction. Furthermore, this reinstatement resulted in significant growth enhancement [163]. Future efforts for correcting the disease could include epi-editors for IGF2 activation, or inhibition through methylation of H19/IGF2 IG-DMR locus to block CTCF from binding and, hence, allow for IGF2 expression.

4. Conclusions

The new advancement of CRISPR/Cas9 epigenome editors provides promising tools for editing and possibly treating rare IDs. Dead Cas9 fused or bound to an 'epi- effector' domain can modulate gene expression in most conceivable ways able to ameliorate or treat rare IDs caused by aberrant gene expression of imprinted genes. Thus, the epigenome editors based on CRISPR/Cas system represents new ways of activating existing but silenced alleles on the other parent-of-origin chromosome or ways to decrease the expression of genes, which are improperly biallelically expressed. However, the therapeutic potential of the systems reviewed is limited as efficient delivery systems need to be further developed. Additional investigation is also required to identify critical therapeutic window for every individual disease. Albeit many challenges are ahead, the CRISPR systems have beyond doubt opened up novel door for treatment of rare IDs based on epigenome editing, which has not been possible before.

Author Contributions: Conceptualization: P.N. and L.A.S.; writing—original draft preparation: P.N. and L.A.S.; writing—review and editing: P.N., L.A.S.; visualization: P.N. and L.A.S.; writing and manuscript preparation: P.K. and R.S.; funding: R.S. All authors have read and agreed to the published version of the manuscript.

Funding: This research was funded by the European Union's Horizon 2020 research and innovation program under the Marie Skłodowska-Curie grant agreement no. 765269, RVO 68378050 by the Czech Academy of Sciences (CAS), LM2015040, LMS2018126 (Czech Centre for Phenogenomics) CZ.1.05/1.1.00/02.0109 (Biotechnology and Biomedicine Centre of the Academy of Sciences and Charles University in Vestec), by MEYS (Ministry of Education, Youth and Sports).

Conflicts of Interest: The authors declare no conflict of interest.

References

1. Jinek, M.; Chylinski, K.; Fonfara, I.; Hauer, M.; Doudna, J.A.; Charpentier, E. A Programmable Dual-RNA-Guided DNA Endonuclease in Adaptive Bacterial Immunity. *Science* **2012**, *337*, 816–821. [CrossRef] [PubMed]
2. Jinek, M.; Jiang, F.; Taylor, D.W.; Sternberg, S.H.; Kaya, E.; Ma, E.; Anders, C.; Hauer, M.; Zhou, K.; Lin, S.; et al. Structures of Cas9 Endonucleases Reveal RNA-Mediated Conformational Activation. *Science* **2014**, *343*, 1247997. [CrossRef] [PubMed]
3. Gilbert, L.A.; Horlbeck, M.A.; Adamson, B.; Villalta, J.E.; Chen, Y.; Whitehead, E.H.; Guimaraes, C.; Panning, B.; Ploegh, H.L.; Bassik, M.C.; et al. Genome-Scale CRISPR-Mediated Control of Gene Repression and Activation. *Cell* **2014**, *159*, 647–661. [CrossRef] [PubMed]
4. Kato, T.; Hara, S.; Goto, Y.; Ogawa, Y.; Okayasu, H.; Kubota, S.; Tamano, M.; Terao, M.; Takada, S. Creation of mutant mice with megabase-sized deletions containing custom-designed breakpoints by means of the CRISPR/Cas9 system. *Sci. Rep.* **2017**, *7*, 59. [CrossRef]
5. Kitamoto, K.; Taketani, Y.; Fujii, W.; Inamochi, A.; Toyono, T.; Miyai, T.; Yamagami, S.; Kuroda, M.; Usui, T.; Ouchi, Y. Generation of mouse model of TGFBI-R124C corneal dystrophy using CRISPR/Cas9-mediated homology-directed repair. *Sci. Rep.* **2020**, *10*, 1–10. [CrossRef] [PubMed]
6. Ran, F.A.; Hsu, P.D.; Lin, C.Y.; Gootenberg, J.S.; Konermann, S.; Trevino, A.E.; Scott, D.A.; Inoue, A.; Matoba, S.; Zhang, Y.; et al. Double nicking by RNA-guided CRISPR cas9 for enhanced genome editing specificity. *Cell* **2013**, *154*, 1380–1389. [CrossRef] [PubMed]
7. Chen, X.; Tasca, F.; Wang, Q.; Liu, J.; Janssen, J.M.; Brescia, M.D.; Bellin, M.; Szuhai, K.; Kenrick, J.; Frock, R.L.; et al. Expanding the editable genome and CRISPR-Cas9 versatility using DNA cutting-free gene targeting based on in trans paired nicking. *Nucleic Acids Res.* **2020**, *48*, 974–995. [CrossRef] [PubMed]
8. Vigouroux, A.; Oldewurtel, E.; Cui, L.; Bikard, D.; Teeffelen, S. Tuning dCas9's ability to block transcription enables robust, noiseless knockdown of bacterial genes. *Mol. Syst. Biol.* **2018**, *14*. [CrossRef]
9. Perez-Pinera, P.; Kocak, D.D.; Vockley, C.M.; Adler, A.F.; Kabadi, A.M.; Polstein, L.R.; Thakore, P.I.; Glass, K.A.; Ousterout, D.G.; Leong, K.W.; et al. RNA-guided gene activation by CRISPR-Cas9–based transcription factors. *Nat. Methods* **2013**, *10*, 973–976. [CrossRef]
10. Maeder, M.L.; Linder, S.J.; Cascio, V.M.; Fu, Y.; Ho, Q.H.; Joung, J.K. CRISPR RNA-guided activation of endogenous human genes. *Nat. Methods* **2013**, *10*, 977–979. [CrossRef]
11. Li, E. Chromatin modification and epigenetic reprogramming in mammalian development. *Nat. Rev. Genet.* **2002**, *3*, 662–673. [CrossRef]
12. Inbar-Feigenberg, M.; Choufani, S.; Butcher, D.T.; Roifman, M.; Weksberg, R. Basic concepts of epigenetics. *Fertil. Steril.* **2013**, *99*, 607–615. [CrossRef]
13. Jones, P.A. Functions of DNA methylation: Islands, start sites, gene bodies and beyond. *Nat. Rev. Genet.* **2012**, *13*, 484–492. [CrossRef] [PubMed]
14. Rasmussen, K.D.; Helin, K. Role of TET enzymes in DNA methylation, development, and cancer. *Genes Dev.* **2016**, *30*, 733–750. [CrossRef]
15. Okano, M.; Bell, D.W.; Haber, D.A.; Li, E. DNA methyltransferases Dnmt3a and Dnmt3b are essential for de novo methylation and mammalian development. *Cell* **1999**, *99*, 247–257. [CrossRef]
16. Bourc'his, D.; Xu, G.L.; Lin, C.S.; Bollman, B.; Bestor, T.H. Dnmt3L and the establishment of maternal genomic imprints. *Science* **2001**, *294*, 2536–2539. [CrossRef] [PubMed]

17. Sadakierska-Chudy, A.; Kostrzewa, R.M.; Filip, M. A Comprehensive View of the Epigenetic Landscape Part I: DNA Methylation, Passive and Active DNA Demethylation Pathways and Histone Variants. *Neurotox. Res.* **2015**, *27*, 84–97. [CrossRef]
18. Hill, P.W.S.; Amouroux, R.; Hajkova, P. DNA demethylation, Tet proteins and 5-hydroxymethylcytosine in epigenetic reprogramming: An emerging complex story. *Genomics* **2014**, *104*, 324–333. [CrossRef]
19. Cortellino, S.; Xu, J.; Sannai, M.; Moore, R.; Caretti, E.; Coz, M.L.; Devarajan, K.; Wessels, A.; Soprano, D.; Abramowitz, K.; et al. Demethylation by Linked Deamination-Base Excision Repair. *Cell* **2011**, *146*, 67–79. [CrossRef]
20. Nabel, C.S.; Jia, H.; Ye, Y.; Shen, L.; Goldschmidt, H.L.; Stivers, J.T.; Zhang, Y.; Kohli, R.M. AID/APOBEC deaminases disfavor modified cytosines implicated in DNA demethylation. *Nat. Chem. Biol.* **2012**, *8*, 751–758. [CrossRef]
21. Dizdaroglu, M.; Bergtold, D.S. Characterization of free radical-induced base damage in DNA at biologically relevant levels. *Anal. Biochem.* **1986**, *156*, 182–188. [CrossRef]
22. Barski, A.; Cuddapah, S.; Cui, K.; Roh, T.Y.; Schones, D.E.; Wang, Z.; Wei, G.; Chepelev, I.; Zhao, K. High-Resolution Profiling of Histone Methylations in the Human Genome. *Cell* **2007**, *129*, 823–837. [CrossRef] [PubMed]
23. Koch, C.M.; Andrews, R.M.; Flicek, P.; Dillon, S.C.; Karaöz, U.; Clelland, G.K.; Wilcox, S.; Beare, D.M.; Fowler, J.C.; Couttet, P.; et al. The landscape of histone modifications across 1% of the human genome in five human cell lines. *Genome Res.* **2007**, *17*, 691–707. [CrossRef] [PubMed]
24. Creyghton, M.P.; Cheng, A.W.; Welstead, G.G.; Kooistra, T.; Carey, B.W.; Steine, E.J.; Hanna, J.; Lodato, M.A.; Frampton, G.M.; Sharp, P.A.; et al. Histone H3K27ac separates active from poised enhancers and predicts developmental state. *Proc. Natl. Acad. Sci. USA* **2010**, *107*, 21931–21936. [CrossRef] [PubMed]
25. Liu, Y.; Liu, K.; Yin, L.; Yu, Y.; Qi, J.; Shen, W.H.; Zhu, J.; Zhang, Y.; Dong, A. H3K4me2 functions as a repressive epigenetic mark in plants. *Epigenet. Chromatin* **2019**, *12*, 40. [CrossRef] [PubMed]
26. Rosenfeld, J.A.; Wang, Z.; Schones, D.E.; Zhao, K.; DeSalle, R.; Zhang, M.Q. Determination of enriched histone modifications in non-genic portions of the human genome. *BMC Genom.* **2009**, *10*, 143. [CrossRef]
27. Lu, D. Epigenetic modification enzymes: Catalytic mechanisms and inhibitors. *Acta Pharm. Sin. B* **2013**, *3*, 141–149. [CrossRef]
28. Biswas, S.; Rao, C.M. Epigenetic tools (The Writers, The Readers and The Erasers) and their implications in cancer therapy. *Eur. J. Pharmacol.* **2018**, *837*, 8–24. [CrossRef]
29. Enríquez, P. CRISPR-mediated epigenome editing. *Yale J. Biol. Med.* **2016**, *89*, 471–486.
30. Surani, M.A.H.; Barton, S.C.; Norris, M.L. Development of reconstituted mouse eggs suggests imprinting of the genome during gametogenesis. *Nature* **1984**, *308*, 548–550. [CrossRef]
31. McGrath, J.; Solter, D. Completion of mouse embryogenesis requires both the maternal and paternal genomes. *Cell* **1984**, *37*, 179–183. [CrossRef]
32. Peters, J. The role of genomic imprinting in biology and disease: An expanding view. *Nat. Rev. Genet.* **2014**, *15*, 517–530. [CrossRef] [PubMed]
33. Williamson, C.M.; Thomas, S.; Beechey, C.V.; Hancock, J.; Cattanach, B.M.; Peters, J. MRC Harwell, Oxfordshire. World Wide Web Site - Mouse Imprinting Data and References. 2013. Available online: http://www.har.mrc.ac.uk/research/genomic_imprinting/ (accessed on 3 March 2020).
34. Chotalia, M.; Smallwood, S.A.; Ruf, N.; Dawson, C.; Lucifero, D.; Frontera, M.; James, K.; Dean, W.; Kelsey, G. Transcription is required for establishment of germline methylation marks at imprinted genes. *Genes Dev.* **2009**, *23*, 105–117. [CrossRef] [PubMed]
35. Barlow, D.P. Genomic Imprinting: A Mammalian Epigenetic Discovery Model. *Annu. Rev. Genet.* **2011**, *45*, 379–403. [CrossRef] [PubMed]
36. Meng, L.; Person, R.E.; Beaudet, A.L. Ube3a-ATS is an atypical RNA polymerase II transcript that represses the paternal expression of Ube3a. *Hum. Mol. Genet.* **2012**, *21*, 3001–3012. [CrossRef]
37. Kato, Y.; Kaneda, M.; Hata, K.; Kumaki, K.; Hisano, M.; Kohara, Y.; Okano, M.; Li, E.; Nozaki, M.; Sasaki, H. Role of the Dnmt3 family in de novo methylation of imprinted and repetitive sequences during male germ cell development in the mouse. *Hum. Mol. Genet.* **2007**, *16*, 2272–2280. [CrossRef]
38. Russo, S.; Calzari, L.; Mussa, A.; Mainini, E.; Cassina, M.; Di Candia, S.; Clementi, M.; Guzzetti, S.; Tabano, S.; Miozzo, M.; et al. A multi-method approach to the molecular diagnosis of overt and borderline 11p15.5

defects underlying Silver–Russell and Beckwith–Wiedemann syndromes. *Clin. Epigenetics* **2016**, *8*, 23. [CrossRef]
39. Wilkins, J.F.; Úbeda, F. Chapter 13—Diseases Associated with Genomic Imprinting. In *Progress in Molecular Biology and Translational Science*; Cheng, X., Blumenthal, R.M., Eds.; Academic Press: Cambridge, MA, USA, 2011; Volume 101, pp. 401–445. ISBN 1877-1173.
40. Eggermann, T.; Netchine, I.; Temple, I.K.; Tümer, Z.; Monk, D.; Mackay, D.; Grønskov, K.; Riccio, A.; Linglart, A.; Maher, E.R. Congenital imprinting disorders: EUCID.net—A network to decipher their aetiology and to improve the diagnostic and clinical care. *Clin. Epigenetics* **2015**, *7*, 23. [CrossRef]
41. Heerboth, S.; Lapinska, K.; Snyder, N.; Leary, M.; Rollinson, S.; Sarkar, S. Use of epigenetic drugs in disease: An overview. *Genet. Epigenetics* **2014**, *1*, 9–19. [CrossRef]
42. Ptak, C.; Petronis, A. Epigenetics and Complex Disease: From Etiology to New Therapeutics. *Annu. Rev. Pharmacol. Toxicol.* **2008**, *48*, 257–276. [CrossRef]
43. El Bahhaj, F.; Dekker, F.J.; Martinet, N.; Bertrand, P. Delivery of epidrugs. *Drug Discov. Today* **2014**, *19*, 1337–1352. [CrossRef] [PubMed]
44. Thakore, P.I.; D'Ippolito, A.M.; Song, L.; Safi, A.; Shivakumar, N.K.; Kabadi, A.M.; Reddy, T.E.; Crawford, G.E.; Gersbach, C.A. Highly specific epigenome editing by CRISPR-Cas9 repressors for silencing of distal regulatory elements. *Nat. Methods* **2015**, *12*, 1143–1149. [CrossRef] [PubMed]
45. Liao, H.K.; Hatanaka, F.; Araoka, T.; Reddy, P.; Wu, M.Z.; Sui, Y.; Yamauchi, T.; Sakurai, M.; O'Keefe, D.D.; Núñez-Delicado, E.; et al. In Vivo Target Gene Activation via CRISPR/Cas9-Mediated Trans-epigenetic Modulation. *Cell* **2017**, *171*, 1495–1507.e15. [CrossRef] [PubMed]
46. Chavez, A.; Scheiman, J.; Vora, S.; Pruitt, B.W.; Tuttle, M.; P R Iyer, E.; Lin, S.; Kiani, S.; Guzman, C.D.; Wiegand, D.J.; et al. Highly efficient Cas9-mediated transcriptional programming. *Nat. Methods* **2015**, *12*, 326–328. [CrossRef]
47. Morita, S.; Noguchi, H.; Horii, T.; Nakabayashi, K.; Kimura, M.; Okamura, K.; Sakai, A.; Nakashima, H.; Hata, K.; Nakashima, K.; et al. Targeted DNA demethylation in vivo using dCas9-peptide repeat and scFv-TET1 catalytic domain fusions. *Nat. Biotechnol.* **2016**, *34*, 1060–1065. [CrossRef]
48. Gilbert, L.A.; Larson, M.H.; Morsut, L.; Liu, Z.; Brar, G.A.; Torres, S.E.; Stern-Ginossar, N.; Brandman, O.; Whitehead, E.H.; Doudna, J.A.; et al. XCRISPR-mediated modular RNA-guided regulation of transcription in eukaryotes. *Cell* **2013**, *154*, 442. [CrossRef]
49. Pflueger, C.; Tan, D.; Swain, T.; Nguyen, T.; Pflueger, J.; Nefzger, C.; Polo, J.M.; Ford, E.; Lister, R. A modular dCas9-SunTag DNMT3A epigenome editing system overcomes pervasive off-target activity of direct fusion dCas9-DNMT3A constructs. *Genome Res.* **2018**, *28*, 1193–1206. [CrossRef]
50. Wu, Z.; Yang, H.; Colosi, P. Effect of genome size on AAV vector packaging. *Mol. Ther.* **2010**, *18*, 80–86. [CrossRef]
51. Grieger, J.C.; Samulski, R.J. Packaging Capacity of Adeno-Associated Virus Serotypes: Impact of Larger Genomes on Infectivity and Postentry Steps. *J. Virol.* **2005**, *79*, 9933–9944. [CrossRef]
52. Saleh, A.F.; Lázaro-Ibáñez, E.; Forsgard, M.A.M.; Shatnyeva, O.; Osteikoetxea, X.; Karlsson, F.; Heath, N.; Ingelsten, M.; Rose, J.; Harris, J.; et al. Extracellular vesicles induce minimal hepatotoxicity and immunogenicity. *Nanoscale* **2019**, *11*, 6990–7001. [CrossRef]
53. Matharu, N.; Rattanasopha, S.; Tamura, S.; Maliskova, L.; Wang, Y.; Bernard, A.; Hardin, A.; Eckalbar, W.L.; Vaisse, C.; Ahituv, N. CRISPR-mediated activation of a promoter or enhancer rescues obesity caused by haploinsufficiency. *Science* **2019**, *363*, eaau0629. [CrossRef] [PubMed]
54. György, B.; Fitzpatrick, Z.; Crommentuijn, M.H.W.; Mu, D.; Maguire, C.A. Naturally enveloped AAV vectors for shielding neutralizing antibodies and robust gene delivery in vivo. *Biomaterials* **2014**, *35*, 7598–7609. [CrossRef] [PubMed]
55. Colella, P.; Ronzitti, G.; Mingozzi, F. Emerging Issues in AAV-Mediated In Vivo Gene Therapy. *Mol. Ther. Methods Clin. Dev.* **2018**, *8*, 87–104. [CrossRef] [PubMed]
56. Braun, S.M.G.; Kirkland, J.G.; Chory, E.J.; Husmann, D.; Calarco, J.P.; Crabtree, G.R. Rapid and reversible epigenome editing by endogenous chromatin regulators. *Nat. Commun.* **2017**, *8*. [CrossRef]
57. MacLeod, R.S.; Cawley, K.M.; Gubrij, I.; Nookaew, I.; Onal, M.; O'Brien, C.A. Effective CRISPR interference of an endogenous gene via a single transgene in mice. *Sci. Rep.* **2019**, *9*, 1–12. [CrossRef]

58. Hilton, I.B.; D'Ippolito, A.M.; Vockley, C.M.; Thakore, P.I.; Crawford, G.E.; Reddy, T.E.; Gersbach, C.A. Epigenome editing by a CRISPR-Cas9-based acetyltransferase activates genes from promoters and enhancers. *Nat. Biotechnol.* **2015**, *33*, 510–517. [CrossRef]
59. Kearns, N.A.; Pham, H.; Tabak, B.; Genga, R.M.; Silverstein, N.J.; Garber, M.; Maehr, R. Functional annotation of native enhancers with a Cas9-histone demethylase fusion. *Nat. Methods* **2015**, *12*, 401–403. [CrossRef]
60. Stepper, P.; Kungulovski, G.; Jurkowska, R.Z.; Chandra, T.; Krueger, F.; Reinhardt, R.; Reik, W.; Jeltsch, A.; Jurkowski, T.P. Efficient targeted DNA methylation with chimeric dCas9-Dnmt3a-Dnmt3L methyltransferase. *Nucleic Acids Res.* **2017**, *45*, 1703–1713. [CrossRef]
61. Cano-Rodriguez, D.; Gjaltema, R.A.F.; Jilderda, L.J.; Jellema, P.; Dokter-Fokkens, J.; Ruiters, M.H.J.; Rots, M.G. Writing of H3K4Me3 overcomes epigenetic silencing in a sustained but context-dependent manner. *Nat. Commun.* **2016**, *7*, 1–11. [CrossRef]
62. Rivenbark, A.G.; Stolzenburg, S.; Beltran, A.S.; Yuan, X.; Rots, M.G.; Strahl, B.D.; Blancafort, P. Epigenetic reprogramming of cancer cells via targeted DNA methylation. *Epigenetics* **2012**, *7*, 350–360. [CrossRef]
63. Bernstein, D.L.; Le Lay, J.E.; Ruano, E.G.; Kaestner, K.H. TALE-mediated epigenetic suppression of CDKN2A increases replication in human fibroblasts. *J. Clin. Invest.* **2015**, *125*, 1998–2006. [CrossRef]
64. Chen, H.; Kazemier, H.G.; De Groote, M.L.; Ruiters, M.H.J.; Xu, G.-L.; Rots, M.G. Induced DNA demethylation by targeting Ten-Eleven Translocation 2 to the human ICAM-1 promoter. *Nucleic Acids Res.* **2014**, *42*, 1563–1574. [CrossRef] [PubMed]
65. Maeder, M.L.; Angstman, J.F.; Richardson, M.E.; Linder, S.J.; Cascio, V.M.; Tsai, S.Q.; Ho, Q.H.; Sander, J.D.; Reyon, D.; Bernstein, B.E.; et al. Targeted DNA demethylation and activation of endogenous genes using programmable TALE-TET1 fusion proteins. *Nat. Biotechnol.* **2013**, *31*, 1137–1142. [CrossRef] [PubMed]
66. Huang, Y.-H.; Su, J.; Lei, Y.; Brunetti, L.; Gundry, M.C.; Zhang, X.; Jeong, M.; Li, W.; Goodell, M.A. DNA epigenome editing using CRISPR-Cas SunTag-directed DNMT3A. *Genome Biol.* **2017**, *18*, 176. [CrossRef] [PubMed]
67. Xu, X.; Tao, Y.; Gao, X.; Zhang, L.; Li, X.; Zou, W.; Ruan, K.; Wang, F.; Xu, G.; Hu, R. A CRISPR-based approach for targeted DNA demethylation. *Cell Discov.* **2016**, *2*, 16009. [CrossRef] [PubMed]
68. Zalatan, J.G.; Lee, M.E.; Almeida, R.; Gilbert, L.A.; Whitehead, E.H.; La Russa, M.; Tsai, J.C.; Weissman, J.S.; Dueber, J.E.; Qi, L.S.; et al. Engineering Complex Synthetic Transcriptional Programs with CRISPR RNA Scaffolds. *Cell* **2015**, *160*, 339–350. [CrossRef] [PubMed]
69. Qi, L.; Lo, A. Genetic and epigenetic control of gene expression by CRISPR-Cas systems. *F1000Research* **2017**, *6*, 747. [CrossRef] [PubMed]
70. Xu, X.; Tan, X.; Tampe, B.; Wilhelmi, T.; Hulshoff, M.S.; Saito, S.; Moser, T.; Kalluri, R.; Hasenfuss, G.; Zeisberg, E.M.; et al. High-fidelity CRISPR/Cas9- based gene-specific hydroxymethylation rescues gene expression and attenuates renal fibrosis. *Nat. Commun.* **2018**, *9*, 1–15. [CrossRef]
71. Amabile, A.; Migliara, A.; Capasso, P.; Biffi, M.; Cittaro, D.; Naldini, L.; Lombardo, A. Inheritable Silencing of Endogenous Genes by Hit-and-Run Targeted Epigenetic Editing. *Cell* **2016**, *167*, 219–232.e14. [CrossRef]
72. Williams, R.M.; Senanayake, U.; Artibani, M.; Taylor, G.; Wells, D.; Ahmed, A.A.; Sauka-Spengler, T. Genome and epigenome engineering CRISPR toolkit for in vivo modulation of cis-regulatory interactions and gene expression in the chicken embryo. *Development* **2018**, *145*. [CrossRef]
73. Shi, Y.; Lan, F.; Matson, C.; Mulligan, P.; Whetstine, J.R.; Cole, P.A.; Casero, R.A.; Shi, Y. Histone demethylation mediated by the nuclear amine oxidase homolog LSD1. *Cell* **2004**, *119*, 941–953. [CrossRef] [PubMed]
74. Kwon, D.Y.; Zhao, Y.T.; Lamonica, J.M.; Zhou, Z. Locus-specific histone deacetylation using a synthetic CRISPR-Cas9-based HDAC. *Nat. Commun.* **2017**, *8*, 15315. [CrossRef] [PubMed]
75. Hirai, H.; Tani, T.; Kikyo, N. Structure and functions of powerful transactivators: VP16, MyoD and FoxA. *Int. J. Dev. Biol.* **2011**, *54*, 1589–1596. [CrossRef] [PubMed]
76. Cheng, A.W.; Wang, H.; Yang, H.; Shi, L.; Katz, Y.; Theunissen, T.W.; Rangarajan, S.; Shivalila, C.S.; Dadon, D.B.; Jaenisch, R. Multiplexed activation of endogenous genes by CRISPR-on, an RNA-guided transcriptional activator system. *Cell Res.* **2013**, *23*, 1163–1171. [CrossRef]
77. Konermann, S.; Brigham, M.D.; Trevino, A.E.; Joung, J.; Abudayyeh, O.O.; Barcena, C.; Hsu, P.D.; Habib, N.; Gootenberg, J.S.; Nishimasu, H.; et al. Genome-scale transcriptional activation by an engineered CRISPR-Cas9 complex. *Nature* **2015**, *517*, 583–588. [CrossRef]

78. Chavez, A.; Tuttle, M.; Pruitt, B.W.; Ewen-Campen, B.; Chari, R.; Ter-Ovanesyan, D.; Haque, S.J.; Cecchi, R.J.; Kowal, E.J.K.; Buchthal, J.; et al. Comparison of Cas9 activators in multiple species. *Nat. Methods* **2016**, *13*, 563–567. [CrossRef]
79. Campa, C.C.; Weisbach, N.R.; Santinha, A.J.; Incarnato, D.; Platt, R.J. Multiplexed genome engineering by Cas12a and CRISPR arrays encoded on single transcripts. *Nat. Methods* **2019**, *16*, 887–893. [CrossRef]
80. Qi, L.S.; Larson, M.H.; Gilbert, L.A.; Doudna, J.A.; Weissman, J.S.; Arkin, A.P.; Lim, W.A. Repurposing CRISPR as an RNA-Guided Platform for Sequence-Specific Control of Gene Expression. *Cell* **2013**, *152*, 1173–1183. [CrossRef]
81. Gasperini, M.; Hill, A.J.; McFaline-Figueroa, J.L.; Martin, B.; Kim, S.; Zhang, M.D.; Jackson, D.; Leith, A.; Schreiber, J.; Noble, W.S.; et al. A Genome-wide Framework for Mapping Gene Regulation via Cellular Genetic Screens. *Cell* **2019**, *176*, 377–390.e19. [CrossRef]
82. Li, K.; Liu, Y.; Cao, H.; Zhang, Y.; Gu, Z.; Liu, X.; Yu, A.; Kaphle, P.; Dickerson, K.E.; Ni, M.; et al. Interrogation of enhancer function by enhancer-targeting CRISPR epigenetic editing. *Nat. Commun.* **2020**, *11*, 1–16. [CrossRef]
83. Connoly, J.B. Lentiviruses in gene therapy clinical reseach. *Gene Ther.* **2002**, *9*, 1730–1734. [CrossRef] [PubMed]
84. Yáñez-Muñoz, R.J.; Balaggan, K.S.; MacNeil, A.; Howe, S.J.; Schmidt, M.; Smith, A.J.; Buch, P.; MacLaren, R.E.; Anderson, P.N.; Barker, S.E.; et al. Effective gene therapy with nonintegrating lentiviral vectors. *Nat. Med.* **2006**, *12*, 348–353. [CrossRef] [PubMed]
85. Wold, W.; Toth, K. Adenovirus Vectors for Gene Therapy, Vaccination and Cancer Gene Therapy. *Curr. Gene Ther.* **2014**, *13*, 421–433. [CrossRef]
86. Naso, M.F.; Tomkowicz, B.; Perry, W.L.; Strohl, W.R. Adeno-Associated Virus (AAV) as a Vector for Gene Therapy. *BioDrugs* **2017**, *31*, 317–334. [CrossRef]
87. Landegger, L.D.; Pan, B.; Askew, C.; Wassmer, S.J.; Gluck, S.D.; Galvin, A.; Taylor, R.; Forge, A.; Stankovic, K.M.; Holt, J.R.; et al. A synthetic AAV vector enables safe and efficient gene transfer to the mammalian inner ear. *Nat. Biotechnol.* **2017**, *35*, 280–284. [CrossRef] [PubMed]
88. Grieger, J.C.; Choi, V.W.; Samulski, R.J. Production and characterization of adeno-associated viral vectors. *Nat. Protoc.* **2006**, *1*, 1412–1428. [CrossRef]
89. Hudry, E.; Andres-Mateos, E.; Lerner, E.P.; Volak, A.; Cohen, O.; Hyman, B.T.; Maguire, C.A.; Vandenberghe, L.H. Efficient Gene Transfer to the Central Nervous System by Single-Stranded Anc80L65. *Mol. Ther. Methods Clin. Dev.* **2018**, *10*, 197–209. [CrossRef]
90. Hoffmann, M.D.; Aschenbrenner, S.; Grosse, S.; Rapti, K.; Domenger, C.; Fakhiri, J.; Mastel, M.; Orner, K.B.; Eils, R.; Grimm, D.; et al. Cell-specific CRISPR-Cas9 activation by microRNA-dependent expression of anti-CRISPR proteins. *Nucleic Acids Res.* **2019**, *47*, 75. [CrossRef]
91. Thakore, P.I.; Kwon, J.B.; Nelson, C.E.; Rouse, D.C.; Gemberling, M.P.; Oliver, M.L.; Gersbach, C.A. RNA-guided transcriptional silencing in vivo with S. aureus CRISPR-Cas9 repressors. *Nat. Commun.* **2018**, *9*, 1674. [CrossRef]
92. Chew, W.L.; Tabebordbar, M.; Cheng, J.K.W.; Mali, P.; Wu, E.Y.; Ng, A.H.M.; Zhu, K.; Wagers, A.J.; Church, G.M. A multifunctional AAV–CRISPR–Cas9 and its host response. *Nat. Methods* **2016**. [CrossRef]
93. Vogt, S.; Stadlmayr, G.; Grillari, J.; Rüker, F.; Wozniak-Knopp, G. Engineering of Surface Proteins in Extracellular Vesicles for Tissue-Specific Targeting. In *Current Topics in Biochemical Engineering*; IntechOpen: London UK, 2019.
94. Göran Ronquist, K. Extracellular vesicles and energy metabolism. *Clin. Chim. Acta* **2019**, *488*, 116–121. [CrossRef] [PubMed]
95. Van Gestel, M.A.; Boender, A.J.; De Vrind, V.A.J.; Garner, K.M.; Luijendijk, M.C.M.; Adan, R.A.H. Recombinant adeno-associated virus: Efficient transduction of the rat VMH and clearance from blood. *PLoS ONE* **2014**, *9*, e97639. [CrossRef] [PubMed]
96. Maguire, C.A.; Balaj, L.; Sivaraman, S.; Crommentuijn, M.H.W.; Ericsson, M.; Mincheva-Nilsson, L.; Baranov, V.; Gianni, D.; Tannous, B.A.; Sena-Esteves, M.; et al. Microvesicle-associated AAV vector as a novel gene delivery system. *Mol. Ther.* **2012**, *20*, 960–971. [CrossRef]
97. Polstein, L.R.; Gersbach, C.A. A light-inducible CRISPR-Cas9 system for control of endogenous gene activation. *Nat. Chem. Biol.* **2015**, *11*, 198–200. [CrossRef] [PubMed]

98. Nihongaki, Y.; Yamamoto, S.; Kawano, F.; Suzuki, H.; Sato, M. CRISPR-Cas9-based photoactivatable transcription system. *Chem. Biol.* **2015**, *22*, 169–174. [CrossRef] [PubMed]
99. Bubeck, F.; Hoffmann, M.D.; Harteveld, Z.; Aschenbrenner, S.; Bietz, A.; Waldhauer, M.C.; Börner, K.; Fakhiri, J.; Schmelas, C.; Dietz, L.; et al. Engineered anti-CRISPR proteins for optogenetic control of CRISPR–Cas9. *Nat. Methods* **2018**, *15*, 924–927. [CrossRef]
100. Zetsche, B.; Volz, S.E.; Zhang, F. A split-Cas9 architecture for inducible genome editing and transcription modulation. *Nat. Biotechnol.* **2015**, *33*, 139–142. [CrossRef]
101. Gao, Y.; Xiong, X.; Wong, S.; Charles, E.J.; Lim, W.A.; Qi, L.S. Complex transcriptional modulation with orthogonal and inducible dCas9 regulators. *Nat. Methods* **2016**, *13*, 1043–1049. [CrossRef]
102. Tague, E.P.; Dotson, H.L.; Tunney, S.N.; Sloas, D.C.; Ngo, J.T. Chemogenetic control of gene expression and cell signaling with antiviral drugs. *Nat. Methods* **2018**, *15*, 519–522. [CrossRef]
103. Maji, B.; Moore, C.L.; Zetsche, B.; Volz, S.E.; Zhang, F.; Shoulders, M.D.; Choudhary, A. Multidimensional chemical control of CRISPR-Cas9. *Nat. Chem. Biol.* **2017**, *13*, 9–11. [CrossRef]
104. Stojic, L.; Lun, A.T.L.; Mangei, J.; Mascalchi, P.; Quarantotti, V.; Barr, A.R.; Bakal, C.; Marioni, J.C.; Gergely, F.; Odom, D.T. Specificity of RNAi, LNA and CRISPRi as loss-of-function methods in transcriptional analysis. *Nucleic Acids Res.* **2018**, *46*, 5950–5966. [CrossRef] [PubMed]
105. Kampmann, M. CRISPRi and CRISPRa screens in mammalian cells for precision biology and medicine HHS Public Access. *ACS Chem. Biol.* **2018**, *13*, 406–416. [CrossRef] [PubMed]
106. Van Buggenhout, G.; Fryns, J.-P. Angelman syndrome (AS, MIM 105830). *Eur. J. Hum. Genet.* **2009**, *17*, 1367–1373. [CrossRef]
107. Williams, C.A.; Driscoll, D.J.; Dagli, A.I. Clinical and genetic aspects of Angelman syndrome. *Genet. Med.* **2010**, *12*, 385–395. [CrossRef] [PubMed]
108. Sandanam, T.; Beange, H.; Robson, L.; Woolnough, H.; Buchholz, T.; Smith, A. Manifestations in institutionalised adults with Angelman syndrome due to deletion. *Am. J. Med. Genet.* **1997**, *70*, 415–420. [CrossRef]
109. Malcolm, S.; Clayton-Smith, J.; Nichols, M.; Pembrey, M.E.; Armour, J.A.L.; Jeffreys, A.J.; Robb, S.; Webb, T. Uniparental paternal disomy in Angelman's syndrome. *Lancet* **1991**, *337*, 694–697. [CrossRef]
110. Buiting, K.; Groß, S.; Lich, C.; Gillessen-Kaesbach, G.; El-Maarri, O.; Horsthemke, B. Epimutations in Prader-Willi and Angelman Syndromes: A Molecular Study of 136 Patients with an Imprinting Defect. *Am. J. Hum. Genet.* **2003**, *72*, 571–577. [CrossRef]
111. Matsuura, T.; Sutcliffe, J.S.; Fang, P.; Galjaard, R.-J.; Jiang, Y.; Benton, C.S.; Rommens, J.M.; Beaudet, A.L. De novo truncating mutations in E6-AP ubiquitin-protein ligase gene (UBE3A) in Angelman syndrome. *Nat. Genet.* **1997**, *15*, 74–77. [CrossRef]
112. Kishino, T.; Lalande, M.; Wagstaff, J. UBE3A/E6-AP mutations cause Angelman syndrome. *Nat. Genet.* **1997**, *15*, 70–73. [CrossRef]
113. Dittrich, B.; Robinson, W.P.; Knoblauch, H.; Buiting, K.; Schmidt, K.; Gillessen-Kaesbach, G.; Horsthemke, B. Molecular diagnosis of the Prader-Willi and Angelman syndromes by detection of parent-of-origin specific DNA methylation in 15q11-13. *Hum. Genet.* **1992**, *90*, 313–315. [CrossRef]
114. Kantor, B.; Kaufman, Y.; Makedonski, K.; Razin, A.; Shemer, R. Establishing the epigenetic status of the Prader–Willi/Angelman imprinting center in the gametes and embryo. *Hum. Mol. Genet.* **2004**, *13*, 2767–2779. [CrossRef] [PubMed]
115. Rougeulle, C.; Cardoso, C.; Fontés, M.; Colleaux, L.; Lalande, M. An imprinted antisense RNA overlaps UBE3A and a second maternally expressed transcript. *Nat. Genet.* **1998**, *19*, 15–16. [CrossRef] [PubMed]
116. Silva-Santos, S.; van Woerden, G.M.; Bruinsma, C.F.; Mientjes, E.; Jolfaei, M.A.; Distel, B.; Kushner, S.A.; Elgersma, Y. Ube3a reinstatement identifies distinct developmental windows in a murine Angelman syndrome model. *J. Clin. Invest.* **2015**, *125*, 2069–2076. [CrossRef] [PubMed]
117. Huang, H.-S.; Allen, J.A.; Mabb, A.M.; King, I.F.; Miriyala, J.; Taylor-Blake, B.; Sciaky, N.; Dutton, J.W., Jr.; Lee, H.-M.; Chen, X.; et al. Topoisomerase inhibitors unsilence the dormant allele of Ube3a in neurons. *Nature* **2011**, *481*, 185–189. [CrossRef] [PubMed]
118. Meng, L.; Ward, A.J.; Chun, S.; Bennett, C.F.; Beaudet, A.L.; Rigo, F. Towards a therapy for Angelman syndrome by targeting a long non-coding RNA. *Nature* **2015**, *518*, 409–412. [CrossRef]

119. Daily, J.L.; Nash, K.; Jinwal, U.; Golde, T.; Rogers, J.; Peters, M.M.; Burdine, R.D.; Dickey, C.; Banko, J.L.; Weeber, E.J. Adeno-Associated Virus-Mediated Rescue of the Cognitive Defects in a Mouse Model for Angelman Syndrome. *PLoS ONE* **2011**, *6*, e27221. [CrossRef]
120. Bird, L.M.; Tan, W.-H.; Bacino, C.A.; Peters, S.U.; Skinner, S.A.; Anselm, I.; Barbieri-Welge, R.; Bauer-Carlin, A.; Gentile, J.K.; Glaze, D.G.; et al. A therapeutic trial of pro-methylation dietary supplements in Angelman syndrome. *Am. J. Med. Genet. A* **2011**, *155A*, 2956–2963. [CrossRef]
121. Bi, X.; Sun, J.; Ji, A.X.; Baudry, M. Potential therapeutic approaches for Angelman syndrome. *Expert Opin. Ther. Targets* **2016**, *20*, 601–613. [CrossRef]
122. Vojta, A.; Dobrinic´, P.; Tadic´, V.; Boc˘kor, L.; Korac´, P.; Julg, B.; Klasic´, M.; Zoldoš, V. Repurposing the CRISPR-Cas9 system for targeted DNA methylation. *Nucleic Acids Res.* **2016**, *44*, 5615–5628. [CrossRef]
123. Kim, S.-J.; Miller, J.L.; Kuipers, P.J.; German, J.R.; Beaudet, A.L.; Sahoo, T.; Driscoll, D.J. Unique and atypical deletions in Prader–Willi syndrome reveal distinct phenotypes. *Eur. J. Hum. Genet.* **2012**, *20*, 283–290. [CrossRef]
124. Wang, S.E.; Jiang, Y. Potential of Epigenetic Therapy for Prader-Willi Syndrome. *Trends Pharmacol. Sci.* **2019**, *40*, 605–608. [CrossRef] [PubMed]
125. Tan, Q.; Potter, K.J.; Burnett, L.C.; Orsso, C.E.; Inman, M.; Ryman, D.C.; Haqq, A.M. Prader–Willi-Like Phenotype Caused by an Atypical 15q11.2 Microdeletion. *Genes* **2020**, *11*, 128. [CrossRef] [PubMed]
126. Bazeley, P.S.; Shepelev, V.; Talebizadeh, Z.; Butler, M.G.; Fedorova, L.; Filatov, V.; Fedorov, A. snoTARGET shows that human orphan snoRNA targets locate close to alternative splice junctions. *Gene* **2008**, *408*, 172–179. [CrossRef] [PubMed]
127. Sahoo, T.; del Gaudio, D.; German, J.R.; Shinawi, M.; Peters, S.U.; Person, R.E.; Garnica, A.; Cheung, S.W.; Beaudet, A.L. Prader-Willi phenotype caused by paternal deficiency for the HBII-85 C/D box small nucleolar RNA cluster. *Nat. Genet.* **2008**, *40*, 719–721. [CrossRef]
128. De Smith, A.J.; Purmann, C.; Walters, R.G.; Ellis, R.J.; Holder, S.E.; Van Haelst, M.M.; Brady, A.F.; Fairbrother, U.L.; Dattani, M.; Keogh, J.M.; et al. A deletion of the HBII-85 class of small nucleolar RNAs (snoRNAs) is associated with hyperphagia, obesity and hypogonadism. *Hum. Mol. Genet.* **2009**, *18*, 3257–3265. [CrossRef]
129. Duker, A.L.; Ballif, B.C.; Bawle, E.V.; Person, R.E.; Mahadevan, S.; Alliman, S.; Thompson, R.; Traylor, R.; Bejjani, B.A.; Shaffer, L.G.; et al. Paternally inherited microdeletion at 15q11.2 confirms a significant role for the SNORD116 C/D box snoRNA cluster in Prader–Willi syndrome. *Eur. J. Hum. Genet.* **2010**, *18*, 1196–1201. [CrossRef]
130. Bieth, E.; Eddiry, S.; Gaston, V.; Lorenzini, F.; Buffet, A.; Conte Auriol, F.; Molinas, C.; Cailley, D.; Rooryck, C.; Arveiler, B.; et al. Highly restricted deletion of the SNORD116 region is implicated in Prader–Willi Syndrome. *Eur. J. Hum. Genet.* **2015**, *23*, 252–255. [CrossRef]
131. Butler, M.G.; Christian, S.L.; Kubota, T.; Ledbetter, D.H. A 5-year-old white girl with Prader-Willi syndrome and a submicroscopic deletion of chromosome 15q11q13. *Am. J. Med. Genet.* **1996**, *65*, 137–141. [CrossRef]
132. Burnett, L.C.; LeDuc, C.A.; Sulsona, C.R.; Paull, D.; Rausch, R.; Eddiry, S.; Carli, J.F.M.; Morabito, M.V.; Skowronski, A.A.; Hubner, G.; et al. Deficiency in prohormone convertase PC1 impairs prohormone processing in Prader-Willi syndrome. *J. Clin. Invest.* **2017**, *127*, 293–305. [CrossRef]
133. Heksch, R.; Kamboj, M.; Anglin, K.; Obrynba, K. Review of Prader-Willi syndrome: The endocrine approach. *Transl. Pediatr.* **2017**, *6*, 274–285. [CrossRef]
134. Vogels, A.; De Hert, M.; Descheemaeker, M.J.; Govers, V.; Devriendt, K.; Legius, E.; Prinzie, P.; Fryns, J.P. Psychotic disorders in Prader–Willi syndrome. *Am. J. Med. Genet. Part A* **2004**, *127A*, 238–243. [CrossRef] [PubMed]
135. Costa, R.A.; Ferreira, I.R.; Cintra, H.A.; Gomes, L.H.F.; Guida, L.d.C. Genotype-Phenotype Relationships and Endocrine Findings in Prader-Willi Syndrome. *Front. Endocrinol. (Lausanne)* **2019**, *10*, 864. [CrossRef] [PubMed]
136. Cruvinel, E.; Budinetz, T.; Germain, N.; Chamberlain, S.; Lalande, M.; Martins-Taylor, K. Reactivation of maternal SNORD116 cluster via SETDB1 knockdown in Prader-Willi syndrome iPSCs. *Hum. Mol. Genet.* **2014**, *23*, 4674–4685. [CrossRef] [PubMed]
137. Li, H.; Rauch, T.; Chen, Z.X.; Szabó, P.E.; Riggs, A.D.; Pfeifer, G.P. The histone methyltransferase SETDB1 and the DNA methyltransferase DNMT3A interact directly and localize to promoters silenced in cancer cells. *J. Biol. Chem.* **2006**, *281*, 19489–19500. [CrossRef] [PubMed]

138. Langouët, M.; Glatt-Deeley, H.R.; Chung, M.S.; Dupont-Thibert, C.M.; Mathieux, E.; Banda, E.C.; Stoddard, C.E.; Crandall, L.; Lalande, M. Zinc finger protein 274 regulates imprinted expression of transcripts in Prader-Willi syndrome neurons. *Hum. Mol. Genet.* **2017**, *27*, 505–515. [CrossRef] [PubMed]
139. Kim, Y.; Lee, H.-M.; Xiong, Y.; Sciaky, N.; Hulbert, S.W.; Cao, X.; Everitt, J.I.; Jin, J.; Roth, B.L.; Jiang, Y. Targeting the histone methyltransferase G9a activates imprinted genes and improves survival of a mouse model of Prader–Willi syndrome. *Nat. Med.* **2017**, *23*, 213–222. [CrossRef] [PubMed]
140. Temple, I.K.; Gardner, R.J.; Robinson, D.O.; Kibirige, M.S.; Ferguson, A.W.; Baum, J.D.; Barber, J.C.K.; James, R.S.; Shield, J.P.H. Further Evidence for an Imprinted Gene for Neonatal Diabetes Localised to Chromosome 6q22–q23. *Hum. Mol. Genet.* **1996**, *5*, 1117–1121. [CrossRef]
141. Shield, J.P.; Gardner, R.J.; Wadsworth, E.J.; Whiteford, M.L.; James, R.S.; Robinson, D.O.; Baum, J.D.; Temple, I.K. Aetiopathology and genetic basis of neonatal diabetes. *Arch. Dis. Child. Fetal Neonatal Ed.* **1997**, *76*, F39–F42. [CrossRef]
142. Gardner, R.J.; Mackay, D.J.G.; Mungall, A.J.; Polychronakos, C.; Siebert, R.; Shield, J.P.H.; Temple, I.K.; Robinson, D.O. An imprinted locus associated with transient neonatal diabetes mellitus. *Hum. Mol. Genet.* **2000**, *9*, 589–596. [CrossRef]
143. Pivnick, E.K.; Qumsiyeh, M.B.; Tharapel, A.T.; Summitt, J.B.; Wilroy, R.S. Partial duplication of the long arm of chromosome 6: A clinically recognisable syndrome. *J. Med. Genet.* **1990**, *27*, 523–526. [CrossRef]
144. Temple, I.K.; Shield, J.P.H. 6q24 transient neonatal diabetes. *Rev. Endocr. Metab. Disord.* **2010**, *11*, 199–204. [CrossRef] [PubMed]
145. Kamiya, M.; Judson, H.; Okazaki, Y.; Kusakabe, M.; Muramatsu, M.; Takada, S.; Takagi, N.; Arima, T.; Wake, N.; Kamimura, K.; et al. The cell cycle control gene ZAC/PLAGL1 is imprinted—a strong candidate gene for transient neonatal diabetes. *Hum. Mol. Genet.* **2000**, *9*, 453–460. [CrossRef] [PubMed]
146. Mackay, D.; Coupe, A.M.; Shield, J.; Storr, J.; Temple, I.; Robinson, D. Relaxation of imprinted expression of ZAC and HYMAI in a patient with transient neonatal diabetes mellitus. *Hum. Genet.* **2002**, *110*, 139–144. [CrossRef] [PubMed]
147. Arima, T.; Yamasaki, K.; John, R.M.; Kato, K.; Sakumi, K.; Nakabeppu, Y.; Wake, N.; Kono, T. The human HYMAI/PLAGL1 differentially methylated region acts as an imprint control region in mice. *Genomics* **2006**, *88*, 650–658. [CrossRef]
148. Abdollahi, A. LOT1 (ZAC1/PLAGL1) and its family members: Mechanisms and functions. *J. Cell. Physiol.* **2007**, *210*, 16–25. [CrossRef]
149. Rodríguez-Henche, N.; Jamen, F.; Leroy, C.; Bockaert, J.; Brabet, P. Transcription of the mouse PAC1 receptor gene: Cell-specific expression and regulation by Zac1. *Biochim. Biophys. Acta Gene Struct. Expr.* **2002**, *1576*, 157–162.
150. Arima, T.; Drewell, R.A.; Oshimura, M.; Wake, N.; Surani, M.A. A Novel Imprinted Gene, HYMAI, Is Located within an Imprinted Domain on Human Chromosome 6 Containing ZAC. *Genomics* **2000**, *67*, 248–255. [CrossRef]
151. Yorifuji, T.; Higuchi, S.; Hosokawa, Y.; Kawakita, R. Chromosome 6q24-related diabetes mellitus. *Clin. Pediatr. Endocrinol.* **2018**, *27*, 59–65. [CrossRef]
152. Zhang, M.; Chen, X.; Shen, S.; Li, T.; Chen, L.; Hu, M.; Cao, L.; Cheng, R.; Zhao, Z.; Luo, F. Sulfonylurea in the treatment of neonatal diabetes mellitus children with heterogeneous genetic backgrounds. *J. Pediatr. Endocrinol. Metab.* **2015**, *28*, 877. [CrossRef]
153. Fu, J.-L.; Wang, T.; Xiao, X.-H. Relapsed 6q24-related transient neonatal diabetes mellitus successfully treated with sulfonylurea. *Chin. Med. J. (Engl.)* **2019**, *132*, 846–848. [CrossRef]
154. Abu-Amero, S.; Monk, D.; Frost, J.; Preece, M.; Stanier, P.; Moore, G.E. The genetic aetiology of Silver-Russell syndrome. *J. Med. Genet.* **2008**, *45*, 193–199. [CrossRef] [PubMed]
155. Wakeling, E.L.; Brioude, F.; Lokulo-Sodipe, O.; O'Connell, S.M.; Salem, J.; Bliek, J.; Canton, A.P.M.; Chrzanowska, K.H.; Davies, J.H.; Dias, R.P.; et al. Diagnosis and management of Silver–Russell syndrome: First international consensus statement. *Nat. Rev. Endocrinol.* **2017**, *13*, 105–124. [CrossRef] [PubMed]
156. Gicquel, C.; Rossignol, S.; Cabrol, S.; Houang, M.; Steunou, V.; Barbu, V.; Danton, F.; Thibaud, N.; Merrer, M.L.; Burglen, L.; et al. Epimutation of the telomeric imprinting center region on chromosome 11p15 in Silver-Russell syndrome. *Nat. Genet.* **2005**, *37*, 1003–1007. [CrossRef]
157. Netchine, I.; Rossignol, S.; Dufourg, M.-N.; Azzi, S.; Rousseau, A.; Perin, L.; Houang, M.; Steunou, V.; Esteva, B.; Thibaud, N.; et al. 11p15 Imprinting Center Region 1 Loss of Methylation Is a Common and

Specific Cause of Typical Russell-Silver Syndrome: Clinical Scoring System and Epigenetic-Phenotypic Correlations. *J. Clin. Endocrinol. Metab.* **2007**, *92*, 3148–3154. [CrossRef] [PubMed]
158. Azzi, S.; Rossignol, S.; Steunou, V.; Sas, T.; Thibaud, N.; Danton, F.; Le Jule, M.; Heinrichs, C.; Cabrol, S.; Gicquel, C.; et al. Multilocus methylation analysis in a large cohort of 11p15-related foetal growth disorders (Russell Silver and Beckwith Wiedemann syndromes) reveals simultaneous loss of methylation at paternal and maternal imprinted loci. *Hum. Mol. Genet.* **2009**, *18*, 4724–4733. [CrossRef]
159. Gaston, V.; Le Bouc, Y.; Soupre, V.; Burglen, L.; Donadieu, J.; Oro, H.; Audry, G.; Vazquez, M.-P.; Gicquel, C. Analysis of the methylation status of the KCNQ1OT and H19 genes in leukocyte DNA for the diagnosis and prognosis of Beckwith–Wiedemann syndrome. *Eur. J. Hum. Genet.* **2001**, *9*, 409–418. [CrossRef]
160. Pianka, M.A.; McIntosh, A.T.; Patel, S.D.; Bakhshi, P.R.; Jung, M. Close yet so far away: A look into the management strategies of genetic imprinting disorders. *Am. J. Stem Cells* **2018**, *7*, 72–81.
161. Eggermann, T.; Begemann, M.; Binder, G.; Spengler, S. Silver-Russell syndrome: Genetic basis and molecular genetic testing. *Orphanet J. Rare Dis.* **2010**, *5*, 19. [CrossRef]
162. Saal, H.M.; Harbison, M.D.; Netchine, I. Silver-Russell Syndrome. In *GeneReviews((R))*; Adam, M.P., Ardinger, H.H., Pagon, R.A., Wallace, S.E., Bean, L.J.H., Stephens, K., Amemiya, A., Eds.; University of Washington: Seattle, WA, USA, 1993.
163. Han, L.; Szabó, P.E.; Mann, J.R. Postnatal Survival of Mice with Maternal Duplication of Distal Chromosome 7 Induced by a Igf2/H19 Imprinting Control Region Lacking Insulator Function. *PLoS Genet.* **2010**, *6*, e1000803. [CrossRef]

frontiers | Frontiers in Drug Discovery

REVIEW
published: 02 May 2022
doi: 10.3389/fddsv.2022.899587

Advances in Modelling COVID-19 in Animals

Petr Nickl [1,2†], *Miles Joseph Raishbrook* [1,2†], *Linn Amanda Syding* [1†] *and Radislav Sedlacek* [1,2*]

[1]*Laboratory of Transgenic Models of Diseases, Institute of Molecular Genetics of the CAS, v.v.i, Vestec, Czechia,* [2]*Czech Centre for Phenogenomics, Institute of Molecular Genetics of the CAS, v.v.i, Vestec, Czechia*

Severe acute respiratory syndrome coronavirus 2 (SARS-CoV2) is a positive-sense-single stranded RNA virus and the cause of the coronavirus disease 2019 (COVID-19). The World Health Organisation has confirmed over 250 million cases with over 5.1 million deaths as a result of this pandemic since December 2019. A global outbreak of such intensity and perseverance is due to the novelty of SARS-CoV2 virus, meaning humans lack any pre-existing immunity to the virus. Humanised animal models, from rodents to primates, simulating SARS-CoV2 transmission, cell entry and immune defence in humans have already been crucial to boost understanding of its molecular mechanisms of infection, reveal at-risk populations, and study the pathophysiology *in vivo*. Focus is now turning towards using this knowledge to create effective vaccines and therapeutic agents, as well as optimise their safety for translatable use in humans. SARS-CoV2 possesses remarkable adaptability and rapid mutagenic capabilities thus exploiting innovative animal models will be pivotal to outmanoeuvre it during this pandemic. In this review, we summarise all generated SARS-CoV2-related animal models to date, evaluate their suitability for COVID-19 research, and address the current and future state of the importance of animal models in this field.

Keywords: COVID-19, mouse, model, SARS-CoV2, sensitised, humanized, mice

OPEN ACCESS

Edited by:
Bruno Villoutreix, Institut National de la Santé et de la Recherche Médicale (INSERM), France

Reviewed by:
Venkata Ramireddy Narala, Yogi Vemana University, India
Dhanasekaran Sakthivel, ZIP Diagnostics Pty Ltd., Australia

**Correspondence:*
Radislav Sedlacek
radislav.sedlacek@img.cas.cz

†These authors have contributed equally to this work and share first authorship

Specialty section:
This article was submitted to Anti-Infective Agents, a section of the journal Frontiers in Drug Discovery

Received: 18 March 2022
Accepted: 14 April 2022
Published: 02 May 2022

Citation:
Nickl P, Raishbrook MJ, Syding LA and Sedlacek R (2022) Advances in Modelling COVID-19 in Animals. Front. Drug. Discov. 2:899587. doi: 10.3389/fddsv.2022.899587

1 COVID-19 ORIGIN AND SARS-COV2 TRANSMISSION

A pandemic is defined as a disease that is prevalent in an entire country or the world, and thus is undoubtedly the correct term for the coronavirus disease 2019 (COVID-19) outbreak. COVID-19 is caused by the severe acute respiratory syndrome coronavirus 2 (SARS-CoV2) which has been pinpointed to have originated from Wuhan, China in December 2019 and has since then spread over all continents including Antarctica (Triggle et al., 2021). Before the COVID-19 outburst there were already two identified and relatively well-known human coronaviruses causing severe respiratory pneumonia namely, SARS-CoV and MERS-CoV. They both originate from bats but spilled over to intermediate hosts namely, civets and dromedary camels, respectively. The origin of SARS-CoV2 is also suggested, based on its sequence similarity to the SARS-CoV, to have originated from bats and later spilled over to an animal reservoir, however it is not yet confirmed (Forni et al., 2017). Bats are and continue to be a copious source for novel viral sequences (Jiang et al., 2022). The bat species are among one of the oldest mammals and they exhibit great diversity and are widely spread across the globe (X. M. Zhang et al., 1992). Cross-species mixing between different kinds of bats has facilitated a maintenance of less discriminatory viruses capable of infecting a broader variety of hosts. Bats are thus a carrier of a pool of viruses able to perform inter- species transmission, which has been a reason for concern long before the COVID-19 outbreak (Calisher et al., 2006). SARS-CoV2 is a pneumotropic virus that mainly spreads through respiratory secretions like coughing and sneezing. The transmission may also occur *via* contaminated surfaces where the virus can

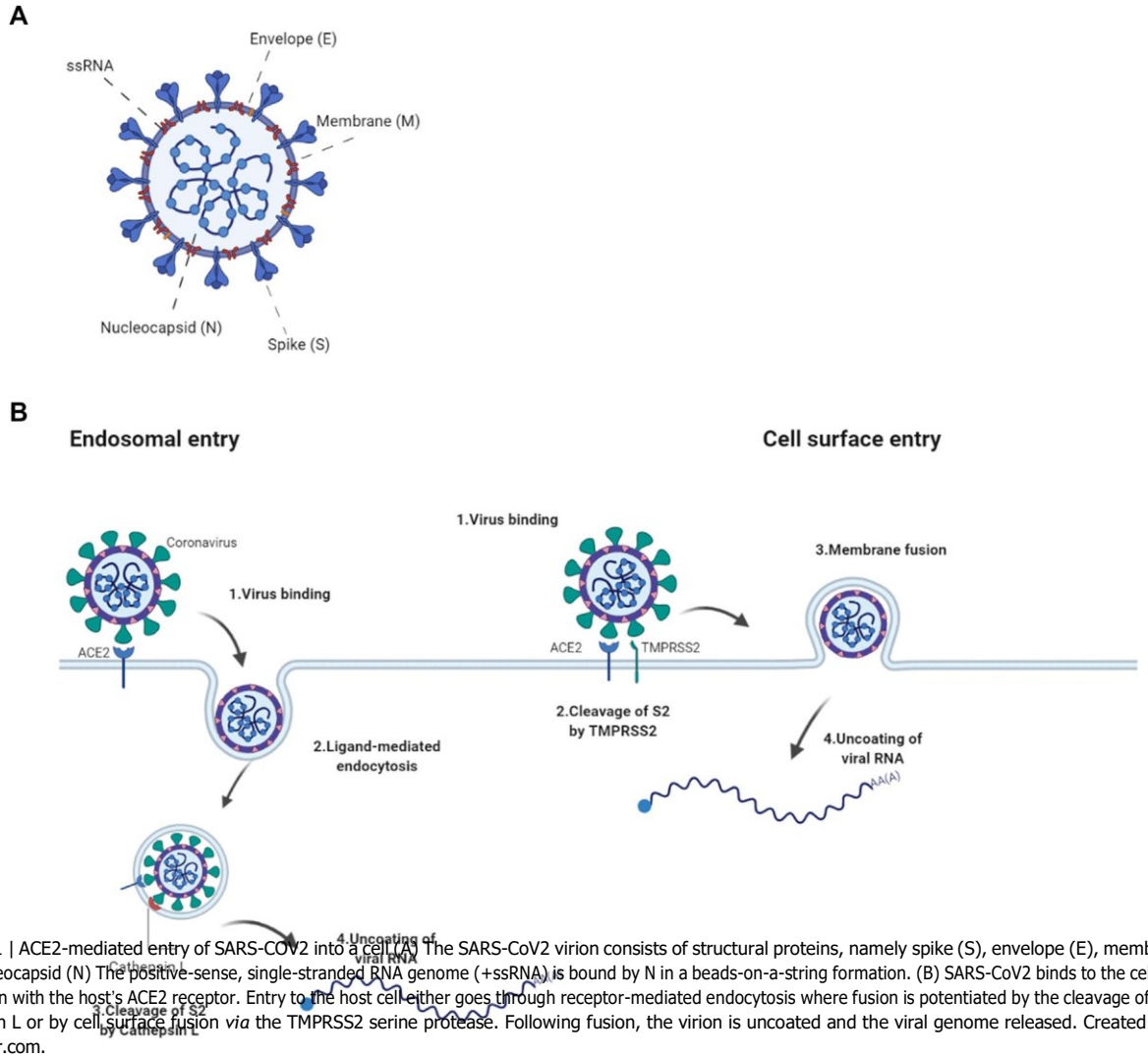

FIGURE 1 | ACE2-mediated entry of SARS-COV2 into a cell.(A) The SARS-CoV2 virion consists of structural proteins, namely spike (S), envelope (E), membrane (M), nucleocapsid (N) The positive-sense, single-stranded RNA genome (+ssRNA) is bound by N in a beads-on-a-string formation. (B) SARS-CoV2 binds to the cell *via* S interaction with the host's ACE2 receptor. Entry to the host cell either goes through receptor-mediated endocytosis where fusion is potentiated by the cleavage of S2 by Cathepsin L or by cell surface fusion *via* the TMPRSS2 serine protease. Following fusion, the virion is uncoated and the viral genome released. Created with Biorender.com.

survive up to 6 days, making preventive measures such as surface disinfection, hand hygiene and masks important in combating transmission (Leclerc et al., 2020).

Once infected, COVID-19 manifests in a large variety of symptoms however, the most common ones include fever, sore throat, fatigue, cough, dyspnoea and immune system dysregulation, often ending with cytokine storm (Ragab et al., 2020). SARS-CoV2 is not only capable of affecting the respiratory system by pulmonary infiltration and inflammation but can spread to multiple organ systems. For the majority of people the disease symptoms are mild and the infection runs its course without any medical intervention but for approximately 5–10%, it severely affects the fitness of the individual and for another 2% it has a mortal outcome (Gavriatopoulou et al., 2021).

The SARS-CoV2 consists of approximately 29.9kB of single- stranded, non-segmented, positive-sense RNA.(Triggle et al., 2021). The genome is composed by 13–15 open reading frames largely resembling the make-up of MERS-CoV and SARS-CoV. The genome contains 11 protein coding genes with ultimate expression of 12 expressed proteins (Lu et al., 2020). Structurally, it consists of four proteins namely, spike (S), envelope (E), membrane (M) and nucleocapsid (N) (Figure 1A). These proteins play important parts in entry, fusion and replication in the host cells. The non-structural have roles imperative to viral pathogenesis by regulating early transcription, helicase activity, gene transactivation and countering antiviral response (J Alsaadi and Jones, 2019; Tang et al., 2020).

The spike glycoprotein plays a pivotal role in the pathogenesis of SARS-CoV2 as it pivotal for the entry into the host cell. It is assembled as a homotrimer and inserted in multiple copies into the virus membrane, giving the virus a crown-like appearance, thus its name coronavirus (Jackson et al., 2022). It consists of two functional subunits, S1 and S2, that both part take in the entry of the virus. The S1 subunit has a receptor-binding domain (RBD) and is responsible for anchoring the host cell upon binding between the RBD and the human angiotensin-converting enzyme 2 (hACE2), thus stabilizing the virus (Hoffmann et al., 2020). Once the RBD region of the S1 subunit binds to the hACE2, the virus enters the host's endosomes *via* ligand-mediated endocytosis or membrane- fusion. Once bound to the ACE2, the S protein undergoes conformational changes, which are important to therapeutically limit its infection cycle (Wrapp et al., 2020). Although several mutations have been found in the RBD of the S1 subunit, its affinity to and interaction with the hACE2 is preserved in most species however not in mouse (Chan et al., 2020; Wrapp et al., 2020). The S2 subunit functions as a fusion protein between the virus and the host cell membrane. The S2 exhibit three different conformational changes during the process namely, i) native state before fusion, ii) intermediate state and iii) post fusion hairpin state (Qing and Gallagher, 2020; Walls et al., 2020). Finally the S protein is cleaved either by the host cell surface serine protease TMPRSS or by host's Cathepsin L in the endosomal compartment at the S2′ cleavage site (Figure 1B; Simmons et al., 2005). The cleavage releases a fusion peptide, which initiates the fusion pore formation. Once the pore expands and the cell membranes of both the virion and the host are combined, the viral genome can be released in to the cytoplasm. The cell membrane or endosomal fusion, represent the two different modes of entry for the viral genome to be released.

The N protein, composed by two separate domains, is present in the nucleocapsid complex that tightly binds the RNA genome of the virus. Both the N-terminal and C-terminal domain can bind to RNA but is more efficient when both bind simultaneously (Chang et al., 2006). The N protein bind the viral RNA genome in a beads-on-a-string conformation. The ribonucleotide protein (RNP) complex is subsequently packaged in to viral particles enveloped by a fatty lipid bi-layer (Fehr and Perlman, 2015).

The envelope protein is a relatively small protein that plays a substantial role in viral assembly. The protein assemble in to the host membrane forming protein-lipid pores referred to as viroporins. The envelope protein is highly conserved between SARS-CoV and SARS-CoV2 (Fehr and Perlman, 2015).

SARS-CoV2's membrane protein is the most abundant structural protein and is a transmembrane with a short NH2 terminal on the outside and a long cytoplasmic COOH terminus. Completion of viral assembly is potentiated partly by the binding between M proteins and N proteins leading to a stabilization of the N-Protein and RNA complex internally (Thomas, 2020).

2 INFECTION ROUTE AND ACE2 FUNCTION

The primary route of entry for the SARS-CoV2 is the upper respiratory tract. The virus gains access to the host cells by binding to the ACE2 receptors and subsequently introduced in to the cytoplasm *via* receptor-mediated endocytosis. The virus particles then goes through uncoating. The RNA and proteins needed for translation are released followed by transcription and assembly, finally the viral loads are shed thus completing the viral replication cycle (Jiang et al., 2020). As the virus sheds, the newly replicated and released particles bind upon another host cell and the cycle starts again. The ACE2 receptor is a carboxypeptidase consisting of 805 amino acids that removes a single amino acid from the C terminus of its substrates (Turner and Hooper, 2002). The ACE2 receptors are expressed in alveolar epithelial cells and capillary endothelial cells that are abundant in organs such as the lungs, kidneys, brain and gut hence explaining the multisystem infection found in a substantial amount of patients (Samavati and Uhal, 2020). The physiological role of ACE2 in humans is to convert angiotensin I and II to angiotensin 1–9 and angiotensin 1–7, respectively. This is one of the steps making up the Renin Angiotensin Aldosterone System (RAAS) a system, which functions to elevate blood volume and arterial tone *via* sodium and water reabsorption and vascular tone (Nehme et al., 2019). Infection results in a decrease of physiologically available ACE2 receptors thus disrupts the RAAS system, leading to potential downstream complications such as inflammation and circulatory dysfunction (Guo et al., 2020).

3 TRANSLATIONAL STUDIES: IMPORTANCE OF MOUSE MODELS

Since the start of the COVID-19 pandemic, we have gained substantial knowledge about the SARS-CoV2 virus in terms of its genetic make-up, transmission, infection and pathogenesis. This allows us to develop therapeutic agents to combat it. However, to perform scientifically sound and reliable research it is of the utmost importance to work with an appropriate model organism for *in vivo* study. The laboratory mouse is the most used animal in medical research as they are inexpensive, easy to handle, are genetically very similar to humans and can be genetically modified relatively easy (Sellers, 2017). They are often present as inbred strains, making it a highly controlled system, which is desirable in medical research. The mouse as an organism for translational research in COVID-19 medical research is however not well suited for COVID-19 as the ACE2 receptor of the mouse is not efficiently bound by the SARS- CoV2 virus, thus rendering the mouse immune to severe infection. This seemingly huge barrier has been surpassed by the generation of various modified mouse models capable of infection (Jia et al., 2020), as exemplified in the text below.

The COVID-19 outbreak pointed out a desperate need for relevant animal models for SARS-CoV2 research. As mentioned above wild type mouse cells and tissues are not very susceptible to SARS-CoV2 due to lack of human ACE2 specifically. Basically, mouse Ace2 does not bind the virus efficiently enough to mediate cell entry. To overcome this obstacle and study COVID-19 in mouse models, researchers have developed several approaches such as "*murinisation*" of SARS-CoV2 (Dinnon et al., 2020; Gu

TABLE 1 | Overview of COVID-19 mouse models and their characteristics.

Transgenic mouse model/background	Promoter/tissue	SARS-CoV2 dose/Most affected tissues/Symptoms/Lethality (intranasal route-IN, intravascular-IV)	References
Krt18-hACE2 (C57BL/6	Epithelial cell cytokeratin-18 promoter, epithelial cells	2.5×10^4 PFU (IN)/lung, kidney, brain, heart, spleen/severe interstitial pneumonia/lethal	McCray et al. (2007), Winkler et al., (2020)
HFH4-hACE2 (C3H, C57BL/6)	HFH4/FOXJ1 - lung ciliated epithelial cell-specific promoter, predominantly expressed in lung (also detected in brain, liver, kidney and gut)	3×10^4 $TCID_{50}$ (IN)/lung, heart, eye, brain/ severe interstitial pneumonia/lethal	Menachery et al. (2016), Jiang et al. (2020)
pCAGGS-hACE2 (C57BL/6 or BALB/c)	Cytomegalovirus enhancer with chicken β-actin promoter/universal expression	2×10^5 or 10^3 $TCID_{50}$ (IN) of SARS-CoV/ lungs, brain/acute wasting syndrome/lethal	Tseng et al. (2007)
Ace2-hACE2 Ace2-hACE2-IRES-tdTomato (ICR,C57Bl/6	Murine angiotensin converting enzyme 2/ intestine, brain, heart, kidney	10^5 $TCID_{50}$ (IN)/lung, intestine, brain/ moderate interstitial pneumonia/non-lethal	Bao et al. (2020a), Sun S.-H. et al. (2020), Yang et al. (2007b)
hACE2(LoxP-STOP) (C57Bl/6J)	Cytomegalovirus enhancer with chicken β-actin promoter/conditioned expression of hACE2-IRES-eGFP cassette	4.5 l g FFU (IN)/lung, brain/dramatic weight loss and rapid mortality/lethal (ubiquitous expression)	Bruter et al. (2021), Dolskiy et al. (2022)
Rosa26-chACE2 (C57Bl/6N)	Cytomegalovirus enhancer with chicken β-actin promoter/conditioned expression	2×10^3 PFU (IN)/not characterized/weight loss and rapid mortality/lethal (ubiquitous expression)	Czech Centre for Phenogenomics (2021)
Sensitised mouse models	**Promoter/tissue**	**SARS-CoV2 dose/Most affected tissues/Symptoms/Lethality (intranasal route-IN, intravascular-IV)**	**References**
AdV-hACE2/AdV-hACE2-GFP (BALB/c; C57BL/6J; $Rag1^{-/-}$ C57BL/6, $Stat1^{-/-}$ C57BL/6; DBA/2J; AG129)	Cytomegalovirus promoter, lung	10^5 FFU (IN); 10^5 PFU(IN, IV)/lung, heart, brain, liver, spleen/weight loss/non-lethal	Hassan et al. (2020), Sun J. et al. (2020)
AAV-hACE2 (C57BL/6J,B6(Cg) Ifnar1tm1.2Ees/J($Ifnar1^{-/-}$); C57BL/6NCrl	Cytomegalovirus promoter/lung*	3×10^7 PFU/ml (IN); 1×10^4 PFU (IN)/lung (other organs not characterized)/weight loss/ non-lethal (*note: Localization of AAV-hACE2 expression is dependent on route of AAV application and used AAV serotype.)	Israelow et al. (2020), De Gasparo et al. (2021)
Lenti-hACE2 (C57BL/6J, IFNAR−/−)	Elongation factor 1 alpha promoter/lung	2×10^5 pfu (IN); 10^5 $CCID_{50}$ per mouse (IN)/ lung (inflammatory response)/mild symptoms of the COVID-19 disease, weight loss/non-lethal	Rawle et al. (2021), Katzman et al. (2022)

et al., 2020) or humanisation of mouse models (McCray et al., 2007; Tseng et al., 2007; Menachery et al., 2016). Alternatively they used different animal models which are sensitive to known SARS-CoV2 variants, such as hamsters, ferrets or non-human primates (Enkirch and von Messling, 2015; Finch et al., 2020; Munster et al., 2020; Rockx et al., 2020; Gruber et al., 2021).

Several transgenic mouse models have been developed and used in COVID-19 research to overcome limits of mouse Ace2 and generate inexpensive models with high-throughput study potential. The models are based on ubiquitous or cell/tissue specific expression of human ACE2, a protein well-known for its importance in SARS-CoV2 entry in the cell.

3.1 K18-hACE2 Model

This mouse model expresses hACE2 under control of the epithelial cell cytokeratin-18 promoter, expressed in subset of epithelial cells (Table 1). Even though the model has been generated to study SARS-CoV during 2003 epidemics, it remains relevant for SARS-CoV2 research too (McCray et al., 2007). K18-hACE2 model is susceptible to both strains of SARS- CoV, one and 2. In the context of COVID-19 research, the model responds to the infection by progressive weight loss, high viral titres in the lung at the beginning of infection, and with progressing infection increasing viral titres in the brain and gut. Other less severely affected organs are heart, kidney and spleen (Figure 2). (McCray et al., 2007; Rathnasinghe et al., 2020).

3.2 HFH4-hACE2 Model

The model expresses hACE2 under lung ciliated epithelial cell- specific promoter (HFH4/FOXJ1), which was supposed to drive lung-specific hACE2 expression. However, detailed characterization of the model revealed a moderate hACE2 expression in other tissues such as the brain, eye, heart, liver, kidney and gut (Figure 2). The model is highly responsive to SARS-CoV2 infection with main replication of the virus in lungs, eyes, heart and brain accompanied with severe symptoms such as interstitial pneumonia sometimes succumbed to lethal encephalitis (Table 1) (Menachery et al., 2016; Jiang et al., 2020).

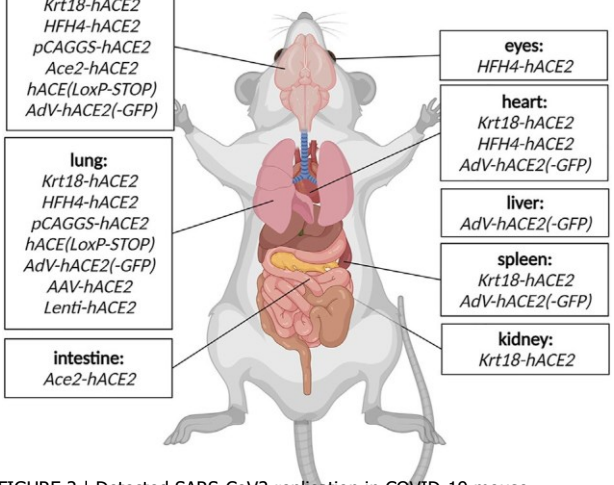

FIGURE 2 | Detected SARS-CoV2 replication in COVID-19 mouse models. The organs where viral replication has been detected in specific COVID mouse models are depicted schematically. Created with Biorender.com.

3.3 pCAGG-hACE2 Model

A model generated with multiple random integrations of pCAG- hACE2 cassette throughout the genome. Cytomegalovirus enhancer with chicken β-actin promoter (CAG) allows ubiquitous and constant expression of hACE2 in all tissues but mainly in lung, brain, heart and kidney (Table 1). This model is highly susceptible to SARS-CoV1 and 2 after intranasal application. The infection starts with initial exponential growth of viral titre in lungs and continues with gradual transmission to the brain. Slight presence of the virus was also observed in heart, kidney, spleen and small intestine (Figure 2). Of note, the lethal titre of the virus for the pCAGG-hACE2 model (2×10^2 to 2×10^4 $TCID_{50}$) is lower than in case of K18-hACE2 model (10^4 to 10^5 $TCID_{50}$) This fact might be connected to multiple insertion of pCAGG-hACE2 cassette in the genome in combination with ubiquitous and strong expression of hACE2 (Tseng et al., 2007; Asaka et al., 2021).

3.4 Ace2-hACE2 Model

Two major Ace2-hACE2 models have been generated to more closely mimic expression pattern of Ace2. The first model by was generated by random integration of a hACE2 cDNA under control of Ace2 promoter (Yang X. H. et al., 2007). The model indeed recapitulates endogenous expression of Ace2 in tissues such as lung, kidney, heart and intestines; the model is responsive to SARS-CoV2 infection with the major impact on lung tissue (Bao et al., 2020b).

The second Ace2-hACE2 model, generated by Sun S.-H. et al. (2020), is based on replacement of Ace2 coding sequence with hACE2 and tdTomato cDNA (Table 1). Therefore, the expression of transgenic cassette hACE2-IRES-tdTomato is under control of endogenous Ace2 promoter and present only in one or two copies depending on zygosity. Despite the lack of clinical symptoms or elevated mortality, this model responds to SARS-CoV2 infection by interstitial pneumonia of distinct scale depending on age. Sun's group also points out different abundance of hACE2 throughout-tissues in human (kidney, heart, oesophagus, bladder, ileum) and hACE2 in their model (liver, spleen, small intestine, ovary, and brain), however without further explanation. Furthermore, the group identified brain, lung and trachea as the main tissues of SARS-CoV2 replication (Figure 2; Sun S.-H. et al., 2020).

3.5 hACE2(LoxP-STOP) Model

hACE2 (LoxP-STOP) also termed TgCAGLoxPStopACE2GFP is a model generated by random integration of a loxP-CRE dependent cassette under the CAG promoter (Table 1). In the presence of Cre recombinase, the STOP cassette is removed and expression of hACE2 cDNA and eGFP is turned on. This model allows for conditioned, tissue-specific and traceable expression of hACE2-IRES-GFP transgene (Bruter et al., 2021). Dolskiy and collective have tested two inducible and ubiquitously expressed Cre-ERT2 drivers (UBC-ACE2 and Rosa26-ACE2) to promote conditioned hACE2 expression. In this case, the most severely affected organs were lung and brain (Figure 2). Their results further suggested that severity and infection progress is dependent on the particular Cre driver, more specifically on its expression potency. Furthermore, relatively recent changes in renin-angiotensin system due to hACE2 overexpression can be another factor influencing response to the infection (Dolskiy et al., 2022).

3.6 Rosa26-chACE2

A model similar to the previous one, but a CAG-LoxP-STOP-LoxP-hACE2 cassette is inserted in Rosa26 locus in a site-specific manner (Table 1). Therefore, transgene copy number depends on zygosity. The model has not been validated yet through SARS- CoV2 infection. It is available at Czech Centre for Phenogenomics and will be soon available *via* European Mouse Mutant Archive (EMMA) (Czech Centre for Phenogenomics, 2021).

Of note, transgenic models have an important role in SARS- CoV2 research. However, their ectopic expression of ACE2 protein, specifically in case of K18-hACE2, HFH4-hACE2, and pCAGG-hACE2 models may lead to different response, development and impact of the infection. This fact to some extend limits translatability of gathered data to clinical practise (Shou et al., 2021). Therefore, ACE2 under control of endogenous Ace2 promoter or conditional expression might provide more precise understanding of systemic or tissue-specific importance of ACE2 in the context of COVID-19.

3.7 Sensitised Mouse Models

In order to circumvent the desperate need for COVID-19 mouse models in the peak of pandemics, researchers focused on development of alternative SARS-CoV2-sensitive mouse models. Paradoxically, a rapid generation of such models was mediated by viruses. Inhalation or intranasal application of a viral

vector carrying hACE2 gene under strong promoter may lead to humanisation of upper and lower respiratory tracts. This approach allows fast, affordable and versatile generation of a sensitive model in various mouse strains and genetic backgrounds. It has been shown that the most suitable viral vectors for rapid humanisation happen to be adeno-associated virus, adenovirus, and lentivirus.

3.8 AAV-hACE2

Two independent groups have used Adeno-Associated vector of serotype 9 to deliver a cassette with hACE2 under control of CMV to the lung (Table 1; Israelow et al. (2020) have used commercially available AAV-CMV-hACE2 plasmid for AAV production and applied the vector virus *via* injection into the trachea. The De Gasparo's group assembled the AAV-CMV- hACE2 plasmid by subcloning hACE2 cDNA isolated form HEK293 cells and the vector was administered with forced inhalation into the lung and upper respiratory system. Both groups confirmed functionality of AAV-mediated humanisation where treated mice became susceptible to SARS- CoV2 infection accompanied with progressive inflammatory immune response in lung (Figure 1; Israelow et al., 2020; De Gasparo et al., 2021). In addition to establishing a new sensitized model, Israelow and collective focused on deciphering the role of type I interferon during SARS-CoV2 infection. Whereas, De Gasparo and collective tested bispecific antibodies that reduced SARS-CoV2 infection and weight loss associated with ongoing virus infection. Humanisation with AAV offers rapid, adaptable mouse model with long-term transgene expression and low immunogenicity which is crucial for immunological studies (De Gasparo et al., 2021; Kovacech et al., 2022).

3.9 AdV-hACE2

Replication defective Adenovirus encoding hACE2 (AdV-hACE2) was used to humanise several mouse strains in order to overcome unavailability of transgenic models (Table 1). The vector is delivered intranasally and it is capable to sensitise lung tissue for SARS-CoV2 entry and replication. In other organs, low levels of SARS-CoV2 replication was also identified, such as heart, spleen, brain and liver (Figure 2). Sensitised models suffer from weight loss, develop lung pathologies and respond positively to treatment with neutralising antibodies. However, the model has limitations in the form of bronchial inflammation associated with AdV delivery (Hassan et al., 2020).

3.10 Lenti-hACE2

Lentiviral vectors can be also used for sensitising a mouse to SARS-CoV2. Two independent publications describe utility of a lentiviral vector encoding hACE2 and its ability to avoid significant immune response in lung tissue before SARS-CoV2 exposure (Table 1). The advantage of lentiviral systems is their integrative character, with possibly stable long-term expression allowing re-infection studies in the sensitised mice. Both publications emphasize the role of IFNAR1 depletion and its impact on SARS-CoV2 progression in sensitised models. However, the collectives also point out the presence of mild COVID-19 symptoms in the models, probably due to relatively low expression of hACE2 by lentivirus (Rawle et al., 2021; Katzman et al., 2022).

Transgenic mouse models, expressing hACE2, represent convenient systems for large-scale, rapid (compared to other animal models), and relatively inexpensive SARS-CoV2 research. However, their availability during pandemics has been limited and their expansion in larger cohorts is time- consuming and expensive. Furthermore, distinct transgenic models differ in their response to infection, some suffer from lethal neuroinvasion, some show only mild symptoms. In general, variability of these models is significant, and no universal transgenic model has been established yet (Yang XH. et al., 2007; Yang XH. et al., 2007; McCray et al., 2007; Tseng et al., 2007; Menachery et al., 2016; Jiang et al., 2020; Sun J. et al. (2020) Bruter et al., 2021; Dolskiy et al., 2022).

In contrast with transgenic models stand virus-sensitised models, which can be generated on wide variety of genetic backgrounds and genotypes in relatively large scale and short- time. Sensitised models often do not develop severe disease mainly due to absence of neuroinvasion, but their symptoms and impact on lung tissue resembles pathology in COVID-19 patients. Moreover, the distribution and scale of hACE2 expression varies with tropism of a used viral vector or promoter. Importantly, use of viral vectors may be associated with a risk of potential inflammation leading to interference with subsequent SARS-CoV2 infection (Hassan et al., 2020; Israelow et al., 2020; De Gasparo et al., 2021; Rawle et al., 2021; Katzman et al., 2022).

3.11 Other Animal Models

Alternatives to mouse models are other animals that are naturally susceptible to SARS-CoV2, such as hamsters (*Mesocricetus auratus*, *Phodopus roborovskii*, *Cricetulus griseus*), ferrets (*Mustela putorius furo*) minks (*Neovison vison*) (Shuai et al., 2021)and non-human primates (*Macaca mulatta*, *Macaca fascicularis*, *Chlorocebus aethiops*) (Enkirch and von Messling, 2015; Finch et al., 2020; Gruber et al., 2021; Munster et al., 2020; Rockx et al., 2020). In these models there is no need for genetic modifications in order to study COVID-19 progression. Nevertheless, the models are less frequently used either due to lack of research tools, limited availability, high costs, complex husbandry or associated ethical concerns.

3.12 Murinised SARS-CoV2

While most efforts have been made in generating mouse models humanising the ACE2 to potentiate study of entry and infection *in vivo*, efforts have also been made in murinising the SARS- CoV2 virus itself. In a study by Muruato et al. (2021), they used a reverse genetic system and *in vivo* adaptation to successfully generate SARS-CoV2 strains capable of infecting mice (Muruato et al., 2021). Following infection of the murinised SARS-CoV2 strain the mouse lung exhibited substantial damage manifested with inflammation, immune infiltration, and pneumonia. The infection with the adapted virus was however only exhibited in the upper respiratory tract, thus is inappropriate for studies focusing on multisystem infection. It is worth mentioning that the novel adaptation of the virus was shown to keep its ability to

infect human airway cells (Muruato et al., 2021). This system, with a murinised SARS-CoV and a standard wild type laboratory mouse, overcomes tropism leading to encephalitis seen in infected transgenic mouse models whilst offering a system applicable for both *in vivo* mouse studies and *in vitro* studies on human primary cells (McCray et al., 2007; Winkler et al., 2020). In a study from 2020 the investigators had also produced a murinised SARS-CoV2 *via* reverse genetics to remodel the interaction between the mouse ACE2 and the virus which resulted in a recombinant virus able to infect the BALB/c mice. It was able replicate in both young and old mice however leading to more severe disease in older mice and exhibiting more clinically relevant phenotypes as compared to the disease presentation between non-modified SARS-CoV2 and transgenic mouse models (Dinnon et al., 2020). This gives the murinised ACE2 system better face validity, however the construct validity is decreased.

4 RECENT TRANSLATIONAL APPLICATIONS OF RODENT MODELS SUSCEPTIBLE TO SARS-COV2

The transgenic and transiently sensitised, humanised mouse models of SARS-CoV2 infection have gifted scientists the opportunity to study the potential destruction this, so far, relentless virus can cause to its host *in vivo*. Towards the beginning of the pandemic, initial studies using these models focused on the mechanisms in which viral entry can occur as well as their points of entry, the tissues primarily affected and the pathology of those tissues. These ongoing attempts to recreate infection have assisted our understanding of the infection timeline and has provided a guide to possible symptoms to be aware of in COVID-19 patients. Discussed here are animal studies performed in order to obtain risk assessments of new variants and evaluate the efficacy and safety of candidate anti- viral drugs for treatment in COVID-19 patients.

4.1 Risk Assessments of Variants of Concern

Particular mutations in the RBD have been key to identifying variants of concern. N501Y is one substitution that is characteristic of the Alpha (B.1.1.7) variant but is also found in the Beta (B.1.351), Gamma (B.1.1.28) and Omicron (B.1.1.529) variants (European Centre for Disease Prevention and Control, 2021; He et al., 2021). This means that N501Y is present in all but one variant of concern. *In silico* models predicted that this substitution occurs at a key residue for the RBD that is directly responsible for its strengthened affinity for ACE2 (Shahhosseini et al., 2021). The influence of N501Y was proved using a hamster model, where both donors and recipients inoculated with virus carrying N501Y showed significantly increased viral load in nasal washes and lung and trachea homogenates at 1–4 dpi compared to virus carrying a predecessor 'wild-type' spike protein. Substitutions S982A and D1118H were also shown to decrease viral fitness (Liu et al., 2022). Interestingly, N501Y increases the infectivity of hosts expressing both either hACE2 or mACE2 (Pan et al., 2021), as it has been revealed that variants with this substitution possess an 8-fold higher affinity for the receptor (Bayarri-Olmos et al., 2021). While this demonstrates a key application of using animals in order to evaluate the potential potency of infection with rapidly evolving variants, we need more studies that apply these principles in the established transgenic and sensitised animal models expressing hACE2. This is because, ultimately, we will require data on how mutations in SARS-CoV2 will affect transmission between, and the health of, humans in the future. Studies of this nature have been carried out. K18-hACE2 mice infected with B.1.1.7 show increased weight loss and hyperthermia earlier compared to mice exposed to B.1.351 or the initial WA-1 variant of concern. However, B.1.1.7 and B.1.351 infected mice display more severe clinical manifestations overall compared to WA-1 in a viral dose-dependent manner, with WA-1 infected mice displaying a 50% lower mortality rate at a dose of 10^3 pfu (Horspool et al., 2021). Again in K18-hACE2 mice, whilst both WA- 1 and B.1.1.7 inoculated intranasally caused COVID-19-like disease in the mice, a lower dose of B.1.1.7 was required to cause a severe disease state (Bayarri-Olmos et al., 2021). In contrast, C57Bl/6J hACE2 knock-in mice display reduced viral load in lung and nasal turbinate, and a more minor lung pathology and inflammatory response on exposure to WA-1, B.1.1.7 or B.1.351 variants compared to the K18-hACE2 model, where viral RNA is concentrated at the epithelia of larger airways (Winkler et al., 2022). This is most likely attributed to the difference in approach of hACE2 expression in these two mouse lines and highlights the benefits of multiple rodent models of infection, chosen depending on the study focus, but also shows how different models could be affected when exposed to differing strains. Here, studies using models that more accurately recreate human infection to novel strains will possess increased extrapolative power.

The appearance of the B.1.1.529 (Omicron) variant in late 2021 came with heightened suspicions whether the current vaccines and therapies in progress would still provide suitable protection against a variant with >30 mutations in the RBD compared to variants described so far (Hodcroft, 2021). Halfmann et al. found that K18-hACE2 mice inoculated with
B.1.351 showed significantly increased viral load in nasal turbinate and lung tissue homogenates at 3 dpi, and greater weight loss at 6 dpi compared to B.1.1.529 infected mice (Halfmann et al., 2022), suggesting reduced severity in viral manifestation on infection with the Omicron lineage in comparison to Beta lineage. These studies show the potential of exploiting the current animal models available in order to screen variants with specific mutations to assess their risk to humans, and for practitioners and governments to make appropriate decisions regarding patient care and infection control strategies.

4.2 Screening the Efficacy of Anti-Viral Therapies

The current pandemic has called for the development of anti-viral drugs in order to reduce or eliminate viral infection in, especially,

hospitalised COVID-19 patients. Due to the haste in which these drugs are required to ease the pressure of the pandemic on the world, drug development processes for SARS-CoV2 may be accelerated straight to clinical trials in humans, bypassing preclinical animal safety and efficacy studies.

Anti-viral molecules have been tested in a mouse setting though. PF-07304814 is a phosphate prodrug that on administration is processed into its active form PF-00835231, a potent cysteine protease inhibitor of coronavirus $3CL^{pro}$, that was originally considered as a treatment for the 2002 SARS-CoV epidemic in 2003 (Hoffman et al., 2020). PF-00835231 is effective against alpha, beta, and gamma coronaviruses by preventing viral replication through inhibition of essential proteolysis by $3CL^{pro}$. BALB/C mice infected with SARS-CoV2 MA10 display no weight loss and complete viral elimination when PF-00835231 is administered subcutaneously twice per day at a dose of 300 mg/kg. Initial weight loss is observed in mice receiving 30–100 mg/kg doses, which recovered to the starting weight at 4 dpi with viral load decreasing in dose-dependent manner. Significant decreases in viral load were also measured in SARS-COV2 exposed mice expressing hACE2 on treatment with PF-00835231. Additionally, this trend is also obtained even when treatment was delayed by 1dpi (Boras et al., 2021), highlighting the importance of identifying infection early, especially in high-risk patients. Despite hACE2 being expressed under a CMV promoter, which may not accurately follow the expected human expression of ACE2, this work shows the power of this inhibitor to prevent viral replication and poses a good option for further development into human clinics.

PF-07321332 (Nirmatrelvir) is another $3CL^{pro}$ inhibitor, which is the active component of the Pfizer-produced PAXLOVID™ (Pfizer, 2021), that gained approval in the UK (Medicines & Healthcare products Regulatory Agency, 2021a) and the United States (U.S. Food and Drug Administration, 2021a) at the end of 2021, and in the EU in January 2022 for treatment of COVID-19 (European Medicines Agency, 2022). An efficacy study in mice investigated the anti-viral activity of PF- 07321332 in BALB/C mice infected with mouse-adapted SARS- CoV2 MA10. Mice treated *via* oral administration were protected from weight loss, had significantly reduced lung viral titre at 4 dpi and showed markedly decreased nucleocaspid presence in lung sections (Owen et al., 2021). Syrian hamsters have been shown to be protected from severe B.1.351 infection when treated with PF- 07321332. Significant dose-dependent reductions in viral lung titre and improved weight retention at 4 dpi, as well as lung anatomy closely resembling uninfected hamsters was observed in those treated with PF-07321332. Hamsters were also completely protected from infection when co-housed for 2 days with a B.1.617.2 (Delta) variant positive cage mate when treated with PF-07321332 compared to those not (Abdelnabi et al., 2022). These rodent models support the continuing development and protective ability of PAXLOVID™ use in COVID-19 patients against multiple variants of concern, including the benefits of easy oral administration. Yet, further validation in humanised ACE2 rodent models, such as the hACE2 model used in Bao et al. (2020a) may be required for increased value *in vivo,* as the mentioned studies comprised of mouse adapted SARS-CoV2 infection and wild-type Syrian hamsters as part of their models. These studies could also be extended to examine potential side effects or long term ramifications for patients prescribed this anti-viral treatment. Synthesis and study of additional $3CL^{pro}$ inhibitors with favourable oral, intraperitoneal, and intravenous bioavailability have been reported and trialled in Sprague-Dawley rats and a CRISPR/Cas9 generated hACE2 expressing mice model (Qiao et al., 2021). However more work is required in this area, and PF-07321332 seems to have won the race for clinical trial approval.

Molnupiravir is another anti-viral drug that instead enforces a high mutagenesis rate *via* integration of its active form, β-D-N4- hydroxycytidine triphosphate (NHC), into viral RNA in the place of cytidine or uridine (Sheahan et al., 2020; Kabinger et al., 2021). It has so far gained approval for at-risk and hospitalised patients in the United States (U.S. Food and Drug Administration, 2021b) and the UK (Medicines & Healthcare products Regulatory Agency, 2021b). NHC shows potent viral inhibition and significantly reduces viral load in cell culture (Zhou et al., 2021) and diminishes weight loss, indicators of lung haemorrhage and lung viral titre at 500 mg/kg dosage in C57Bl/6 mice infected with either mouse adapted SARS-MA15 or MERS-CoV. Importantly, initiating NHC treatment before 24 h post infection showed to be crucial to maintaining reductions in weight loss, lung haemorrhaging, viral lung titre and lung and alveolar injury scores (Sheahan et al., 2020). However, a warning of mutagenic toxicity to host DNA during NHC treatment has been given, where mutations in a reporter gene increased in a dose-dependent manner with NHC. It has been suggested that the possible conversion of NHC to dNHC (2'-deoxyribose form of NHC) could be the cause of this increased mutational rate in the host genome (Zhou et al., 2021), and should be investigated further in an *in vivo* model focusing on tissues with natural proliferative tendency.

One study utilised immunodeficient mice with hACE2- and hTMPRSS2- expressing human lung tissue implanted in the animals' backs. This *in vivo* tissue model was susceptible to SARS-CoV, MERS-CoV and SARS-CoV2 infection, showed histopathological symptoms echoing viral damage and a 1000- fold increase in proinflammatory cytokines. Beginning NHC treatment at 12- and 24-h post-infection was extremely effective at reducing viral load, however if treatment started 12 h prior to infection, viral titre in the implanted human lung tissue was measured at >100,000-fold lower than the vehicle control, bestowing the protective potential of Molnupiravir in high-risk patients (Wahl et al., 2021). Molunipiravir-derived inhibitors have also shown to be effective at impeding SARS- CoV2 transmission in ferrets (Cox et al., 2021), and reducing viral replication and its associated lung pathologies in SARS-CoV2- susceptible Syrian hamsters, with amplified viral RNA mutations detected in hamsters that started treatment 12 h pre-infection compared to 12 h post-infection or vehicle control (Rosenke et al., 2021). When used in combination with Favipiravir, another anti- viral drug that acts through lethal mutagenesis but requires higher doses for optimal SARS-CoV2 suppression (Kaptein et al., 2020), hamsters treated with sub-optimal doses of a Molnupiravir/Favipiravir cocktail displayed lower viral loads

than hamsters treated with only one alone, with an implied additional transmission protection from cage-mates (Abdelnabi et al., 2021b).

These examples show that animal models can serve effectively in the screening of anti-virals in the current and future pandemics, and could assist in the recommendation of single or combinational therapies to complement human clinical trials. Finally, Molnupiravir has also shown its high protective ability against the B.1.1.7 and B.1.351 variants in Syrian hamsters (Abdelnabi et al., 2021a) and emphasises NHC's potent anti- viral mechanism is not dependent on specific sequences in the viral genome which may be mutated in future variants of concern, such is the case with e.g. monoclonal antibody treatment.

5 FUTURE RESEARCH DIRECTIONS

5.1 Risk Factors Suitable for Rodent Research

This pandemic has revealed that certain individuals are risk of developing severe COVID-19 illness or death. Factors such as age, male sex, and ethnicity have been attributed to a tendency to suffer from severe symptoms (Ebinger et al., 2020; Mughal et al., 2020; Williamson et al., 2020), as well as patients with comorbidities such as diabetes, hypertension and obesity (Alguwaihes et al., 2020; Ebinger et al., 2020; Huang et al., 2020; Li X. et al., 2020; Mughal et al., 2020; Williamson et al., 2020; Goyal et al., 2022). Whereas asthma may actually be protective (Avdeev et al., 2020; Skevaki et al., 2020; Zhu et al., 2020). Genetic or induced mouse models of these disease states are already well established, and the opportunity to combine transgenic and sensitised SARS-CoV2 models with models of human conditions potentially vulnerable to COVID-19 is waiting to be seized. This will allow us to further study comorbidities that may aggravate SARS-CoV2 transmission and pathophysiology, or contribute to any long-term damaging effects in humans. The human population is genetically and culturally diverse, but isolating comorbidities or genetic traits for study in a controlled environment will be vital.

5.1.1 Age

A report from early in the pandemic described that every additional 10 years of age associates with a 1.5-fold increased chance of requiring a higher level of hospitalised care during COVID-19 infection (Ebinger et al., 2020). SARS-COV2-related deaths peak in those aged 80+, who possess more than a 20-fold higher chance of death than those aged 50–59 (Williamson et al., 2020). This most likely attributed to an increase in comorbidities with age, even if yet to be detected. Rodents experience a much shorter life span than humans, making them an excellent model for studying age-related changes in COVID-19 research. ACE2 receptor expression has been described to both increase (Baker et al., 2021; Wark et al., 2021) and decrease (Chen et al., 2020; J.; Gu et al., 2021; Xudong et al., 2006; Yoon et al., 2016) with age in humans and rodents. However, Berni Canani et al. (2021) observed no significant differences in ACE2 expression between children <10 years old and adults 20–80 years old, and Li M.-Y. et al. (2020) detected this same trend when comparing expression across multiple tissues in adults above or below 49 years of age. These contradicting reports suggest that ACE2 expression alone may not be a robust marker for identifying severe risk of SARS-CoV2 infection, and other factors in combination with ACE2 receptor expression must possess a decisive role. Comprehensive studies encompassing widespread tissue analysis of ACE2 expression in multiple age groups could well be accomplished to solve this, surely context- dependent, matter in rodent models of infection.

5.1.2 Diabetes

Diabetic patients are at increased risk of hospitalisation and mortality on infection with SARS-CoV2 (Ebinger et al., 2020), and are significantly more likely to require oxygen, intubation, antibiotics or dexamethasone on admission to hospital than non- diabetic patients (Alguwaihes et al., 2020). This is not entirely surprising considering increased cellular glucose levels assists in supporting viral replication (Codo et al., 2020). Overexpression of hACE2 boosts glucose tolerance and pancreatic β-cell function in diabetic mice (Bindom et al., 2010), whilst *ACE2*$^{-/y}$ knockout mice display impaired glucose tolerance alongside hepatic steatosis (Cao et al., 2016). Infection-induced downregulation of ACE2, and the resulting angiotensin II excess, therefore intensifies an already unbalanced glucose homeostasis. For these reasons, a bi-directional relationship between diabetes and COVID-19 infection has been proposed (Muniangi- Muhitu et al., 2020).

HFD-induced diabetic DPP4$^{H/M}$ male C57Bl/6 mice have been shown to be more vulnerable to severe signs of disease on infection with MERS-CoV when compared to lean controls, displaying prolonged weight loss and lung inflammation up to 21dpi (Kulcsar et al., 2019). Ma et al. (2021) however is the only study we found to date that has addressed the effect of the current SARS-CoV2 in a hACE2 expressing mouse model of diabetes. Ob/ob mice showed greater weight loss and increased lung immune infiltration when compared to non-diabetic mice at 5 dpi. Interestingly, this study also observed higher fasting blood glucose levels in both wild type and ob/ob mice infected with SARS-CoV2, compared to non-infected. Insulin tolerance was also non-significantly reduced in infected ob/ob mice (Ma et al., 2021). This is an alarming observation, and shows the potency of COVID-19 infection to disturb glucose homeostasis, not only in diabetic patients. Given that genetically-, chemically- or diet-induced rodent models of type 1 and type 2 diabetes are well established (King, 2012) in scientific literature, more research utilising hACE2-expressing rodents combined with these diabetic models will be extremely beneficial to understanding the risk posed on diabetic and non-diabetic people, both during and after contracting COVID-19.

5.1.3 Obesity

Obesity is another major risk factor for severe COVID-19 symptoms (Alguwaihes et al., 2020; Goyal et al., 2022) and COVID-19-related hospitalisation and mortality (Popkin et al., 2020). Its involvement in instigating this is likely intertwined with other comorbidities such as diabetes and hypertension. ACE2 is

expressed in subcutaneous and visceral adipose tissue (Al-Benna, 2020), and SARS-CoV2 nucleocapsids were detected in up to 5% of adipocytes in a small cohort of deceased COVID-19 patients (Basolo et al., 2022). Consequently, more adipose tissue will lead to surges in viral penetration and illness.

C57Bl/6 male mice fed a high-fat diet (HFD) display higher ACE2 expression in the lungs and trachea but reduced Tmprss2 expression in the oesophagus, whereas obese females display reduced ACE2 expression in the oesophagus and trachea with no differences in lung tissue (Sarver and Wong, 2021). This, at least in rodents, shows how obesity affects the expression of key SARS-CoV2 entry proteins differently in the two sexes, and should be investigated further in order to understand whether human patients should be treated according to sex. Further, HFD-fed rats see a 3.8- and 6-fold increase in lung Ace2 expression, and a 5.1- and 3.4-fold increase in Tmprss2 expression compared to standard and ketogenic diet fed rats, respectively. AT_1R and AT_2R levels were also significantly increased in HFD fed rats. Interestingly though, mice fed a ketogenic diet saw reduced AT_1R expression in pulmonary tissue compared to rats fed standard chow (da Eira et al., 2021), and this type of diet may help to safeguard diabetic or hypertensive humans. It would be meaningful to see further studies into the potential protective effects of certain diets on SARS-CoV2 infected rodent models.

The obesity-prone C57Bl/6N strain can provide valuable information in support of increased weight and diet on disease advancement and severity in SARS-CoV2 infected rodent models. Zhang et al., utilising leptin receptor dysfunctional C57BL/KsJ- db/db mice, observed a maintained 10% weight loss and more severe pulmonary pathology and inflammation in the obese model compared to db/+ controls inoculated with a mouse- adapted SARS-CoV2. Viral load was also significantly higher in obese lungs, nasal turbinates and trachea (Zhang et al., 2021). HFD-fed C57Bl/6N mice transduced with AdV-hACE2 also display more severe lung pathology than lean mice at 10 days post SARS-CoV2 infection, however a more comprehensive inflammatory profile should be included when studying models such as these (Rai et al., 2021).

This presented evidence further supports the role of obesity in severe COVID-19 patients, and in a way embodies the fusion of two pandemics. Researchers may now also look towards rodent models, preferably expressing hACE2 under its namesake promoter, to develop treatments to ease symptoms and reduce mortality in these patients in the short term. Patients may then turn to improve their diet and lifestyle habits post-recovery.

5.1.4 Hypertension

As the ACE2 receptor is responsible for initial SARS-CoV2 cell entry, it is logical that hypertension was among the top clinical presentations in patients suffering from severe COVID-19 (Huang et al., 2020; Li X. et al., 2020), through viral disruption of RAAS. ACE2 usually acts a negative regulator of RAAS, lowering blood pressure with anti-inflammatory effects. A number of RAAS modulators have been tested on rat primary *in vitro* cultures that principally act to increase or decrease ACE2 mRNA or protein levels (Hu et al., 2021), which in regards to a COVID-19 patient may either encourage additional viral penetration or further increase blood pressure, respectively. ACE inhibitors or ARB drugs however, seem to display a protective effect against SARS-CoV2 infection and in-hospital mortality (Hippisley-Cox et al., 2020). Nevertheless, these types of studies mainly take into account hospital admissions and must account for a large number of comorbidities and variables.

Diet-induced obese C57Bl/6J mice display weight loss, improved glucose tolerance and reduced expression of inflammatory cytokines when treated with ACE inhibitors (Premaratna et al., 2012). $ACE^{-/-}$ mice show a similar trend (Jayasooriya et al., 2008), displaying the potential for this treatment to ease multiple COVID-19-related risk factors at once. There are a high number of inbred, outbred and transgenic rodent models used for hypertension research (Lerman et al., 2019). Jiang et al. (2022) recently published that SARS-CoV2 viral load in the lungs is higher in transgenic hACE2-expressing mice that have been induced into hypertension compared to normotensive hACE2 mice. Further, AT_1R blocker treatment improved lung pathology, reduced blood pressure and downregulated IL-6 and TNF-α expression in hypertensive hACE2 mice. This signifies that treatment provided protection to the organs on SARS-CoV2 infection overall, despite increased viral penetration in the heart and kidneys initially at early infection (Jiang et al., 2022). A recent preprint article reported that the ACE inhibitor Lisinopril can raise the ACE2 expression landscape in the lungs, small intestine, kidney and brain of healthy mice, an effect that persists to at least 21 days post-termination of treatment (Brooks et al., 2022). Captopril, which also acts as an ACE inhibitor, appears to improve lung pathology and reduce inflammation during SARS-CoV2 infection in an angiotensin II-induced hypertensive and hACE2-expressing mouse model, without any detectable effect on viral load (Gao et al., 2021). These reports reinforce the potential but need for further clarification on RAAS modulators in COVID-19 research, but studies focusing specifically on hypertension in rodents on infection with the SARS-CoV2 virus are lacking. Nonetheless, with blood pressure measurements by techniques such as tail-cuff plethysmography and radiotelemetry readily available for use in rodents (Burger et al., 2014) and with a number of hypertension remedies on the market, future COVID-19 animal research focused on hypertension risk or the efficacy of RAAS modulators would benefit from integrating these methodologies into their study design for a greater *in vivo* view of hypertension in the current pandemic.

5.2 Insights Into Long-COVID

Post-acute COVID-19 sequelae or 'long-COVID' is a condition in which patients continue to suffer multiple COVID-19-related symptoms weeks or even months after testing negative for the virus, and can come in continuous or relapsing forms. The mechanisms behind symptom persistence are still unclear as presentation varies from patient to patient. Large scale studies from around the globe have witnessed exhaustive lists of symptoms (Davis et al., 2021; Hossain et al., 2021; C. Huang

et al., 2021; Pérez-González et al., 2022), with those who were hospitalised or required intensive care during primary infection especially at risk (Xie et al., 2022).

Rodent models of post-acute COVID-19 syndrome have been close to non-existent so far. This is likely due to subsided infections, or death, of animals in the models currently available, and the incorporation of early terminal analysis into experiment design. To more accurately study the long-term effects of SARS-CoV2 infection we require models that are even more 'comprehensively human' than those presented in Table 1, which more closely mimic aspects such as our own immune system. Researching viral infections by utilising non-human primates is an attractive option, due to marked similarities in physiology and immune responses to antigens with humans with the possibility for longitudinal studies in controlled environments (Estes et al., 2018). The rhesus macaque, African green monkey and pigtail macaque are susceptible to SARS-CoV2 infection and show mild-moderate COVID-19-associated lung pathologies (Clancy et al., 2021). Further, Böszörményi et al. (2021) observed that infected macaques show worsening lung lesions in CT scans, increases in specific cytokines in plasma, mild to moderate histopathological signs of pneumonia and the presence of viral RNA levels in a myriad of tissues up to 38 dpi, despite all subjects testing negative for SARS-CoV2 after 14 dpi. This suggests that these non-human primates are also susceptible to post-acute COVID-19 in a similar way to humans (Böszörményi et al., 2021).

For many researchers however, rodents are a preferred model based on their lower maintenance costs, shorter gestation period and the wealth of tools for transgenic manipulation. A promising example of a mouse model with a humanised immune system is MISTRG6. These immunodeficient mice express seven human cytokine genes knocked into their respective locus in the mouse's genome, and tolerate human hematopoietic stem cell engraftment (Rongvaux et al., 2014). MISTRG6 mice that transiently express hACE2 sustain prolonged viral titres and RNA, more severe lung pathology, and immune cell signatures to at least 35dpi of SARS-CoV2 compared to controls, emulating severe COVID-19 disease in humans. Convalescent plasma therapy showed a protective effect in these mice in regards to weight loss and viral clearance, however only prophylactic monoclonal antibody treatment improved prevention of T cell lung infiltration (Sefik et al., 2021). This again highlights the importance of early diagnosis in high risk patients, and it will be interesting to see more therapies tested on this model over longer time periods.

Finally, a recent preprint article has described their tracking of 10-weeks- and 1-year-old BALB/C mice for 120 days post infection with mouse adapted SARS-CoV2 MA10. Younger mice cleared infection twice as fast as older mice, with cytokine responses enduring in the latter until 30 dpi. Interestingly though, mice in the younger age group displayed a greater capability for tissue repair, and Molnupiravir was also effective at reducing disease prevalence in the older age group (Dinnon et al., 2022). Although this study is yet to be peer- reviewed, long-term mouse studies such as this will prove valuable in the fight against post-acute COVID-19 syndrome.

6 CONCLUDING REMARKS

The COVID-19 pandemic prompted a global scientific effort to produce a number of diverse animal models that mimic SARS- CoV2 infection. Mice have been and continue to be the preferred model organism used in scientific research due to their easy manipulation, short breeding time and genetic similarity to humans. However, the SARS-CoV2 virus binds inefficiently to the ACE2 receptor in mice thus preventing severe infection. This seemingly large barrier has been surmounted by the generation of transgenic and humanised mouse models. Additionally, efforts have been placed in reverse engineering the virus itself to increase its affinity to the mouse ACE2 receptor and causing COVID-19 symptoms. The aim of this review was to highlight individual COVID-19 mouse models and the tissue-specific replication of the virus and pathophysiology upon infection. We substantiate the review with examples of how these models have been used in regards to risk assessment of novel strains, developing therapeutics and elucidating the mechanisms of risk factors such as old age, diabetes, obesity and hypertension. We believe that this review can be used as a comprised guide for investigators researching which mouse model or which strategy to employ in regards to future COVID-19 research.

AUTHOR CONTRIBUTIONS

PN, MR, and LS wrote the article with equal contributions. RS supervised.

REFERENCES

Abdelnabi, R., Foo, C. S., de Jonghe, S., Maes, P., Weynand, B., and Neyts, J. (2021a). Molnupiravir Inhibits Replication of the Emerging SARS-CoV-2 Variants of Concern in a Hamster Infection Model. *J. Infect. Dis.* 224 (5), 749–753. doi:10.1093/infdis/jiab361

Abdelnabi, R., Foo, C. S., Jochmans, D., Vangeel, L., de Jonghe, S., Augustijns, P., et al. (2022). The Oral Protease Inhibitor (PF-07321332) Protects Syrian Hamsters against Infection with SARS-CoV-2 Variants of Concern. *Nat. Commun.* 13 (1). doi:10.1038/s41467-022-28354-0

Abdelnabi, R., Foo, C. S., Kaptein, S. J. F., Zhang, X., Do, T. N. D., Langendries, L., et al. (2021b). The Combined Treatment of Molnupiravir and Favipiravir Results in a Potentiation of Antiviral Efficacy in a SARS-CoV-2 Hamster Infection Model. *EBioMedicine* 72, 103595. doi:10.1016/j.ebiom.2021.103595

Al-Benna, S. (2020). Association of High Level Gene Expression of ACE2 in Adipose Tissue with Mortality of COVID-19 Infection in Obese Patients. *Obes. Med.* 19, 100283. doi:10.1016/j.obmed.2020.100283

Alguwaihes, A. M., Al-Sofiani, M. E., Megdad, M., Albader, S. S., Alsari, M. H., Alelayan, A., et al. (2020). Diabetes and Covid-19 Among Hospitalized Patients in Saudi Arabia: a Single-centre Retrospective Study. *Cardiovasc. Diabetol.* 19 (1), 205. doi:10.1186/s12933-020-01184-4

Alsaadi, E. J. A., and Jones, I. M. (2019). Membrane Binding Proteins of Coronaviruses. *Future Virol.* 14 (4), 275–286. doi:10.2217/fvl-2018-0144 Asaka, M. N., Utsumi, D., Kamada, H., Nagata, S., Nakachi, Y., Yamaguchi, T., et al.

(2021). Highly Susceptible SARS-CoV-2 Model in CAG Promoter-Driven

hACE2-Transgenic Mice. *JCI Insight* 6 (19), e152529. doi:10.1172/JCI.INSIGHT.152529

Avdeev, S., Moiseev, S., Brovko, M., Yavorovskiy, A., Umbetova, K., Akulkina, L., et al. (2020). Low Prevalence of Bronchial Asthma and Chronic Obstructive Lung Disease Among Intensive Care Unit Patients with COVID-19. *Allergy* 75 (10), 2703–2704. doi:10.1111/all.14420

Baker, S. A., Kwok, S., Berry, G. J., and Montine, T. J. (2021). Angiotensin-converting Enzyme 2 (ACE2) Expression Increases with Age in Patients Requiring Mechanical Ventilation. *PLoS ONE* 16 (2 February), e0247060. doi:10.1371/journal.pone.0247060

Bao, L., Deng, W., Huang, B., Gao, H., Liu, J., Ren, L., et al. (2020a). The Pathogenicity of SARS-CoV-2 in hACE2 Transgenic Mice. *Nature* 583 (7818), 830–833. doi:10.1038/s41586-020-2312-y

Bao, L., Gao, H., Deng, W., Lv, Q., Yu, H., Liu, M., et al. (2020b). Transmission of Severe Acute Respiratory Syndrome Coronavirus 2 via Close Contact and Respiratory Droplets Among Human Angiotensin-Converting Enzyme 2 Mice.

J. Infect. Dis. 222 (4), 551–555. doi:10.1093/INFDIS/JIAA281

Basolo, A., Poma, A. M., Bonuccelli, D., Proietti, A., Macerola, E., Ugolini, C., et al. (2022). Adipose Tissue in COVID-19: Detection of SARS-CoV-2 in Adipocytes and Activation of the Interferon-Alpha Response. *J. Endocrinol. Invest.* 45, 1021–1029. doi:10.1007/s40618-022-01742-5

Bayarri-Olmos, R., Johnsen, L. B., Idorn, M., Reinert, L. S., Rosbjerg, A., Vang, S., et al. (2021). The alpha/B.1.1.7 SARS-CoV-2 Variant Exhibits Significantly Higher Affinity for ACE-2 and Requires Lower Inoculation Doses to Cause Disease in K18-hACE2 Mice. *ELife* 10, e70002. doi:10.7554/eLife.70002

Berni Canani, R., Comegna, M., Paparo, L., Cernera, G., Bruno, C., Strisciuglio, C., et al. (2021). Age-Related Differences in the Expression of Most Relevant Mediators of SARS-CoV-2 Infection in Human Respiratory and Gastrointestinal Tract. *Front. Pediatr.* 9. doi:10.3389/fped.2021.697390

Bindom, S. M., Hans, C. P., Xia, H., Boulares, A. H., and Lazartigues, E. (2010). Angiotensin I-Converting Enzyme Type 2 (ACE2) Gene Therapy Improves Glycemic Control in Diabetic Mice. *Diabetes* 59 (10), 2540–2548. doi:10.2337/ db09-0782

Boras, B., Jones, R. M., Anson, B. J., Arenson, D., Aschenbrenner, L., Bakowski, M. A., et al. (2021). Preclinical Characterization of an Intravenous Coronavirus 3CL Protease Inhibitor for the Potential Treatment of COVID19. *Nat. Commun.* 12 (1), 6055. doi:10.1038/s41467-021-26239-2

Böszörményi, K. P., Stammes, M. A., Fagrouch, Z. C., Kiemenyi-Kayere, G., Niphuis, H., Mortier, D., et al. (2021). The post-acute Phase of Sars-Cov-2 Infection in Two Macaque Species Is Associated with Signs of Ongoing Virus Replication and Pathology in Pulmonary and Extrapulmonary Tissues. *Viruses* 13 (8), 1673. doi:10.3390/v13081673

Brooks, S. D., Smith, R. L., Moreira, A. S., and Ackerman, H. C. (2022). Oral Lisinopril Raises Tissue Levels of ACE2, The SARS-CoV-2 Receptor, in Healthy Male and Female Mice. *Front. Pharmacol.* 13, 798349. doi:10.3389/fphar.2022. 798349

Bruter, A. V., Korshunova, D. S., Kubekina, M. V., Sergiev, P. V., Kalinina, A. A., Ilchuk, L. A., et al. (2021). Novel Transgenic Mice with Cre-dependent Co-expression of GFP and Human ACE2: a Safe Tool for Study of COVID-19 Pathogenesis. *Transgenic Res.* 30 (3), 289–301. doi:10.1007/S11248-021-00249- 8/TABLES/1

Burger, D., Reudelhuber, T. L., Mahajan, A., Chibale, K., Sturrock, E. D., and Touyz, R. M. (2014). Effects of a Domain-Selective ACE Inhibitor in a Mouse Model of Chronic Angiotensin II-dependent Hypertension. *Clin. Sci.* 127 (1), 57–63. doi:10.1042/CS20130808

Calisher, C. H., Childs, J. E., Field, H. E., Holmes, K. V., and Schountz, T. (2006). Bats: Important Reservoir Hosts of Emerging Viruses. *Clin. Microbiol. Rev.* 19 (3), 531–545. doi:10.1128/CMR.00017-06

Cao, X., Yang, F., Shi, T., Yuan, M., Xin, Z., Xie, R., et al. (2016). Angiotensin-converting Enzyme 2/angiotensin-(1-7)/Mas axis Activates Akt Signaling to Ameliorate Hepatic Steatosis. *Sci. Rep.* 6, 21592. doi:10.1038/srep21592

Chan, J. F.-W., Yip, C. C.-Y., To, K. K.-W., Tang, T. H.-C., Wong, S. C.-Y., Leung, K.-H., et al. (2020). Improved Molecular Diagnosis of COVID-19 by the Novel, Highly Sensitive and Specific COVID-19-RdRp/Hel Real-Time Reverse Transcription-PCR Assay Validated *In Vitro* and with Clinical Specimens.

J. Clin. Microbiol. 58 (5), e00310–20. doi:10.1128/JCM.00310-20

Chang, C.-k., Sue, S.-C., Yu, T.-h., Hsieh, C.-M., Tsai, C.-K., Chiang, Y.-C., et al. (2006). Modular Organization of SARS Coronavirus Nucleocapsid Protein.

J. Biomed. Sci. 13 (1), 59–72. doi:10.1007/s11373-005-9035-9

Chen, J., Jiang, Q., Xia, X., Liu, K., Yu, Z., Tao, W., et al. (2020). Individual Variation of the SARS-CoV-2 Receptor ACE2 Gene Expression and Regulation. *Aging Cell* 19 (7), e13168. doi:10.1111/acel.13168

Clancy, C. S., Shaia, C., Munster, V., de Wit, E., Hawman, D., Okumura, A., et al. (2021). Histologic Pulmonary Lesions of SARS-CoV-2 in 4 Nonhuman Primate Species: An Institutional Comparative Review. *Vet. Pathol.*, 3009858211067468. doi:10.1177/03009858211067468

Codo, A. C., Davanzo, G. G., Monteiro, L. d. B., de Souza, G. F., Muraro, S. P., Virgilio-da-Silva, J. V., et al. (2020). Elevated Glucose Levels Favor SARS-CoV- 2 Infection and Monocyte Response through a HIF-1α/Glycolysis-dependent Axis. *Cel Metab.* 32 (3), 437–446. e5. doi:10.1016/j.cmet.2020.07.007

Cox, R. M., Wolf, J. D., and Plemper, R. K. (2021). Therapeutically Administered Ribonucleoside Analogue MK-4482/EIDD-2801 Blocks SARS-CoV-2 Transmission in Ferrets. *Nat. Microbiol.* 6 (1), 11–18. doi:10.1038/s41564-020-00835-2

Czech Centre for Phenogenomics (2021). *Covid-19 Mouse Models Available at CCP - Czech Centre for Phenogenomics*. Vestec, Czechia. https://www. phenogenomics.cz/2021/09/covid-19-mouse-models-available-at-ccp/.

da Eira, D., Jani, S., and Ceddia, R. B. (2021). Obesogenic and Ketogenic Diets Distinctly Regulate the SARS-CoV-2 Entry Proteins ACE2 and TMPRSS2 and the Renin-Angiotensin System in Rat Lung and Heart Tissues. *Nutrients* 13 (10), 3357. doi:10.3390/nu13103357

Davis, H. E., Assaf, G. S., McCorkell, L., Wei, H., Low, R. J., Re'em, Y., et al. (2021). Characterizing Long COVID in an International Cohort: 7 Months of Symptoms and Their Impact. *EClinicalMedicine* 38, 101019. doi:10.1016/j. eclinm.2021.101019

De Gasparo, R., Pedotti, M., Simonelli, L., Nickl, P., Muecksch, F., Cassaniti, I., et al. (2021). Bispecific IgG Neutralizes SARS-CoV-2 Variants and Prevents Escape in Mice. *Nature* 593 (7859), 424–428. doi:10.1038/s41586-021-03461-y

Dinnon, K. H., III, Leist, S. R., Okuda, K., Dang, H., Fritch, E. J., Gully, K. L., et al. (2022). A Model of Persistent post SARS-CoV-2 Induced Lung Disease for Target Identification and Testing of Therapeutic Strategies. *BioRxiv*. doi:10. 1101/2022.02.15.480515

Dinnon, K. H., Leist, S. R., Schäfer, A., Edwards, C. E., Martinez, D. R., Montgomery, S. A., et al. (2020). A Mouse-Adapted Model of SARS-CoV-2 to Test COVID-19 Countermeasures. *Nature* 586 (7830), 560–566. doi:10.1038/ s41586-020-2708-8

Dolskiy, A. A., Gudymo, A. S., Taranov, O. S., Grishchenko, I. V., Shitik, E. M., Prokopov, D. Y., et al. (2022). The Tissue Distribution of SARS-CoV-2 in Transgenic Mice with Inducible Ubiquitous Expression of hACE2. *Front. Mol. Biosciences* 8, 1339. doi:10.3389/FMOLB.2021.821506/BIBTEX

Ebinger, J. E., Achamallah, N., Ji, H., Claggett, B. L., Sun, N., Botting, P., et al. (2020). Pre-existing Traits Associated with Covid-19 Illness Severity. *PLoS ONE* 15 (7 July), e0236240. doi:10.1371/journal.pone.0236240

Enkirch, T., and von Messling, V. (2015). Ferret Models of Viral Pathogenesis.

Virology 479-480, 259–270. doi:10.1016/J.VIROL.2015.03.017

Estes, J. D., Wong, S. W., and Brenchley, J. M. (2018). Nonhuman Primate Models of Human Viral Infections. *Nat. Rev. Immunol.* 18 (6), 390–404. doi:10.1038/ s41577-018-0005-7

European Centre for Disease Prevention and Control (2021). *Assessment of the Further Emergence of the SARS-CoV-2 Omicron VOC in the Context of the Ongoing Delta VOC Transmission in the EU/EEA, 18th Update*. Stockholm, Sweden: ECDC. Available at: https://www.ecdc.europa.eu/en/publications- data/covid-19-assessment-further-emergence-omicron-18th-risk-assessment (Accessed February 25, 2022).

European Medicines Agency (2021). *EMA Issues Advice on Use of Lagevrio (Molnupiravir) for the Treatment of COVID-19*. Amsterdam, Netherlands: European Medicines Agency. Available at: https://www.ema.europa.eu/en/ news/ema-issues-advice-use-lagevrio-molnupiravir-treatment-covid-19 (Accessed February 10, 2022).

European Medicines Agency (2022). *Paxlovid*. European Medicines Agency. Available at: https://www.ema.europa.eu/en/medicines/human/EPAR/paxlovid (Accessed February 11, 2022).

Fehr, A. R., and Perlman, S. (2015). Coronaviruses: an Overview of Their Replication and Pathogenesis. *Methods Mol. Biol.* 1282, 1–23. doi:10.1007/ 978-1-4939-2438-7_1

Finch, C. L., Crozier, I., Lee, J. H., Byrum, R., Cooper, T. K., Liang, J., et al. (2020). Characteristic and Quantifiable COVID-19-like Abnormalities in CT- and PET/CT-imaged Lungs of SARS-CoV-2-Infected Crab-Eating Macaques (*Macaca fascicularis*). *BioRxiv*. doi:10.1101/2020.05.14.096727

Forni, D., Cagliani, R., Clerici, M., and Sironi, M. (2017). Molecular Evolution of Human Coronavirus Genomes. *Trends Microbiol.* 25 (1), 35–48. doi:10.1016/j. tim.2016.09.001

Gao, W.-C., Ma, X., Wang, P., Ma, X., Wang, P., He, X.-Y., et al. (2021). Captopril Alleviates Lung Inflammation in SARS-CoV-2-Infected Hypertensive Mice. *Zoolog. Res.* 42 (5), 633–636. doi:10.24272/J.ISSN.2095-8137.2021.206

Gavriatopoulou, M., Ntanasis-Stathopoulos, I., Korompoki, E., Fotiou, D., Migkou, M., Tzanninis, I.-G., et al. (2021). Emerging Treatment Strategies for COVID-19 Infection. *Clin. Exp. Med.* 21 (2), 167–179. doi:10.1007/ s10238-020-00671-y

Goyal, A., Gupta, Y., Kalaivani, M., Praveen, P. A., Ambekar, S., and Tandon, N. (2022). SARS-CoV-2 Seroprevalence in Individuals with Type 1 and Type 2 Diabetes Compared with Controls. *Endocr. Pract.* 28 (2), 191–198. doi:10.1016/ j.eprac.2021.12.009

Gruber, A. D., Firsching, T. C., Trimpert, J., and Dietert, K. (2021). Hamster Models of COVID-19 Pneumonia Reviewed: How Human Can They Be? *Vet. Pathol.*, 030098582110571. doi:10.1177/03009858211057197

Gu, H., Chen, Q., Yang, G., He, L., Fan, H., Deng, Y.-Q., et al. (2020). Rapid Adaptation of SARS-CoV-2 in BALB/c Mice: Novel Mouse Model for Vaccine Efficacy. *BioRxiv*. doi:10.1101/2020.05.02.073411

Gu, J., Yin, J., Zhang, M., Li, J., Wu, Y., Chen, J., et al. (2021). Study on the Clinical Significance of Ace2 and its Age-Related Expression. *Jir* Vol. 14, 2873–2882. doi:10.2147/JIR.S315981

Guo, T., Fan, Y., Chen, M., Wu, X., Zhang, L., He, T., et al. (2020). Cardiovascular Implications of Fatal Outcomes of Patients with Coronavirus Disease 2019 (COVID-19). *JAMA Cardiol.* 5 (7), 811–818. doi:10.1001/jamacardio.2020.1017

Halfmann, P. J., Iida, S., Iwatsuki-Horimoto, K., Maemura, T., Kiso, M., Scheaffer, S. M., et al. (2022). SARS-CoV-2 Omicron Virus Causes Attenuated Disease in Mice and Hamsters. *Nature* 603, 687–692. doi:10.1038/s41586-022-04441-6

Hassan, A. O., Case, J. B., Winkler, E. S., Thackray, L. B., Kafai, N. M., Bailey, A. L., et al. (2020). A SARS-CoV-2 Infection Model in Mice Demonstrates Protection by Neutralizing Antibodies. *Cell* 182 (3), 744–753. doi:10.1016/J.CELL.2020.06.011

He, X., Hong, W., Pan, X., Lu, G., and Wei, X. (2021). SARS-CoV-2 Omicron Variant: Characteristics and Prevention. *MedComm* 2 (4), 838–845. doi:10. 1002/mco2.110

Hippisley-Cox, J., Young, D., Coupland, C., Channon, K. M., Tan, P. S., Harrison, D. A., et al. (2020). Risk of Severe COVID-19 Disease with ACE Inhibitors and Angiotensin Receptor Blockers: Cohort Study Including 8.3 Million People. *Heart* 106 (19), 1503–1511. doi:10.1136/heartjnl-2020-317393

Hodcroft, E. B. (2021). *CoVariants: SARS-CoV-2 Mutations and Variants of Interest*. Available at https://covariants.org/ (Accessed February 10, 2022). Hoffman, R. L., Kania, R. S., Brothers, M. A., Davies, J. F., Ferre, R. A., Gajiwala, K. S., et al. (2020). Discovery of Ketone-Based Covalent Inhibitors of Coronavirus 3CL Proteases for the Potential Therapeutic Treatment of COVID-19. *J. Med. Chem.* 63 (21), 12725–12747. doi:10.1021/acs.jmedchem.0c01063

Hoffmann, M., Kleine-Weber, H., Schroeder, S., Krüger, N., Herrler, T., Erichsen, S., et al. (2020). SARS-CoV-2 Cell Entry Depends on ACE2 and TMPRSS2 and Is Blocked by a Clinically Proven Protease Inhibitor. *Cell* 181 (2), 271–280. e8. doi:10.1016/j.cell.2020.02.052

Horspool, A. M., Ye, C., Wong, T. Y., Russ, B. P., Lee, K. S., Winters, M. T., et al. (2021). SARS-CoV-2 B.1.1.7 and B.1.351 Variants of Concern Induce Lethal Disease in K18-hACE2 Transgenic Mice Despite Convalescent Plasma Therapy. *BioRxiv*. doi:10.1101/2021.05.05.442784

Hossain, M. A., Hossain, K. M. A., Saunders, K., Uddin, Z., Walton, L. M., Raigangar, V., et al. (2021). Prevalence of Long COVID Symptoms in Bangladesh: A Prospective Inception Cohort Study of COVID-19 Survivors. *BMJ Glob. Health* 6 (12), e006838. doi:10.1136/bmjgh-2021-006838

Hu, Y., Liu, L., and Lu, X. (2021). Regulation of Angiotensin-Converting Enzyme 2: A Potential Target to Prevent COVID-19? *Front. Endocrinol.* 12. doi:10.3389/ fendo.2021.725967

Huang, C., Huang, L., Wang, Y., Li, X., Ren, L., Gu, X., et al. (2021). 6-month Consequences of COVID-19 in Patients Discharged from Hospital: a Cohort Study. *The Lancet* 397 (10270), 220–232. doi:10.1016/S0140-6736(20)32656-8

Huang, S., Wang, J., Liu, F., Liu, J., Cao, G., Yang, C., et al. (2020). COVID-19 Patients with Hypertension Have More Severe Disease: a Multicenter Retrospective Observational Study. *Hypertens. Res.* 43 (8), 824–831. doi:10. 1038/s41440-020-0485-2

Israelow, B., Song, E., Mao, T., Lu, P., Meir, A., Liu, F., et al. (2020). Mouse Model of SARS-CoV-2 Reveals Inflammatory Role of Type I Interferon Signaling. *J. Exp. Med.* 217 (12). doi:10.1084/JEM.20201241

Jackson, C. B., Farzan, M., Chen, B., and Choe, H. (2022). Mechanisms of SARS- CoV-2 Entry into Cells. *Nat. Rev. Mol. Cel Biol* 23 (1), 3–20. doi:10.1038/ s41580-021-00418-x

Jayasooriya, A. P., Mathai, M. L., Walker, L. L., Begg, D. P., Denton, D. A., Cameron-Smith, D., et al. (2008). Mice Lacking Angiotensin-Converting Enzyme Have Increased Energy Expenditure, with Reduced Fat Mass and Improved Glucose Clearance. *Proc. Natl. Acad. Sci. U.S.A.* 105 (18), 6531–6536. www.pnas.orgcgi. doi:10.1073/pnas.0802690105

Jia, H., Yue, X., and Lazartigues, E. (2020). ACE2 Mouse Models: a Toolbox for Cardiovascular and Pulmonary Research. *Nat. Commun.* 11 (1), 5165. doi:10. 1038/s41467-020-18880-0

Jiang, R.-D., Di, Liu, M.-Q., Liu, Y., Shan, C., Zhou, Y.-W., Shen, X.-R., et al. (2020). Pathogenesis of SARS-CoV-2 in Transgenic Mice Expressing Human Angiotensin-Converting Enzyme 2. *Cell* 182 (1), 50–58. e8. doi:10.1016/J.CELL.2020.05.027

Jiang, X., Li, H., Liu, Y., Bao, L., Zhan, L., Gao, H., et al. (2022). The Effects of ATIR Blocker on the Severity of COVID-19 in Hypertensive Inpatients and Virulence of SARS-CoV-2 in Hypertensive hACE2 Transgenic Mice. *J. Cardiovasc. Trans. Res.* 15, 38–48. doi:10.1007/s12265-021-10147-3

Kabinger, F., Stiller, C., Schmitzová, J., Dienemann, C., Kokic, G., Hillen, H. S., et al. (2021). Mechanism of Molnupiravir-Induced SARS-CoV-2 Mutagenesis. *Nat. Struct. Mol. Biol.* 28 (9), 740–746. doi:10.1038/s41594-021-00651-0

Kaptein, S. J. F., Jacobs, S., Langendries, L., Seldeslachts, L., ter Horst, S., Liesenborghs, L., et al. (2020). Favipiravir at High Doses Has Potent Antiviral Activity in SARS-CoV-2−infected Hamsters, whereas Hydroxychloroquine Lacks Activity. *Proc. Natl. Acad. Sci. U.S.A.* 117 (43), 26955–26965. doi:10.1073/pnas.2014441117/-/DCSupplemental

Katzman, C., Israely, T., Melamed, S., Politi, B., Sittner, A., Yahalom-Ronen, Y., et al. (2022). Modeling Sars-Cov-2 Infection in Mice Using Lentiviral Hace2 Vectors Infers Two Modes of Immune Responses to Sars-Cov-2 Infection. *Viruses* 14 (1), 11. doi:10.3390/V14010011/S1

King, A. J. (2012). The Use of Animal Models in Diabetes Research. *Br. J. Pharamacology* 166, 877–894. doi:10.1111/j.1476-5381.2012.01911.x

Kovacech, B., Fialova, L., Filipcik, P., Skrabana, R., Zilkova, M., Paulenka-Ivanovova, N., et al. (2022). Monoclonal Antibodies Targeting Two Immunodominant Epitopes on the Spike Protein Neutralize Emerging SARS-CoV-2 Variants of Concern. *EBioMedicine* 76, 103818. doi:10.1016/j10.1016/j.ebiom.2022.103818

Kulcsar, K. A., Coleman, C. M., Beck, S. E., and Frieman, M. B. (2019). Comorbid Diabetes Results in Immune Dysregulation and Enhanced Disease Severity Following MERS-CoV Infection. *JCI Insight* 4 (20), e131774. doi:10.1172/jci. insight.131774

Leclerc, Q. J., Fuller, N. M., Knight, L. E., Funk, S., Knight, G. M., and Knight, G. M. (2020). What Settings Have Been Linked to SARS-CoV-2 Transmission Clusters? *Wellcome Open Res.* 5, 83. doi:10.12688/wellcomeopenres.15889.1

Lerman, L. O., Kurtz, T. W., Touyz, R. M., Ellison, D. H., Chade, A. R., Crowley, S. D., et al. (2019). Animal Models of Hypertension: A Scientific Statement from the American Heart Association. *Hypertension* 73 (6), e87–e120. doi:10.1161/ HYP.0000000000000090

Li, M.-Y., Li, L., Zhang, Y., and Wang, X.-S. (2020). Expression of the SARS-CoV-2 Cell Receptor Gene ACE2 in a Wide Variety of Human Tissues. *Infect. Dis. Poverty* 9 (1). doi:10.1186/s40249-020-00662-x

Li, X., Xu, S., Yu, M., Wang, K., Tao, Y., Zhou, Y., et al. (2020). Risk Factors for Severity and Mortality in Adult COVID-19 Inpatients in Wuhan. *J. Allergy Clin. Immunol.* 146 (1), 110–118. doi:10.1016/j.jaci.2020.04.006

Liu, Y., Liu, J., Plante, K. S., Plante, J. A., Xie, X., Zhang, X., et al. (2022). The N501Y Spike Substitution Enhances SARS-CoV-2 Infection and Transmission. *Nature* 602 (7896), 294–299. doi:10.1038/s41586-021-04245-0

Lu, R., Zhao, X., Li, J., Niu, P., Yang, B., Wu, H., et al. (2020). Genomic Characterisation and Epidemiology of 2019 Novel Coronavirus: Implications for Virus Origins and Receptor Binding. *The Lancet* 395 (10224), 565–574. doi:10.1016/s0140-6736(20)30251-8

Ma, Y., Lu, D., Bao, L., Qu, Y., Liu, J., Qi, X., et al. (2021). SARS-CoV-2 Infection Aggravates Chronic Comorbidities of Cardiovascular Diseases and Diabetes in Mice. *Anim. Models Exp. Med.* 4 (1), 2–15. doi:10.1002/ ame2.12155

McCray, P. B., Pewe, L., Wohlford-Lenane, C., Hickey, M., Manzel, L., Shi, L., et al. (2007). Lethal Infection of K18- hACE2 Mice Infected with Severe Acute Respiratory Syndrome Coronavirus. *J. Virol.* 81 (2), 813–821. doi:10.1128/JVI.
02012-06

Medicines & Healthcare products Regulatory Agency (2021b). *First Oral Antiviral for COVID-19, Lagevrio (Molnupiravir), Approved by MHRA. [Press release]* London, United Kingdom. Available at: https://www.gov.uk/government/news/ first-oral-antiviral-for-covid-19-lagevrio-molnupiravir-approved-by-mhra (Accessed February 24, 2022).

Medicines & Healthcare products Regulatory Agency (2021a). *Oral COVID-19 Antiviral, Paxlovid, Approved by UK regulator. [Press release]*. London, United Kingdom (Available at: https://www.gov.uk/government/news/ oral-covid-19-antiviral-paxlovid-approved-by-uk-regulator (Accessed February 24, 2022).

Menachery, V. D., Yount, B. L., Sims, A. C., Debbink, K., Agnihothram, S. S., Gralinski, L. E., et al. (2016). SARS-like WIV1-CoV Poised for Human Emergence. *Proc. Natl. Acad. Sci. U.S.A.* 113 (11), 3048–3053. doi:10.1073/ PNAS.1517719113

Mughal, M. S., Kaur, I. P., Jaffery, A. R., Dalmacion, D. L., Wang, C., Koyoda, S., et al. (2020). COVID-19 Patients in a Tertiary US Hospital: Assessment of Clinical Course and Predictors of the Disease Severity. *Respir. Med.* 172, 106130. doi:10.1016/j.rmed.2020.106130

Muniangi-Muhitu, H., Akalestou, E., Salem, V., Misra, S., Oliver, N. S., and Rutter, G. A. (2020). Covid-19 and Diabetes: A Complex Bidirectional Relationship. *Front. Endocrinol.* 11. doi:10.3389/fendo.2020.582936

Munster, V. J., Feldmann, F., Williamson, B. N., van Doremalen, N., Pérez-Pérez, L., Schulz, J., et al. (2020). Respiratory Disease in Rhesus Macaques Inoculated with SARS-CoV-2. *Nature* 585 (7824), 268–272. doi:10.1038/S41586-020-
2324-7

Muruato, A., Vu, M. N., Johnson, B. A., Davis-Gardner, M. E., Vanderheiden, A., Lokugamage, K., et al. (2021). Mouse-adapted SARS-CoV-2 Protects Animals from Lethal SARS-CoV challenge. *Plos Biol.* 19 (11), e3001284. doi:10.1371/ journal.pbio.3001284

Nehme, A., Zouein, F. A., Zayeri, Z. D., and Zibara, K. (2019). An Update on the Tissue Renin Angiotensin System and its Role in Physiology and Pathology. *Jcdd* 6 (2), 14. doi:10.3390/jcdd6020014

Owen, D. R., Allerton, C. M. N., Anderson, A. S., Aschenbrenner, L., Avery, M., Berritt, S., et al. (2021). An Oral SARS-CoV-2 M Pro Inhibitor Clinical Candidate for the Treatment of COVID-19. *Science* 374 (6575), 1586–1593. https://www.science.org. doi:10.1126/science.abl4784

Pan, T., Chen, R., He, X., Yuan, Y., Deng, X., Li, R., et al. (2021). Infection of Wild-type Mice by SARS-CoV-2 B.1.351 Variant Indicates a Possible Novel Cross- Species Transmission Route. *Sig Transduct Target. Ther.* 6 (1), 420. doi:10.1038/ s41392-021-00848-1

Pérez-González, A., Araújo-Ameijeiras, A., Fernández-Villar, A., Crespo, M., Poveda, E., Cabrera, J. J., et al. (2022). Long COVID in Hospitalized and Non-hospitalized Patients in a Large Cohort in Northwest Spain, a Prospective Cohort Study. *Sci. Rep.* 12 (1), 3369. doi:10.1038/s41598-022-07414-x

Popkin, B. M., Du, S., Green, W. D., Beck, M. A., Algaith, T., Herbst, C. H., et al. (2020). Individuals with Obesity and COVID-19: A Global Perspective on the Epidemiology and Biological Relationships. *Obes. Rev.* 21 (11), e13128. doi:10.1111/obr.13128

Premaratna, S. D., Manickam, E., Begg, D. P., Rayment, D. J., Hafandi, A., Jois, M., et al. (2012). Angiotensin-converting Enzyme Inhibition Reverses Diet-Induced
Obesity, Insulin Resistance and Inflammation in C57BL/6J Mice. *Int. J. Obes.* 36 (2), 233–243. doi:10.1038/ijo.2011.95

Qiao, J., Li, Y.-S., Zeng, R., Liu, F.-L., Luo, R.-H., Huang, C., et al. (2021). SARS-CoV-2 M Pro Inhibitors with Antiviral Activity in a Transgenic Mouse Model. *Science* 371 (6536), 1374–1378. https://pymol.org. doi:10.1126/science.abf1611 Qing, E., and Gallagher, T. (2020). SARS Coronavirus Redux. *Trends Immunol.* 41 (4), 271–273. doi:10.1016/j.it.2020.02.007

Ragab, D., Salah Eldin, H., Taeimah, M., Khattab, R., and Salem, R. (2020). The COVID-19 Cytokine Storm; what We Know So Far. *Front. Immunol.* 11. doi:10.3389/fimmu.2020.01446

Rai, P., Chuong, C., LeRoith, T., Smyth, J. W., Panov, J., Levi, M., et al. (2021). Adenovirus Transduction to Express Human ACE2 Causes Obesity-specific Morbidity in Mice, Impeding Studies on the Effect of Host Nutritional Status on SARS-CoV-2 Pathogenesis. *Virology* 563, 98–106. doi:10.1016/j.virol.2021.
08.014

Rathnasinghe, R., Strohmeier, S., Amanat, F., Gillespie, V. L., Krammer, F., García- Sastre, A., et al. (2020). Comparison of Transgenic and Adenovirus hACE2 Mouse Models for SARS-CoV-2 Infection. *BioRxiv*. doi:10.1101/2020.07.06. 190066

Rawle, D. J., Le, T. T., Dumenil, T., Yan, K., Tang, B., Nguyen, W., et al. (2021). ACE2-lentiviral Transduction Enables Mouse SARS-CoV-2 Infection and Mapping of Receptor Interactions. *Plos Pathog.* 17 (7), e1009723. doi:10.1371/JOURNAL.PPAT.1009723

Rockx, B., Kuiken, T., Herfst, S., Bestebroer, T., Lamers, M. M., Oude Munnink, B. B., et al. (2020). Comparative Pathogenesis of COVID-19, MERS, and SARS in a Nonhuman Primate Model. *Science* 368 (6494), 1012–1015. doi:10.1126/ SCIENCE.ABB7314

Rongvaux, A., Willinger, T., Martinek, J., Strowig, T., Gearty, S. v., Teichmann, L. L., et al. (2014). Development and Function of Human Innate Immune Cells in a Humanized Mouse Model. *Nat. Biotechnol.* 32 (4), 364–372. doi:10.1038/nbt.2858 Rosenke, K., Hansen, F., Schwarz, B., Feldmann, F., Haddock, E., Rosenke, R., et al. (2021). Orally Delivered MK-4482 Inhibits SARS-CoV-2 Replication in the Syrian Hamster Model. *Nat. Commun.* 12 (1). doi:10.1038/s41467-021-22580-8 Samavati, L., and Uhal, B. D. (2020). ACE2, Much More Than Just a Receptor for SARS-COV-2. *Front. Cell Infect. Microbiol.* 10. doi:10.3389/fcimb.2020.00317 Sarver, D. C., and Wong, G. W. (2021). Obesity Alters Ace2 and Tmprss2 Expression in Lung, Trachea, and Esophagus in a Sex-dependent Manner: Implications for COVID-19. *Biochem. Biophysical Res. Commun.* 538, 92–96. doi:10.1016/j.bbrc.2020.10.066

Sefik, E., Israelow, B., Mirza, H., Zhao, J., Qu, R., Kaffe, E., et al. (2021). A Humanized Mouse Model of Chronic COVID-19. *Nat. Biotechnol*. doi:10.1038/s41587-021-01155-4

Sellers, R. S. (2017). Translating Mouse Models. *Toxicol. Pathol.* 45 (1), 134–145. doi:10.1177/0192623316675767

Shahhosseini, N., Babuadze, G., Wong, G., and Kobinger, G. P. (2021). Mutation Signatures and In Silico Docking of Novel Sars-Cov-2 Variants of Concern. *Microorganisms* 9 (5), 926. doi:10.3390/microorganisms9050926

Sheahan, T. P., Sims, A. C., Zhou, S., Graham, R. L., Pruijssers, A. J., Agostini, M. L., et al. (2020). An Orally Bioavailable Broad-Spectrum Antiviral Inhibits SARS- CoV-2 in Human Airway Epithelial Cell Cultures and Multiple Coronaviruses in Mice. *Sci. Transl. Med.* 12 (541). doi:10.1126/SCITRANSLMED.ABB5883

Shou, S., Liu, M., Yang, Y., Kang, N., Song, Y., Tan, D., et al. (2021). Animal Models for COVID-19: Hamsters, Mouse, Ferret, Mink, Tree Shrew, and Non-human Primates. *Front. Microbiol.* 12. doi:10.3389/fmicb.2021.626553

Shuai, L., Zhong, G., Yuan, Q., Wen, Z., Wang, C., He, X., et al. (2021). Replication, Pathogenicity, and Transmission of SARS-CoV-2 in Minks. *Natl. Sci. Rev.* 8 (3), 2021. doi:10.1093/NSR/NWAA291

Simmons, G., Gosalia, D. N., Rennekamp, A. J., Reeves, J. D., Diamond, S. L., and Bates, P. (2005). Inhibitors of Cathepsin L Prevent Severe Acute Respiratory Syndrome Coronavirus Entry. *Proc. Natl. Acad. Sci. U.S.A.* 102 (33), 11876–11881. doi:10.1073/pnas.0505577102

Skevaki, C., Karsonova, A., Karaulov, A., Xie, M., and Renz, H. (2020). Asthma-associated Risk for COVID-19 Development. *J. Allergy Clin. Immunol.* 146 (6), 1295–1301. doi:10.1016/j.jaci.2020.09.017

Su, Y., Yuan, D., Chen, D. G., Ng, R. H., Wang, K., Choi, J., et al. (2022). Multiple Early Factors Anticipate post-acute COVID-19 Sequelae. *Cell* 185, 881–895. doi:10.1016/j.cell.2022.01.014

Sun, J., Zhuang, Z., Zheng, J., Li, K., Wong, R. L.-Y., Liu, D., et al. (2020). Generation ofa Broadly Useful Model for COVID-19 Pathogenesis, Vaccination, and Treatment. *Cell* 182 (3), 734–743. e5. doi:10.1016/j.cell.2020.06.010

Sun, S.-H., Chen, Q., Gu, H.-J., Yang, G., Wang, Y.-X., Huang, X.-Y., et al. (2020). A Mouse Model of SARS-CoV-2 Infection and Pathogenesis. *Cell Host and Microbe* 28 (1), 124–133. e4. doi:10.1016/J.CHOM.2020.05.020/ ATTACHMENT/34A485A8-CAD9-409E-AA5B-0EF7B1B54781/MMC1.PDF

Tang, C., Deng, Z., Li, X., Yang, M., Tian, Z., Chen, Z., et al. (2020). Helicase of Type 2 Porcine Reproductive and Respiratory Syndrome Virus Strain HV Reveals a Unique Structure. *Viruses* 12 (2), 215. doi:10.3390/ v12020215

Thomas, S. (2020). The Structure of the Membrane Protein of SARS-CoV-2 Resembles the Sugar Transporter SemiSWEET. *Pai* 5 (1), 342–363. doi:10. 20411/pai.v5i1.377

Triggle, C. R., Bansal, D., Ding, H., Islam, M. M., Farag, E. A. B. A., Hadi, H. A., et al. (2021). A Comprehensive Review of Viral Characteristics, Transmission, Pathophysiology, Immune Response, and Management of SARS-CoV-2 and COVID-19 as a Basis for Controlling the Pandemic. *Front. Immunol.* 12, 631139. doi:10.3389/fimmu.2021.631139

Tseng, C.-T. K., Huang, C., Newman, P., Wang, N., Narayanan, K., Watts, D. M., et al. (2007). Severe Acute Respiratory Syndrome Coronavirus Infection of Mice Transgenic for the Human Angiotensin-Converting Enzyme 2 Virus Receptor.
J. Virol. 81 (3), 1162–1173. doi:10.1128/JVI.01702-06/ASSET/DACA1C30- 425C-4D1C-8B34-1CE2B664B6C9/ASSETS/GRAPHIC/ZJV0030787060008. JPEG

Turner, A. J., and Hooper, N. M. (2002). The Angiotensin-Converting Enzyme Gene Family: Genomics and Pharmacology. *Trends Pharmacol. Sci.* 23 (4), 177–183. doi:10.1016/s0165-6147(00)01994-5

U.S. Food and Drug Administration (2021b). *Coronavirus (COVID-19) Update: FDA Authorizes Additional Oral Antiviral for Treatment of COVID-19 in Certain Adults*. Silver Spring, MD: FDA. Available at: https://www.fda.gov/news-events/press- announcements/coronavirus-covid-19-update-fda-authorizes-additional-oral- antiviral-treatment-covid-19-certain (Accessed February 11, 2022).

U.S. Food and Drug Administration (2021a). *Coronavirus (COVID-19) Update: FDA Authorizes First Oral Antiviral for Treatment of COVID-19*. Silver Spring, MD: FDA. Available at: https://www.fda.gov/news-events/press-announcements/coronavirus- covid-19-update-fda-authorizes-first-oral-antiviral-treatment-covid-19 (Accessed February 10, 2022).

Wahl, A., Gralinski, L. E., Johnson, C. E., Yao, W., Kovarova, M., Dinnon, K. H., et al. (2021). SARS-CoV-2 Infection Is Effectively Treated and Prevented by EIDD-2801. *Nature* 591 (7850), 451–457. doi:10.1038/ s41586-021-03312-w

Walls, A. C., Park, Y.-J., Tortorici, M. A., Wall, A., McGuire, A. T., and Veesler, D. (2020). Structure, Function, and Antigenicity of the SARS-CoV-2 Spike Glycoprotein. *Cell* 181 (2), 281–292. e6. doi:10.1016/j.cell.2020.02.058

Wark, P. A. B., Pathinayake, P. S., Kaiko, G., Nichol, K., Ali, A., Chen, L., et al. (2021). ACE2 Expression Is Elevated in Airway Epithelial Cells from Older and Male Healthy Individuals but Reduced in Asthma. *Respirology* 26 (5), 442–451. doi:10.1111/resp.14003

Williamson, E. J., Walker, A. J., Bhaskaran, K., Bacon, S., Bates, C., Morton, C. E., et al. (2020). Factors Associated with COVID-19-Related Death Using OpenSAFELY. *Nature* 584 (7821), 430–436. doi:10.1038/s41586-020-2521-4

Winkler, E. S., Chen, R. E., Alam, F., Yildiz, S., Case, J. B., Uccellini, M. B., et al. (2022). SARS-CoV-2 Causes Lung Infection without Severe Disease in Human ACE2 Knock- In Mice. *J. Virol.* 96 (1), e0151121. doi:10.1128/JVI10.1128/JVI.01511-21

Winkler, E. S., Bailey, A. L., Kafai, N. M., Nair, S., McCune, B. T., Yu, J., et al. (2020). SARS-CoV-2 Infection of Human ACE2-Transgenic Mice Causes Severe Lung Inflammation and Impaired Function. *Nat. Immunol.* 21 (11), 1327–1335. doi:10.1038/s41590-020-0778-2

Wrapp, D., Wang, N., Corbett, K. S., Goldsmith, J. A., Hsieh, C.-L., Abiona, O., et al. (2020). Cryo-EM Structure of the 2019-nCoV Spike in the Prefusion Conformation. *Science* 367 (6483), 1260–1263. doi:10.1126/science. abb2507

Xie, Y., Xu, E., Bowe, B., and Al-Aly, Z. (2022). Long-term Cardiovascular Outcomes of COVID-19. *Nat. Med.* 28, 583–590. doi:10.1038/s41591-022-01689-3

Xudong, X., Junzhu, C., Xingxiang, W., Furong, Z., and Yanrong, L. (2006). Age- and Gender-Related Difference of ACE2 Expression in Rat Lung. *Life Sci.* 78 (19), 2166–2171. doi:10.1016/j.lfs.2005.09.038

Yang, X. H., Deng, W., Tong, Z., Liu, Y. X., Zhang, L. F., Zhu, H., et al. (2007b). Mice Transgenic for Human Angiotensin-Converting Enzyme 2 Provide a Model for SARS Coronavirus Infection. *Comp. Med.* 57 (5), 450–459.

Yang, X. H., Deng, W., Tong, Z., Liu, Y.-x., Zhang, L., and Zhu, H. (2007a). Mice Transgenic for Human Angiotensin-Converting Enzyme 2 Provide a Model for SARS Coronavirus Infection. *Comp. Med.* 57, 450–459. *Ingenta Connect*. from https://www.ingentaconnect.com/content/aalas/cm/2007/00000057/00000005/ art00003# (Retrieved March 6, 2022).

Yong, S. J. (2021). Long COVID or post-COVID-19 Syndrome: Putative Pathophysiology, Risk Factors, and Treatments. *Infect. Dis.* 53 (Issue 10), 737–754. doi:10.1080/23744235.2021.1924397

Yoon, H. E., Kim, E. N., Kim, M. Y., Lim, J. H., Jang, I.-A., Ban, T. H., et al. (2016). Age-Associated Changes in the Vascular Renin-Angiotensin System in Mice. *Oxidative Med. Cell Longevity* 2016, 1–14. doi:10.1155/ 2016/6731093

Zhang, X., Kousoulas, K. G., and Storz, J. (1992). The Hemagglutinin/esterase Gene of Human Coronavirus Strain OC43: Phylogenetic Relationships to Bovine and Murine Coronaviruses and Influenza C Virus. *Virology* 186 (1), 318–323. doi:10.1016/0042-6822(92)90089-8

Zhang, Y.-N., Zhang, Z.-R., Zhang, H.-Q., Li, X.-D., Li, J.-Q., Zhang, Q.-Y., et al. (2021). Increased Morbidity of Obese Mice Infected with Mouse-Adapted SARS-CoV-2. *Cell Discov* 7 (Issue 1), 74. doi:10.1038/s41421-021- 00305-x

Zhou, S., Hill, C. S., Sarkar, S., Tse, L. v., Woodburn, B. M. D., Schinazi, R. F., et al. (2021). β-d-N4-hydroxycytidine Inhibits SARS-CoV-2 through Lethal Mutagenesis but Is Also Mutagenic to Mammalian Cells. *J. Infect. Dis.* 224 (3), 415–419. doi:10.1093/infdis/jiab247

Zhu, Z., Hasegawa, K., Ma, B., Fujiogi, M., Camargo, C. A., Jr., and Liang, L. (2020). Association of Asthma and its Genetic Predisposition with the Risk of Severe COVID-19. *J. Allergy Clin. Immunol.* 146 (2), 327–e4. doi:10.1016/j.jaci.2020. 05.02110.1016/j.jaci.2020.06.001

Conflict of Interest: The authors declare that the research was conducted in the absence of any commercial or financial relationships that could be construed as a potential conflict of interest.